University of Alberta

Molecular Basis of TopBP1 BRCT Domain Interactions in the DNA Damage Response

by

Charles Chung Yun Leung

A thesis submitted to the Faculty of Graduate Studies and Research
in partial fulfillment of the requirements for the degree of

Doctor of Philosophy

Department of Biochemistry

Fall 2011
Edmonton, Alberta

Abstract

Topoisomerase IIβ binding protein 1 (TopBP1) is a critical regulatory protein that integrates diverse signals in the DNA damage response. In response to DNA replication stress, TopBP1 participates in a series of protein interactions to collectively activate the key Ser/Thr kinase, Ataxia telangiectasia and Rad3 related (ATR), and control the DNA replication checkpoint. These phosphorylation-dependent interactions are mediated by the numerous conserved BRCT domains within TopBP1. Our studies utilize X-ray crystallography in combination with other biochemical and biophysical techniques to elucidate the molecular basis underlying various TopBP1 BRCT-mediated interactions in DNA damage response signalling.

Contrary to previous studies suggesting that the single BRCT6 domain of TopBP1 recognizes a phospho-peptide of the transcription factor, E2F1, and binds to poly(ADP-ribose) chains, the crystal structure of BRCT6 provides evidence that both the phospho-peptide binding pocket and PAR-binding motif are non-functional. Our studies of distinct phospho-peptide interactions involving the tandem BRCT7/8 and BRCT4/5 repeats of TopBP1 shed light on critical interactions required for activation of ATR and the DNA replication checkpoint. In addition, the mode of phospho-peptide recognition presented by these BRCT repeats uncover new and exciting perspectives in BRCT domain function that were previously unknown. Analysis of the structures of TopBP1

BRCT7/8 and in complex with a BACH1 phospho-peptide provides the first demonstration of pThr specificity and an uncharacteristic plasticity at the BRCT domain interface for canonical tandem BRCT domains. Our structural investigations of interactions between TopBP1 BRCT4/5 and a MDC1 phospho-peptide reveal a novel tandem BRCT domain packing arrangement, as well as an unexpected dimerization of two BRCT4/5 domains needed to stabilize interactions with a single phospho-peptide.

Taken together, our studies of TopBP1 BRCT domain interactions provide molecular insights into crucial protein interactions involved in DNA replication checkpoint signalling and also highlight the extraordinary functional diversity of BRCT domains.

Acknowledgements

Firstly, I would like to thank my supervisor, Dr. Mark Glover, for his support and guidance. Thank you for being so patient with me and giving me the freedom to explore my research interests. Mark is a brilliant scientist who has been a great mentor and someone I will undoubtedly try to model myself after in the future.

My research on TopBP1 has been an ongoing collaboration with Dr. Junjie Chen (University of Texas MD Anderson Cancer Center). If not for his amazing discoveries in TopBP1 and BRCT domains, none of this work would be possible. Thanks to Dr. Zihua Gong especially, who led the work on the TopBP1-BACH1 and TopBP1-MDC1 projects. Other collaborations with Dr. David Baker (University of Washington) and Dr. Frank Hanel (Hans Knoell Institute) have also been instrumental for one of my projects.

My committee members, Dr. Charles Holmes and Dr. Howard Young, have been very supportive during my graduate studies. A special thanks to my internal examiner, Dr. Frederick West, and my external examiner, Dr. Alba Guarne, for making the trip from Hamilton.

Past and present members of the Glover lab (Stephen, Steve, Ross, Dave, Megan, Nina, Danny, Nico, Curtis, Gina, Jun, Joyce, Ruth, Yun, Zahra and Inbal) have provided tremendous help and expertise over the years. Members of 451/308 have made working in the lab extremely fun and memorable. Thanks to my summer/499 students, especially Mark, who did tremendous work for two consecutive summers. Thanks to Sheraz for helping with the synchrotron shipping and maintaining the crystallography equipment. Thanks to Sue for keeping all the paper work for scholarships and reimbursements in order.

I will always remember the fun times I've had in Edmonton, especially with all the great friends. Stephen has been by my side since my first day in the lab and has become my best friend. I will forever cherish our friendship. All the friends from the department, especially Angela, Roshani, Nobu, Ian, Tamara, Allison, OJ, Grant, Delaine, Shem and Sean, have made staying and hanging out in the department fun. I have enjoyed being a member of all the sports teams, including EUPA ultimate, intramural softball, ultimate and flag football. Finally, a very special thanks and love to Angela, who is the sunshine of my life and the source of 99% of my happiness.

Most importantly, thanks to mom, dad and bro for their unconditional love and support. Mom and dad have sacrificed so much for me and I owe all my successes (and failures) to them. I am so proud of my family and I hope to never let them down.

Table of Contents

Page

Page

Page

Page

List of Tables

Page

List of Figures

Page

Page

Page

Page

List of Abbreviations

Å	Angstrom (10^{-10}) meters
BME	β-mercaptoethanol
CMCF	Canadian Macromolecular Crystallography Facility
DDR	DNA damage response
dsDNA	Double-stranded DNA
DSB	Double-stranded break
DTT	Dithiothreitol
EDTA	(Ethylenedinitrilo)-tetraacetic acid
EMSA	Electrophoretic mobility shift assay
FITC	Fluorescein isothiocyanate
FP	Fluorescence polarization
GST	Glutatione S-transferase
HEPES	4-(2-hydroxyethyl)-1-piperazineethanesulfonic acid
HR	Homologous recombination
ITC	Isothermal titration calorimetry
IPTG	Isopropyl β-D-thiogalactopyranoside
LB	Luria Bertani
LC-MS	Liquid chromatography-mass spectrometry
MALDI-TOF	Matrix assisted laser desorption ionization-time of flight
MME	Monomethyl ether
PAGE	Polyacrylamide gel electrophoresis
PAR	Poly(ADP-ribose)
PCR	Polymerase chain reaction
PDB	Protein Data Bank
PEG	Polyethylene glycol
PMSF	Phenylmethyl sulfonyl fluoride
SAD	Single wavelength anomalous dispersion
SCN	Thiocyanate

SDS	Sodium dodecyl sulphate
Se-Met	Seleno-methionine
SSB	Single-stranded break
ssDNA	Single-stranded DNA
TCEP	(Tris(2-carboxyethyl)phosphine)
TRIS	Tris(hydroxymethyl)aminomethane

Chapter 1

Introduction

A version of this chapter is accepted in:

Leung CC, Glover J N (2011) BRCT domains: Easy as one, two three. *Cell Cycle*. **10**:2461-70.

1.1. DNA damage and cancer

1.1.1. A brief history of DNA damage and repair

The concept that radiation can cause damage to the genetic material of cells can be traced back to as early as the 1930s, a period where major advances in energy and radiation technology eventually led to the construction of the atomic bomb (Friedberg, 1997). Knowledge of the molecular mechanisms underlying this phenomenon, however, was primitive and poorly understood. A major breakthrough came in the discovery of the DNA structure by James Watson and Francis Crick in the 1950s (Watson & Crick, 1953). The realization that our genetic material is composed of nucleotide base pairing between two complementary parental strands shed light on a possible mechanism for DNA replication and the transferring of genetic material. Yet, the idea that DNA structure is damaged and requires repair by enzymes was still not proposed until direct evidence for DNA repair mechanisms emerged for the processes of enzymatic photoactivation in the 1950s and excision repair in the 1960s (Boyce & Howard-Flanders, 1964; Goodgal et al, 1957; Pettijohn & Hanawalt, 1964; Setlow & Carrier, 1964). As Francis Crick later in 1974 stated "We totally missed the possible role of enzymes in DNA repair.... I later came to realize that DNA is so precious that probably many distinct repair mechanisms would exist" (Crick, 1974). With the discovery of excision repair, the link between defective DNA repair and cancer was subsequently determined in the late 1960s from studies of the cancer predisposing genetic disorder, Xeroderma pigmentosum (XP) (Cleaver, 1968; Setlow et al, 1969). Together, these pioneering studies have paved the way for the dynamic and exciting field of DNA repair.

1.1.2. Striving to preserve genomic integrity

It is now clear that the fundamental, dependent nature of DNA creates enormous stakes for preserving genomic integrity. The unavoidable assault by

genotoxic agents amasses tens of thousands of lesions/cell/day. It is therefore an absolute necessity that cells are equipped with a vast network of repair machineries. The importance for maintaining genomic integrity is perhaps reflected in the investment cells are willing to make to overcome or repair different types of DNA damages. A specialized low fidelity class of DNA polymerases (Y family and Polζ) is solely devoted to replicate past damaged DNA during DNA replication stress (Goodman & Tippin, 2000). It is also estimated that more than 10^4 ATP molecules are used in the homologous recombination (HR) pathway to alleviate one DNA double-stranded break (DSB) (Hoeijmakers, 2009). Ultimately if the damage permeates past cellular repair, the ensuing mutations and chromosomal aberrations can cause cell death, or be passed onto future generations and lead to genomic instability and cancer.

1.1.3. Hallmarks of cancer

Defining characteristics of cancer have been highly debated in the past decade. The hallmarks of cancer were initially defined by Hanahan and Weinberg to describe six distinctive and complementary capabilities in cancers (Hanahan & Weinberg, 2000). These included activated growth signalling, evading cell death, sustained angiogenesis, tissue invasion and metastasis, limitless replicative potential and evading growth suppressors. However, as our understanding of cancers has evolved, additional hallmarks that express the state of cancer cells have been proposed. As a result, an updated map of cancer hallmarks proposed by Negrini et al. includes evading immune surveillance, metabolic stress, mitotic stress, DNA damage and DNA replication stress, and genomic instability (Fig. 1-1) (Negrini et al, 2010).

Genomic instability is a fundamental trait in all cancers and is prevalent at all stages of cancer. Several forms of genomic instability exist, although the major form is chromosomal instability, which is characterized by the high rate of

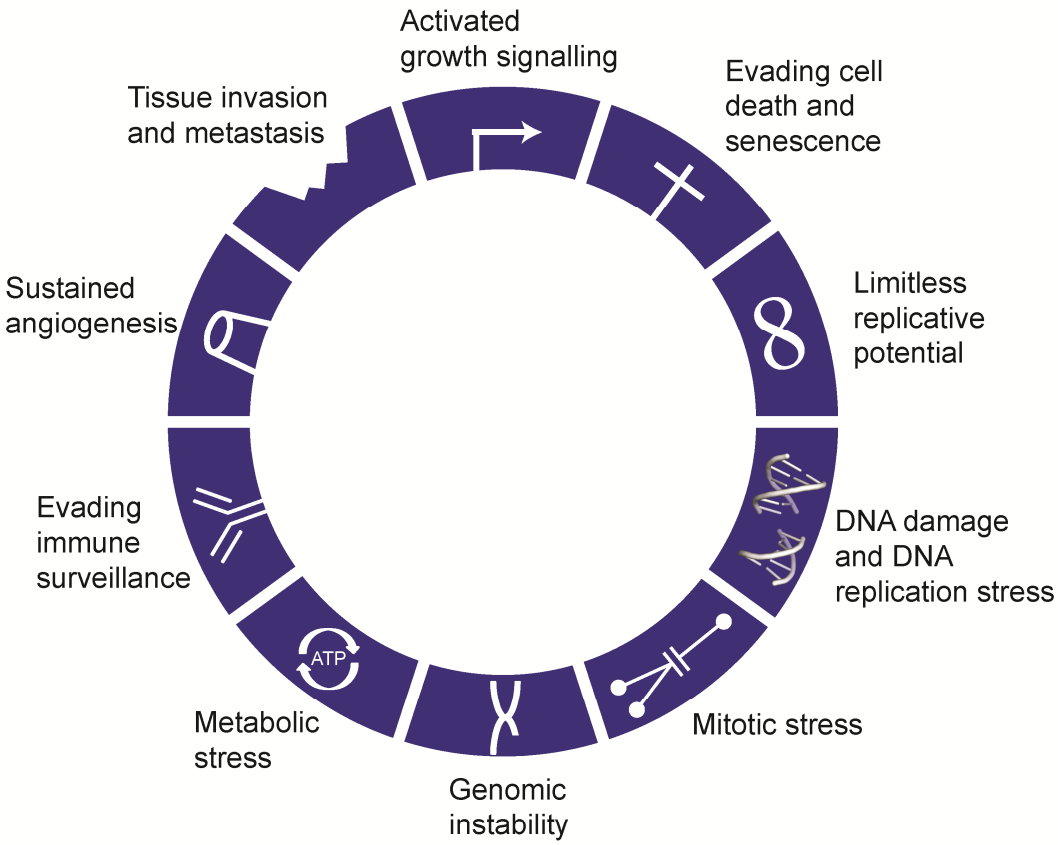

Figure 1-1. Genomic instability and DNA damage/DNA replication stress are hallmarks of cancer. Adapted from Negrini et al. (Negrini et al, 2010).

chromosomal aberrations in cancer cells. Other forms of genomic instability include microsatellite instability and increased frequency of base-pair mutations (Negrini et al, 2010). It is now clear that genomic instability and DNA damage/replication stress work hand in hand to fuel tumour development. In hereditary cancers, germline mutations in DNA repair genes, such as *Breast cancer associated 1 and 2 (BRCA1 and BRCA2)*, *Nijmegen breakage syndrome protein 1 (NBS1)* and *RAD50*, generate genomic instability and predispose to various cancers (Ciccia & Elledge, 2010). Aberrant proliferation from activated oncogenes also induces DNA replication stress and ensuing DNA DSBs, which drive chromosomal instability in sporadic cancers (Halazonetis et al, 2008). Since DNA damage and replication stress are driving forces for cancer development, understanding their underlying regulatory mechanisms may prove to be an effective avenue for the development of cancer treatments.

1.1.4 Sources of DNA damage

DNA integrity is constantly threatened on two fronts: sources that come from within cells (endogenous) and from the environment (exogenous) (Table 1-1). Each type of genotoxic agent elicits a specific pattern of damage to the DNA structure. Mismatch during DNA replication, depurination of DNA to form abasic sites, interconversion between DNA bases from deamination and alkylation of DNA bases are spontaneous occurrences in cells (De Bont & van Larebeke, 2004; Lindahl, 1993). Reactive oxygen and nitrogen species generated by cell metabolism also create several kinds of single-stranded DNA breaks (SSBs) and over 70 oxidized DNA base and sugar products in DNA (Hoeijmakers, 2009). Exogenous DNA damages are either chemical or physical, but can be avoided or minimized in most cases. Chemical genotoxic sources include chemotherapy agents that are used to intentionally generate DNA lesions. For example, cross-linking agents such as mitomycin C (MMC) and cisplatin form covalent linkages

Table 1-1. Magnitude of different sources of DNA damage

Endogenous DNA damage	**DNA Lesions Generated**	**Number Lesions/Cell/Day**	
Depurination	AP site	10000	
Cytosine deamination	Base transition	100-500	
SAM-induced methylation	3meA	600	
	7meG	4000	
	O^6meG	10-30	
Oxidation	8oxoG		
Exogenous DNA damage	**Dose Exposure (mSv)**	**DNA Lesions Generated**	**Estimated Number Lesions/Cell**
Peak hr sunlight	-	Pyrimidine dimers, (6-4) photoproducts	100,000/day
Cigarette smoke	-	Aromatic DNA adducts	45-1029
Chest X-rays	0.02	DSBs	0.0008
Dental X-rays	0.005	DSBs	0.0002
Mammography	0.4	DSBs	0.016
Body CT	7	DSBs	0.28
Head CT	2	DSBs	0.08
Coronary angioplasty	22	DSBs	0.88
Tumor PET scan (^{18}F)	10	DSBs	0.4
^{131}I treatment	70-150	DSBs	2.8-6
External beam therapy	1800-2000	DSBs	72-80
Airline travel	0.005/HR	DSBs	0.0002/hr
Space mission (60 days)	50	DSBs	2
Chernobyl accident	300	DSBs	12
Hiroshima and Nagasaki atomic bombs	5-4000	DSBs	0.2-160

Table adapted from Ciccia et al. (Ciccia & Elledge, 2010)

between bases in DNA, and alkylating agents such as methyl methanesulfonate (MMS) attach alkyl groups to DNA bases. Physical sources include UV light and ionizing radiation (IR). UV induces pyrimidine dimers and (6-4) photoproducts, whereas X-rays create oxidized DNA bases, DNA SSBs and DSBs. If left unrepaired, these damages to DNA can manifest into mutations and chromosomal aberrations that ultimately lead to genomic instability.

1.2 DNA damage response: a multifaceted response machinery

1.2.1. DNA Repair pathways

The plethora of DNA lesion types requires customized DNA repair mechanisms that are capable of detecting and fixing the specific damage. Collectively termed the DNA damage response (DDR), cells are armed with elaborate signalling pathways that sense, amplify and transduce signals down to the effector molecules to operate a wide range of cellular responses necessary to ensure genomic integrity. These cellular responses include: DNA repair, cell cycle control, chromatin remodelling, apoptosis and senescence, replisome stability, transcription and RNA processing (Jackson & Bartek, 2009). Since repair of damaged DNA is time-dependent, the DDR is intimately linked to cell cycle control. Cell cycle checkpoints are present at every phase to ensure that DNA lesions are repaired before proceeding into the next cell cycle phase (Zhou & Elledge, 2000). As shown in Figure 1-2, the decision to enter a specific repair pathway is dictated by the lesion type. Small base adducts are repaired by base excision repair (BER), where the damaged base is often recognized by a glycosylase enzyme to remove the damaged base (Almeida & Sobol, 2007). The resulting abasic site is then repaired by nuclease, polymerase and ligase proteins. The nucleotide excision repair (NER) pathway repairs larger, helix distorting adducts. In NER, the lesion is removed along with 22-30 flanking oligonucleotides, which creates a short ssDNA stretch that requires polymerases

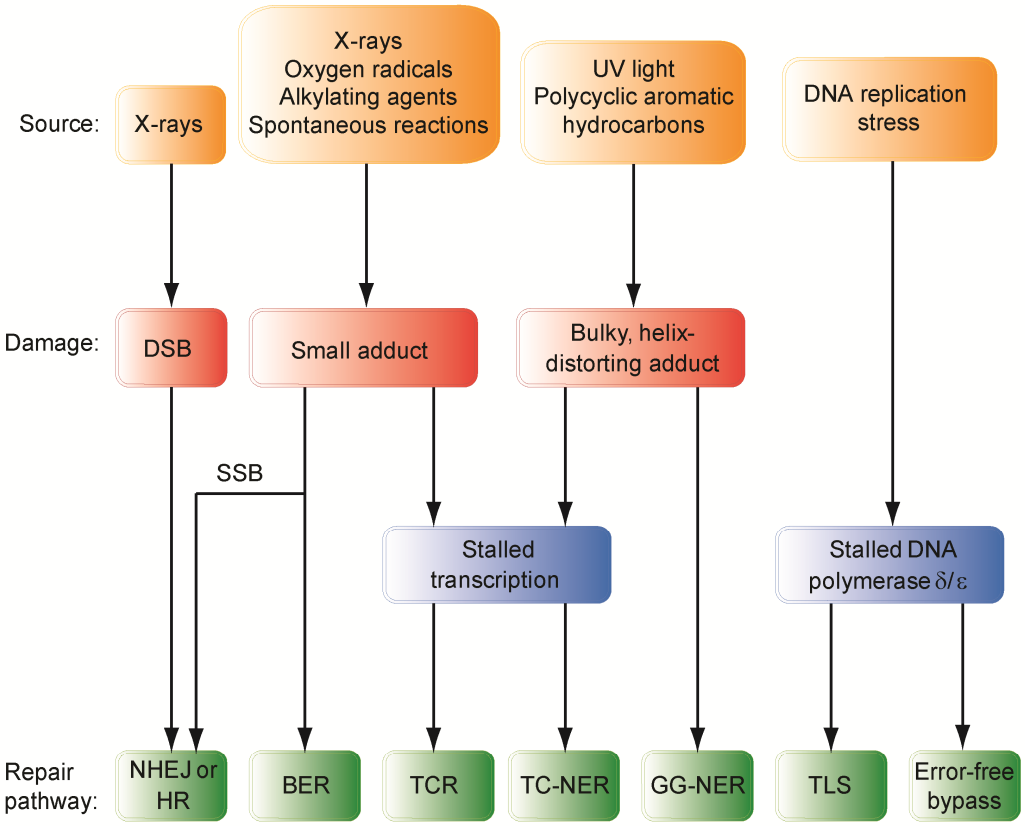

Figure 1-2. DNA repair pathways in the DNA damage response. Different types of DNA lesions generated from genotoxic agents activate distinct repair pathways. SSBs during DNA replication create DSBs, which are repaired by homologous recombination (HR). Other pathways shown include non-homologous end joining (NHEJ), base excision repair (BER), transcription-coupled repair (TCR), transcription-coupled nucleotide excision repair (TC-NER), global genome nucleotide excision repair (GG-NER), translesion synthesis (TLS) and error-free bypass. Adapted from Hoeijmakers (Hoeijmakers, 2009).

to fill in the gap before ligation (Friedberg, 2001). If a DNA lesion blocks transcription, transcription-coupled repair (TCR) or a specialized arm of NER, transcription-coupled NER (TC-NER), work in tandem with the transcription machinery for repair (Sarasin & Stary, 2007). DNA DSBs are considered the most cytotoxic type of lesion and are repaired by two different pathways: non-homologous end joining (NHEJ) and homologous recombination (HR). NHEJ is active throughout all cell cycle stages (primarily in G1). NHEJ utilizes a network of proteins to detect, process and ligate the DNA ends together (Lieber, 2010; Weinfeld et al, 2011). This process renders NHEJ error-prone, and bases can be lost or added during the process. HR occurs only in S and G2 phase, since the sister chromatid is required as a template to properly align the broken ends. HR is characterized by end resection to create ssDNA ends, strand invasion and exchange, and Holliday junction resolution (Huen et al, 2010; West, 2003). Some notable HR proteins include the Mre11-Rad50-Nbs1 (MRN) complex (performs end resection), Breast cancer associated 1 and 2 (BRCA1, BRCA2) and Rad51 (performs strand exchange). In contrast to NHEJ, HR is error-free and is also used to repair collapsed replication forks from DNA replication stress and inter-strand cross-links.

DNA replication stress is triggered when active replication forks encounter barriers or lesions on the DNA. Depending on the type of lesion or barrier, the fork may choose to repair the damage before restarting or bypass and repair the trailing damage via post-replication repair (PRR). Post-replication repair consists of two different mechanisms (translesion synthesis (TLS) and error-free bypass/template switching), and the choice of pathways depends on the ubiquitination state of the DNA processivity clamp, Proliferating cell nuclear antigen (PCNA) (Ulrich & Walden, 2010). TLS requires a damage-tolerant polymerase to complete DNA replication. Although DNA replication is successful, the damage remains intact and can contribute to mutagenesis. In contrast, error-free bypass incorporates template switching, which involves

strand invasion and Holliday junction resolution in a manner that is analogous to homologous recombination.

1.2.2. DNA repair pathways as targets for cancer therapy

Due to the importance of the DDR pathways in maintaining genomic integrity, mutations in DDR genes are linked to genetic disorders and cancer. For example, mutations in the *Ataxia telangiectasia mutated* (*ATM*) gene, which encodes for a critical Ser/Thr kinase that is central for DNA DSB repair, causes the cancer predisposing Ataxia telangiectasia (A-T) disease (Canman & Lim, 1998; Lavin et al, 2005). Mutations in the *BRCA1* and *BRCA2* genes are also linked to inherited breast and ovarian cancers (Futreal et al, 1994; Wooster et al, 1994).

Since most cancer cells proliferate more rapidly than normal cells and are DDR-impaired to some extent, DNA repair mechanisms are intriguing targets for chemotherapy agents. DDR inhibitors may work in multiple ways: DDR inhibitors can be used in combination therapy with DNA-damaging agents (both radiotherapy and chemotherapies) to enhance efficacy; DDR inhibitors can be used as monotherapy against cancers that are defective in DRR, which is the basis for the emerging concept of synthetic lethality (Helleday et al, 2008).

Two genes are said to be "synthetic lethal" if mutation in either gene is compatible with survival but defects in both genes are incompatible and causes death. This can also translate to DDR, where two genes that govern separate repair pathways contribute to cell survival. As described in Figure 1-3A, a cancer cell lacking pathway "B" is synthetic lethal when a DDR inhibitor of pathway "A" is introduced. However, since a normal cell has both pathways intact, it can still survive even if pathway "A" is inhibited. One of the most promising examples is in treatment of BRCA-deficient cells and tumours with inhibitors of PARP, a DNA SSB repair protein (Ashworth, 2008; Bryant et al, 2005; Farmer et al, 2005; Fong et al, 2009). The specificity for BRCA-deficient cancer cells is due to inability to repair DNA DSBs that are indirectly generated by PARP inhibition (Fig 1-3B).

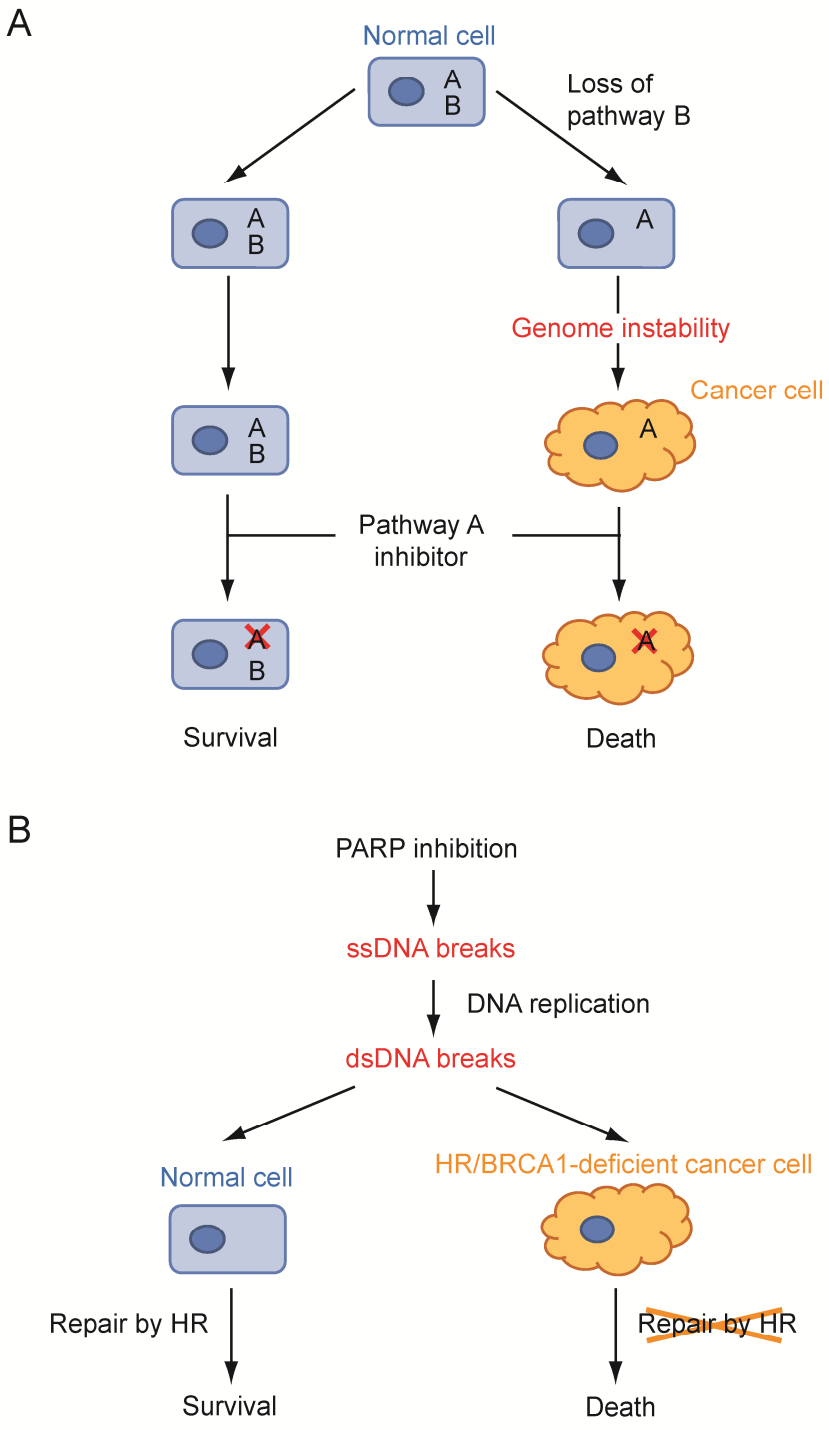

Figure 1-3. Exploiting DDR pathways using synthetic lethality. (A) Losing pathways A and B in cancer cells causes death, whereas retaining a single pathway in normal cells retains survival. (B) Example of PARP inhibitors in treatment of BRCA1-deficient cancer cells. Adapted from Jackson et al. (Jackson & Bartek, 2009).

Because DNA SSBs are converted to DSBs during DNA replication, normal cells have the ability to repair DSBs through HR, while HR-defective BRCA-deficient cancer cells are no longer capable of repairing DNA DSBs and subsequently die.

1.3 DNA replication stress and checkpoint control

1.3.1. DNA replication stress and DNA replication checkpoint

DNA replication is perhaps the most critical task for cells, as absolute fidelity must be maintained so that genomic defects are not passed onto the daughter cells. Failure to complete chromosome duplication can lead to mitotic catastrophe, chromosomal rearrangements and cell death (Canman, 2001; Morrison & Rieder, 2004).

A variety of sources, both endogenous and exogenous, pose threats to the replication machinery during fork progression. Replication forks can stall at endogenous genomic sites that contain secondary structures or protein barriers. These include repetitive sequences, converging transcriptional machinery associated with highly transcribed regions (such as rDNA and tRNA genes) and fragile sites (Branzei & Foiani, 2005; Hyrien, 2000; Lambert & Carr, 2005; Paulsen & Cimprich, 2007; Rothstein et al, 2000). Endogenous and exogenous events that generate DNA lesions also present an obstacle for fork progression. For example, an inter-strand crosslink blocks unwinding from the helicase and therefore prevents the whole replication fork from advancing. In most cases, the replisome remains on the fork in a favourable conformation that can resume replication once the barrier is removed or the lesion is repaired. The fork may also choose to bypass the lesion, which is subsequently repaired in an error or error-free way via post-replication repair mechanisms (ie. translesion synthesis or template switching). In other scenarios, the replisome can dissociate from the fork and result in fork collapse.

A common threat to both replication fork stall and collapse is the generation of ssDNA tracts (Fig. 1-4). Depending on the location of the lesion or barrier, ssDNA can form on either the leading or lagging strand, or both strands. Fork collapse commonly generates longer tracts of ssDNA, thus being more severe in comparison to stalled forks. Exposed ssDNA is prone to fork reversal and structural rearrangements that are often targets for nucleases. DNA SSB-induced DSBs generate unique one-ended DSBs (Fig. 1-4), which require a sub-pathway of HR, break-induced replication (BIR), for repair (Llorente et al, 2008).

It is therefore imperative that mechanisms are in place to stabilize stalled or collapsed replication forks. The DNA replication checkpoint is triggered in response to replication stress to coordinate the cellular events necessary to ensure that DNA is repaired and faithfully replicated before cell cycle progression (Nyberg et al, 2002; Osborn et al, 2002). At the apex of the DNA replication checkpoint is Ataxia telangiectasia and Rad3 related (ATR), a Ser/Thr kinase that phosphorylates and regulates the activity of an array of proteins, such as Checkpoint kinase 1 (CHK1), at the replication fork (Cimprich & Cortez, 2008). ATR is a member of the phosphoinositide 3-kinase-related protein kinases (PIKKs) and shares many biochemical and functional similarities to another PIKK, ATM. Together, ATM and ATR are regarded as master regulators of DDR, amassing more than 900 putative phosphorylation sites in over 700 substrate proteins (Matsuoka et al, 2007). Although there is significant crosstalk between ATM and ATR, ATM generally responds to DNA DSBs whereas ATR responds to replication stress (Cimprich & Cortez, 2008; Shiloh, 2003).

1.3.2. Sensing replication stress: ATR activation pathway

The ability of ATR to function relies on the coordinated assembly of a macromolecular complex at the stalled replication fork (Burrows & Elledge, 2008; Ciccia & Elledge, 2010; Cimprich & Cortez, 2008). Following uncoupling of the fork in response to replication stress, the exposed ssDNA regions are

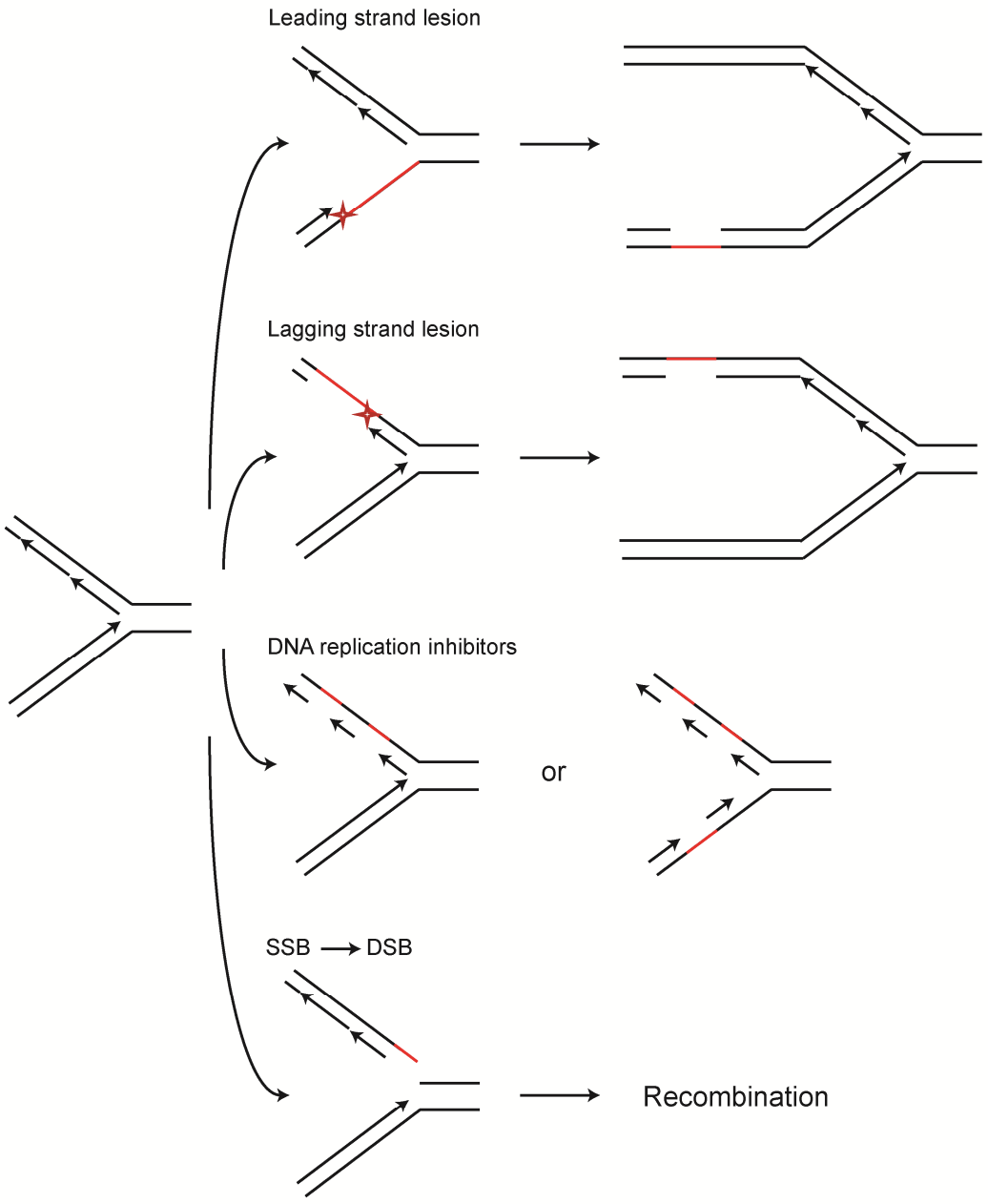

Figure 1-4. Generation of ssDNA regions from DNA replication stress. DNA lesions (red star) on the leading and lagging strand stall DNA polymerases and ensuing ssDNA (red line) can be left behind the progressing replication fork. Inhibitors of DNA polymerases (eg. Aphidicolin) increases regions of ssDNA and short DNA primers. SSBs often create one-ended DSBs that carry ssDNA overhangs. Adapted from Flynn et al. (Flynn & Zou, 2011).

quickly coated by the ssDNA-binding heterotrimeric protein replication protein A (RPA), which acts as the DNA replication stress sensor (Fig. 1-5). RPA then binds to ATRIP of the ATR-ATRIP complex to recruit ATR to stalled forks (Zou & Elledge, 2003). This interaction is mediated by the N-terminal RPA binding domain of ATRIP and the N-terminal oligosaccharide/oligonucleotide binding (OB)-fold domain of the RPA70 large subunit (Ball et al, 2007; Ball et al, 2005). RPA also recruits the Rad17-RFC clamp loader complex and Rad9-Hus1-Rad1 (9-1-1) DNA clamp to facilitate the Rad17-RFC dependent loading of 9-1-1 to ssDNA-dsDNA junctions (Ellison & Stillman, 2003; Majka et al, 2006; Zou et al, 2003). The proximal colocalization of these two complexes allows the ATR activating protein, Topoisomerase IIβ binding protein 1 (TopBP1), to stimulate ATR activity by interactions with Rad9 and regions in both ATR and ATRIP (Delacroix et al, 2007; Kumagai et al, 2006; Lee et al, 2007; Mordes et al, 2008). Activated ATR then phosphorylates an assortment of replication fork proteins to coordinate downstream processes such as cell cycle arrest, replication fork stability, DNA repair, transcription control, apoptosis and senescence (Ciccia & Elledge, 2010; Cimprich & Cortez, 2008). One of the hallmark ATR substrates is CHK1, which phosphorylates the phosphatase Cdc25 to control cell cycle progression. Activation of CHK1 requires the cumulative effort of other protein factors, such as the CHK1 regulator, Claspin, and the Timeless (TIM)-TIM interacting protein (TIPIN) complex to recruit CHK1 into proximity of ATR phosphorylation (Kemp et al, 2010; Kumagai et al, 2004).

1.4 BRCT domain: a versatile signalling module in structure and function

1.4.1. Phospho-peptide binding modules in DNA damage response

The elaborate signalling network in the DNA damage response relies heavily on protein phosphorylation by Ser/Thr kinases for regulation. There are two major classes of DDR kinases: PIKKs (ATM, ATR, DNA-PK) (Bakkenist & Kastan, 2004; Shiloh, 2003) and checkpoint effector kinases (CHK1, CHK2 and

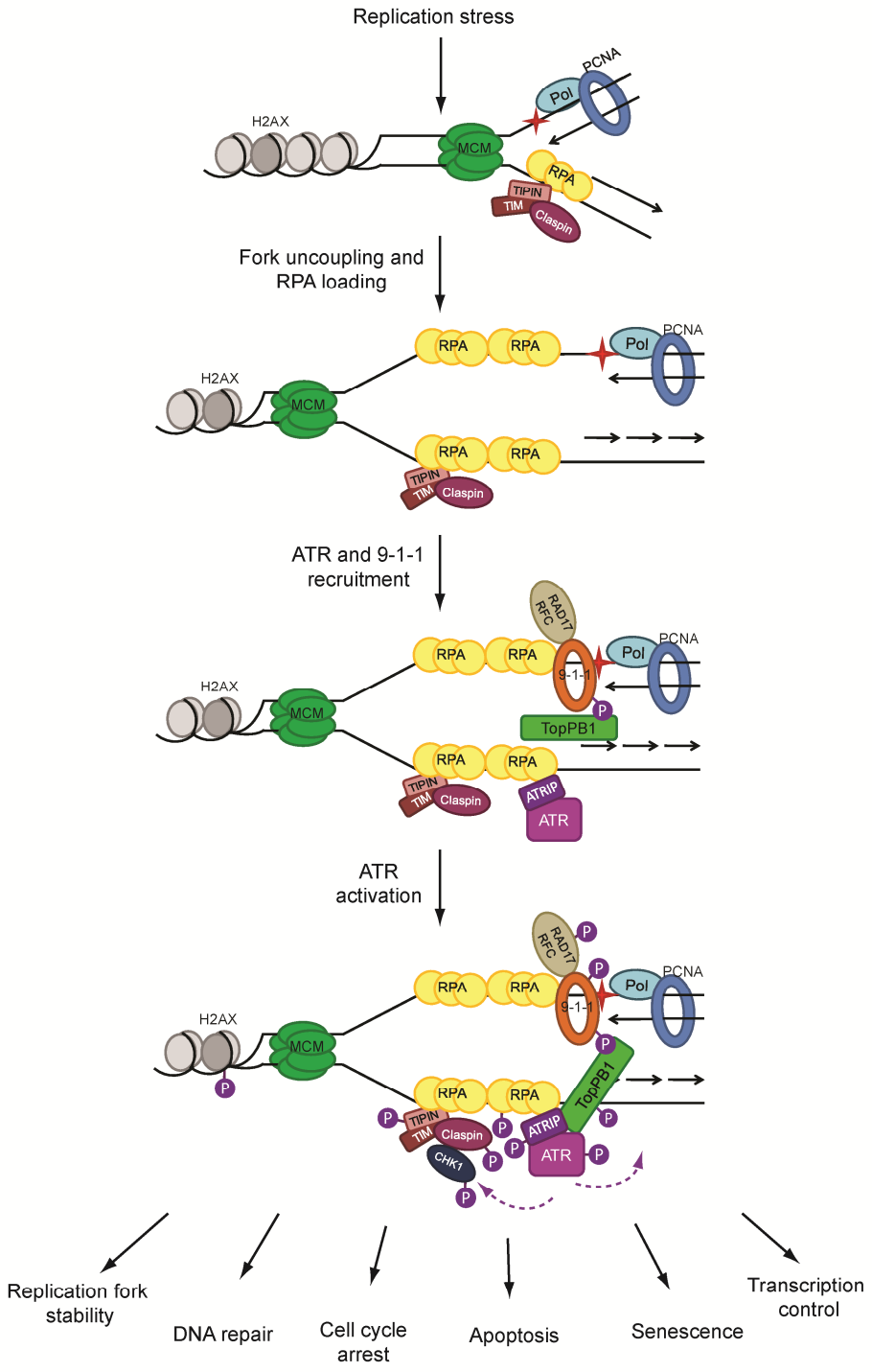

Figure 1-5. ATR activation pathway at stalled replication forks. ATR activation requires the organization of RPA, RAD17-RFC complexes, 9-1-1 complex, ATR-ATRIP heterodimer and TopBP1 to stalled replication forks. Once ATR is activated, it can phosphorylate (purple circles) replication fork proteins to control various cellular functions. Adapted from Ciccia et al. (Ciccia & Elledge, 2010).

MK2) (Reinhardt & Yaffe, 2009). Phosphorylated proteins are recognized by specialized 14-3-3, forkhead associated (FHA) and BRCA1 C-terminal (BRCT) domains present in downstream DDR proteins. Interestingly, these phospho-peptide binding modules commonly match the conserved phospho-peptide motifs targeted by their cognate kinases. 14-3-3 domains preferentially bind the targets of checkpoint kinases, while the BRCT and FHA domains can bind to the phosphorylated targets of ATM/ATR (Fig. 1-6) (Mohammad & Yaffe, 2009). While the kinases involved show little or no substrate specificity for serine or threonine residues, the binding modules can discriminate between their phospho-threonine (pThr) or phospho-serine (pSer) targets. 14-3-3 domains do not discriminate between pThr or pSer, FHA domains show profound specificity for pThr-peptides, and certain BRCT domains show preference for pSer-peptides.

The structural basis for 14-3-3 and FHA domain phospho-peptide recognition has been established through a number of crystal structures in complex with phospho-peptides. The α-helical 14-3-3 domain packs as a dimer via interactions with three N-terminal helices (α_1, α_2 and α_4) of each protomer (Fig. 1-7A). Basic residues from α_3 and α_5 helices of each protomer form a small positively charged pocket to recognize the pSer/pThr of the phospho-peptide (Yaffe & Smerdon, 2001). In 14-3-3ζ, side chains of Lys49 and Arg56 from α_3-helix and Arg127 and Tyr128 from α_5-helix protrude outwards to coordinate the phosphate group (Fig. 1-7B) (Yaffe et al, 1997). Other interactions mediated by residues in α_5, α_7 and α_9 helices hydrogen bond with the phospho-peptide main chain to ensure an extended conformation. 14-3-3 domains are more promiscuous for their peptide targets, and can in fact utilize the same basic phosphate-binding pocket to bind to both phosphorylated (pSer and pThr) and non-phosphorylated ligands. In particular, Tyr128 makes a conserved hydrogen bond with the side chain of pSer (14-3-3ζ in complex with histone H3 phospho-acetylated peptide (Macdonald et al, 2005)), pThr (14-3-3ζ in complex with serotonin *N*-acetyltransferase (Obsil et al, 2001)) and Asp (14-3-3β in complex

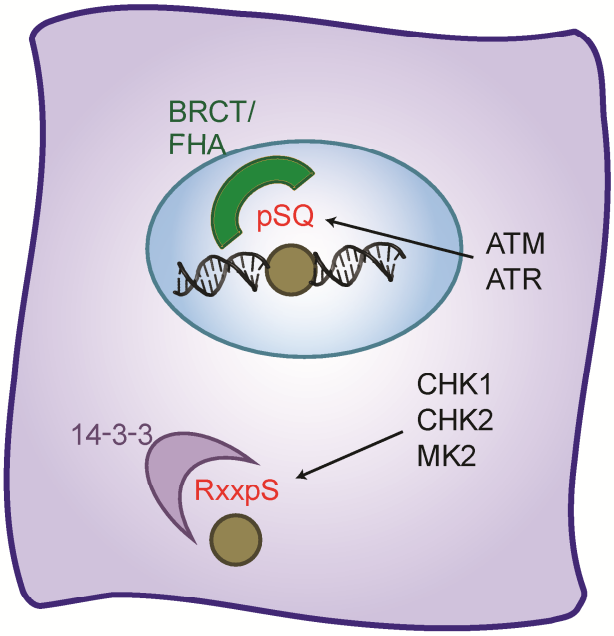

Figure 1-6. Kinase-specific phospho-peptide binding modules in DDR. BRCT and FHA domains preferentially bind to ATM/ATR phosphorylated motifs, which allow for protein complexes to form at DNA damaged sites. 14-3-3 domains recognize motifs phosphorylated by CHK1, CHK2 and MK2 effector kinases to regulate the cell cycle. Adapted from Mohammad et al. (Mohammad & Yaffe, 2009).

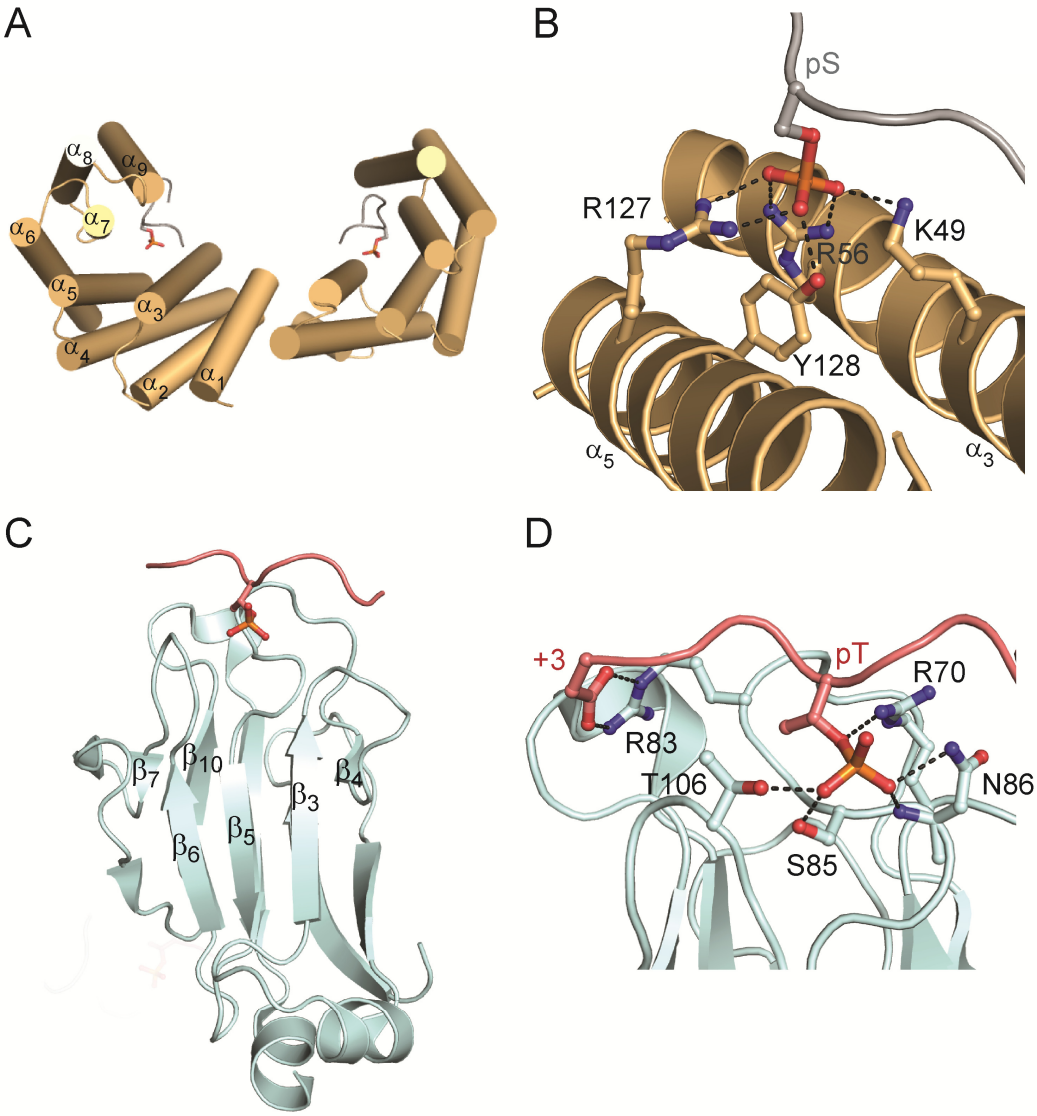

Figure 1-7. Structural basis for phospho-peptide recognition by 14-3-3 and FHA domains. (A) Crystal structure of 14-3-3ζ in complex with an optimized phospho-peptide (PDB ID: 1QJA). The pSer of the peptide (grey) is shown as sticks and α-helices of the 14-3-3 domain are labelled. (B) The pSer is coordinated by residues (shown as sticks and labelled) of α_3 and α_5 helices. Hydrogen bonds and electrostatic interactions are represented as dotted lines. (C) Crystal structure of *S. cerevisiae* RAD53 FHA domain in complex with an optimized phospho-peptide (PDB ID: 1G6G). The pThr of the peptide (pink) is shown as sticks and β-strands of the FHA domain are labelled. (D) Recognition of the pThr and +3 residues by loop residues of the FHA domain.

with Exoenzyme S peptide (Ottmann et al, 2007)). FHA domains consist of two β-sheets folded into a β-sandwich. A series of loops connecting the β-strands form a binding surface for the phospho-peptide (Fig. 1-7C). Besides tailoring specificity for a pThr, FHA domains commonly select for the +3 residue with respect to the pThr, which can be an aspartate, branched aliphatic residue, or hydrophobic or uncharged polar residue (Liang & Van Doren, 2008). Another class of FHA domains, such as in polynucleotide kinase/phosphatase (PNKP), choose to recognize the -3, -2 and +1 residues instead. In FHA domains, the pThr is coordinated by highly conserved residues from the β_3-β_4 and β_4-β_5 loops. For example in *S. cerevisiae* Rad53, Arg70 (β_3-β_4 loop) and Ser85 (β_4-β_5 loop) make direct hydrogen bonds with the phosphate oxygen atoms (Fig. 1-7D). Other variant residues (Asn86 and Thr106) also contribute to pThr interactions. A small hydrophobic cavity forms extensive van der Waals interactions with the γ-methyl of pThr to favour pThr over pSer (Pennell et al, 2010). Depending on the characteristics of the +3 residue side chain, residues from the β_4-β_5, β_6-β_7 or β_{10}-β_{11} loops of the FHA domains can be involved. In the Rad53 FHA domain for example, Arg83 in the β_4-β5 loop is positioned to form a salt bridge with the +3 Asp of the phospho-peptide (Fig. 1-7D). There also exists a smaller class of FHA domains that binds di-phospho-peptides that have a pSer/pThr at the -3 or -4 positions. The solution structures of Dun1 and Ki67 FHA domains in complex with their respective di-phospho-peptides show that the second pSer or pThr is stabilized by Arg residues of a single loop near the N-terminus, which could account for the lack of discrimination for pThr or pSer (Byeon et al, 2005; Lee et al, 2008).

1.4.2. BRCT domains: past and present

The BRCT domain was originally identified in the tumour suppressor protein, Breast cancer associated 1 (BRCA1). Truncation and missense mutations in this region correlate with an increased risk for breast and ovarian cancers,

underscoring its importance in the tumour suppressor function of BRCA1 (Futreal et al, 1994; Miki et al, 1994). Subsequent bioinformatics analysis revealed that BRCT domains exist in a myriad of proteins, most of which have roles in DNA metabolism and repair (Bork et al, 1997; Callebaut & Mornon, 1997). The conserved phospho-peptide binding function was later identified in BRCA1 and other tandem BRCT domains, as well as various single BRCT domains (Manke et al, 2003; Yu et al, 2003). For example, the tandem BRCT domain pair in BRCA1 recognizes the phosphorylated peptide motif pSer-Pro-Thr-Phe in various protein partners such as BRCA1-associated C-terminal helicase/Fanconi anemia group J protein (BACH1/FANCJ), CtIP and Abraxas/Coiled-coil domain-containing protein 98 (CCDC98), and the ability of BRCA1 to recognize different binding partners in DDR signalling regulates BRCA1 recruitment and function (Kim et al, 2007; Liu et al, 2007; Manke et al, 2003; Wang et al, 2007; Yu & Chen, 2004; Yu et al, 2003).

It is now evident that BRCT domains possess an array of activities other than phosphorylated protein interactions. Besides the conserved phospho-peptide recognition exhibited by tandem BRCT domains, BRCT domains have also been implicated in phosphorylation-independent protein interactions, DNA binding and poly(ADP-ribose) (PAR) binding. This diversity can be credited not only to variations in sequence and structure within a single BRCT domain, but also to the unique ability of BRCT domains to assemble as multi-domain complexes with other BRCT domains or even other functional domains, adding another level of complexity, specificity and regulation.

1.4.3. BRCT domain structure and assembly

The BRCT domain fold was first revealed in the crystal structure of the X-ray repair cross-complementing protein 1 (XRCC1) N-terminal BRCT domain (Zhang et al, 1998) and comprises of a central four-stranded β-sheet flanked by a single α-helix (α_2) on one side and 2 α-helices (α_1 and α_3) on the opposite side

(Fig. 1-8A). Comparison of various BRCT domain structures illustrate that deviations in structure and sequence are mainly localized to the connecting loops, whereas conserved residues are situated in the hydrophobic core and in residues involved in recognizing the phosphorylated amino acid in phospho-peptide targets (Glover et al, 2004; Rodriguez & Songyang, 2008).

Interestingly, the domain architecture of BRCT domains is remarkably diverse. BRCT domains range from isolated individual domains to multiple tandem BRCT repeats, or even as fusions with other functional domains (Table 1-2). Single BRCT domains represent a large class of BRCT domains that exist as single copies in proteins such as Poly(ADP-ribose) polymerase 1 (PARP-1) and DNA Ligase III (Lig3). They can also be found in multiple but isolated copies, such as in XRCC1, where two distinct single BRCT domains are separated by 135 amino acids in sequence. In tandem BRCT repeats, multiple BRCT domains are separated by a variable linker region. The initial crystal structure of the tandem BRCT domains in BRCA1 shed light on the canonical BRCT-BRCT domain packing, which occurs through a hydrophobic interface consisting of the α_2 helix of the N-terminal BRCT and α_1' and α_3' helices of the C-terminal BRCT (Fig. 1-8B) (Williams et al, 2001). Mutations at this hydrophobic interface in BRCA1 (M1775R and A1708E) are linked to breast and ovarian cancer, highlighting the requirement for an intact tandem BRCT interface for normal function (Futreal et al, 1994; Miki et al, 1994). This conserved BRCT-BRCT domain packing has since been observed in numerous BRCT repeat structures such as in Mediator of DNA damage checkpoint protein 1 (MDC1), BRCA1-associated RING domain protein 1 (BARD1), *S. pombe* Crb2 and *S. pombe* Brc1, and their functional role in phospho-peptide binding is well established (Birrane et al, 2007; Edwards et al, 2008; Kilkenny et al, 2008; Lee et al, 2005; Stucki et al, 2005; Williams et al, 2010). However, variations in tandem BRCT domain structure also exist. For example, the tandem BRCT domains of DNA Ligase IV (LigIV) do not pack together and are separated by a significantly longer inter-BRCT linker, which ultimately ensures its

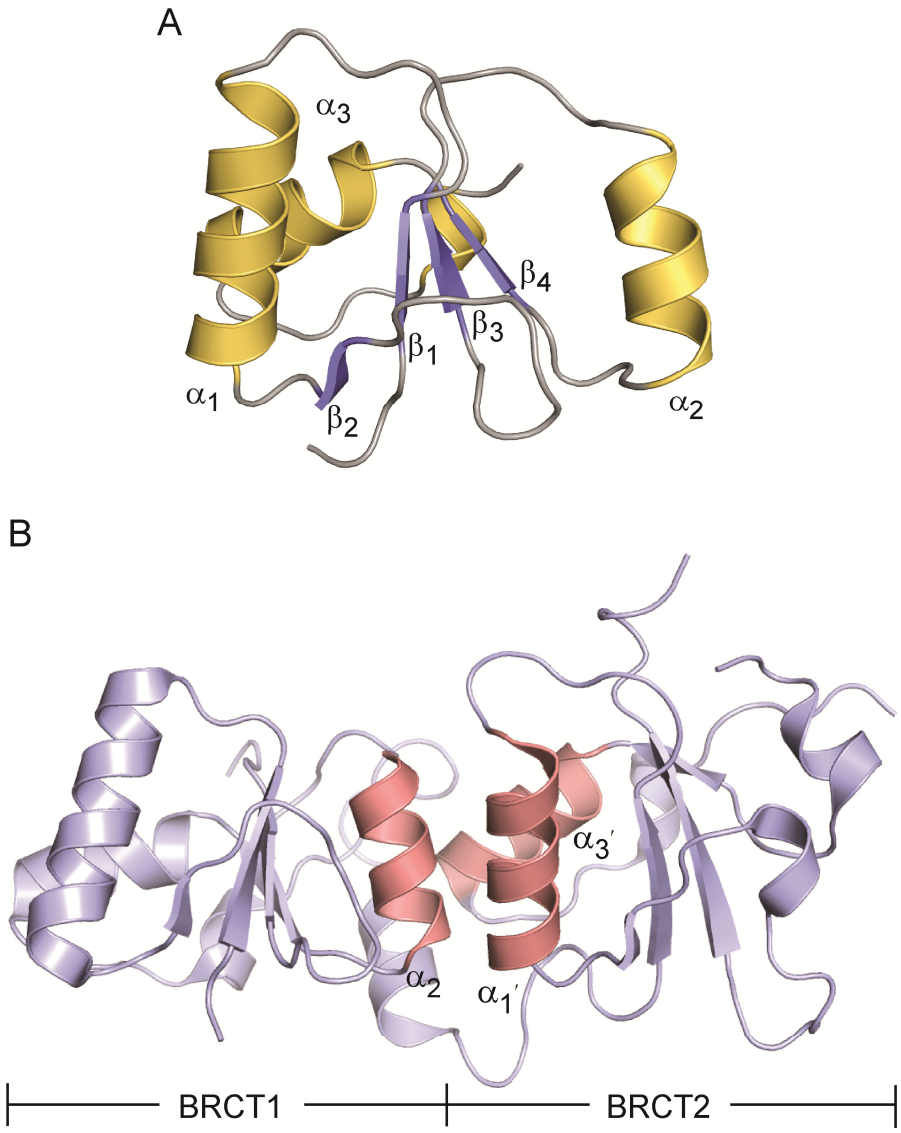

Figure 1-8. Structures of single and tandem BRCT domains. (A) Crystal structure of the N-terminal BRCT domain of XRCC1 (PDB ID: 1CDZ). β-strands (blue) and α-helices (yellow) are coloured and labelled. (B) Crystal structure of the BRCA1 tandem BRCT domains (PDB ID: 1JNX). Helices involved in the BRCT-BRCT domain interface are coloured red and labelled.

Table 1-2. BRCT domain architecture found in proteins.

Homo-Domain Assembly

Domain Architecture	**Examples**	**PDB ID***
BRCT	XRCC1, Lig3, PARP-1, TDT, ECT2, DNA Pol μ, REV1, RFC, PES1, DNA Pol λ, MCPH1, FCP1, TopBP1	1CDZ, 1IN1, 2COK, 2COE, 2COU[1], 2HTF, 2EBW, 2EBU, 2EP8, 2JW5, 2WT8, 3EF0[2], 3JVE
BRCT-BRCT	BRCA1, 53BP1, MDC1, BARD1, *S. pombe* Crb2, LigIV, *S. pombe* Brc1, TopBP1	1JNX, 1KZY, 2ADO, 2NTE, 2VXB, 3II6, 3L40, 3AL2
BRCT-BRCT-BRCT	TopBP1	2XNK

Hetero-Domain Assembly

Domain Architecture	**Examples**	**PDB ID**
FN3-BRCT	*S. cerevisiae* Chs5p	Not available
FHA-BRCT-BRCT	NBS1	3I0N/3HUE[2]

* Unless otherwise specified, listed structures are of the human proteins

[1] Structure of the mouse homolog

[2] Structure of the *S. pombe* homolog

unique mode of recognition for X-ray repair cross-complementing protein 4 (XRCC4) (Dore et al, 2006; Sibanda et al, 2001; Wu et al, 2009). A triple BRCT domain module also exists in TopBP1 BRCT0/1/2, suggesting even higher order tandem BRCT domain architecture. Interestingly, the packing of BRCT0/BRCT1 and BRCT1/BRCT2 at the interface are significantly different from canonical tandem BRCT domains (Huo et al, 2010; Rappas et al, 2011). This unconventional BRCT domain interface is likely a consequence of the shorter inter-BRCT linker regions, suggesting a role for the inter-BRCT linker in driving the packing of tandem BRCT domains. Whereas longer linker lengths ranging from 30-60 amino acids permit the parallel juxtaposition characteristic of canonical tandem BRCT domain packing, shorter linkers restrict the packing of adjacent BRCT repeats such that they interact in a twisted orientation.

The diversity in BRCT domain architecture extends to other functional domains, although the significance of these hetero-domain modules is still unclear. A single BRCT domain is packed alongside an N-terminal fibronectin type III (FN3) domain in *S. cerevisiae* Chs5p, a component of the exomer coat complex. Studies in yeast suggest that both the FN3 and BRCT domain act as a single module and are both required for localization and cargo delivery function (Martín-García et al, 2010). The tandem BRCT repeats in the DNA DSB repair protein Nijmegen breakage syndrome protein 1 (NBS1) are coupled to an N-terminal FHA domain, another phospho-peptide binding domain (Lloyd et al, 2009; Williams et al, 2009). This unique FHA-BRCT-BRCT domain setup may present an intriguing platform for cross-talk between the two adjacent functional phospho-peptide interacting modules.

1.4.4. Phosphorylation-dependent interactions

The initial discovery of phospho-peptide binding by BRCT domains included both single BRCT and tandem BRCT domains. Evidence for single BRCT domain phospho-peptide interactions have mainly been restricted to *in vitro*

phospho-peptide binding studies (Yu et al, 2003), and a clear molecular basis for binding specificity is still lacking. Furthermore, there is conflicting data supporting existing single BRCT phospho-peptide interactions, such as in the proposed interaction between hFCP1 BRCT and phosphorylated RNA polymerase II. Although Yu et al. demonstrated a direct phosphorylation-dependent interaction between a RNA polymerase II peptide and hFCP1 BRCT *in vitro* (Yu et al, 2003), structural and biochemical data from Ghosh et al. have shown that the BRCT phosphate-binding pocket is dispensable for FCP1 function (Ghosh et al, 2008). Clearly, more structural characterization is required to elucidate the mechanism of single BRCT domain phospho-peptide interactions.

In contrast to single BRCT domains, a combination of biochemical and structural studies of a number of BRCT repeat proteins with their cognate phosphorylated protein targets have established a conserved mode of phospho-peptide binding by BRCT repeats. Crystal structures of the BRCA1, MDC1, *S. pombe* Brc1 and *S. pombe* Crb2 repeats bound to their respective phospho-peptides reveal a conserved bipartite recognition involving two distinct pockets: a pSer binding pocket in the N-terminal BRCT and a secondary specificity pocket at the BRCT-BRCT interface that generally provides selectivity for a hydrophobic residue at the +3 position in the phospho-peptide with respect to the pSer (Fig. 1-9A) (Clapperton et al, 2004; Glover et al, 2004; Kilkenny et al, 2008; Shen & Tong, 2008; Shiozaki et al, 2004; Stucki et al, 2005; Varma et al, 2005; Williams et al, 2010; Williams et al, 2004). In the conserved phosphate-binding pockets of BRCA1 and MDC1, the phosphate moiety interacts with two side chains (S1655/T1898, K1702/K1936 in BRCA1/MDC1, respectively) and a main chain NH (G1656/G1899 in BRCA1/MDC1) (Fig. 1-9B). The minimal phospho-peptide sequence bound by BRCT repeats consists of four residues (pS/pT-X-X-X), in which the +3 residue dictates the majority of the binding specificity (Campbell et al, 2010). The +3 residue sits in a cleft situated at the hydrophobic interface between the two BRCT domains, and conserved residues at the BRCT-BRCT

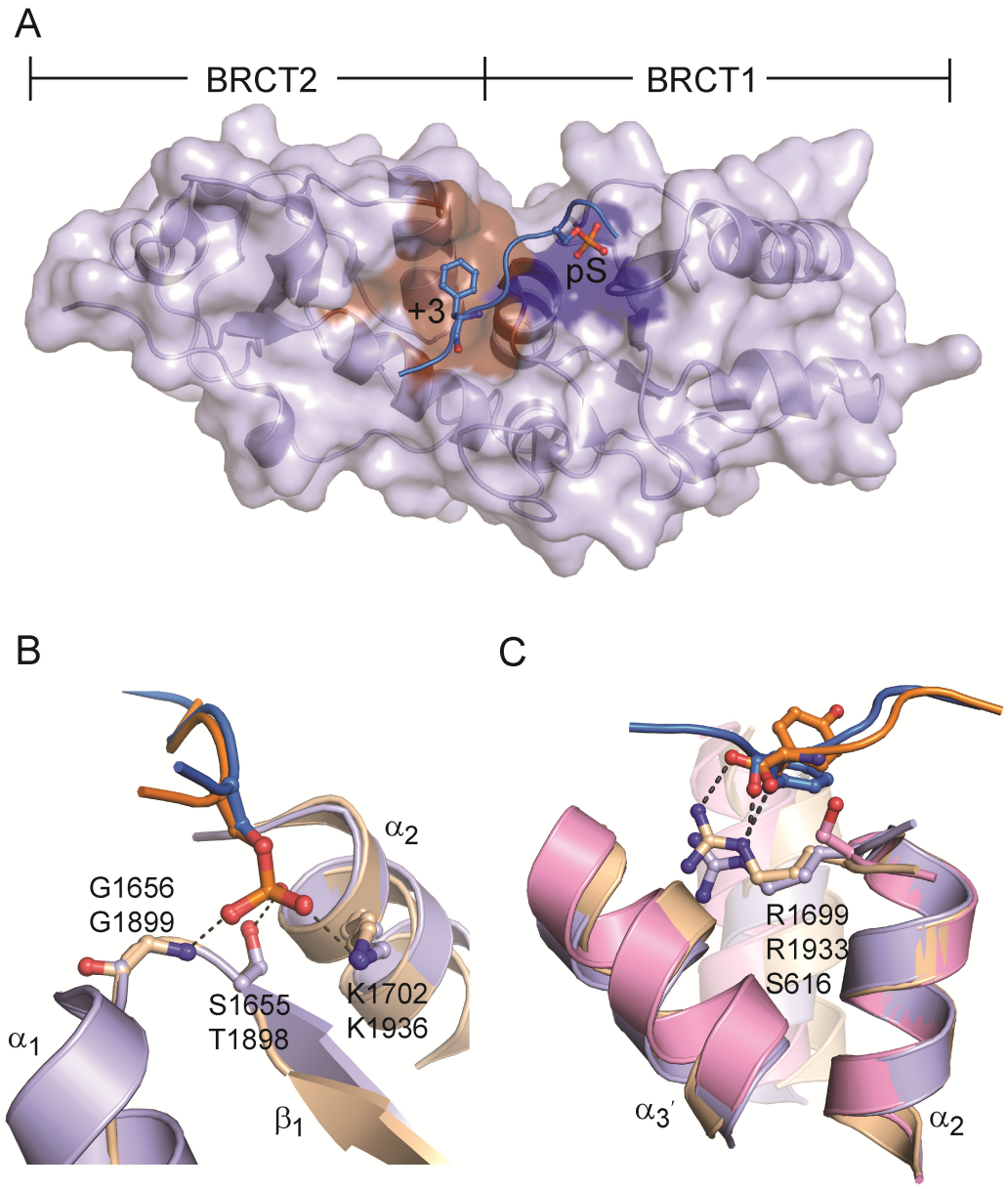

Figure 1-9. Molecular basis of phospho-peptide binding by tandem BRCT domains. (A) Conserved phospho-peptide recognition of BRCA1 BRCT1/2 (PDB ID: 1T15) consists of a phosphate-binding pocket (blue) and +3 binding pocket (brown). The surface representation of BRCA1 BRCT1/2 is shown and the BACH1 peptide pS and +3 side chains are represented as sticks and labelled. (B) pSer coordination by BRCA1 (blue) and MDC1 (beige, PDB ID: 2AZM). Phosphate contact residues for BRCA1/MDC1 (top/bottom) are labelled and equivalent hydrogen bonding and electrostatic interactions are indicated by black dotted lines. (C) +3 phospho-peptide main chain recognition at the BRCT-BRCT interface for BRCA1 (blue), MDC1 (beige) and BARD1 (pink, BARD1 PDB ID: 2NTE). The equivalent Arg residue in BRCA1/MDC1/BARD1 (top/middle/bottom) is labelled.

interface determine the binding specificity for the +3 residue. In particular, a conserved arginine residue (R1699/R1933 in BRCA1/MDC1, respectively) has a pivotal role in recognizing the peptide main chain at the +3 position (Fig. 1-9C). In BARD1, the conserved arginine is substituted for a serine residue (S616), suggesting that the phospho-peptide binding properties of BARD1 may be different (Birrane et al, 2007; Edwards et al, 2008; Rodriguez et al, 2003; Thanassoulas et al, 2010). Interestingly, both BRCA1 and MDC1 have peptide targets that are internal (BACH1/CtIP/ACCA for BRCA1, MMSET for MDC1) or terminate (Abraxas for BRCA1, γ-H2AX for MDC1) at the +3 position (Manke et al, 2003; Pei et al, 2011; Ray et al, 2006; Stewart et al, 2003; Wang et al, 2007; Yu & Chen, 2004; Yu et al, 2003). Peptide binding studies have shown that the presence of a C-terminal carboxylate increases binding affinity to BRCA1 and MDC1, although the differences between the carboxy and amidated phospho-peptides are more profound for MDC1 (Campbell et al, 2010; Lee et al, 2005; Stucki et al, 2005). Comparison of the peptide-bound structures suggests that positioning of the +3 side chain determines the angle of incidence of the C-terminal carboxylate, which is more favourable in MDC1, and thereby tunes the degree of preference for the carboxylate (Campbell et al, 2010).

In another layer of complexity, tandem BRCT domain phospho-peptide binding may also be further regulated by interactions with neighbouring domains, such as in the NBS1 FHA-BRCT-BRCT hetero-domain module. Structural studies of *S. pombe* NBS1 with a Ctp1 phospho-peptide show a structural rearrangement in the tandem BRCT domain interface (Williams et al, 2009) that is triggered by an arginine switch located at the FHA-BRCT1 domain interface and activated upon FHA domain binding to the phospho-peptide. Since both the NBS1 FHA domain and BRCT repeat are capable of binding to similar phospho-peptide motifs in MDC1, (Chapman & Jackson, 2008; Hari et al, 2010; Lloyd et al, 2009; Melander et al, 2008; Spycher et al, 2008) interaction from the FHA

domain may regulate the phospho-peptide binding ability of the adjacent BRCT repeat by initiating a tandem BRCT domain structural rearrangement.

The structure of the N-terminal region of TopBP1 shows an unexpected packing of BRCT1/2 with another BRCT domain at the N-terminus, forming a triple BRCT repeat module. This region interacts with Rad9, a component of the trimeric Rad9-Hus1-Rad1 (9-1-1) clamp, which is a prerequisite for stimulating ATR activity and subsequent DNA replication checkpoint activation (Delacroix et al, 2007; Lee et al, 2007). Interestingly, both BRCT1 and BRCT2 contain putative phosphate-binding pockets, but peptide binding data suggests that only the BRCT1 pocket is responsible for the phosphorylation-dependent interaction with Rad9 (Huo et al, 2010; Rappas et al, 2011). Recent studies of Treslin recognition by the same TopBP1 N-terminal BRCT repeat in DNA replication suggests that the phosphate-binding pockets of BRCT1 and BRCT2 preferentially bind to separate phospho-peptide motifs (pT969 for BRCT1 and pS1001 for BRCT2) in Treslin (Boos et al, 2011). This presents an intriguing mechanism for dual phospho-peptide recognition within a single tandem BRCT repeat.

There is also the rare scenario where the putative phosphate-binding pocket exists in the C-terminal BRCT rather than the N-terminal BRCT domain of a BRCT repeat, such as in TopBP1 BRCT4/5 and PTIP BRCT1/2. TopBP1 BRCT5 is required for TopBP1 localization DNA damage sites (Yamane et al, 2002), although the mechanism is unknown. In addition, TopBP1 BRCT4/5 has been shown to bind 53BP1, an interaction that is important for 53BP1-mediated checkpoint control in response to DSBs during G1 (Cescutti et al, 2010). It is likely that the phosphate-binding pocket in BRCT5 for TopBP1 function is critical for these interactions. However, the absence of a downstream +3 hydrophobic pocket implies a smaller peptide binding surface and potentially a weaker interaction compared to canonical tandem BRCT domain interactions.

1.4.5. Phosphorylation-independent protein interactions

Both single BRCT and tandem BRCT domains have also been implicated in protein-protein interactions in regions that are distinct from the putative phosphate-binding pockets. Perhaps the best examples for single BRCT domain interactions involve heterodimeric complexes between the two single BRCT domains in XRCC1 binding with other single BRCT domains. The interaction between the C-terminal BRCT (BRCT2) of XRCC1 and Lig3 BRCT domain is well established in short-patch base excision repair (Caldecott et al, 1994; Nash et al, 1997; Taylor et al, 1998; Thornton et al, 2001). The recent crystal structure of the XRCC1-Lig3 heterodimer provides the structural principles for a single BRCT-BRCT domain complex. The XRCC1-Lig3 interface involves extensive contacts between the α_1-helices of each BRCT, as well as an extended linker preceding the XRCC1 BRCT that further stabilizes interactions with the Lig3 BRCT domain (Fig. 1-10) (Cuneo et al, 2011). The N-terminal BRCT of XRCC1 (BRCT1) and PARP-1 BRCT also interact to regulate PARP-1 activity (Beernink et al, 2005; Masson et al, 1998). Like XRCC1 BRCT1, TopBP1 BRCT6 also interacts with the PARP-1 BRCT domain, (Wollmann et al, 2007) providing evidence for a common mode of interaction mediated by the BRCT domain of PARP-1. A putative protein-binding surface has also been suggested in the N-terminal BRCT domain of Microcephalin (MCPH1/BRIT1). The conserved phosphate-binding residues (S1655 and K1702 in BRCA1) are absent in MCPH1 (E14 and T59, respectively) and the pocket is instead replaced by a larger, more acidic surface that is conserved in MCPH1 homologs and required for its role in regulating chromosomal condensation (Jeffers et al, 2008; Richards et al, 2010).

Protein-protein interactions mediated by tandem BRCT domains are demonstrated in crystal structures involving the BRCT repeats of LigIV, *S. pombe* Crb2 and 53BP1 in complex with their respective protein binding partners. A common theme observed in each of these interactions is the presence of a

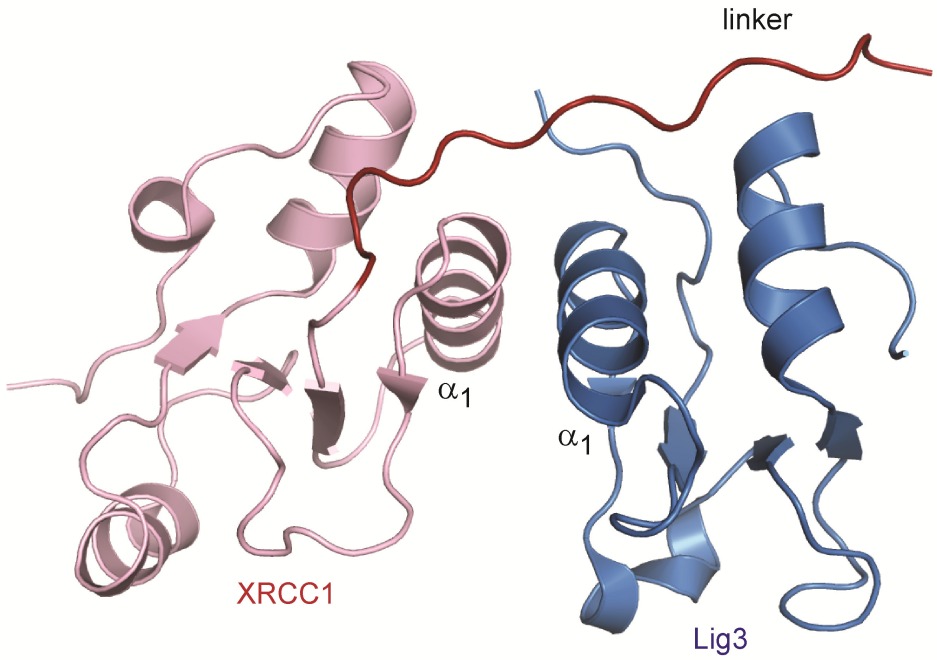

Figure 1-10. Crystal structure of XRCC1-Lig3 BRCT-BRCT heterodimer. The α_1-helix of XRCC1 (pink) and Lig3 (blue) is labelled. The N-terminal linker of XRCC1 (red) is also highlighted. PDB ID: 3PC8.

β-hairpin motif in the inter-BRCT linker, which is responsible for extensive contacts at the protein binding interface (Watts & Brissett, 2010). In the 53BP1 BRCT1/2-p53 DNA binding domain (DBD) complex crystal structure, the 53BP1 BRCT-BRCT linker adopts an extended β-hairpin loop that, together with the α_4-helix, contacts the conserved L_2 and L_3 loops of the p53 DBD (Fig. 1-11A) (Derbyshire et al, 2002; Joo et al, 2002). A distal salt bridge between the 53BP1 BRCT1 α_3-helix residue D1833 and p53 R181 also makes a minor contribution to the overall binding interface. The *S. pombe* Crb2 checkpoint function relies on the BRCT repeat-mediated homodimerization of Crb2 (Du et al, 2004; Soulier & Lowndes, 1999). At the interface of the Crb2 dimer, the extended β-hairpin loop of the Crb2 BRCT-BRCT linker from each protomer participates in an extensive symmetrical hydrogen bonding network (Fig. 1-11B) (Kilkenny et al, 2008). The LigIV-XRCC4 interaction is critical for non-homologous end joining (NHEJ) and in V(D)J recombination (Critchlow et al, 1997; Grawunder et al, 1997; Grawunder et al, 1998; Li et al, 1995). Interestingly, the tandem BRCT domains of LigIV contain an unusually long linker region, and packing of the tandem BRCT domains is not observed. In the crystal structures of the human and yeast ortholog of XRCC4 in complex with the tandem BRCT domains of LigIV (Dore et al, 2006; Sibanda et al, 2001; Wu et al, 2009), the extended LigIV linker forms a distinct helix-loop-helix (HLH) clamp structure that wraps around the linear coiled-coil tails of the XRCC4 homodimer to stabilize the interaction (Fig. 1-11C). Further contacts are made by the β-hairpin of the linker region and α_1 of LigIV BRCT2, which bind on opposite ends of the XRCC4 coiled-coil tails.

The inter-BRCT domain linker has evolved a role in facilitating protein-protein interactions in addition to its role in dictating the orientation and packing of tandem BRCT repeats. Whereas shorter linker lengths affect the overall tandem BRCT domain structure by restricting the BRCT packing orientation, as evident in the TopBP1 BRCT0/1/2 structure (Huo et al, 2010; Rappas et al, 2011),

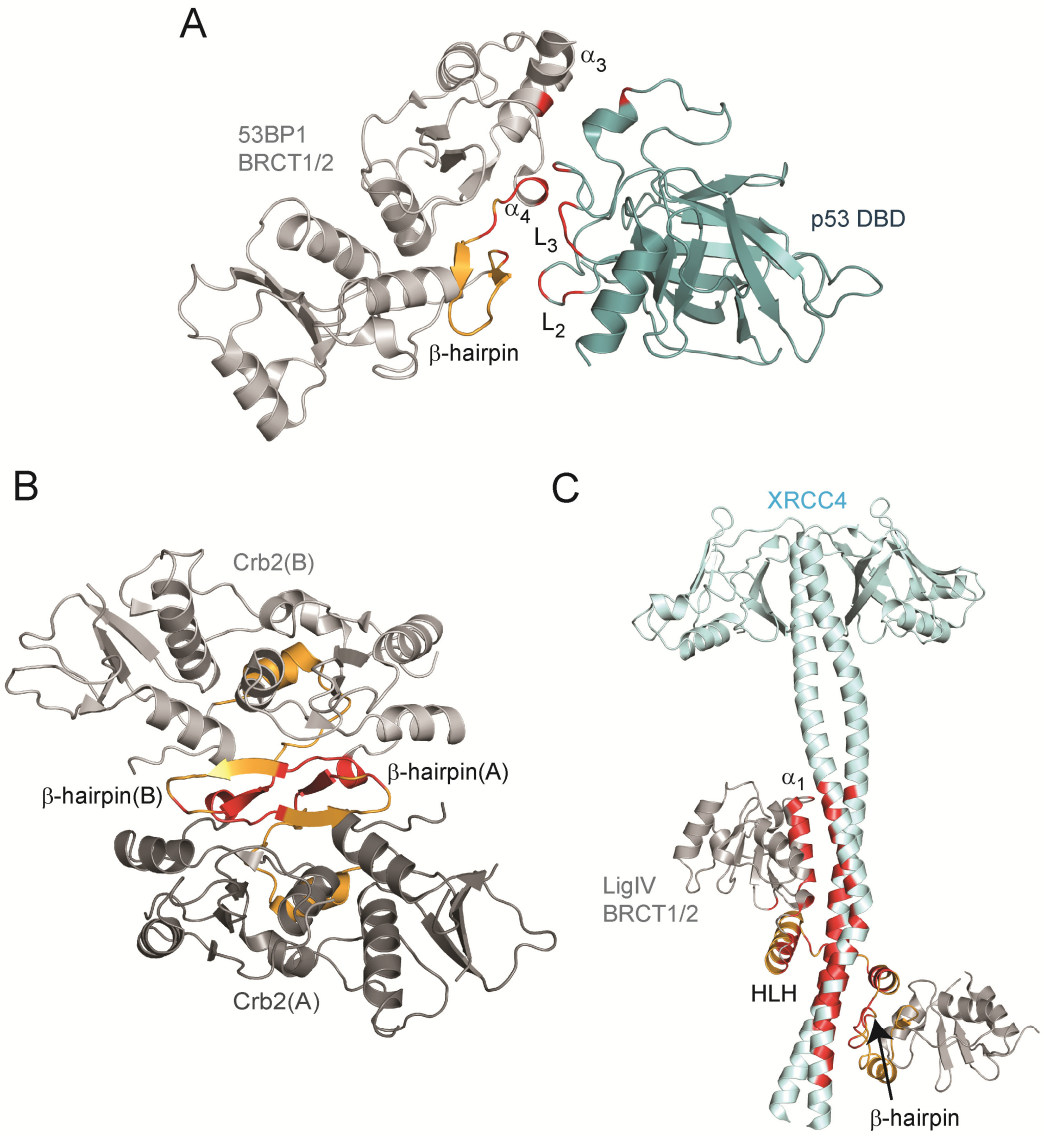

Figure 1-11. Tandem BRCT domain linker-mediated protein interactions. The inter-BRCT linker is shown in orange and contact regions are highlighted in red. Secondary structure motifs involved in interactions are labelled. (A) Structure of 53BP1 BRCT repeats (grey) in complex with p53 DBD (teal). (B) Structure of the *S. pombe* Crb2 homodimer. Each protomer is labelled (A and B). (C) LigIV (grey) in complex with XRCC4 homodimer (light cyan).

the flexibility of longer linkers to form common structure motifs, such as a β-hairpin and/or HLH, can be utilized for protein-protein interactions.

1.4.6. DNA Binding

DNA binding activity in single and tandem BRCT domains have also been demonstrated in XRCC1, TopBP1 and BRCA1 (Yamane et al, 2000; Yamane & Tsuruo, 1999), although the relevance of these interactions to the cellular function of these proteins is still unclear. However, a well characterized DNA binding function exists in the BRCT domain of Replication factor C (RFC) p140, a subunit of the five protein RFC complex (Burbelo et al, 1993; Fotedar et al, 1996; Tsurimoto & Stillman, 1991). The RFC BRCT domain selectively recognizes the 5′-phosphate DNA terminus within a 3′ overhanging DNA end (Allen et al, 1998; Kobayashi et al, 2006), and structural investigations by NMR spectroscopy shed light on the mechanism of DNA recognition. Interestingly, a α-helix N-terminal to the BRCT domain inserts into the major groove of the DNA to stabilize the interaction (Fig. 1-12A,B) (Kobayashi et al, 2010; Kobayashi et al, 2006). In a mode analogous to phospho-peptide recognition, conserved residues in the phosphate-binding pocket of RFC (T415, G416, K458, R423) coordinate the recessed 5′-phosphate (Fig. 1-12C). This mechanism of DNA binding may also be shared with bacterial NAD+-dependent DNA ligase (LigA), which also houses the conserved phosphate-binding residues and is highly similar to RFC (Bork et al, 1997). As in RFC, the BRCT domain of LigA has DNA binding activity and mutations in these conserved residues (T599, G600) markedly reduce DNA binding and ligation activity (Feng et al, 2004; Wilkinson et al, 2005). In light of this evidence, the mechanism of DNA recognition by the RFC BRCT domain may represent a conserved mode of DNA recognition for this subset of single BRCT domains. TopBP1 BRCT7/8 also displays unique specificity for damaged DNA containing bulky lesions. Using an *in vitro* partially reconstituted checkpoint system, Choi et al. showed that a C-terminal fragment of TopBP1, containing

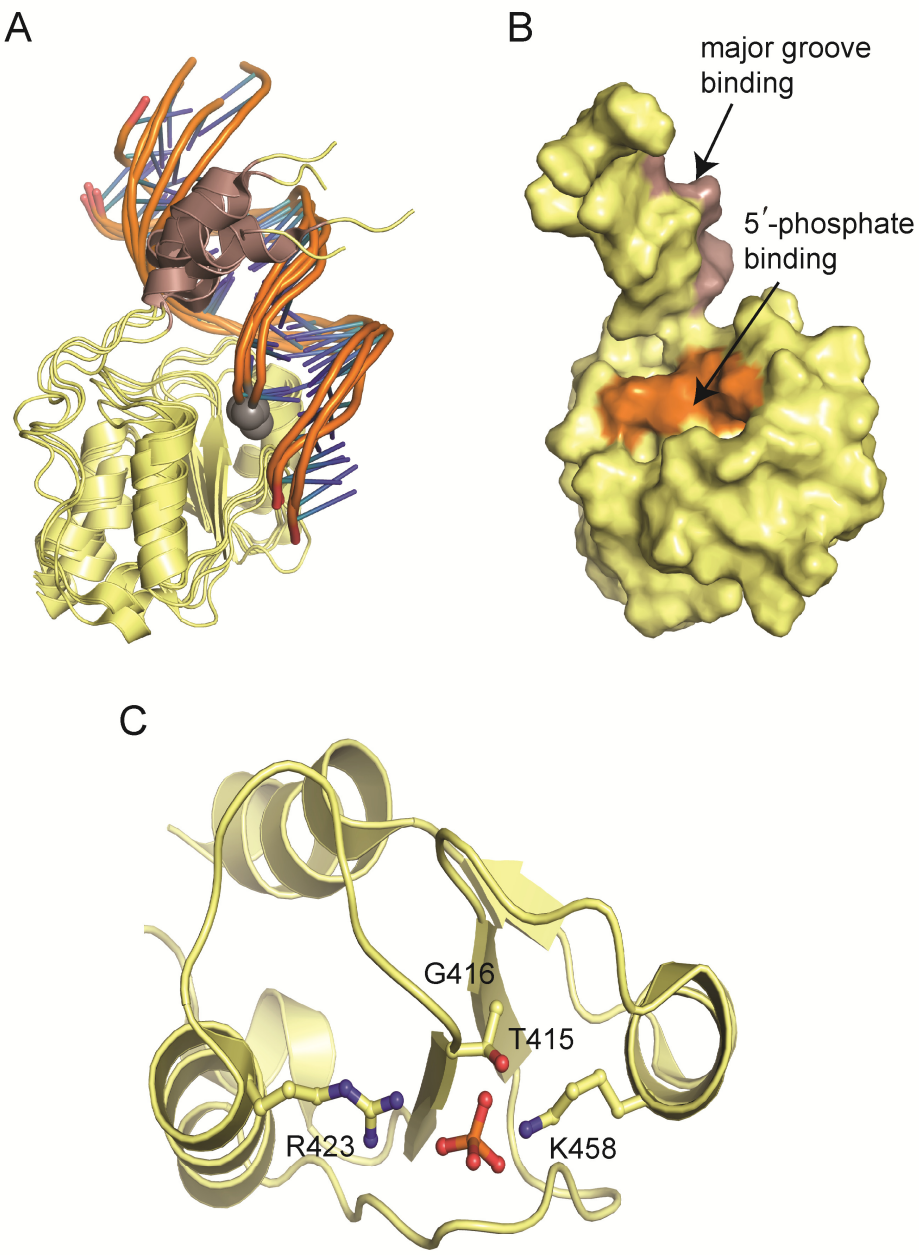

Figure 1-12. Model of the RFC p140 BRCT domain in complex with dsDNA. (A) Representative ensemble by Kobayashi et al. based on the four best structures from HADDOCK (PDB ID: 2K7F). The N-terminal α-helix is shown in purple and the 5′-phosphate is represented as a grey sphere. (B) Surface representation of RFC BRCT domain. Binding surfaces with the DNA major groove (purple) and with the 5′-phosphate (orange) are marked. (C) Conserved phosphate-binding pocket of RFC BRCT domain, as represented by one model in the ensemble. The 5′-phosphate group and contact residues are represented as sticks and labelled.

BRCT7/8 and the adjacent ATR-activation domain (AAD), preferentially binds benzo[a]pyrene diol epoxide (BPDE)-treated DNA and stimulates ATR activity, (Choi et al, 2009) which is critical for DNA replication checkpoint activation in response to DNA replication stress. The implication of BRCT domains directly detecting damaged DNA offers intriguing possibilities that proteins with BRCT domains can act as DNA damage sensors in addition to transducers of DDR signalling.

1.4.7. Poly(ADP-ribose) binding

Although still poorly understood, single BRCT domains have been implicated in binding poly(ADP-ribose) (PAR), a post-translational modification catalyzed by Poly (ADP-ribose) polymerases (PARP) in DDR signalling. A consensus PAR-binding motif is found in TopBP1 BRCT6 and the N-terminal BRCT of XRCC1 (Pleschke et al, 2000), although there is more evidence supporting XRCC1 BRCT1 as a validated PAR-binding module. XRCC1 BRCT1 preferentially recognizes ribosylated PARP-1 and a peptide of the XRCC1 PAR-binding sequence binds to PAR *in vitro* (Dantzer et al, 2000; El-Khamisy et al, 2003; Masson et al, 1998; Pleschke et al, 2000; Schreiber et al, 2002).

1.5 TopBP1: a prototypic BRCT domain protein in DNA damage response signalling

TopBP1 was originally identified in a two-hybrid screen as a binding partner of Topoisomerase IIβ, although its functional significance still remains unclear (Yamane et al, 1997). Implications of TopBP1 in numerous aspects of DNA metabolism such as DNA replication initiation and cell cycle control were initially limited to studies in its yeast orthologs (Araki et al, 1995; Saka et al, 1994). Over the past decade, studies of TopBP1 orthologs in metazoans have cemented TopBP1 as a key regulator of genomic stability and the DNA damage response (Garcia et al, 2005; Sokka et al, 2010).

The domain structure of TopBP1 includes nine BRCT domains and an ATR-activation domain (AAD) of unknown structure between BRCT6 and BRCT7 (Fig. 1-13). Originally observed to contain eight BRCT domains using sequence analysis, recent structural studies confirmed that BRCT1/2 in fact buttresses a cryptic BRCT domain (BRCT0) at its N-terminus (Huo et al, 2010; Rappas et al, 2011). Besides the triple BRCT domain at the N-terminus, TopBP1 contains two tandem BRCT repeats (BRCT4/5 and BRCT7/8) and two single BRCT domains (BRCT3 and BRCT6). Interestingly, orthologs of TopBP1 vary in length and number of BRCT domains, suggesting that higher order eukaryotes may have acquired additional BRCT domain function as a result of increased complexities in genome maintenance (Fig. 1-13). Due to the abundance of BRCT repeats present in TopBP1, it is speculated that the diverse roles of TopBP1 in DNA replication and checkpoint signalling are associated with the ability of TopBP1 to act as a scaffolding protein and facilitate various protein-protein interactions.

TopBP1 BRCT6 interacts with the E2F1 transcription factor to regulate E2F1 activity in response to DNA damage (Liu et al, 2003). This interaction is dependent on E2F1 phosphorylation at Ser31 by ATM. BRCT6 is also a target for poly(ADP)-ribosylation (Wollmann et al, 2007). A phosphorylation-dependent interaction involving Treslin and TopBP1 BRCT0/1/2 is pivotal for replication initiation (Kumagai et al, 2010). This interaction is also conserved between the *S. cerevisiae* orthologs, $Dpb11^{TopBP1}$ and $Sld3^{Treslin}$ (Boos et al, 2011; Tanaka et al, 2007; Zegerman & Diffley, 2007). TopBP1 BRCT4/5 interacts with 53BP1 to regulate the checkpoint function of 53BP1 in G1 (Cescutti et al, 2010). There is also evidence that TopBP1 C-terminal BRCT7/8 domains bind to an internal pSer binding motif in TopBP1, inducing TopBP1 oligomerization that is needed for E2F1-mediated apoptosis (Liu et al, 2006).

Other TopBP1 BRCT-domain mediated interactions highlight the role of TopBP1 as a key regulator in DNA replication stress. It is now apparent that

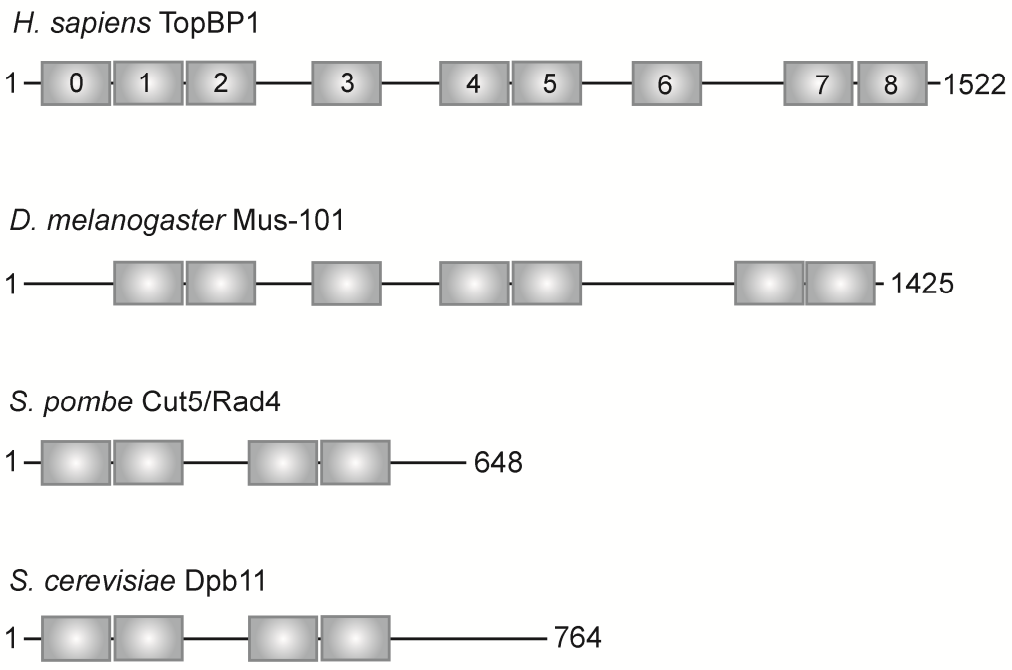

Figure 1-13. TopBP1 conservation in different orthologs. BRCT domains are represented as grey boxes and numbered in human TopBP1.

regulation of the DNA replication checkpoint by TopBP1 is governed by at least three distinct BRCT-mediated interactions. Activation of ATR through the AAD of TopBP1 requires the interaction between the TopBP1 BRCT0/1/2 domains and the phosphorylated tail of the Rad9 component of the 9-1-1 complex (Delacroix et al, 2007; Lee et al, 2007). The C-terminal end of Rad9 is constitutively phosphorylated at Ser387 by Casein kinase 2 (CK2) (Takeishi et al, 2010), and binding to this phospho-peptide motif (pS-E-G-E-G) is dependent on the phosphate-binding pocket in BRCT1 of TopBP1 (Rappas et al, 2011). Recent work from our collaborator, Dr. Junjie Chen (University of Texas MD Anderson Cancer Center), identified BACH1/FANCJ and MDC1 as additional binding partners of TopBP1. Interestingly, both binding events contribute at different stages of ATR activation. The interaction between TopBP1 and BACH1 is mediated by the S phase-specific phosphorylation of BACH1 at Thr1133 and the C-terminal TopBP1 BRCT7/8 domains (Gong et al, 2010). Binding to BACH1 regulates BACH1 helicase activity and stimulates RPA chromatin loading, which is a prerequisite for ATR-ATRIP accumulation and activation at stalled replication forks. The discovery of a separate BACH1 binding motif for TopBP1 is particularly intriguing, since BACH1 was originally identified as a BRCA1 BRCT-interacting partner (Cantor et al, 2001; Yu et al, 2003). The missing link for TopBP1 BRCT5-dependent accumulation at replication forks was uncovered with the identification of the binding partner MDC1, another key adaptor protein in the repair of DNA DSBs (Wang et al, 2011; Yamane et al, 2002). TopBP1 BRCT5 specifically recognizes the SDT repeats of MDC1, which consist of six CK2 phosphorylated Ser-Asp-Thr peptide motifs, to sustain TopBP1 accumulation and ATR activation at stalled replication forks.

1.6 Research goals and thesis organization

The goals of this thesis are to elucidate the molecular mechanisms underlying interactions mediated by TopBP1 BRCT domains in DNA damage

repair and DNA replication stress. Chapter 2 summarizes the materials and methods used throughout the thesis. Chapter 3 reports the crystal structure of TopBP1 BRCT6 and provides insights into potential phospho-peptide binding and poly(ADP-ribose) binding roles in DNA repair. The BRCT6 structure reveals a degenerate phospho-peptide binding pocket, suggesting that it is unlikely to bind its cognate E2F1 phospho-peptide in a canonical way. Chapter 4 describes the structural basis for the interaction between TopBP1 BRCT7/8 and BACH1 in DNA replication checkpoint control. The crystal structure of TopBP1 BRCT7/8 in complex with a BACH1 phospho-peptide provides the basis for pThr recognition by BRCT domains, and comparisons between the apo and bound structures reveal a unique structural rearrangement at the BRCT-BRCT interface upon binding BACH1. In Chapter 5, I present the structural basis for MDC1 targeted recognition by TopBP1 BRCT4/5, another key step in the regulation of the DNA replication checkpoint. The crystal structure of TopBP1 BRCT4/5 is the first demonstration of a BRCT repeat containing a C-terminal phosphate binding pocket. Additionally, the structure in complex with a MDC1 di-phospho-peptide indicates a peptide-induced dimerization model, where two BRCT5 protomers recognize a single MDC1 di-phospho-peptide. Chapter 6 summarizes results from our studies and provides perspectives into the role of TopBP1 in DNA replication checkpoint control, as well as novel aspects of BRCT domain function. Finally, Appendices A and B describe brief work done to characterize the poly-ubiquitin binding specificities of the RAP80 and RAD18 DDR proteins.

1.7 References

Allen BL, Uhlmann F, Gaur LK, Mulder BA, Posey KL, Jones LB, Hardin SH (1998) DNA recognition properties of the N-terminal DNA binding domain within the large subunit of replication factor C. *Nucleic Acids Res* **26:** 3877-3882

Almeida KH, Sobol RW (2007) A unified view of base excision repair: lesion-dependent protein complexes regulated by post-translational modification. *DNA Repair (Amst)* **6:** 695-711

Araki H, Leem SH, Phongdara A, Sugino A (1995) Dpb11, which interacts with DNA polymerase II(epsilon) in Saccharomyces cerevisiae, has a dual role in S-phase progression and at a cell cycle checkpoint. *Proc Natl Acad Sci U S A* **92:** 11791-11795

Ashworth A (2008) A synthetic lethal therapeutic approach: poly(ADP) ribose polymerase inhibitors for the treatment of cancers deficient in DNA double-strand break repair. *J Clin Oncol* **26:** 3785-3790

Bakkenist CJ, Kastan MB (2004) Initiating cellular stress responses. *Cell* **118:** 9-17

Ball HL, Ehrhardt MR, Mordes Da, Glick GG, Chazin WJ, Cortez D (2007) Function of a conserved checkpoint recruitment domain in ATRIP proteins. *Mol Cell Biol* **27:** 3367-3377

Ball HL, Myers JS, Cortez D (2005) ATRIP binding to replication protein A-single-stranded DNA promotes ATR-ATRIP localization but is dispensable for Chk1 phosphorylation. *Mol Biol Cell* **16:** 2372-2381

Beernink PT, Hwang M, Ramirez M, Murphy MB, Doyle Sa, Thelen MP (2005) Specificity of protein interactions mediated by BRCT domains of the XRCC1 DNA repair protein. *J Biol Chem* **280:** 30206-30213

Birrane G, Varma AK, Soni A, Ladias Jaa (2007) Crystal structure of the BARD1 BRCT domains. *Biochemistry* **46:** 7706-7712

Boos D, Sanchez-Pulido L, Rappas M, Pearl LH, Oliver AW, Ponting CP, Diffley JF (2011) Regulation of DNA Replication through Sld3-Dpb11 Interaction Is Conserved from Yeast to Humans. *Curr Biol*

Bork P, Hofmann K, Bucher P, Neuwald AF, Altschul SF, Koonin EV (1997) A superfamily of conserved domains in DNA damage-responsive cell cycle checkpoint proteins. *The FASEB Journal* **11:** 68-76

Boyce RP, Howard-Flanders P (1964) Release of Ultraviolet Light-Induced Thymine Dimers from DNA in E. Coli K-12. *Proc Natl Acad Sci U S A* **51:** 293-300

Branzei D, Foiani M (2005) The DNA damage response during DNA replication. *Curr Opin Cell Biol* **17:** 568-575

Bryant HE, Schultz N, Thomas HD, Parker KM, Flower D, Lopez E, Kyle S, Meuth M, Curtin NJ, Helleday T (2005) Specific killing of BRCA2-deficient tumours with inhibitors of poly(ADP-ribose) polymerase. *Nature* **434:** 913-917

Burbelo PD, Utani a, Pan ZQ, Yamada Y (1993) Cloning of the large subunit of activator 1 (replication factor C) reveals homology with bacterial DNA ligases. *Proc Natl Acad Sci U S A* **90:** 11543-11547

Burrows AE, Elledge SJ (2008) How ATR turns on: TopBP1 goes on ATRIP with ATR. *Genes Dev* **22:** 1416-1421

Byeon IJ, Li H, Song H, Gronenborn AM, Tsai MD (2005) Sequential phosphorylation and multisite interactions characterize specific target recognition by the FHA domain of Ki67. *Nat Struct Mol Biol* **12:** 987-993

Caldecott KW, McKeown CK, Tucker JD, Ljungquist S, Thompson LH (1994) An interaction between the mammalian DNA repair protein XRCC1 and DNA ligase III. *Mol Cell Biol* **14:** 68-76

Callebaut I, Mornon JP (1997) From BRCA1 to RAP1: a widespread BRCT module closely associated with DNA repair. *FEBS letters* **400:** 25-30

Campbell SJ, Edwards RA, Glover JNM (2010) Comparison of the structures and peptide binding specificities of the BRCT domains of MDC1 and BRCA1. *Structure* **18:** 167-176

Canman CE (2001) Replication checkpoint: preventing mitotic catastrophe. *Curr Biol* **11:** R121-124

Canman CE, Lim DS (1998) The role of ATM in DNA damage responses and cancer. *Oncogene* **17:** 3301-3308

Cantor SB, Bell DW, Ganesan S, Kass EM, Drapkin R, Grossman S, Wahrer DC, Sgroi DC, Lane WS, Haber DA, Livingston DM (2001) BACH1, a novel helicase-like protein, interacts directly with BRCA1 and contributes to its DNA repair function. *Cell* **105:** 149-160

Cescutti R, Negrini S, Kohzaki M, Halazonetis TD (2010) TopBP1 functions with 53BP1 in the G1 DNA damage checkpoint. *EMBO J* **29:** 3723-3732

Chapman JR, Jackson SP (2008) Phospho-dependent interactions between NBS1 and MDC1 mediate chromatin retention of the MRN complex at sites of DNA damage. *EMBO Rep* **9:** 795-801

Choi J-H, Lindsey-Boltz La, Sancar A (2009) Cooperative activation of the ATR checkpoint kinase by TopBP1 and damaged DNA. *Nucleic Acids Res* **37:** 1501-1509

Ciccia A, Elledge SJ (2010) The DNA damage response: making it safe to play with knives. *Mol Cell* **40:** 179-204

Cimprich Ka, Cortez D (2008) ATR: an essential regulator of genome integrity. *Nat Rev Mol Cell Biol* **9:** 616-627

Clapperton Ja, Manke Ia, Lowery DM, Ho T, Haire LF, Yaffe MB, Smerdon SJ (2004) Structure and mechanism of BRCA1 BRCT domain recognition of phosphorylated BACH1 with implications for cancer. *Nat Struct Mol Biol* **11:** 512-518

Cleaver JE (1968) Defective repair replication of DNA in xeroderma pigmentosum. *Nature* **218:** 652-656

Crick F (1974) The double helix: a personal view. *Nature* **248:** 766-769

Critchlow SE, Bowater RP, Jackson SP (1997) Mammalian DNA double-strand break repair protein XRCC4 interacts with DNA ligase IV. *Curr Biol* **7:** 588-598

Cuneo MJ, Gabel SA, Krahn JM, Ricker MA, London RE (2011) The structural basis for partitioning of the XRCC1/DNA ligase III-{alpha} BRCT-mediated dimer complexes. *Nucleic Acids Res*

Dantzer F, de La Rubia G, Ménissier-De Murcia J, Hostomsky Z, de Murcia G, Schreiber V (2000) Base excision repair is impaired in mammalian cells lacking Poly(ADP-ribose) polymerase-1. *Biochemistry* **39:** 7559-7569

De Bont R, van Larebeke N (2004) Endogenous DNA damage in humans: a review of quantitative data. *Mutagenesis* **19:** 169-185

Delacroix S, Wagner JM, Kobayashi M, Yamamoto K-i, Karnitz LM (2007) The Rad9-Hus1-Rad1 (9-1-1) clamp activates checkpoint signaling via TopBP1. *Genes Dev* **21:** 1472-1477

Derbyshire DJ, Basu BP, Serpell LC, Joo WS, Date T, Iwabuchi K, Doherty AJ (2002) Crystal structure of human 53BP1 BRCT domains bound to p53 tumour suppressor. *EMBO J* **21:** 3863-3872

Dore AS, Furnham N, Davies OR, Sibanda BL, Chirgadze DY, Jackson SP, Pellegrini L, Blundell TL (2006) Structure of an Xrcc4-DNA ligase IV yeast ortholog complex reveals a novel BRCT interaction mode. *DNA Repair* **5:** 362-368

Du LL, Moser BA, Russell P (2004) Homo-oligomerization is the essential function of the tandem BRCT domains in the checkpoint protein Crb2. *J Biol Chem* **279:** 38409-38414

Edwards RA, Lee MS, Tsutakawa SE, Williams RS, Nazeer I, Kleiman FE, Tainer JA, Glover JN (2008) The BARD1 C-terminal domain structure and interactions with polyadenylation factor CstF-50. *Biochemistry* **47:** 11446-11456

El-Khamisy SF, Masutani M, Suzuki H, Caldecott KW (2003) A requirement for PARP-1 for the assembly or stability of XRCC1 nuclear foci at sites of oxidative DNA damage. *Nucleic Acids Res* **31:** 5526-5533

Ellison V, Stillman B (2003) Biochemical characterization of DNA damage checkpoint complexes: clamp loader and clamp complexes with specificity for 5' recessed DNA. *PLoS biology* **1:** E33

Farmer H, McCabe N, Lord CJ, Tutt AN, Johnson DA, Richardson TB, Santarosa M, Dillon KJ, Hickson I, Knights C, Martin NM, Jackson SP, Smith GC, Ashworth A (2005) Targeting the DNA repair defect in BRCA mutant cells as a therapeutic strategy. *Nature* **434:** 917-921

Feng H, Parker JM, Lu J, Cao W (2004) Effects of deletion and site-directed mutations on ligation steps of NAD+-dependent DNA ligase: a biochemical analysis of BRCA1 C-terminal domain. *Biochemistry* **43:** 12648-12659

Flynn RL, Zou L (2011) ATR: a master conductor of cellular responses to DNA replication stress. *Trends Biochem Sci* **36:** 133-140

Fong PC, Boss DS, Yap TA, Tutt A, Wu P, Mergui-Roelvink M, Mortimer P, Swaisland H, Lau A, O'Connor MJ, Ashworth A, Carmichael J, Kaye SB, Schellens JH, de Bono JS (2009) Inhibition of poly(ADP-ribose) polymerase in tumors from BRCA mutation carriers. *N Engl J Med* **361:** 123-134

Fotedar R, Mossi R, Fitzgerald P, Rousselle T, Maga G, Brickner H, Messier H, Kasibhatla S, Hübscher U, Fotedar a (1996) A conserved domain of the large subunit of replication factor C binds PCNA and acts like a dominant negative inhibitor of DNA replication in mammalian cells. *EMBO J* **15:** 4423-4433

Friedberg EC (1997) *Correcting the Blueprint of Life. An Historical Accounting of the Discovery DNA Repairing Mechanisms*, Cold Spring Harbor, NY: Cold Spring Harbor Laboratory Press.

Friedberg EC (2001) How nucleotide excision repair protects against cancer. *Nat Rev Cancer* **1:** 22-33

Futreal PA, Liu Q, Shattuck-Eidens D, Cochran C, Harshman K, Tavtigian S, Bennett LM, Haugen-Strano A, Swensen J, Miki Y, et al. (1994) BRCA1 mutations in primary breast and ovarian carcinomas. *Science* **266:** 120-122

Garcia V, Furuya K, Carr AM (2005) Identification and functional analysis of TopBP1 and its homologs. *DNA Repair* **4:** 1227-1239

Ghosh A, Shuman S, Lima CD (2008) The structure of Fcp1, an essential RNA polymerase II CTD phosphatase. *Mol Cell* **32:** 478-490

Glover JNM, Williams RS, Lee MS (2004) Interactions between BRCT repeats and phosphoproteins: tangled up in two. *Trends Biochem Sci* **29:** 579-585

Gong Z, Kim JE, Leung CC, Glover JN, Chen J (2010) BACH1/FANCJ acts with TopBP1 and participates early in DNA replication checkpoint control. *Mol Cell* **37:** 438-446

Goodgal SH, Rupert CS, Herriot R (1957) *The chemical basis of heredity*, Vol. 336, Baltimore: The Johns Hopkins Press.

Goodman MF, Tippin B (2000) Sloppier copier DNA polymerases involved in genome repair. *Curr Opin Genet Dev* **10:** 162-168

Grawunder U, Wilm M, Wu X, Kulesza P, Wilson TE, Mann M, Lieber MR (1997) Activity of DNA ligase IV stimulated by complex formation with XRCC4 protein in mammalian cells. *Nature* **388:** 492-495

Grawunder U, Zimmer D, Kulesza P, Lieber MR (1998) Requirement for an interaction of XRCC4 with DNA ligase IV for wild-type V(D)J recombination and DNA double-strand break repair in vivo. *J Biol Chem* **273:** 24708-24714

Halazonetis TD, Gorgoulis VG, Bartek J (2008) An oncogene-induced DNA damage model for cancer development. *Science* **319:** 1352-1355

Hanahan D, Weinberg RA (2000) The hallmarks of cancer. *Cell* **100:** 57-70

Hari FJ, Spycher C, Jungmichel S, Pavic L, Stucki M (2010) A divalent FHA/BRCT-binding mechanism couples the MRE11-RAD50-NBS1 complex to damaged chromatin. *EMBO Rep* **11:** 387-392

Helleday T, Petermann E, Lundin C, Hodgson B, Sharma RA (2008) DNA repair pathways as targets for cancer therapy. *Nat Rev Cancer* **8:** 193-204

Hoeijmakers JH (2009) DNA damage, aging, and cancer. *N Engl J Med* **361:** 1475-1485

Huen MS, Sy SM, Chen J (2010) BRCA1 and its toolbox for the maintenance of genome integrity. *Nat Rev Mol Cell Biol* **11:** 138-148

Huo Y-G, Bai L, Xu M, Jiang T (2010) Crystal structure of the N-terminal region of human Topoisomerase IIβ binding protein 1. *Biochem Biophys Res Commun* **401:** 401-405

Hyrien O (2000) Mechanisms and consequences of replication fork arrest. *Biochimie* **82:** 5-17

Jackson SP, Bartek J (2009) The DNA-damage response in human biology and disease. *Nature* **461:** 1071-1078

Jeffers LJ, Coull BJ, Stack SJ, Morrison CG (2008) Distinct BRCT domains in Mcph1/Brit1 mediate ionizing radiation-induced focus formation and centrosomal localization. *Oncogene* **27:** 139-144

Joo WS, Jeffrey PD, Cantor SB, Finnin MS, Livingston DM, Pavletich NP (2002) Structure of the 53BP1 BRCT region bound to p53 and its comparison to the Brca1 BRCT structure. *Genes Dev* **16:** 583-593

Kemp MG, Akan Z, Yilmaz S, Grillo M, Smith-Roe SL, Kang TH, Cordeiro-Stone M, Kaufmann WK, Abraham RT, Sancar A, Unsal-Kacmaz K (2010) Tipin-replication

protein A interaction mediates Chk1 phosphorylation by ATR in response to genotoxic stress. *J Biol Chem* **285:** 16562-16571

Kilkenny ML, Doré AS, Roe SM, Nestoras K, Ho JCY, Watts FZ, Pearl LH (2008) Structural and functional analysis of the Crb2-BRCT2 domain reveals distinct roles in checkpoint signaling and DNA damage repair. *Genes Dev* **22:** 2034-2047

Kim H, Huang J, Chen J (2007) CCDC98 is a BRCA1-BRCT domain-binding protein involved in the DNA damage response. *Nat Struct Mol Biol* **14:** 710-715

Kobayashi M, Ab E, Bonvin AMJJ, Siegal G (2010) Structure of the DNA-bound BRCA1 C-terminal region from human replication factor C p140 and model of the protein-DNA complex. *J Biol Chem* **285:** 10087-10097

Kobayashi M, Figaroa F, Meeuwenoord N, Jansen LET, Siegal G (2006) Characterization of the DNA binding and structural properties of the BRCT region of human replication factor C p140 subunit. *J Biol Chem* **281:** 4308-4317

Kumagai A, Kim S-M, Dunphy WG (2004) Claspin and the activated form of ATR-ATRIP collaborate in the activation of Chk1. *J Biol Chem* **279:** 49599-49608

Kumagai A, Lee J, Yoo HY, Dunphy WG (2006) TopBP1 activates the ATR-ATRIP complex. *Cell* **124:** 943-955

Kumagai A, Shevchenko A, Dunphy WG (2010) Treslin collaborates with TopBP1 in triggering the initiation of DNA replication. *Cell* **140:** 349-359

Lambert S, Carr AM (2005) Checkpoint responses to replication fork barriers. *Biochimie* **87:** 591-602

Lavin MF, Birrell G, Chen P, Kozlov S, Scott S, Gueven N (2005) ATM signaling and genomic stability in response to DNA damage. *Mutat Res* **569:** 123-132

Lee H, Yuan C, Hammet A, Mahajan A, Chen ES, Wu MR, Su MI, Heierhorst J, Tsai MD (2008) Diphosphothreonine-specific interaction between an SQ/TQ cluster and an FHA domain in the Rad53-Dun1 kinase cascade. *Mol Cell* **30:** 767-778

Lee J, Kumagai A, Dunphy WG (2007) The Rad9-Hus1-Rad1 checkpoint clamp regulates interaction of TopBP1 with ATR. *J Biol Chem* **282:** 28036-28044

Lee MS, Edwards RA, Thede GL, Glover JN (2005) Structure of the BRCT repeat domain of MDC1 and its specificity for the free COOH-terminal end of the gamma-H2AX histone tail. *J Biol Chem* **280:** 32053-32056

Li Z, Otevrel T, Gao Y, Cheng HL, Seed B, Stamato TD, Taccioli GE, Alt FW (1995) The XRCC4 gene encodes a novel protein involved in DNA double-strand break repair and V(D)J recombination. *Cell* **83:** 1079-1089

Liang X, Van Doren SR (2008) Mechanistic insights into phosphoprotein-binding FHA domains. *Acc Chem Res* **41:** 991-999

Lieber MR (2010) The mechanism of double-strand DNA break repair by the nonhomologous DNA end-joining pathway. *Annu Rev Biochem* **79:** 181-211

Lindahl T (1993) Instability and decay of the primary structure of DNA. *Nature* **362:** 709-715

Liu K, Lin F-T, Ruppert JM, Lin W-C (2003) Regulation of E2F1 by BRCT domain-containing protein TopBP1. *Mol Cell Biol* **23:** 3287-3304

Liu K, Paik JC, Wang B, Lin FT, Lin WC (2006) Regulation of TopBP1 oligomerization by Akt/PKB for cell survival. *EMBO J* **25:** 4795-4807

Liu Z, Wu J, Yu X (2007) CCDC98 targets BRCA1 to DNA damage sites. *Nat Struct Mol Biol* **14:** 716-720

Llorente B, Smith CE, Symington LS (2008) Break-induced replication: what is it and what is it for? *Cell Cycle* **7:** 859-864

Lloyd J, Chapman JR, Clapperton JA, Haire LF, Hartsuiker E, Li J, Carr AM, Jackson SP, Smerdon SJ (2009) A supramodular FHA/BRCT-repeat architecture mediates Nbs1 adaptor function in response to DNA damage. *Cell* **139:** 100-111

Macdonald N, Welburn JP, Noble ME, Nguyen A, Yaffe MB, Clynes D, Moggs JG, Orphanides G, Thomson S, Edmunds JW, Clayton AL, Endicott JA, Mahadevan LC (2005) Molecular basis for the recognition of phosphorylated and phosphoacetylated histone h3 by 14-3-3. *Mol Cell* **20:** 199-211

Majka J, Binz SK, Wold MS, Burgers PM (2006) Replication protein A directs loading of the DNA damage checkpoint clamp to 5'-DNA junctions. *J Biol Chem* **281:** 27855-27861

Manke Ia, Lowery DM, Nguyen A, Yaffe MB (2003) BRCT repeats as phosphopeptide-binding modules involved in protein targeting. *Science* **302:** 636-639

Martín-García R, de León N, Sharifmoghadam MR, Curto M-Á, Hoya M, Bustos-Sanmamed P, Valdivieso M-H (2010) The FN3 and BRCT motifs in the exomer component Chs5p define a conserved module that is necessary and sufficient for its function. *Cellular and molecular life sciences : CMLS*

Masson M, Niedergang C, Schreiber V, Muller S, Menissier-de Murcia J, de Murcia G (1998) XRCC1 is specifically associated with poly(ADP-ribose) polymerase and negatively regulates its activity following DNA damage. *Mol Cell Biol* **18:** 3563-3571

Matsuoka S, Ballif BA, Smogorzewska A, McDonald ER, 3rd, Hurov KE, Luo J, Bakalarski CE, Zhao Z, Solimini N, Lerenthal Y, Shiloh Y, Gygi SP, Elledge SJ (2007) ATM and ATR substrate analysis reveals extensive protein networks responsive to DNA damage. *Science* **316:** 1160-1166

Melander F, Bekker-Jensen S, Falck J, Bartek J, Mailand N, Lukas J (2008) Phosphorylation of SDT repeats in the MDC1 N terminus triggers retention of NBS1 at the DNA damage-modified chromatin. *J Cell Biol* **181:** 213-226

Miki Y, Swensen J, Shattuck-Eidens D, Futreal Pa, Harshman K, Tavtigian S, Liu Q, Cochran C, Bennett LM, Ding W (1994) A strong candidate for the breast and ovarian cancer susceptibility gene BRCA1. *Science* **266:** 66-71

Mohammad D, Yaffe MB (2009) 14-3-3 proteins, FHA domains and BRCT domains in the DNA damage response. *DNA Repair* **8:** 1009-1017

Mordes Da, Glick GG, Zhao R, Cortez D (2008) TopBP1 activates ATR through ATRIP and a PIKK regulatory domain. *Genes Dev* **22:** 1478-1489

Morrison C, Rieder CL (2004) Chromosome damage and progression into and through mitosis in vertebrates. *DNA Repair* **3:** 1133-1139

Nash Ra, Caldecott KW, Barnes DE, Lindahl T (1997) XRCC1 protein interacts with one of two distinct forms of DNA ligase III. *Biochemistry* **36:** 5207-5211

Negrini S, Gorgoulis VG, Halazonetis TD (2010) Genomic instability--an evolving hallmark of cancer. *Nat Rev Mol Cell Biol* **11:** 220-228

Nyberg KA, Michelson RJ, Putnam CW, Weinert TA (2002) Toward maintaining the genome: DNA damage and replication checkpoints. *Annu Rev Genet* **36:** 617-656

Obsil T, Ghirlando R, Klein DC, Ganguly S, Dyda F (2001) Crystal structure of the 14-3-3zeta:serotonin N-acetyltransferase complex. a role for scaffolding in enzyme regulation. *Cell* **105:** 257-267

Osborn AJ, Elledge SJ, Zou L (2002) Checking on the fork: the DNA-replication stress-response pathway. *Trends Cell Biol* **12:** 509-516

Ottmann C, Yasmin L, Weyand M, Veesenmeyer JL, Diaz MH, Palmer RH, Francis MS, Hauser AR, Wittinghofer A, Hallberg B (2007) Phosphorylation-independent interaction between 14-3-3 and exoenzyme S: from structure to pathogenesis. *EMBO J* **26:** 902-913

Paulsen RD, Cimprich Ka (2007) The ATR pathway: fine-tuning the fork. *DNA Repair* **6:** 953-966

Pei H, Zhang L, Luo K, Qin Y, Chesi M, Fei F, Bergsagel PL, Wang L, You Z, Lou Z (2011) MMSET regulates histone H4K20 methylation and 53BP1 accumulation at DNA damage sites. *Nature* **470:** 124-128

Pennell S, Westcott S, Ortiz-Lombardia M, Patel D, Li J, Nott TJ, Mohammed D, Buxton RS, Yaffe MB, Verma C, Smerdon SJ (2010) Structural and functional analysis of phosphothreonine-dependent FHA domain interactions. *Structure* **18:** 1587-1595

Pettijohn D, Hanawalt P (1964) Evidence for Repair-Replication of Ultraviolet Damaged DNA in Bacteria. *J Mol Biol* **9:** 395-410

Pleschke JM, Kleczkowska HE, Strohm M, Althaus FR (2000) Poly(ADP-ribose) binds to specific domains in DNA damage checkpoint proteins. *J Biol Chem* **275:** 40974-40980

Rappas M, Oliver AW, Pearl LH (2011) Structure and function of the Rad9-binding region of the DNA-damage checkpoint adaptor TopBP1. *Nucleic Acids Res* **39:** 313-324

Ray H, Moreau K, Dizin E, Callebaut I, Venezia ND (2006) ACCA phosphopeptide recognition by the BRCT repeats of BRCA1. *J Mol Biol* **359:** 973-982

Reinhardt HC, Yaffe MB (2009) Kinases that control the cell cycle in response to DNA damage: Chk1, Chk2, and MK2. *Curr Opin Cell Biol* **21:** 245-255

Richards MW, Leung JW, Roe SM, Li K, Chen J, Bayliss R (2010) A pocket on the surface of the N-terminal BRCT domain of Mcph1 is required to prevent abnormal chromosome condensation. *J Mol Biol* **395:** 908-915

Rodriguez M, Yu X, Chen J, Songyang Z (2003) Phosphopeptide binding specificities of BRCA1 COOH-terminal (BRCT) domains. *J Biol Chem* **278:** 52914-52918

Rodriguez MC, Songyang Z (2008) BRCT domains: phosphopeptide binding and signaling modules. *Front Biosci* **13:** 5905-5915

Rothstein R, Michel B, Gangloff S (2000) Replication fork pausing and recombination or "gimme a break". *Genes Dev* **14:** 1-10

Saka Y, Fantes P, Yanagida M (1994) Coupling of DNA replication and mitosis by fission yeast rad4/cut5. *J Cell Sci Suppl* **18:** 57-61

Sarasin A, Stary A (2007) New insights for understanding the transcription-coupled repair pathway. *DNA Repair (Amst)* **6:** 265-269

Schreiber V, Amé J-C, Dollé P, Schultz I, Rinaldi B, Fraulob V, Ménissier-de Murcia J, de Murcia G (2002) Poly(ADP-ribose) polymerase-2 (PARP-2) is required for efficient base excision DNA repair in association with PARP-1 and XRCC1. *J Biol Chem* **277:** 23028-23036

Setlow RB, Carrier WL (1964) The Disappearance of Thymine Dimers from DNA: An Error-Correcting Mechanism. *Proc Natl Acad Sci U S A* **51:** 226-231

Setlow RB, Regan JD, German J, Carrier WL (1969) Evidence that xeroderma pigmentosum cells do not perform the first step in the repair of ultraviolet damage to their DNA. *Proc Natl Acad Sci U S A* **64:** 1035-1041

Shen Y, Tong L (2008) Structural evidence for direct interactions between the BRCT domains of human BRCA1 and a phospho-peptide from human ACC1. *Biochemistry* **47:** 5767-5773

Shiloh Y (2003) ATM and related protein kinases: safeguarding genome integrity. *Nat Rev Cancer* **3:** 155-168

Shiozaki EN, Gu L, Yan N, Shi Y (2004) Structure of the BRCT repeats of BRCA1 bound to a BACH1 phosphopeptide: implications for signaling. *Mol Cell* **14:** 405-412

Sibanda BL, Critchlow SE, Begun J, Pei XY, Jackson SP, Blundell TL, Pellegrini L (2001) Crystal structure of an Xrcc4-DNA ligase IV complex. *Nat Struct Biol* **8:** 1015-1019

Sokka M, Parkkinen S, Pospiech H, Syvaoja JE (2010) Function of TopBP1 in genome stability. *Subcell Biochem* **50:** 119-141

Soulier J, Lowndes NF (1999) The BRCT domain of the S. cerevisiae checkpoint protein Rad9 mediates a Rad9-Rad9 interaction after DNA damage. *Curr Biol* **9:** 551-554

Spycher C, Miller ES, Townsend K, Pavic L, Morrice Na, Janscak P, Stewart GS, Stucki M (2008) Constitutive phosphorylation of MDC1 physically links the MRE11-RAD50-NBS1 complex to damaged chromatin. *J Biol Chem* **181:** 227-240

Stewart GS, Wang B, Bignell CR, Taylor AM, Elledge SJ (2003) MDC1 is a mediator of the mammalian DNA damage checkpoint. *Nature* **421:** 961-966

Stucki M, Clapperton Ja, Mohammad D, Yaffe MB, Smerdon SJ, Jackson SP (2005) MDC1 directly binds phosphorylated histone H2AX to regulate cellular responses to DNA double-strand breaks. *Cell* **123:** 1213-1226

Takeishi Y, Ohashi E, Ogawa K, Masai H, Obuse C, Tsurimoto T (2010) Casein kinase 2-dependent phosphorylation of human Rad9 mediates the interaction between human Rad9-Hus1-Rad1 complex and TopBP1. *Genes Cells* **15:** 761-771

Tanaka S, Umemori T, Hirai K, Muramatsu S, Kamimura Y, Araki H (2007) CDK-dependent phosphorylation of Sld2 and Sld3 initiates DNA replication in budding yeast. *Nature* **445:** 328-332

Taylor RM, Wickstead B, Cronin S, Caldecott KW (1998) Role of a BRCT domain in the interaction of DNA ligase III-alpha with the DNA repair protein XRCC1. *Curr BIol* **8:** 877-880

Thanassoulas A, Nomikos M, Theodoridou M, Yannoukakos D, Mastellos D, Nounesis G (2010) Thermodynamic study of the BRCT domain of BARD1 and its interaction with the -pSER-X-X-Phe- motif-containing BRIP1 peptide. *Biochim Biophys Acta* **1804:** 1908-1916

Thornton KH, Krishnan VV, West MG, Popham J, Ramirez M, Thelen MP, Cosman M (2001) Expression, purification, and biophysical characterization of the BRCT domain of human DNA ligase IIIalpha. *Protein expression and purification* **21:** 401-411

Tsurimoto T, Stillman B (1991) Replication factors required for SV40 DNA replication in vitro. II. Switching of DNA polymerase alpha and delta during initiation of leading and lagging strand synthesis. *J Biol Chem* **266:** 1961-1968

Ulrich HD, Walden H (2010) Ubiquitin signalling in DNA replication and repair. *Nat Rev Mol Cell Biol* **11:** 479-489

Varma AK, Brown RS, Birrane G, Ladias Jaa (2005) Structural basis for cell cycle checkpoint control by the BRCA1-CtIP complex. *Biochemistry* **44:** 10941-10946

Wang B, Matsuoka S, Ballif Ba, Zhang D, Smogorzewska A, Gygi SP, Elledge SJ (2007) Abraxas and RAP80 form a BRCA1 protein complex required for the DNA damage response. *Science* **316:** 1194-1198

Wang J, Gong Z, Chen J (2011) MDC1 collaborates with TopBP1 in DNA replication checkpoint control. *J Cell Biol* **193:** 267-273

Watson JD, Crick FH (1953) Genetical implications of the structure of deoxyribonucleic acid. *Nature* **171:** 964-967

Watts FZ, Brissett NC (2010) Linking up and interacting with BRCT domains. *DNA Repair* **9:** 103-108

Weinfeld M, Mani RS, Abdou I, Aceytuno RD, Glover JN (2011) Tidying up loose ends: the role of polynucleotide kinase/phosphatase in DNA strand break repair. *Trends Biochem Sci* **36:** 262-271

West SC (2003) Molecular views of recombination proteins and their control. *Nat Rev Mol Cell Biol* **4:** 435-445

Wilkinson A, Smith A, Bullard D, Lavesa-Curto M, Sayer H, Bonner A, Hemmings A, Bowater R (2005) Analysis of ligation and DNA binding by Escherichia coli DNA ligase (LigA). *Biochim Biophys Acta* **1749:** 113-122

Williams JS, Williams RS, Dovey CL, Guenther G, Tainer JA, Russell P (2010) gammaH2A binds Brc1 to maintain genome integrity during S-phase. *EMBO J* **29:** 1136-1148

Williams RS, Dodson GE, Limbo O, Yamada Y, Williams JS, Guenther G, Classen S, Glover JNM, Iwasaki H, Russell P, Tainer JA (2009) Nbs1 flexibly tethers Ctp1 and Mre11-Rad50 to coordinate DNA double-strand break processing and repair. *Cell* **139:** 87-99

Williams RS, Green R, Glover JN (2001) Crystal structure of the BRCT repeat region from the breast cancer-associated protein BRCA1. *Nat Struct Biol* **8:** 838-842

Williams RS, Lee MS, Hau DD, Glover JN (2004) Structural basis of phosphopeptide recognition by the BRCT domain of BRCA1. *Nat Struct Mol Biol* **11:** 519-525

Wollmann Y, Schmidt U, Wieland GD, Zipfel PF, Saluz H-P, Hänel F (2007) The DNA topoisomerase IIbeta binding protein 1 (TopBP1) interacts with poly (ADP-ribose) polymerase (PARP-1). *Journal of cellular biochemistry* **102:** 171-182

Wooster R, Neuhausen SL, Mangion J, Quirk Y, Ford D, Collins N, Nguyen K, Seal S, Tran T, Averill D, et al. (1994) Localization of a breast cancer susceptibility gene, BRCA2, to chromosome 13q12-13. *Science* **265:** 2088-2090

Wu P-Y, Frit P, Meesala S, Dauvillier S, Modesti M, Andres SN, Huang Y, Sekiguchi J, Calsou P, Salles B, Junop MS (2009) Structural and functional interaction between the human DNA repair proteins DNA ligase IV and XRCC4. *Mol Cell Biol* **29:** 3163-3172

Yaffe MB, Rittinger K, Volinia S, Caron PR, Aitken A, Leffers H, Gamblin SJ, Smerdon SJ, Cantley LC (1997) The structural basis for 14-3-3:phosphopeptide binding specificity. *Cell* **91:** 961-971

Yaffe MB, Smerdon SJ (2001) PhosphoSerine/threonine binding domains: you can't pSERious? *Structure* **9:** R33-38

Yamane K, Katayama E, Tsuruo T (2000) The BRCT regions of tumor suppressor BRCA1 and of XRCC1 show DNA end binding activity with a multimerizing feature. *Biochem Biophys Res Commun* **279:** 678-684

Yamane K, Kawabata M, Tsuruo T (1997) A DNA-topoisomerase-II-binding protein with eight repeating regions similar to DNA-repair enzymes and to a cell-cycle regulator. *European journal of biochemistry / FEBS* **250:** 794-799

Yamane K, Tsuruo T (1999) Conserved BRCT regions of TopBP1 and of the tumor suppressor BRCA1 bind strand breaks and termini of DNA. *Oncogene* **18:** 5194-5203

Yamane K, Wu X, Chen J (2002) A DNA damage-regulated BRCT-containing protein, TopBP1, is required for cell survival. *Mol Cell Biol* **22:** 555-566

Yu X, Chen J (2004) DNA damage-induced cell cycle checkpoint control requires CtIP, a phosphorylation-dependent binding partner of BRCA1 C-terminal domains. *Mol Cell Biol* **24:** 9478-9486

Yu X, Chini CCS, He M, Mer G, Chen J (2003) The BRCT domain is a phospho-protein binding domain. *Science* **302:** 639-642

Zegerman P, Diffley JF (2007) Phosphorylation of Sld2 and Sld3 by cyclin-dependent kinases promotes DNA replication in budding yeast. *Nature* **445:** 281-285

Zhang X, Moréra S, Bates Pa, Whitehead PC, Coffer aI, Hainbucher K, Nash Ra, Sternberg MJ, Lindahl T, Freemont PS (1998) Structure of an XRCC1 BRCT domain: a new protein-protein interaction module. *EMBO J* **17:** 6404-6411

Zhou B, Elledge SJ (2000) The DNA damage response: putting checkpoints in perspective. *Nature* **408:** 433-439

Zou L, Elledge SJ (2003) Sensing DNA damage through ATRIP recognition of RPA-ssDNA complexes. *Science* **300:** 1542-1548

Zou L, Liu D, Elledge SJ (2003) Replication protein A-mediated recruitment and activation of Rad17 complexes. *Proc Natl Acad Sci U S A* **100:** 13827-13832

Chapter 2

Materials and Methods

2.1 Design and cloning of TopBP1 constructs

TopBP1 clones encoding various BRCT domains were generously provided by Dr. Junjie Chen (University of Texas MD Anderson Cancer Center) and used as PCR templates for generation of all TopBP1 BRCT domain constructs. DNA fragments for each TopBP1 BRCT domain were designed based on limited trypsin proteolysis and/or multiple sequence alignments with different homologs to determine the optimal fragment for crystallization. All BRCT domain fragments were cloned into pGEX vectors (GE Healthcare) encoding an N-terminal GST tag. All mutants were generated by PCR-directed overlap extension (Heckman & Pease, 2007). Successful clones were verified with DNA sequencing (Molecular Biology Facility, Dept. of Biological Sciences; The Applied Genomics Centre, Dept. of Medical Genetics).

2.1.1. TopBP1 BRCT6

Primers designed with BamHI and NotI restriction sites (Table 2-1) were used in PCR to amplify the gene from a TopBP1 BRCT6 construct provided by Dr. Junjie Chen. Following BamHI and NotI restriction enzyme digests, the inserts were ligated into pGEX-4T-1 vector. Due to the single point mutation (W936R) in the template TopBP1 construct, wildtype TopBP1 BRCT6 was engineered in TopBP1 BRCT6 (893-996) and cloned into pGEX-6P-1 vector.

2.1.2. TopBP1 BRCT7/8

Primers used to create TopBP1 BRCT7/8 DNA fragments with flanking BamHI and NotI restriction sites are listed in Table 2-2. All TopBP1 BRCT7/8 constructs were made in pGEX-6P-1 vector. TopBP1 BRCT7/8 missense variants were engineered in TopBP1 BRCT7/8 (1264-1493).

Table 2-1. List of primers used for TopBP1 BRCT6 domain constructs.

Protein	**5′-primer (forward)**	**3′-primer (reverse)**
TopBP1 BRCT6 (893-1008)	TGCGGCGGATCCGAGGCCCAGTCAGAGAAGGAA	TGCGGCGCGGCCGCTCACCGGCCATCTTGCACTGCGCT
TopBP1 BRCT6 (893-996)	TGCGGCGGATCCGAGGCCCAGTCAGAGAAGGAA	TGCGGCGCGGCCGCTCATTTGGGATTATAAGTATGTGG
TopBP1 BRCT6 (893-982)	TGCGGCGGATCCGAGGCCCAGTCAGAGAAGGAA	TGCGGCGCGGCCGCTCATTTACACTCTTGGGCACAATC
TopBP1 BRCT6 (899-1008)	TGCGGCGGATCCGAAGAAGCCCCAAAGCCACTT	TGCGGCGCGGCCGCTCACCGGCCATCTTGCACTGCGCT
TopBP1 BRCT6 (899-996)	TGCGGCGGATCCGAAGAAGCCCCAAAGCCACTT	TGCGGCGCGGCCGCTCATTTGGGATTATAAGTATGTGG
TopBP1 BRCT6 (899-982)	TGCGGCGGATCCGAAGAAGCCCCAAAGCCACTT	TGCGGCGCGGCCGCTCATTTACACTCTTGGGCACAATC
Mutagenesis:		
Wild type (R936W)	GGAGCAGATTACAGG**TGG**AGTTTTGATGAAACA	TGTTTCATCAAAACTCC**ACC**TGTAATCTGCTCC

All primer sequences are displayed from 5′ to 3′

Restriction sites are underlined

DNA sequence for mutated residue is bolded

Table 2-2. List of primers used for TopBP1 BRCT7/8 domain constructs.

Protein	5′-primer (forward)	3′-primer (reverse)
TopBP1 BRCT7/8 (1264-1490)	TGCGCGGGCGGATCCTTAAAAAAACAGTAC ATATTTCAG	TGCGGCGCGGCCGCTCAAATAGCTTCTGGTAGACA
TopBP1 BRCT7/8 (1264-1493)	TGCGCGGGCGGATCCTTAAAAAAACAGTAC ATATTTCAG	TGCGGCGCGGCCGCTCAAATAAATGAAATAGCTTC
TopBP1 BRCT7/8 (1264-1506)	TGCGCGGGCGGATCCTTAAAAAAACAGTAC ATATTTCAG	TGCGGCGCGGCCGCTCACTTTTGTGATAATCCAGT
TopBP1 BRCT7/8 (1264-1522)	TGCGCGGGCGGATCCTTAAAAAAACAGTAC ATATTTCAG	TGCGGCGCGGCCGCTCAGTGTACTCTAGGTCGTTT
Mutagenesis:		
S1273A	ATATTTCAGTTA**GCA**TCTCTGAATCCT	AGGATTCAGAGA**TGC**TAACTGAAATAT
R1280Q	AATCCTCAAGAA**CAG**ATTGACTATTGT	ACAATAGTCAAT**CTG**TTCTTGAGGATT
N1315A	CATCCACTTCGA**GCA**GAGAAGTATTTA	TAAATACTTCTC**TGC**TCGAAGTGGATG
Q1298A	GTGATAGAAAAG**GCA**TGCTTTGATCCC	GGGATCAAAGCA**TGC**CTTTTCTATCAC
K1317M	CTTCGAAACGAG**ATG**TATTTAGCCTCA	TGAGGCTAAATA**CAT**CTCGTTTCGAAG
R1314Q	GGACATCCACTT**CAA**AACGAGAAGTAT	ATACTTCTCGTT**TTG**AAGTGGATGTCC
R1407A	GTGGATCAGTCT**GCA**GAAGCAGGCTTC	GAAGCCTGCTTC**TGC**AGACTGATCCAC

All primer sequences are displayed from 5′ to 3′

Restriction sites are underlined

DNA sequence for mutated residue is bolded

2.1.3. TopBP1 BRCT4/5

Primers used to create TopBP1 BRCT5 and BRCT4/5 DNA fragments with flanking restriction sites are listed in Table 2-3. TopBP1 BRCT5 fragments were cloned into pGEX-4T-1 and TopBP1 BRCT4/5 was cloned into pGEX-6P-1. All clones were created with BamHI and NotI restriction sites, except for TopBP1 BRCT5 (634-746) and (634-739), which utilized SmaI and NotI restriction sites instead. BRCT5 mutants were engineered in BRCT5 (641-746).

2.2 Protein expression and purification

Constructs cloned in pGEX vectors were transformed into *E. coli* BL21 Gold strain and grown in LB media at 25 °C to an A_{600} of 0.6-0.8 prior to induction with 0.5 mM IPTG overnight at 22 °C.

Harvested cells were resuspended in lysis buffer (50 mM Tris-HCl pH 8.0, 150 mM NaCl, 1 mM EDTA and 0.1 % BME) supplemented with Complete EDTA-free protease inhibitor cocktail tablets (Roche Applied Science). To lyse the cells, the suspension was incubated with 1 mg/mL lysozyme (Sigma-Aldrich) for 30 min. on ice and sonicated with 5-10 5 sec. pulses separated by 30 sec. pauses on ice. The lysate was then centrifuged at 17,000 rpm for 45 min. using the JA-17 rotor (Beckman Coulter) to separate the soluble from insoluble fraction. The GST-tag fusion protein was purified using glutathione affinity chromatography with glutathione sepharose 4B beads (GE Healthcare) and eluted in elution buffer (20 mM Tris-HCl pH 7.5, 150 mM NaCl, 20 mM reduced glutathione and 0.1 % BME).

2.2.1. TopBP1 BRCT6

GST-TopBP1 BRCT6 was cleaved overnight with the site-specific protease designated by the pGEX vector (Thrombin protease (GE Healthcare) at room temperature for TopBP1 BRCT6 (W936R), PreScission protease at 4 °C for TopBP1 BRCT6). The TopBP1 BRCT6 polypeptide was then purified from GST by

Table 2-3. List of primers used for TopBP1 BRCT5 and BRCT4/5 domain constructs.

Protein	5′-primer (forward)	3′-primer (reverse)
TopBP1 BRCT5 (634-746)	TGCGGCCCCGGGTTTCACACCAGTTCCAGTAATG	TGCGGCGCGGCCGCTCATCGTTCTTCTTTAGTTGAATT
TopBP1 BRCT5 (634-739)	TGCGGCCCCGGGTTTCACACCAGTTCCAGTAATG	TGCGGCGCGGCCGCTCATTCAATCAGAAAATGGCT
TopBP1 BRCT5 (641-746)	TGCGGCGGATCCACAGGAATGACTCCTTTAGAG	TGCGGCGCGGCCGCTCATCGTTCTTCTTTAGTTGAATT
TopBP1 BRCT5 (641-739)	TGCGGCGGATCCACAGGAATGACTCCTTTAGAG	TGCGGCGCGGCCGCTCATTCAATCAGAAAATGGCT
TopBP1 BRCT4/5 (549-746)	TGCGGCGGATCCGAAGAAGGCTTATTTAGCCAA	TGCGGCGCGGCCGCTCATCGTTCTTCTTTAGTTGAATT
Mutagenesis:		
RK681/682EE	GAATACTTTGTT**GAGGAA**TCCAATGCAAAG	CTTTGCATTGGA**TTCCTC**AACAAAGTATTC
RK681/682AA	GAATACTTTGTT**GCAGCA**TCCAATGCAAAG	CTTTGCATTGGA**TGCTGC**AACAAAGTATTC
KK686/687EE	AAATCCAATGCA**GAGGAA**GGCATGTTTGCC	GGCAAACATGCC**TTCCTC**TGCATTGGATTT
KK686/687AA	AAATCCAATGCA**GCGGCA**GGCATGTTTGCC	GGCAAACATGCC**TGCCGC**TGCATTGGATTT
K701E	GAAGCTGCAAAG**GAG**TGGAATTTACCT	AGGTAAATTCCA**CTC**CTTTGCAGCTTC
K704M	CGTGGTGGCTCT**ATG**TATGAAGCTGCA	TGCAGCTTCATA**CAT**AGAGCCACCACG
S654A	GTTATTTCATTT**GCC**CAGTGTGCTGGA	TCCAGCACACTG**GGC**AAATGAAATAAC

All primer sequences are displayed from 5′ to 3′

Restriction sites are underlined

DNA sequence for mutated residue is bolded

gel filtration chromatography on a HiLoad 26/60 Superdex 75 column (GE-Amersham) in storage buffer (10 mM Tris-HCl pH 8.0, 150 mM NaCl and 1 mM DTT).

2.2.2. TopBP1 BRCT7/8

For seleno-methionine (Se-Met) labelling, TopBP1 BRCT7/8 was expressed in *E. Coli* BL21-Gold pLys S cells and grown under conditions that inhibit methionine production (Doublie, 1997).

GST was cleaved from GST-TopBP1 BRCT7/8 with PreScission protease at 4 °C overnight. The liberated TopBP1 BRCT7/8 polypeptide was then separated from GST by cation exchange chromatography using the SP Sepharose Fast Flow column (GE-Amersham) (buffer A: 50 mM HEPES pH 6.6, 0.1 % BME; buffer B: 50 mM HEPES pH 6.6, 1 M NaCl, 0.1 % BME). Further purification was achieved using gel filtration chromatography on a HiLoad 26/60 Superdex 75 column in storage buffer (10 mM Tris-HCl pH 7.5, 400 mM NaCl and 1 mM TCEP). Storage buffer components were resolved by dynamic light scattering (DLS) for optimal solubility of the protein. Se-Met TopBP1 BRCT7/8 (1264-1493) was purified in the same manner as native TopBP1 BRCT7/8. Incorporation of Se-Met in the protein was detected by MALDI-TOF mass spectrometry (Mass Spectrometry Facility, Dept. of Chemistry).

2.2.3. TopBP1 BRCT4/5

GST-TopBP1 BRCT5 was cleaved with Thrombin protease overnight at room temperature. BRCT5 was then purified from GST by cation exchange chromatography using the SP Sepharose Fast Flow column (buffer A: 50 mM HEPES pH 7, 0.1 % BME; buffer B: 50 mM HEPES pH 7, 1 M NaCl, 0.1 % BME). BRCT5 was further purified on a Superdex 75 column in storage buffer (10 mM Tris-HCl pH 8, 150 mM NaCl, 1 mM DTT).

GST-TopBP1 BRCT4/5 was cleaved with PreScission protease overnight at 4 °C. BRCT4/5 was then purified by anion exchange chromatography using the Q Sepharose Fast Flow column (buffer A: 50 mM HEPES pH 7, 0.1 % BME; buffer B: 50 mM HEPES pH 7, 1 M NaCl, 0.1 % BME). Since a fraction of GST co-eluted with BRCT4/5, residual GST was removed by incubating the pooled fractions with glutathione sepharose 4B beads (GE Healthcare) prior to a final purification on a HiLoad 26/60 Superdex 75 column in storage buffer (10 mM Tris-HCl pH 7.5, 150 mM NaCl, 1 mM DTT).

2.3 Limited proteolysis

Purified TopBP1 BRCT protein was concentrated to 2 mg/mL and incubated with 500 ng/mL, 50 ng/mL and 5 ng/mL trypsin on ice. 9 μL aliquots of the digest reaction were taken at 5, 15, 30 and 60 min. time points and quenched with 1 μL of 1 mg/mL PMSF. Samples were analyzed by SDS-PAGE. Trypsin resistant fragments were excised and characterized using LC-MS/MS (Mass Spectrometry Facility, Dept. of Chemistry) to determine the coverage of the trypsin fragment. In conditions where the trypsin resistant fragment was relatively pure, an aliquot was quenched with PMSF and analyzed using MALDI-TOF MS (Mass Spectrometry Facility, Dept. of Chemistry) to determine an accurate molecular weight.

2.4 Protein crystallization

2.4.1. TopBP1 BRCT6

Purified TopBP1 BRCT6 (893-996) was concentrated to 10 mg/mL in storage buffer (10 mM Tris-HCl pH 8.0, 150 mM NaCl and 1 mM DTT) for crystallization. Crystals were grown at 4 °C with hanging drop vapour diffusion by mixing 1 μL of protein with 2 μL of reservoir containing 0.1 M Tris-HCl, pH 6.8 and 16 % PEG 2000 MME. After 2 weeks, crystals were flash-cooled in a cryo-protectant consisting of reservoir solution supplemented with 20% glycerol.

2.4.2. TopBP1 BRCT7/8 and in complex with BACH1 phospho-peptide

Purified Se-Met TopBP1 BRCT7/8 (1264-1493) was concentrated to 18 mg/mL for crystallization. Se-Met derivative crystals were grown at room temperature using hanging drop vapour diffusion by mixing 2 μL of protein with 1 μL of reservoir containing 1.35 M Li_2SO_4 and 0.1 M Tris-HCl, pH 8. Crystals were flash-cooled in a cryo-protectant consisting of reservoir solution supplemented with 23 % glycerol. Native TopBP1 BRCT7/8 (1264-1493) concentrated to 12 mg/mL was incubated in a 1:2 molar ratio of protein:peptide (Ac-ESIYFpTPELYDPEDTKK-NH_2, Biomatik) for co-crystallization. Co-crystals were grown at room temperature by mixing 2 μL of protein with 1 μL of reservoir solution (3.5 M sodium formate, pH 8) and flash-cooled in reservoir solution and 15 % glycerol.

2.4.3. TopBP1 BRCT5, TopBP1 BRCT4/5 and BRCT4/5 in complex with MDC1 phospho-peptide

Crystals of TopBP1 BRCT5 (641-746) concentrated to 9 mg/mL were grown at 4 °C using hanging drop vapour diffusion. 2 μL protein was mixed with 1 μL reservoir consisting of 10 % PEG 1000 and 0.1 M Na/K phosphate pH 6.2. Crystals were flash-cooled in cryo-protectant containing reservoir solution and 26 % glycerol.

TopBP1 BRCT4/5 (549-746) was concentrated to 6.5 mg/mL for crystallization. Crystals were grown at room temperature in drops containing 1 μL protein and 1 μL reservoir (20 % PEG 3350 and 0.2 M NaSCN). Cryo-protectant used to flash-cool crystals contained reservoir solution supplemented with 15 % glycerol. For co-crystallization, TopBP1 BRCT4/5 (549-746) concentrated to 12 mg/mL was incubated with 1:6 molar ratio of protein:peptide (Ac-GFIDpSDpTDVEEE-NH_2, Biomatik) for 1 hr on ice. Co-crystals were grown at room temperature by adding 1 μL of protein:peptide mixture with 1 μL of

reservoir solution containing 0.1 M ammonium acetate, 0.1 M bis-Tris pH 5.5 and 17 % PEG 10,000. Co-crystals were flash-cooled in reservoir solution supplemented with 20 % glycerol.

2.5 Structure determination and refinement

2.5.1. TopBP1 BRCT6

Data were collected at the CMCF-1 beamline at the Canadian Light Source (CLS, Saskatoon). Intensity data were scaled and reduced using the HKL-2000 package (Otwinowski & Minor, 1997). Crystals of a TopBP1 BRCT6 variant (W936R) belonged to the space group *C2* with unit cell parameters a = 120.58 Å, b = 88.88 Å, c = 43.31 Å, β = 94.69 Å. In collaboration with Dr. David Baker (University of Washington), the Rosetta comparative modeling methodology (Qian et al, 2007) was employed to generate models for TopBP1 using the solution structure of the first BRCT domain in XRCC1 (PDB ID: 2D8M) as a starting template. The crystal structure of TopBP1 BRCT6 (W936R) was solved using molecular replacement by the program PHASER (McCoy, 2007) with the Rosetta-built model, placing three molecules in the asymmetric unit. Automated model building with ARP/wARP (Cohen et al, 2008) was used to build 263 of 270 residues, resulting in an initial R_{work} and R_{free} of 18.7 % and 23.7 %, respectively at 2.0 Å resolution.

Wildtype TopBP1 BRCT6 crystals were obtained in similar crystallization conditions and in the space group $P2_12_12_1$ with unit cell dimensions a = 35.77 Å, b = 51.82 Å, c = 62.09 Å. The partially refined BRCT6 (W936R) structure was used as a search model for molecular replacement with Phaser to find a solution. The final structure was refined at 1.34 Å resolution with TLS and anisotropic B-factor refinement, which yielded a R_{work} of 15.8 % and R_{free} of 17.3 % (Murshudov et al, 1997; Winn et al, 2001). The final model contains 818 protein atoms and 153 waters. We were unable to model residues 893–900 from the N-terminus and

residue 996 of the C-terminus, which are presumed to be disordered in the crystals. Model building was carried out in COOT (Emsley & Cowtan, 2004) and validated with PROCHECK (Laskowski et al, 1993). The Ramachandran plot contained 90.5% of all residues in most favoured regions, and 9.5 % of residues in additionally allowed regions. Detailed data collection and refinement statistics are listed in Table 2-4. All figures were made in PyMOL (http://www.pymol.org).

Coordinates for TopBP1 BRCT6 have been deposited in Protein Data Bank with the accession code 3JVE.

2.5.2. TopBP1 BRCT7/8 and in complex with BACH1 phospho-peptide

Data were collected at the CMCF-1 beamline at the Canadian Light Source (CLS, Saskatoon). Data for a single-wavelength anomalous dispersion (SAD) experiment was collected at the selenium peak from a TopBP1 BRCT7/8 Se-Met derivative crystal that belonged to the space group *C2* with unit cell parameters a = 120.58 Å, b = 32.75 Å, c = 81.76 Å, β = 109.3 Å. Intensity data were processed using the HKL-2000 package. Two selenium atom positions were found using SHELXD (Sheldrick, 2008) and refined using SOLVE (Terwilliger & Berendzen, 1999). Phases were improved by density modification with RESOLVE (Terwilliger & Berendzen, 1999), resulting in a figure of merit of 0.64. Automated model building was carried out in ARP/wARP using experimental phases and phase restraints to produce 214/235 built residues with side chains. Further model building was carried out in COOT and refinement using TLS and restrained refinement in REFMAC5. The final model lacks the N-terminal residues 1264-1265 and loop residues 1442-1449, which are presumed to be disordered in the crystals. The Ramachandran plot contained 94.8 % of all residues in the core and 5.2 % in allowed regions.

Table 2-4. Data collection and refinement statistics for TopBP1 BRCT6.

	TopBP1 BRCT6 (W936R)	TopBP1 BRCT6
Data Collection:		
Space group	*C2*	$P2_12_12_1$
Unit-cell parameters (Å)		
a, *b*, *c* (Å)	120.58, 88.88, 43.31	35.77, 51.82, 62.09
α, β, γ (°)	90, 94.69, 90	90, 90, 90
Resolution range (Å)	100-2.0 (2.07-2.00)	50-1.30 (1.38-1.34)
R_{sym} [a]	0.097 (0.380)	0.043 (0.326)
I/σ(I)	14.9 (2.5)	30.2 (2.1)
Completeness (%)	96.8 (74.2)	99.0 (91.6)
Redundancy	3.3 (2.4)	6.5 (3.3)
Refinement:		
Resolution (Å)		39.78-1.34
No. of reflections		25049 (1644)
R_{work}/R_{free} (%) [b]		15.8/17.3
No. of atoms		
Overall		971
Protein		818
Waters		153
Average *B* factor (Å^2)		
Overall		12.11
Protein		9.97
Waters		23.57
R.m.s. deviations		
Bonds (Å)		0.009
Angles (°)		1.208

[a] $R_{sym} = \Sigma|I-\langle I\rangle|^2 / \Sigma|I^2|$

[b] $R = \Sigma||F_o|-|F_c||/ \Sigma|F_o|$, R_{free} was calculated from 5 % of the data excluded from refinement

Intensity data from a TopBP1 BRCT7/8-BACH1 peptide complex crystal in space group $P6_222$ with unit cell parameters a = 78.07 Å, b = 78.07 Å, c = 136.77 Å were reduced and scaled using the HKL-2000 package. Phases for the TopBP1 BRCT7/8-BACH1 peptide complex were solved by molecular replacement using the apo TopBP1 BRCT7/8 structure as a model in PHASER. TopBP1 BRCT7/8 N-terminal residues 1264-1265, side chain of residue 1265, loop residues 1442-1449 and C-terminal residues 1492-1493 are disordered and missing from the model. We were also unable to model BACH1 phospho-peptide residues -5 and +6 to +9. The Ramachandran plot contained 92.0 % of all residues in the core and 8.0 % in allowed regions.

Detailed data collection and refinement statistics for the apo and complex structures are listed in Table 2-5. Models were validated with PROCHECK. Secondary structure prediction of the models was performed with DSSP (Kabsch & Sander, 1983) and converted using DSSP2PDB (http://structure.usc.edu/dssp2pdb/). Hydrogen bonding was verified using HBPLUS (McDonald & Thornton, 1994).

Coordinates for TopBP1 BRCT7/8 and TopBP1 BRCT7/8-BACH1 peptide complex have been deposited in the Protein Data Bank (accession codes 3AL2 and 3AL3).

2.5.3. TopBP1 BRCT4/5 and in complex with MDC1 phospho-peptide

Data for BRCT5 and BRCT4/5 crystals were collected at 8.3.1 beamline (Advanced Light Source, Berkeley). Intensity data from a BRCT5 crystal were processed to the space group *$P6_222$* with unit cell dimensions a = 91.00 Å, b = 91.00 Å, c = 114.31 Å. A starting model consisting of an ensemble of N-terminal BRCT domains (PDB ID: 1JNX, 1R1Z and 2ADO) was used in molecular replacement with PHASER, yielding a score of RF_Z = 4.2, TF_Z = 10.8 for a single copy. The solution was then partially built in COOT and refined to 3.3 Å

Table 2-5. Data collection and refinement statistics for TopBP1 BRCT7/8 and TopBP1 BRCT7/8-peptide complex.

	TopBP1 BRCT7/8 (Se-Met)	**TopBP1 BRCT7/8-peptide complex**
Data collection:		
Space group	*C*2	$P6_222$
Cell dimensions		
a, *b*, *c* (Å)	102.58, 32.75, 81.76	78.07, 78.07, 136.77
α, β, γ (°)	90.0, 109.3, 90.0	90.0, 90.0, 120.0
	Peak	
Wavelength	0.97879	0.97949
Resolution (Å)	50.0-2.0	50.0-2.15
R_{sym} [a]	6.2 (31.8)	4.6 (46.5)
$I / \sigma I$	14.1 (2.4)	29.0 (2.6)
Completeness (%)	99.1 (92.9)	99.9 (100.0)
Redundancy	3.6 (2.7)	6.8 (6.2)
Refinement:		
Resolution (Å)	31.0-2.00	33.9-2.15
No. reflections	17624 (902)	14021 (699)
R_{work} / R_{free} [b]	17.0/20.4	19.6/23.6
No. of atoms		
Protein	1755	1731
Peptide	-	92
Ligand	10	3
Water	182	96
Average *B* factor (Å^2)		
Protein	21.3	47.1
Peptide	-	39.8
Ligand	34.8	55.7
Water	32.9	57.1
R.m.s deviations		
Bond lengths (Å)	0.009	0.009
Bond angles (°)	1.346	1.258

[a] $R_{sym} = \Sigma|I-\langle I\rangle|^2 / \Sigma|I^2|$

[b] $R = \Sigma||F_o|-|F_c||/\Sigma|F_o|$, R_{free} was calculated from 5 % of the data excluded from refinement

resolution with TLS and restrained refinement in REFMAC5 to a R_{work} and R_{free} of 0.3887 and 0.4256, respectively.

Data from a BRCT4/5 crystal were scaled and reduced to the space group $P222_1$ with unit cell dimensions a = 35.90 Å, b = 48.80 Å, c = 126.09 Å. The partially refined BRCT5 structure was used in molecular replacement to find two copies (RF_Z = 5.0, TF_Z = 7.8; RF_Z = 3.3, TF_Z = 6.1), which represents one BRCT4/5 molecule in the asymmetric unit. This solution was refined using rigid body and restrained refinement with REFMAC5 (R_{work}/R_{free} = 0.5007/0.5402) before automated model building using ARP/wARP, which successfully built 191 residues with side chains. Further model building in COOT and refinement using PHENIX (Adams et al, 2010) at 1.9 Å resolution yielded a final R_{work} and R_{free} of 0.1723 and 0.2181, respectively. The Ramachandran plot contained 100 % of all residues in favoured regions and 0 % in outlier regions.

Data for crystals of the BRCT4/5-peptide complex were collected at the Canadian Light Source (CLS, Saskatoon). Intensity data were scaled and reduced using the XDS package (Kabsch, 2010) to the space group *P1* with unit cell dimensions a = 58.81 Å, b = 59.10 Å, c = 78.31 Å, α = 102.05 °, β = 98.04 °, γ = 114.34 °. The apo BRCT4/5 structure was used in PHASER to successfully find 4 copies in the asymmetric unit. Model building was carried out in COOT and refined using TLS refinement (1 group/chain) and 2-fold NCS restraints in PHENIX. The wxu_scale was set to 0.1 to reduce the X-ray/ADP weight. The final model was refined at 2.6 Å resolution to a R_{work} and R_{free} of 0.1910 and 0.2340, respectively. The Ramachandran plot contained 94.6 % of all residues in favoured regions, 99.3 % in allowed regions and 0.7 % in outlier regions.

Data collection and refinement statistics for the apo and peptide-bound structures are listed in Table 2-6. Models were validated with MolProbity (Chen et al, 2010). Secondary structure prediction of the models was performed with

Table 2-6. Data collection and refinement statistics for TopBP1 BRCT4/5 and TopBP1 BRCT4/5-peptide complex.

	TopBP1 BRCT5	**TopBP1 BRCT4/5**	**TopBP1 BRCT4/5-peptide complex**
Data collection:			
Space group	*$P6_222$*	*$P222_1$*	*P1*
Cell dimensions			
a, *b*, *c* (Å)	91.00, 91.00, 114.31	35.90, 48.80, 126.09	58.81, 59.10, 78.31
α, β, γ (°)	90, 90, 120	90, 90, 90	102.05, 98.04, 114.34
Resolution (Å)	50-3.30	63.04-1.90	34.57-2.60
R_{sym} [a]	0.048 (0.773)	0.077 (0.497)	0.059 (0.402)
$I / \sigma I$	34.9 (2.7)	18.0 (2.5)	11.9 (2.2)
Completeness (%)	99.9 (100)	99.8 (99.2)	95.2 (95.2)
Redundancy	14.5 (14.4)	3.8 (3.7)	2.1 (2.1)
Refinement:			
Resolution (Å)		38.60-1.90	34.57-2.60
No. reflections		18136 (926)	26637 (1330)
R_{work} / R_{free} [b]		0.1706/0.2149	0.1910/0.2340
No. of atoms			
Protein		1552	5716
Peptide		-	140
Ligand		3	-
Water		253	255
Average *B* factor (Å^2)			
Protein		17.9	52.0
Peptide		-	62.1
Ligand		15.2	-
Water		31.6	51.7
R.m.s deviations			
Bond lengths (Å)		0.008	0.009
Bond angles (°)		1.109	1.126

[a] $R_{sym} = \Sigma|I-\langle I\rangle|/ \Sigma|I|$

[b] $R = \Sigma||F_o|-|F_c||/ \Sigma|F_o|$, R_{free} was calculated from 5 % of the data excluded from refinement

DSSP and converted using DSSP2PDB. Hydrogen bonding was verified using HBPLUS.

Due to the relatively low resolution data and amino acid composition of the di-phospho-peptide, it was difficult to initially model the di-phospho-peptide without ambiguity. Therefore, the four BRCT4/5 protomers were fully refined to obtain the best possible unbiased electron density before building the two peptides. The largest positive peak from the F_o-F_c map (9 σ) was located in the phosphate-binding pocket of BRCT5 in protomer A. This was modelled as the phosphate moiety of the pThr because the γ-methyl group was also noticeable in the electron density. We successfully built two di-phospho-peptide chains spanning residues -3 to +4 relative to the pThr (Fig. 2-1A). Since small deviations were observed between the side chain conformations (Fig. 2-1B), 2-fold NCS restraints were not imposed for the peptide chains during refinement, which also yielded the lowest R_{free} statistics.

2.6 Fluorescence polarization

FP measurements were carried out using an Envision multi-label plate reader (Perkin Elmer) on a 384-well OptiPlate (Perkin Elmer). All peptides were synthesized and purified by Biomatik. FP assays were incubated for 15 min. at room temperature prior to taking FP measurements using an excitation wavelength of 485 nm and emission wavelength of 538 nm. Triplicate data points are represented in graphs as mean ± s.e.m. Curve fitting, K_d and IC_{50} calculations were obtained using PRISM software (GraphPad). K_i calculations were calculated using the IC_{50}-to-Ki converter (Cer et al, 2009).

For λ phosphatase treatment, 400 units of λ PPase (New England Biolabs) were incubated with 200 pmol of FITC-labelled phospho-peptide for 1 hr at 30°C. For heat inactivation, λ PPase was heat inactivated at 65 °C in 50 mM EDTA prior to incubation with FITC-phospho-peptide.

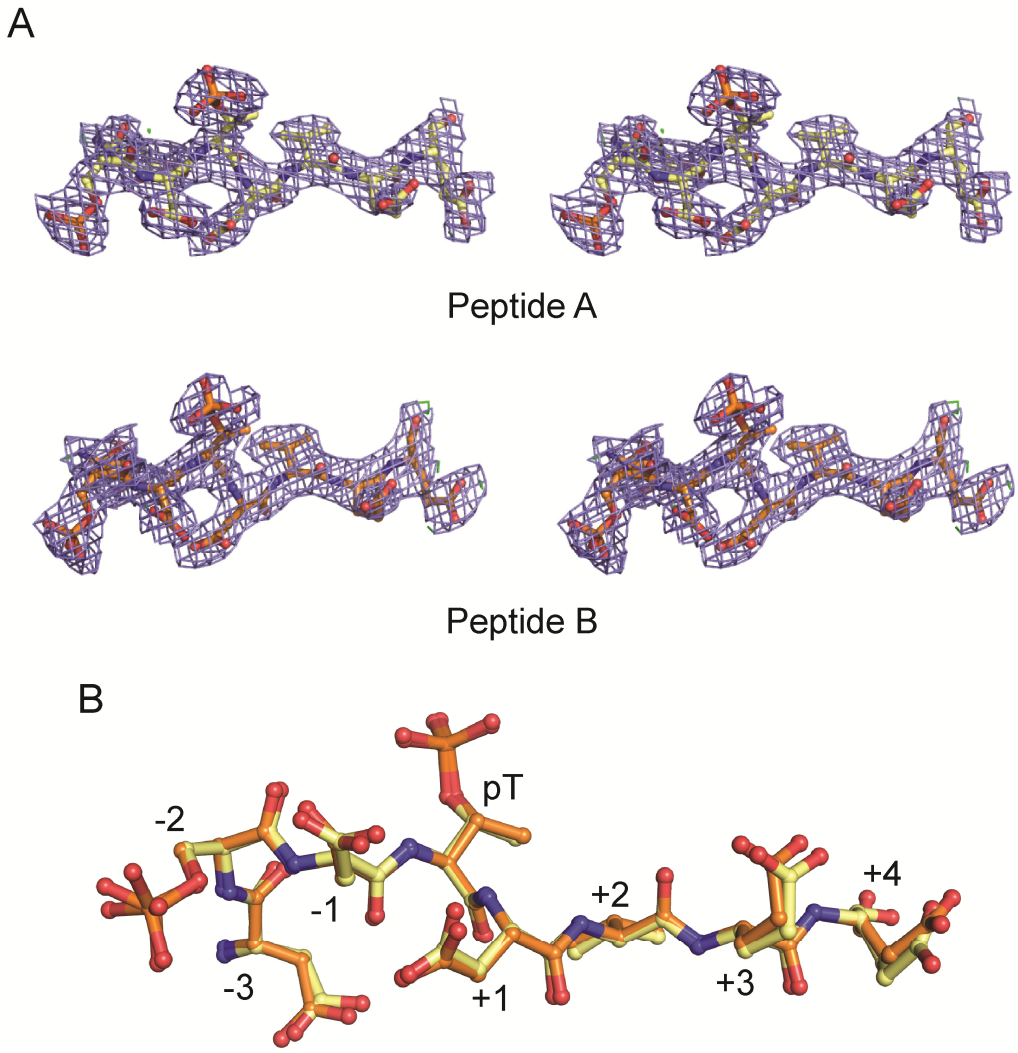

Figure 2-1. Modelling of the TopBP1 BRCT4/5 bound MDC1 di-phospho-peptides. (A) Stereoview of electron densities for the $2|F_o|-|F_c|$ map at 1σ (blue) and $|F_o|-|F_c|$ map at 3σ (green/red) for both peptides. (B) Superimposition of the di-phospho-peptides with residue positions labelled.

2.6.1. TopBP1 BRCT6

Each well consisted of 100 nM FITC-labelled phospho-peptide and increasing GST-fusion protein concentrations in FP buffer (10 mM Tris-HCl pH 7.5, 400 mM NaCl, 1 mM DTT and 0.05 % Tween-20). FITC-labelled phospho-peptides for E2F1 (FITC-RLLDSpSQIVIKK-NH_2) and BACH1 (FITC-GGSRSTpSPTFNK-NH_2) were used for FP.

2.6.2. TopBP1 BRCT7/8 with BACH1 phospho-peptide

For TopBP1 BRCT7/8 FP assays, each well consisted of 10 nM FITC-labelled BACH1 phospho-peptide (FITC-ESIYFpTPELYDPEDT-NH_2) and increasing GST-fusion protein concentrations in FP assay buffer (10 mM Tris-HCl pH 7.5, 400 mM NaCl, 1 mM TCEP, 0.05 % Tween-20). Competition assays were done by titrating increasing peptide concentrations with a saturated concentration of protein and 10 nM FITC-phospho-peptide. Competition assays for MDC1 and BRCA1 were done as previously described (Campbell et al, 2010). The competition peptides used for the assays are: pThr (Ac-ESIYFpTPELYDPEDTKK-NH_2 for TopBP1, Ac-pTPTF-OH for BRCA1, Ac-pTQEY-OH for MDC1) and pSer (Ac-ESIYFpSPELYDPEDTKK-NH_2 for TopBP1, Ac-pSPTF-OH for BRCA1, Ac-pSQEY-OH for MDC1).

2.6.3. TopBP1 BRCT4/5 and BRCT5 with MDC1 phospho-peptide

FP assays were performed with 10 nM FITC-labelled MDC1 di-phospho-peptide (FITC-GFIDpSDpTDVEEE-NH_2) and different GST-fusion protein concentrations in FP assay buffer (10 mM Tris-HCl pH 7.5, 150 mM NaCl, 1 mM DTT, 0.05 % Tween-20).

2.7 Isothermal titration calorimetry

2.7.1. TopBP1 BRCT6

The VP-ITC MicroCalorimetry System (Microcal) was used to perform ITC measurements. GST-BRCT6 and E2F1 phospho-peptide (Ac-RLLDSpSQIVI-NH_2) (Biomatik) were prepared in buffer (10 mM Tris-HCl pH 7.5, 150 mM NaCl and 0.05 % BME) and titration data was measured at 22 °C. Data was analyzed using ORIGIN software (Microcal).

2.8 Electrophoretic mobility shift assay (EMSA)

DNA oligonucleotides (Integrated DNA Technologies) were annealed and radiolabelled with γ^{32}P-ATP and T4 DNA ligase (Invitrogen) to generate DNA substrates. For EMSA, each 5 μL reaction consisted of 0.3 pmol of ^{32}P-labelled DNA substrate, 5 mg/mL BSA, 5 % glycerol, binding buffer (75 mM NaCl, 50 mM HEPES pH 7.5, 2 mM $MgCl_2$, 1 mM EDTA, 2 mM DTT) and increasing concentrations of protein. Binding reactions were incubated at room temperature for 1 hr and resolved at 4 °C on 10 % polyacrylamide gels in Tris/glycine buffer supplemented with 0.1 mM EDTA. Gels were exposed on a phosphor screen and scanned on a Typhoon Imager (GE Healthcare).

2.9 References

Adams PD, Afonine PV, Bunkoczi G, Chen VB, Davis IW, Echols N, Headd JJ, Hung LW, Kapral GJ, Grosse-Kunstleve RW, McCoy AJ, Moriarty NW, Oeffner R, Read RJ, Richardson DC, Richardson JS, Terwilliger TC, Zwart PH (2010) PHENIX: a comprehensive Python-based system for macromolecular structure solution. *Acta Crystallogr D Biol Crystallogr* **66:** 213-221

Campbell SJ, Edwards RA, Glover JNM (2010) Comparison of the structures and peptide binding specificities of the BRCT domains of MDC1 and BRCA1. *Structure* **18:** 167-176

Cer RZ, Mudunuri U, Stephens R, Lebeda FJ (2009) IC50-to-Ki: a web-based tool for converting IC50 to Ki values for inhibitors of enzyme activity and ligand binding. *Nucleic Acids Res* **37:** W441-445

Chen VB, Arendall WB, 3rd, Headd JJ, Keedy DA, Immormino RM, Kapral GJ, Murray LW, Richardson JS, Richardson DC (2010) MolProbity: all-atom structure validation for macromolecular crystallography. *Acta Crystallogr D Biol Crystallogr* **66:** 12-21

Cohen SX, Ben Jelloul M, Long F, Vagin A, Knipscheer P, Lebbink J, Sixma TK, Lamzin VS, Murshudov GN, Perrakis A (2008) ARP/wARP and molecular replacement: the next generation. *Acta Crystallogr D Biol Crystallogr* **64:** 49-60

Doublie S (1997) Preparation of selenomethionyl proteins for phase determination. *Methods Enzymol* **276:** 523-530

Emsley P, Cowtan K (2004) Coot: model-building tools for molecular graphics. *Acta Crystallogr D Biol Crystallogr* **60:** 2126-2132

Heckman KL, Pease LR (2007) Gene splicing and mutagenesis by PCR-driven overlap extension. *Nat Protoc* **2:** 924-932

Kabsch W (2010) Xds. *Acta Crystallogr D Biol Crystallogr* **66:** 125-132

Kabsch W, Sander C (1983) Dictionary of protein secondary structure: pattern recognition of hydrogen-bonded and geometrical features. *Biopolymers* **22:** 2577-2637

Laskowski RA, MacArthur MW, Moss DS, Thornton JM (1993) PROCHECK: a program to check the stereochemical quality of protein structures. *J Appl Crystallogr* **26:** 283-291

McCoy AJ (2007) Solving structures of protein complexes by molecular replacement with Phaser. *Acta Crystallogr D Biol Crystallogr* **63:** 32-41

McDonald IK, Thornton JM (1994) Satisfying hydrogen bonding potential in proteins. *J Mol Biol* **238:** 777-793

Murshudov GN, Vagin AA, Dodson EJ (1997) Refinement of macromolecular structures by the maximum-likelihood method. *Acta Crystallogr D Biol Crystallogr* **53:** 240-255

Otwinowski Z, Minor W (1997) Processing of X-ray Diffraction Data Collected in Oscillation Mode. *Methods Enzymol* **276:** 307-326

Qian B, Raman S, Das R, Bradley P, McCoy AJ, Read RJ, Baker D (2007) High-resolution structure prediction and the crystallographic phase problem. *Nature* **450:** 259-264

Sheldrick GM (2008) A short history of SHELX. *Acta Crystallogr A* **64:** 112-122

Terwilliger TC, Berendzen J (1999) Automated MAD and MIR structure solution. *Acta Crystallogr D Biol Crystallogr* **55:** 849-861

Winn MD, Isupov MN, Murshudov GN (2001) Use of TLS parameters to model anisotropic displacements in macromolecular refinement. *Acta Crystallogr D Biol Crystallogr* **57:** 122-133

Chapter 3

Insights from the crystal structure of TopBP1 BRCT6 in the DNA damage response

A version of this chapter is published in:

Leung CC, Kellogg E, Kuhnert A, Hanel F, Baker D, Glover JN (2010) Insights from the crystal structure of the sixth BRCT domain of Topoisomerase IIβ binding protein 1. *Protein Sci.* **19**:162-7.

3.1 Introduction

The role of TopBP1 as an integrator of DNA damage response signalling relies on its numerous conserved BRCT domains to facilitate protein-protein interactions. Given that the molecular basis of single BRCT domain functions remains unclear, the sixth BRCT domain of TopBP1 was an intriguing target to study because it is implicated in interactions with phospho-peptides, poly(ADP-ribose) polymerase 1 (PARP-1) and poly(ADP-ribose) chains.

TopBP1 BRCT6 interacts with the transcription factor, E2F1, to regulate E2F1 activity in response to DNA damage (Liu et al, 2003). E2F1 belongs to the E2F family of transcription factors that regulate a diverse array of genes encoding proteins involved in DNA replication and cell cycle progression. Unlike other E2F family proteins, E2F1 is specific for inducing apoptosis and is phosphorylated by ATM/ATR in response to DNA damage (DeGregori et al, 1997; Kowalik et al, 1998; Lin et al, 2001). The interaction between TopBP1 BRCT6 and E2F1 is dependent on the E2F1 phosphorylation of Ser31 by ATM, and results in the repression of multiple activities associated with E2F1, including transcriptional activity, induction of apoptosis, and S-phase entry (Liu et al, 2003).

PARP-1 is a member of the PARP family of proteins and has an established role in DNA SSB repair (Dantzer et al, 2000; Dantzer et al, 1999). In response to DNA SSBs, PARP-1 recognizes the nicked DNA ends via two Zinc fingers and catalyzes the synthesis of poly(ADP-ribose) on itself and other target proteins to coordinate numerous activities such as DNA repair, DNA replication, transcription, cytoskeletal organization and protein degradation (Krishnakumar & Kraus, 2010; Schreiber et al, 2006). Wollman et al. have demonstrated that TopBP1 BRCT6 interacts with PARP-1 and is a target for poly(ADP-ribosyl)ation (Wollmann et al, 2007). This consequently disrupts the interaction between the downstream TopBP1 BRCT7 and Miz-1, which is critical for the role of Miz-1 in

mediating cell cycle arrest. Furthermore, TopBP1 BRCT6 also contains a consensus PAR-binding sequence that has been shown in other BRCT domains, such as XRCC1, to bind PAR (Pleschke et al, 2000). Therefore, it is likely that TopBP1 BRCT6 is involved in PARP-1 mediated signalling.

To gain a better understanding of the multiple functions proposed for TopBP1 BRCT6, we solved the crystal structure of TopBP1 BRCT6 to 1.34 Å resolution. The structure reveals a canonical BRCT fold containing a degenerate pSer binding pocket lacking conserved phosphate-binding residues. TopBP1 BRCT6 also lacks the hydrophobic surface that is required for packing of two tandem repeats, suggesting that BRCT6 likely exists and functions as a single BRCT domain. The structure also provides insight into the consensus PAR-binding motif in TopBP1 BRCT6 that likely does not bind PAR, as well as common Glu residues that may be poly(ADP-ribosyl)ated by PARP-1.

3.2 Results

3.2.1. Crystal structure of TopBP1 BRCT6

The crystal structure of TopBP1 BRCT6 was solved to 1.34 Å resolution. TopBP1 BRCT6 both purified and crystallized as a monomer, with one BRCT6 molecule present in the asymmetric unit. Like other BRCT domains, the overall fold of TopBP1 BRCT6 consists of a central four-stranded parallel β-sheet flanked on one side by a single α-helix (α_2) and on the opposite side by a pair of α-helices (α_1 and α_3) (Fig. 3-1A). Structural alignment of the BRCT domain with the N-terminal BRCT domains of BRCA1 and MDC1 also confirm a conserved core involving the β-sheet packed against the α-helices (Fig. 3-1B). In contrast, both the length and orientation of the connecting loops, particularly the β_1-α_1 and β_3-α_2 loops, show less conservation. Unique to the TopBP1 BRCT6 structure is the incorporation of a 3_{10}-helix, which replaces the majority of the β_1-α_1 loop found in other BRCT domains.

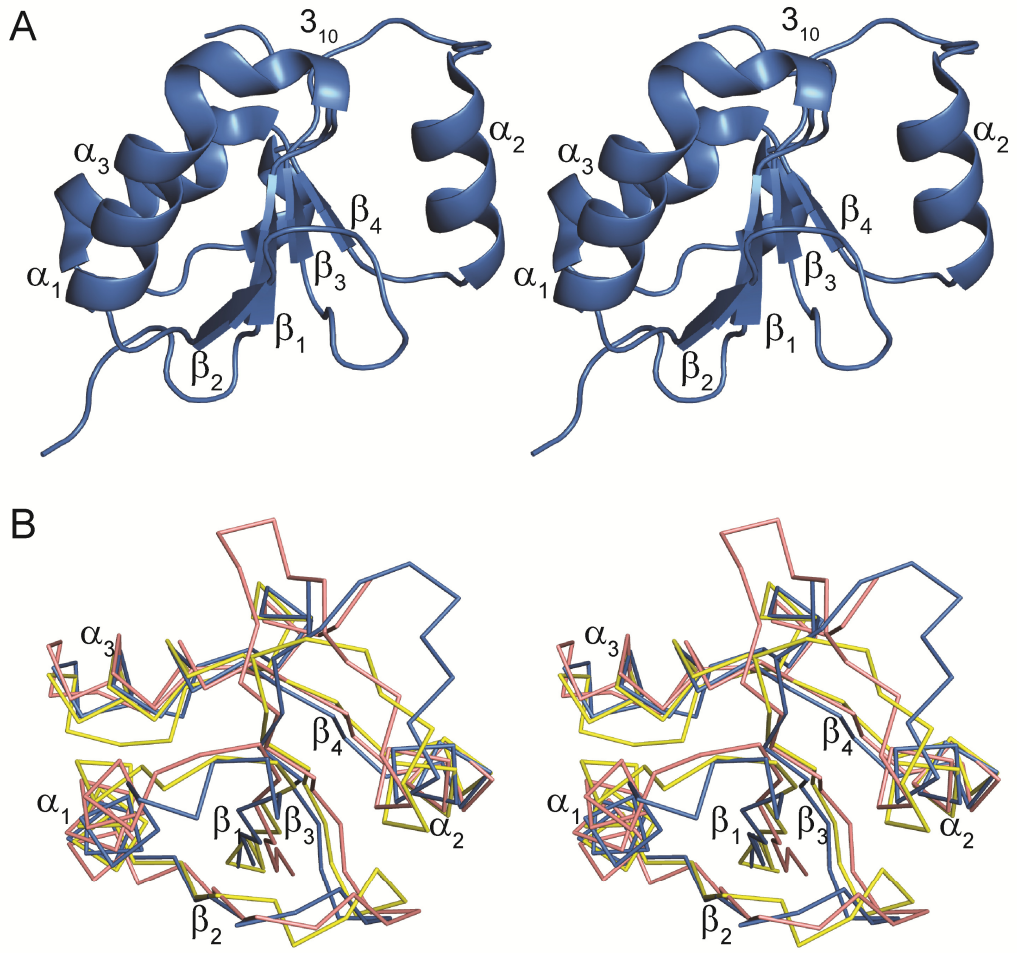

Figure 3-1. Conserved BRCT fold of TopBP1 BRCT6. (A) Ribbon model of TopBP1 BRCT6 in stereoview. Secondary structure elements are labelled. (B) TopBP1 BRCT6 (blue) superimposed with the N-terminal BRCT domains of BRCA1 (pink, PDB ID: 1JNX) and MDC1 (yellow, PDB ID: 2ADO) in stereoview.

3.2.2. TopBP1 BRCT6 contains a degenerate phospho-peptide binding pocket

Contrary to previous reports by Yu et al. (Yu et al, 2003), we were unable to observe binding of an E2F1 phospho-peptide encompassing pSer31 (RLLDSpSQIVI) to TopBP1 BRCT6. To investigate the interaction between TopBP1 BRCT6 and E2F1 *in vitro*, we performed binding experiments using isothermal titration calorimetry (ITC) and fluorescence polarization (FP). While we were able to detect robust binding between the BRCA1 BRCT repeats and its phospho-peptide target derived from BACH1, we were unable to detect interactions between TopBP1 BRCT6 and an E2F1 phospho-peptide in either of these assays (Fig. 3-2).

The crystal structures of tandem BRCT repeats in complex with cognate phospho-peptides, such as in BRCA1 and MDC1, have provided key insights into the mechanism by which the BRCT repeat is selective for a phospho-peptide (Clapperton et al, 2004; Shen & Tong, 2008; Shiozaki et al, 2004; Stucki et al, 2005; Williams et al, 2004). In both BRCA1 and MDC1 structures, the pSer of the bound phospho-peptide is recognized by three structurally conserved residues (Ser1655/Thr1898, Gly1656/Gly1899 and Lys1702/Lys1936 in BRCA1/MDC1 respectively) in the N-terminal BRCT domain (Fig. 3-3). These residues make three essential contacts with the phosphate moiety and form the phosphate recognition pocket in the BRCT domain. In addition, a conserved Thr1700/Thr1934 residue in α_2 makes a hydrogen bond with Ser1655/Thr1898 of BRCA1/MDC1 in order to provide the correct orientation for interaction with the phosphate oxygen. Surprisingly, only Ser1655/Thr1898 is conserved in TopBP1 BRCT6 (Ser913) (Fig. 3-3A and B). Structural alignment of the phosphate binding pocket of BRCA1 with TopBP1 BRCT6 also supports the lack of conservation. The conserved Ser913 of TopBP1 BRCT6 points away from the solvent as a result of the additional 3_{10}-helix between β_1 and α_1. In addition, the substitution of the conserved Gly1656/Gly1899 of BRCA1/MDC1 to Lys914 in the 3_{10}-helix of

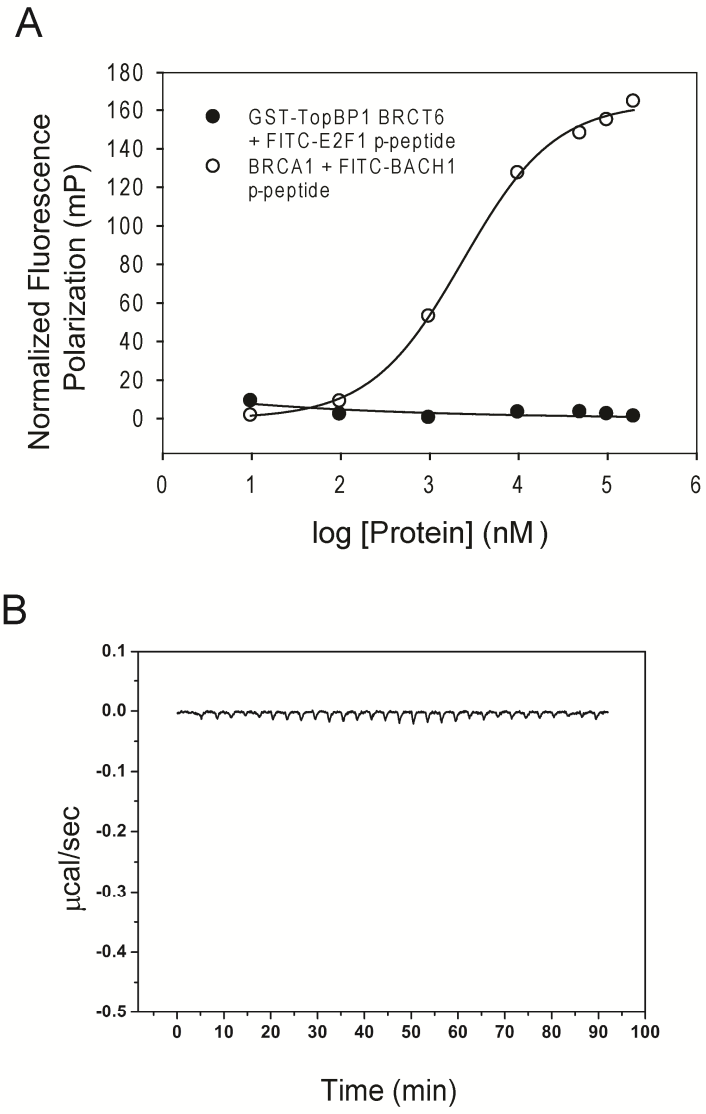

Figure 3-2. Binding assays of TopBP1 BRCT6 and E2F1 phospho-peptide. (A) Fluorescence polarization assay of GST-TopBP1 BRCT6 with FITC-labelled E2F1 phospho-peptide. Binding of BRCA1 and FITC-labelled BACH1 phospho-peptide is shown as a positive control. (B) Isothermal titration calorimetry isotherm of TopBP1 BRCT6 with E2F1 phospho-peptide.

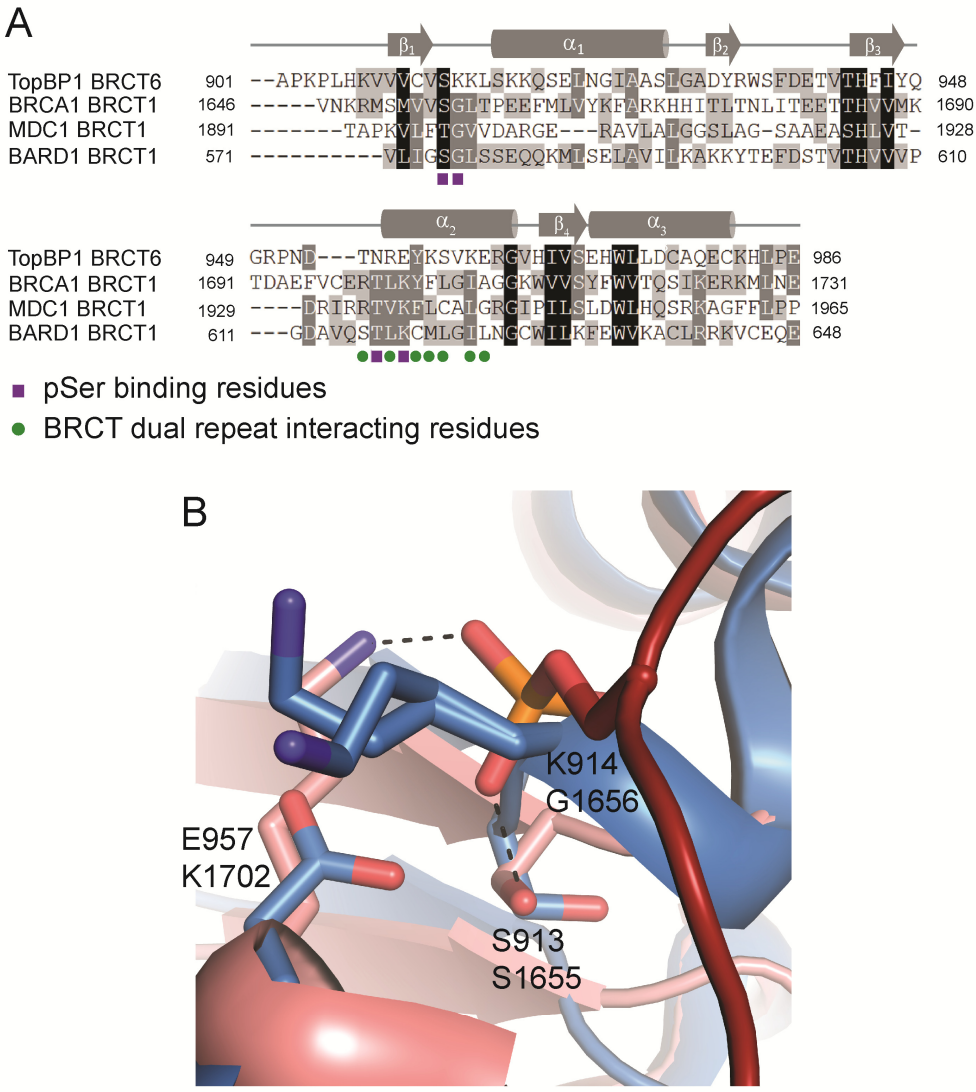

Figure 3-3. Comparison of TopBP1 BRCT6 to phospho-peptide binding tandem BRCT repeats. (A) Sequence alignment of TopBP1 BRCT6 with N-terminal BRCT domains of BRCA1, MDC1 and BARD1. Residues are shaded based on levels of conservation. Secondary structure elements are plotted above the sequences. Conserved residues involved in pSer binding are shown as purple squares. Conserved residues involved in BRCT repeat packing are shown as green circles. (B) Structural alignment of the pSer binding pocket of BRCA1 (pink, PDB ID: 1T15) with TopBP1 BRCT6 (blue). The BACH1 phospho-peptide is shown in red. Hydrogen bonding is designated as dotted lines. Equivalent hydrogen bonding residues in BRCA1 (below) and TopBP1 (above) are displayed.

TopBP1 BRCT6 alters the orientation of the main chain NH such that it is unlikely to form a hydrogen bond with a bound phosphate oxygen. Instead, both Lys914 and Lys915 side chains protrude from the putative pSer binding pocket and are predicted to clash with a putative phospho-peptide. Substitution of the conserved Lys to Glu (Glu957) in α_2 would also repel the negative charge of the phosphate group. Overall, the degenerate phospho-peptide binding pocket in TopBP1 BRCT6 would likely perturb any phospho-peptide interaction.

3.2.3. TopBP1 BRCT6 likely does not form a tandem BRCT repeat

Another requirement for phospho-peptide binding by the tandem BRCT repeats of BRCA1 and MDC1 is the hydrophobic packing of the two BRCT repeats in order to form a specificity pocket for the +3 position of the phospho-peptide. This is facilitated by conserved hydrophobic residues in α_2 of the N-terminal BRCT and α_1 and α_3 of the C-terminal BRCT. Previous studies by Liu et al. have suggested that TopBP1 oligomerization could potentially bring two TopBP1 BRCT6 molecules together in a fashion similar to BRCT repeats to recognize the E2F1 phospho-peptide (Liu et al, 2006). Although TopBP1 BRCT6 purified and crystallized as a monomer, we investigated whether TopBP1 BRCT6 might pack with another BRCT repeat in a similar manner. Interestingly, many of the conserved hydrophobic residues in α_2 that are involved at the BRCT-BRCT interface in BRCA1 and MDC1 are not present in TopBP1 BRCT6 and are replaced by charged residues (Fig. 3-4). These include Arg1699/Thr954, Leu1701/Arg956, Phe1704/Lys959, Leu1705/Ser960, Ile1707/Lys962 and Ala1708/Glu963 in BRCA1/TopBP1, respectively. Crystal packing of TopBP1 BRCT6 also does not provide evidence for a related packing between symmetry molecules (Fig. 3-5). Therefore, it is unlikely that TopBP1 BRCT6 can pack in a dimer analogous to the tandem BRCT repeats in BRCA1 and MDC1.

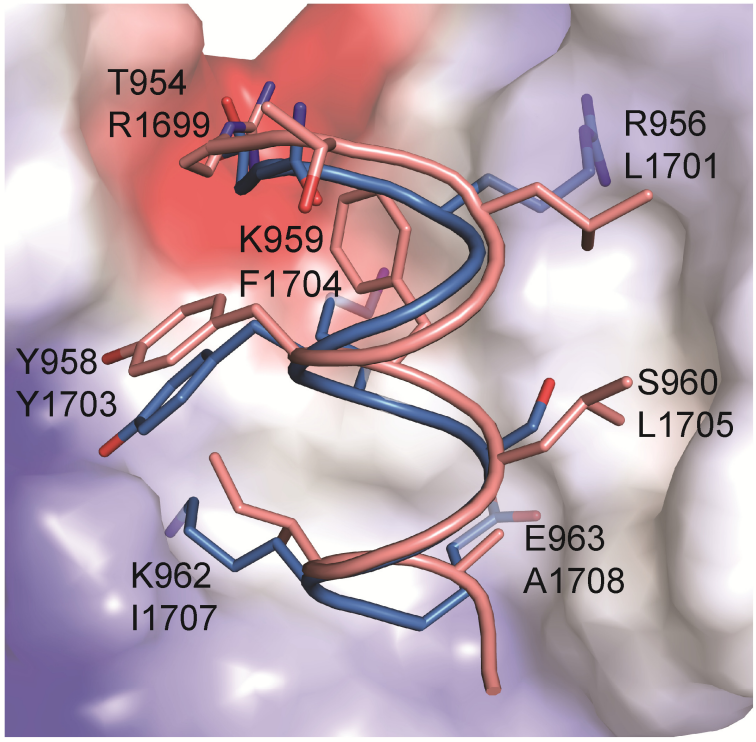

Figure 3-4. Structural alignment of the α_2-helix in BRCA1 (pink, PDB ID: 1JNX) and TopBP1 BRCT6 (blue). The α_2-helix is shown in cartoon representation and packs against the C-terminal BRCT of BRCA1 (represented as electrostatic surface). Equivalent residues of TopBP1 BRCT6 (above) and BRCA1 (below) are shown.

Figure 3-5. Crystal packing of TopBP1 BRCT6. α-helices involved in tandem BRCT-BRCT interfaces are coloured yellow and labelled. Symmetry mates are coloured grey.

3.2.4. Implications for TopBP1 BRCT6 PAR binding and PARP-1 modification

Pleschke et al previously identified a consensus PAR-binding motif (hxbxhhxbhhb, where h is hydrophobic, b is basic and x is any residue) present in a number of proteins (Pleschke et al, 2000). Since TopBP1 BRCT6 contains a similar sequence spanning residues 908 to 918, we wondered if TopBP1 BRCT6 could bind to PAR chains. We established a collaboration with Dr. Frank Hanel (Hans Knoell Institute), whose lab originally characterized the interaction between TopBP1 BRCT6 and PARP-1. Using a PAR binding assay as described by Panzeter et al. (Panzeter et al, 1993), Dr. Anja Kuhnert (Hanel lab) was unable to detect any binding of TopBP1 BRCT6 to PAR chains *in vitro*. This is supported in the BRCT6 structure, where mapping of the consensus PAR-binding motif in BRCT6 reveals a region that is partially buried in the core of the BRCT fold and unlikely involved in mediating interactions (Fig. 3-6). As a result, we hypothesize that TopBP1 BRCT6 is an unlikely candidate for binding PAR chains.

TopBP1 BRCT6 interacts with PARP-1 and can be poly-ADP(ribosyl)ated by PARP-1 *in vitro* (Wollmann et al, 2007). The N-terminal interacting region of PARP-1 is comprised of a Zinc finger DNA binding domain and an auto-modification domain. Intriguingly, this auto-modification domain consists largely of a BRCT domain that shows a relatively high sequence identity to TopBP1 BRCT6 (25% sequence identity) (Yamane et al, 1997). In particular, some putative auto-modification Glu residues in PARP-1 are conserved in TopBP1 BRCT6 and are surface exposed (Fig. 3-6). Because TopBP1 binds to a number of proteins in the DNA damage response, Glu922, Glu963, Glu971 and Glu986 of TopBP1 may serve as potential sites of PARP-1 poly(ADP-ribosyl)ation as an important way of regulating the activities of both TopBP1 and its protein partners. Further studies will be needed to determine if these specific Glu residues in TopBP1 are indeed modified by PARP-1.

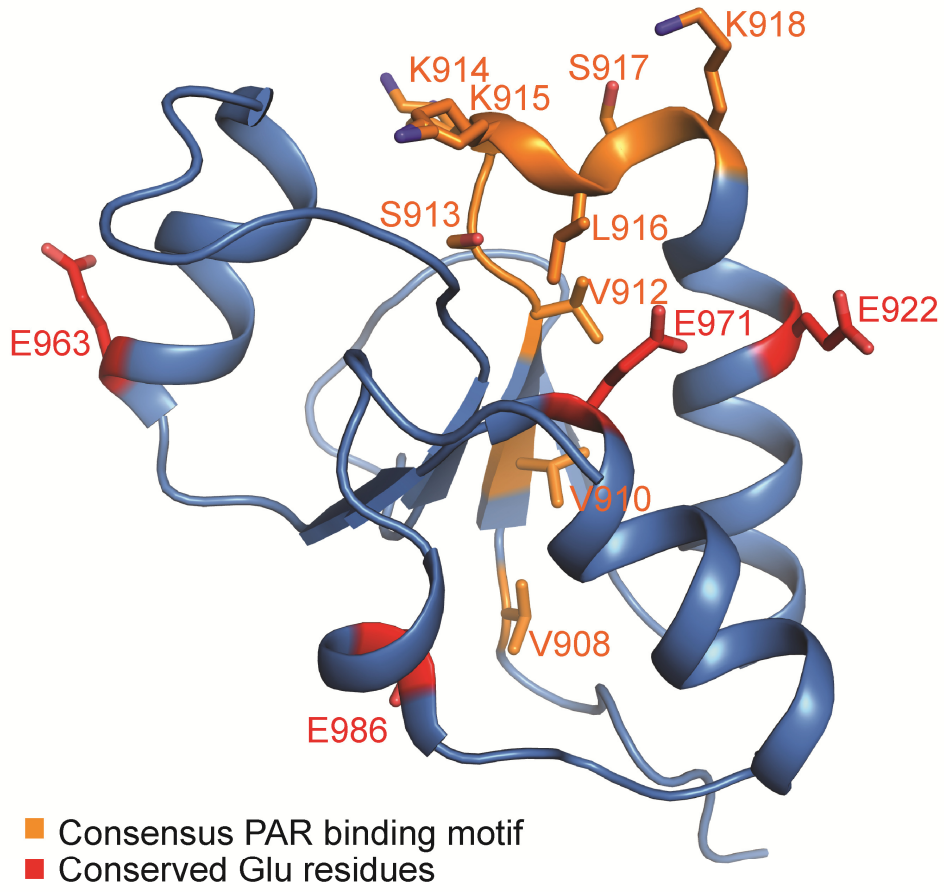

Figure 3-6. Mapping of putative PAR binding and PARP-1 modification residues in TopBP1 BRCT6. Consensus PAR-binding motif residues are shown in orange. Putative PARP-1 auto-modification Glu residues common in TopBP1 BRCT6 are indicated in red.

3.3 Discussion

The sixth BRCT domain of TopBP1 has been implicated in a number of biological functions associated with roles in the DNA damage response. Binding of TopBP1 BRCT6 to phosphorylated E2F1 negatively regulates E2F1-induced apoptosis (Liu et al, 2003). Interactions with PARP-1 disrupt binding of TopBP1 BRCT7 to Miz-1, which is critical for Miz-1-mediated cell cycle arrest (Wollmann et al, 2007). Furthermore, TopBP1 BRCT6 contains a consensus PAR-binding motif that has established PAR binding activity in other proteins (Pleschke et al, 2000). Interestingly, our structural and biochemical studies of TopBP1 BRCT6 do not support these previously suggested phospho-peptide and PAR interactions.

The crystal structure of TopBP1 BRCT6 reveals a degenerate phosphate-binding pocket that likely compromises phosphate coordination. Besides the lack of conserved phosphate-binding residues, the additional 3_{10}-helix would also likely block a phospho-peptide from binding. In support of this, we were also unable to detect any direct interaction *in vitro* between GST-BRCT6 and an E2F1 phospho-peptide using FP or ITC. Although it seems unlikely, interactions between TopBP1 BRCT6 and phospho-E2F1 would have to be extremely weak or require further interactions in order to be stable. Previous studies by Liu et al provided evidence that oligomerization of TopBP1 through a phospho-peptide interaction mediated by the C-terminal BRCT7/8 repeats is required for this interaction (Liu et al, 2006). This oligomerization is dependent on phosphorylation of TopBP1 at Ser1159 by Akt/protein kinase B (PKB). Given the less extensive binding surface and absence of a +3 specificity pocket, one might suspect that the recognition of phospho-peptides by single BRCT domains would be weaker than tandem BRCT domains. Single BRCT domain interactions may participate in more transient signalling processes or may require additional contacts provided within oligomeric complexes and/or from other protein domains, to stabilize these interactions.

The presence of a consensus PAR-binding motif in TopBP1 BRCT6 suggested that another function could be to recognize PAR chains in DDR signalling (Pleschke et al, 2000). In collaboration with Dr. Frank Hanel, we did not detect any measurable binding of TopBP1 BRCT6 to PAR chains, and mapping of the PAR-binding motif in the structure also does not support PAR binding. A consensus PAR-binding motif is also found in the N-terminal BRCT of XRCC1, and there is more evidence supporting XRCC1 BRCT1 as a validated PAR-binding module. XRCC1 BRCT1 preferentially recognizes poly(ADP-ribosyl)ated PARP-1 and a peptide of the XRCC1 PAR-binding sequence binds to PAR *in vitro* (Dantzer et al, 2000; El-Khamisy et al, 2003; Masson et al, 1998; Pleschke et al, 2000). Comparison of the structures of TopBP1 BRCT6 and XRCC1 BRCT1 reveal that their respective PAR-binding motifs are not structurally conserved. Whereas the motif is exposed on the surface of XRCC1 in α_3, α_4 and α_3-α_4 loop, the PAR-binding motif in TopBP1 BRCT6 is localized to the β_1, α_1 and 3_{10}-helix and partially buried in the protein core (Figure 3-7). Taken together, our data suggests that the presence of a PAR-binding motif in TopBP1 BRCT6 is likely an artefact.

TopBP1 BRCT6 also interacts directly with the N-terminal region of PARP-1 containing the DNA-binding domain and BRCT domain. This interaction does not require poly(ADP-ribosyl)ation, although a slight increase in binding was observed in UV-irradiated cells, suggesting that PAR synthesis on either TopBP1 BRCT6 or PARP-1 may increase accessibility and/or affinity of the proteins (Wollmann et al, 2007). Since we have demonstrated that the PAR-binding motif in TopBP1 BRCT6 is non-functional, it is more reasonable to suspect that poly(ADP-ribosyl)ation of TopBP1 BRCT6 mediates binding to PARP-1. Interestingly, the solution structure of the PARP-1 BRCT domain (PDB ID: 2COK, unpublished) reveals a largely electropositive surface, which could potentially complement the negatively charged PAR modifications on TopBP1 BRCT6.

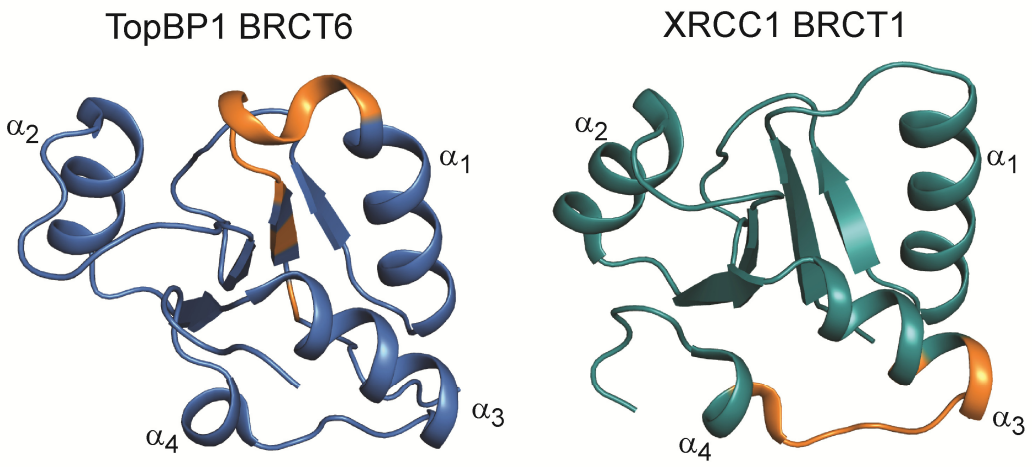

Figure 3-7. The consensus PAR-binding motif is not conserved in TopBP1 and XRCC1. The PAR-binding motif (orange) is mapped in the structures of TopBP1 BRCT6 (left) and XRCC1 BRCT1 (right).

Clearly, further investigations will be required to elucidate the puzzling basis of TopBP1 BRCT6, as well as other single BRCT domains, in phospho-peptide, PAR and PARP-1 interactions.

3.4 References

Clapperton Ja, Manke Ia, Lowery DM, Ho T, Haire LF, Yaffe MB, Smerdon SJ (2004) Structure and mechanism of BRCA1 BRCT domain recognition of phosphorylated BACH1 with implications for cancer. *Nat Struct Mol Biol* **11:** 512-518

Dantzer F, de La Rubia G, Ménissier-De Murcia J, Hostomsky Z, de Murcia G, Schreiber V (2000) Base excision repair is impaired in mammalian cells lacking Poly(ADP-ribose) polymerase-1. *Biochemistry* **39:** 7559-7569

Dantzer F, Schreiber V, Niedergang C, Trucco C, Flatter E, De La Rubia G, Oliver J, Rolli V, Menissier-de Murcia J, de Murcia G (1999) Involvement of poly(ADP-ribose) polymerase in base excision repair. *Biochimie* **81:** 69-75

DeGregori J, Leone G, Miron A, Jakoi L, Nevins JR (1997) Distinct roles for E2F proteins in cell growth control and apoptosis. *Proc Natl Acad Sci U S A* **94:** 7245-7250

El-Khamisy SF, Masutani M, Suzuki H, Caldecott KW (2003) A requirement for PARP-1 for the assembly or stability of XRCC1 nuclear foci at sites of oxidative DNA damage. *Nucleic Acids Res* **31:** 5526-5533

Kowalik TF, DeGregori J, Leone G, Jakoi L, Nevins JR (1998) E2F1-specific induction of apoptosis and p53 accumulation, which is blocked by Mdm2. *Cell Growth Differ* **9:** 113-118

Krishnakumar R, Kraus WL (2010) The PARP side of the nucleus: molecular actions, physiological outcomes, and clinical targets. *Mol Cell* **39:** 8-24

Lin WC, Lin FT, Nevins JR (2001) Selective induction of E2F1 in response to DNA damage, mediated by ATM-dependent phosphorylation. *Genes Dev* **15:** 1833-1844

Liu K, Lin F-T, Ruppert JM, Lin W-C (2003) Regulation of E2F1 by BRCT domain-containing protein TopBP1. *Mol Cell Biol* **23:** 3287-3304

Liu K, Paik JC, Wang B, Lin F-T, Lin W-C (2006) Regulation of TopBP1 oligomerization by Akt/PKB for cell survival. *EMBO J* **25:** 4795-4807

Masson M, Niedergang C, Schreiber V, Muller S, Menissier-de Murcia J, de Murcia G (1998) XRCC1 is specifically associated with poly(ADP-ribose) polymerase and negatively regulates its activity following DNA damage. *Mol Cell Biol* **18:** 3563-3571

Panzeter PL, Zweifel B, Malanga M, Waser SH, Richard M, Althaus FR (1993) Targeting of histone tails by poly(ADP-ribose). *J Biol Chem* **268:** 17662-17664

Pleschke JM, Kleczkowska HE, Strohm M, Althaus FR (2000) Poly(ADP-ribose) binds to specific domains in DNA damage checkpoint proteins. *J Biol Chem* **275:** 40974-40980

Schreiber V, Dantzer F, Ame JC, de Murcia G (2006) Poly(ADP-ribose): novel functions for an old molecule. *Nat Rev Mol Cell Biol* **7:** 517-528

Shen Y, Tong L (2008) Structural evidence for direct interactions between the BRCT domains of human BRCA1 and a phospho-peptide from human ACC1. *Biochemistry* **47:** 5767-5773

Shiozaki EN, Gu L, Yan N, Shi Y (2004) Structure of the BRCT repeats of BRCA1 bound to a BACH1 phosphopeptide: implications for signaling. *Mol Cell* **14:** 405-412

Stucki M, Clapperton Ja, Mohammad D, Yaffe MB, Smerdon SJ, Jackson SP (2005) MDC1 directly binds phosphorylated histone H2AX to regulate cellular responses to DNA double-strand breaks. *Cell* **123:** 1213-1226

Williams RS, Lee MS, Hau DD, Glover JN (2004) Structural basis of phosphopeptide recognition by the BRCT domain of BRCA1. *Nat Struct Mol Biol* **11:** 519-525

Wollmann Y, Schmidt U, Wieland GD, Zipfel PF, Saluz H-P, Hänel F (2007) The DNA topoisomerase IIbeta binding protein 1 (TopBP1) interacts with poly (ADP-ribose) polymerase (PARP-1). *Journal of cellular biochemistry* **102:** 171-182

Yamane K, Kawabata M, Tsuruo T (1997) A DNA-topoisomerase-II-binding protein with eight repeating regions similar to DNA-repair enzymes and to a cell-cycle regulator. *European journal of biochemistry / FEBS* **250:** 794-799

Yu X, Chini CCS, He M, Mer G, Chen J (2003) The BRCT domain is a phospho-protein binding domain. *Science* **302:** 639-642

Chapter 4

Molecular basis of BACH1/FANCJ recognition by TopBP1 BRCT7/8 in DNA replication checkpoint control

A version of this chapter is published in:

Leung CC, Gong Z, Chen J, Glover JN (2011) Molecular basis of BACH1/FANCJ recognition by TopBP1 in DNA replication checkpoint control. *J Biol Chem* **286**: 4292-4301.

Gong Z, Kim JE, Leung CC, Glover JN, Chen J (2010) BACH1/FANCJ acts with TopBP1 and participates early in DNA replication checkpoint control. *Mol Cell* **37:** 438-446.

4.1 Introduction

In response to replication stress, direct activation of the ATR kinase by TopBP1 depends on a secondary interaction initiated by the 9-1-1 complex (Cimprich & Cortez, 2008). This binding event involves the CK2-dependent phosphorylation of Rad9 Ser387 and the N-terminal BRCT0/1/2 repeat in TopBP1. Since TopBP1 contains a number of other conserved BRCT domains, it was plausible that other TopBP1 BRCT-mediated interactions may contribute to DNA replication checkpoint regulation. Studies from Dr. Junjie Chen's group (University of Texas MD Anderson Cancer Center) identified a new interaction between TopBP1 and BACH1/FANCJ that is important for DNA replication checkpoint activation. TopBP1 binding modulates BACH1 helicase activity, which increases ssDNA regions necessary for RPA accumulation at stalled replication forks. Thus, recognition of BACH1 by TopBP1 occurs in an early step in the ATR pathway and is upstream of 9-1-1 binding (Gong et al, 2010). The functional link between TopBP1 and BACH1 was unexpected, since BACH1 is well established in DNA DSB repair, and suggests cross-talk between HR and replication checkpoint pathways. BACH1 was initially identified through its interactions with BRCA1 (Cantor et al, 2001), which involve the recognition of a pSer-Pro-Thr-Phe motif (residues 990-993 of BACH1) by the tandem BRCT repeats of BRCA1 (Yu et al, 2003). This interaction is critical for cell cycle checkpoint (G2/M) function in response to ionizing radiation. Additionally, mutations in BACH1 are found in Fanconi anemia patients and are associated with defects in DNA crosslink repair, and indeed BACH1 is recognized as a member of the family of Fanconi-associated genes, designated FANCJ (Bridge et al, 2005; Levran et al, 2005; Litman et al, 2005).

BACH1 is phosphorylated at Thr1133 during S-phase, which generates a phospho-peptide motif for the C-terminal tandem BRCT7/8 domains of TopBP1. This was particularly intriguing, since previous work suggested that BRCT

domains specifically bind pSer-containing peptide motifs (Mohammad & Yaffe, 2009). For example, *in vitro* peptide library studies show that BRCA1, MDC1, BARD1, and DNA Ligase IV BRCT repeats preferentially bind pSer peptides (Manke et al, 2003; Rodriguez et al, 2003). However, given that checkpoint Ser/Thr kinases such as ATM, ATR and CDKs can phosphorylate both Ser and Thr sites in target proteins, it is reasonable to suspect that a subset of BRCT domains could have pThr peptide binding ability. Indeed, other phospho-peptide binding modules such as 14-3-3 and WW domains are capable of recognizing pSer and pThr binding motifs. In contrast, the FHA binding domain has a unique specificity for pThr binding motifs only (Yaffe & Elia, 2001).

Crystal structures of complexes involving tandem BRCT repeats with their cognate phospho-peptides have provided insight into the molecular basis of BRCT domain interactions. Studies of BRCA1, MDC1, *S. Pombe* Brc1 and *S. Pombe* Crb2 BRCT repeat-peptide complexes reveal a conserved mode of recognition that can be divided into two key regions: a pSer binding pocket in the N-terminal BRCT and a +3 specificity pocket at the BRCT-BRCT interface (Clapperton et al, 2004; Kilkenny et al, 2008; Shen & Tong, 2008; Shiozaki et al, 2004; Stucki et al, 2005; Varma et al, 2005; Williams et al, 2010; Williams et al, 2004). Comparison of the bound and unbound forms of the tandem BRCT domains reveal only subtle changes in structure, suggesting that the binding pocket is largely preformed for peptide binding. Although the current structures provide mechanistic detail of pSer peptide recognition, how BRCT domains can recognize pThr peptide motifs remains elusive.

Here we present the molecular basis of the TopBP1 BRCT7/8-BACH1 interaction involved in DNA replication checkpoint control. In combination with systematic mutagenesis studies *in vitro* and *in vivo*, we illustrate the role of key contact residues in the specificity of TopBP1-BACH1 interactions. Comparison of the apo and bound structures reveal a dramatic rearrangement of the BRCT

domains that is required for specific phospho-peptide recognition. The structure of the TopBP1 BRCT7/8-BACH1 complex also establishes the basis for pThr recognition by BRCT domains. Taken together, our studies provide insights into novel roles of BRCT-phospho-peptide recognition.

4.2 Results

4.2.1. Structures of TopBP1 BRCT7/8 and BACH1 phospho-peptide complex

The crystal structures of TopBP1 BRCT7/8 and its complex with a BACH1 phospho-peptide were determined to 2.0 Å and 2.15 Å, respectively. Like other established tandem BRCT domain structures (Glover et al, 2004), TopBP1 BRCT7/8 packs in a head to tail manner via a hydrophobic interface between the two BRCT domains (Fig. 4-1A). Each BRCT domain consists of a central 4-stranded parallel β-sheet packed on opposite sides by helical elements. Separating BRCT7 and 8 is a prominent linker helix (α_L), which is part of an unusually long linker region compared to other phospho-peptide binding tandem BRCT domains (Fig. 4-2). The conserved phospho-peptide recognition of tandem BRCT repeats is evident in the TopBP1 BRCT7/8-BACH1 phospho-peptide complex, where the pThr sits in a conserved phosphate binding pocket in the N-terminal BRCT7 and the +3 residue is complemented by a hydrophobic cavity formed at the interface of BRCT7 and 8 (Fig. 4-1B). Contacts between the BRCT7/8 domains and BACH1 phospho-peptide span the -2 to +5 positions of the peptide, burying a solvent-accessible surface area of 1208 $Å^2$ at the interface.

Surprisingly, the apo TopBP1 BRCT7/8 structure adopts a conformation that is significantly more open than the TopBP1 BRCT7/8-BACH1 phospho-peptide complex. This is unusual for tandem BRCT repeats, where comparisons of the apo and peptide-bound crystal structures in BRCA1, MDC1, Brc1 and Crb2 BRCT domains only yield subtle structural changes (Clapperton et al, 2004; Glover et al, 2004; Kilkenny et al, 2008; Shiozaki et al, 2004; Stucki et al, 2005)

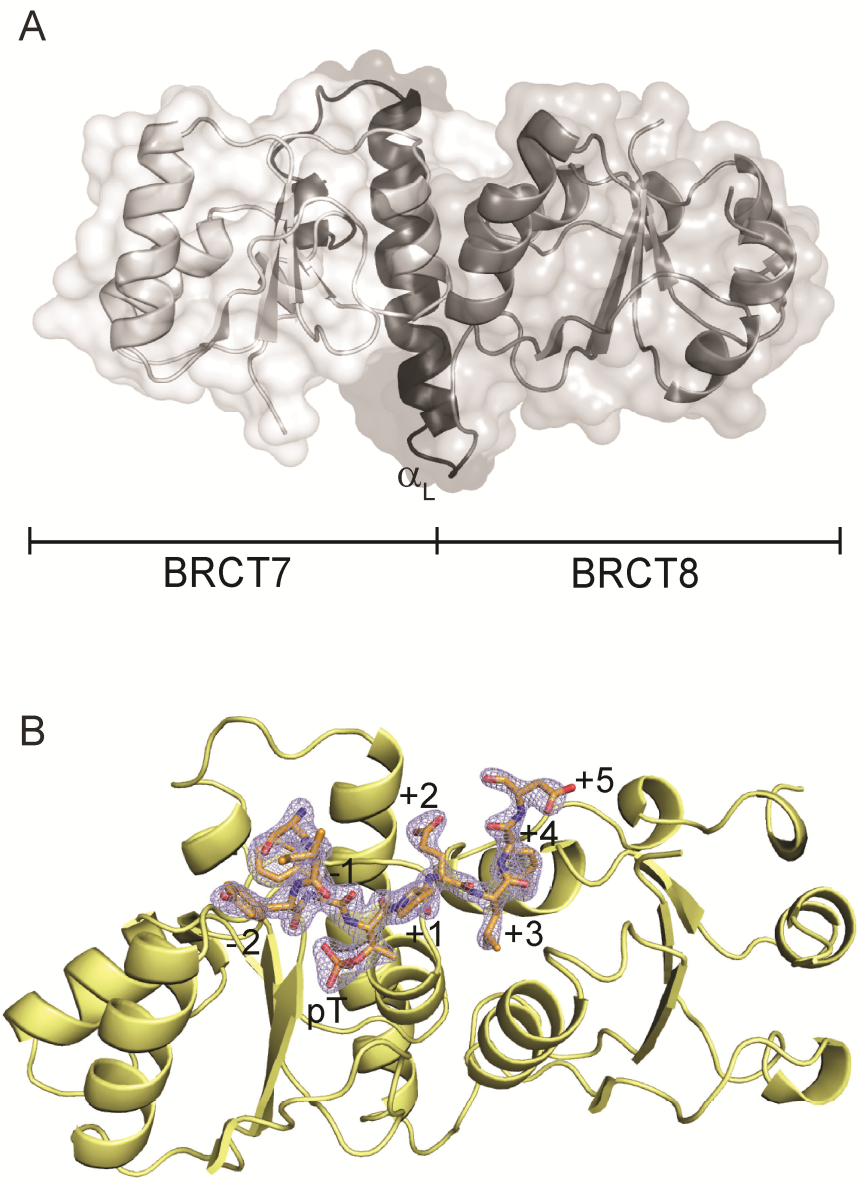

Figure 4-1. Structure of TopBP1 BRCT7/8 and TopBP1 BRCT7/8-BACH1 peptide complex. (A) Cartoon representation of the apo structure of TopBP1 BRCT7/8. The linker region is coloured black and α_L helix is labelled. (B). The BACH1 phospho-peptide (orange) binds in a region spanning the TopBP1 BRCT7/8 domains (yellow). The $2|F_o|-|F_c|$ electron density map at 2σ for the phospho-peptide is shown. Residue positions in the phospho-peptide are labelled.

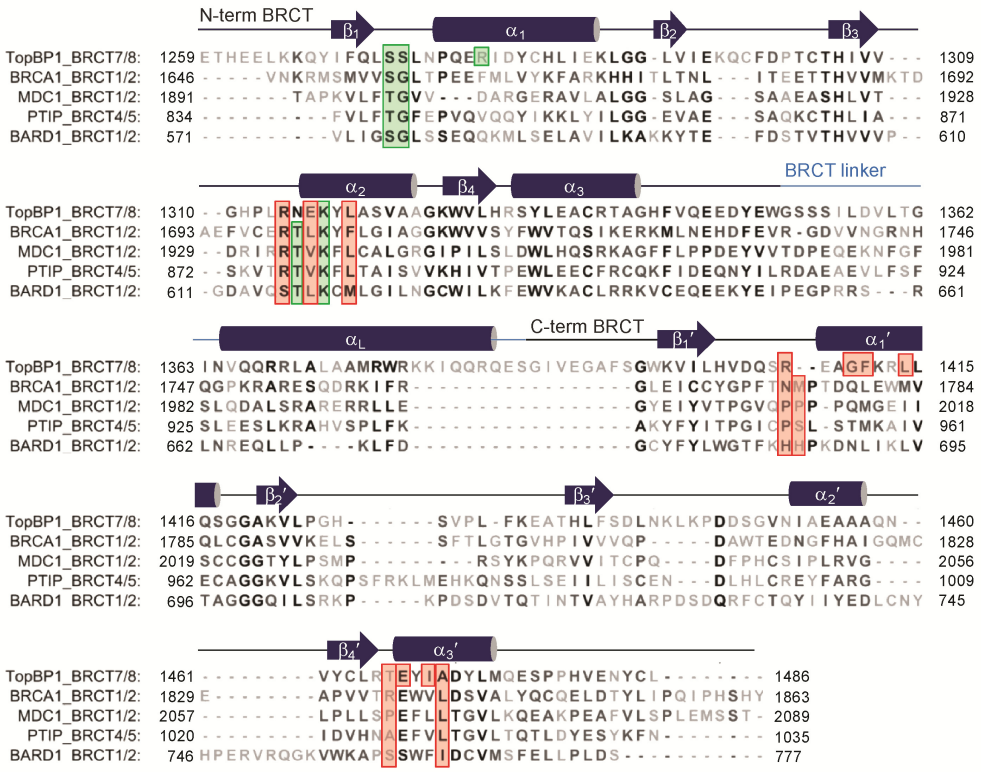

Figure 4-2. Alignment of TopBP1 BRCT7/8 with other phospho-peptide binding tandem BRCT repeats. The secondary structure elements of TopBP1 BRCT7/8 are indicated above the sequence. Residues are shaded based on conservation. Residues involved in phosphate binding are boxed in green. +3/+4 pocket residues are boxed in red.

(Williams et al, 2010; Williams et al, 2001; Williams et al, 2004). This can be further illustrated, for example, in structural alignments of both the apo and bound crystal structures of MDC1 BRCT1/2 with the TopBP1 BRCT7/8-BACH1 peptide complex, which clearly show a better agreement compared to the apo TopBP1 BRCT7/8 structure (Fig. 4-3A). The open structure of TopBP1 BRCT7/8 also does not appear to be a consequence of the crystal packing, since the structure of apo TopBP1 BRCT7/8 crystallized under different conditions in a different space group yielded the same conformation (data not shown). To quantify the degree of conformational change between the apo and peptide-bound structure, we used the program DYNDOM (Hayward & Berendsen, 1998) to define and measure protein domain motion. Both a fixed domain (BRCT7 and α_L (residues 1268-1392)) and moving domain (BRCT8 (residues 1393-1489)) were identified, with the moving domain rotating 23° around a central axis (Fig. 4-3B). The residues defined in inter-domain bending (residues 1388-1393) also conveniently flank the C-terminal end of α_L.

The plasticity of TopBP1 BRCT7/8 may be explained by the difference in the packing interface compared to canonical tandem BRCT repeats. Due to the extensive hydrophobic interface contributed by the α_2-α_1′-α_3′ helices, such as in BRCA1 BRCT1/2 (Williams et al, 2001), tandem BRCT repeats are typically rigid (Fig. 4-4). Consequently, their peptide binding surfaces are considered preformed, aside from minor changes to the backbone or side chain conformation, and the +3 binding cavity is relatively shallow. In contrast, the smaller hydrophobic packing surface at the interface between BRCT7 and 8 of TopBP1 results in a larger cavity (Fig. 4-4). In particular, the TopBP1 equivalent residues of BRCA1 Arg1699, Met1775, Pro1776, Glu1836 and Asp1840, which all contribute to the interface packing at the top of the pocket in BRCA1, do not do so in TopBP1. This allows for a more dynamic interaction of the BRCT domains in TopBP1 BRCT7/8 and explains its conformational change upon peptide binding.

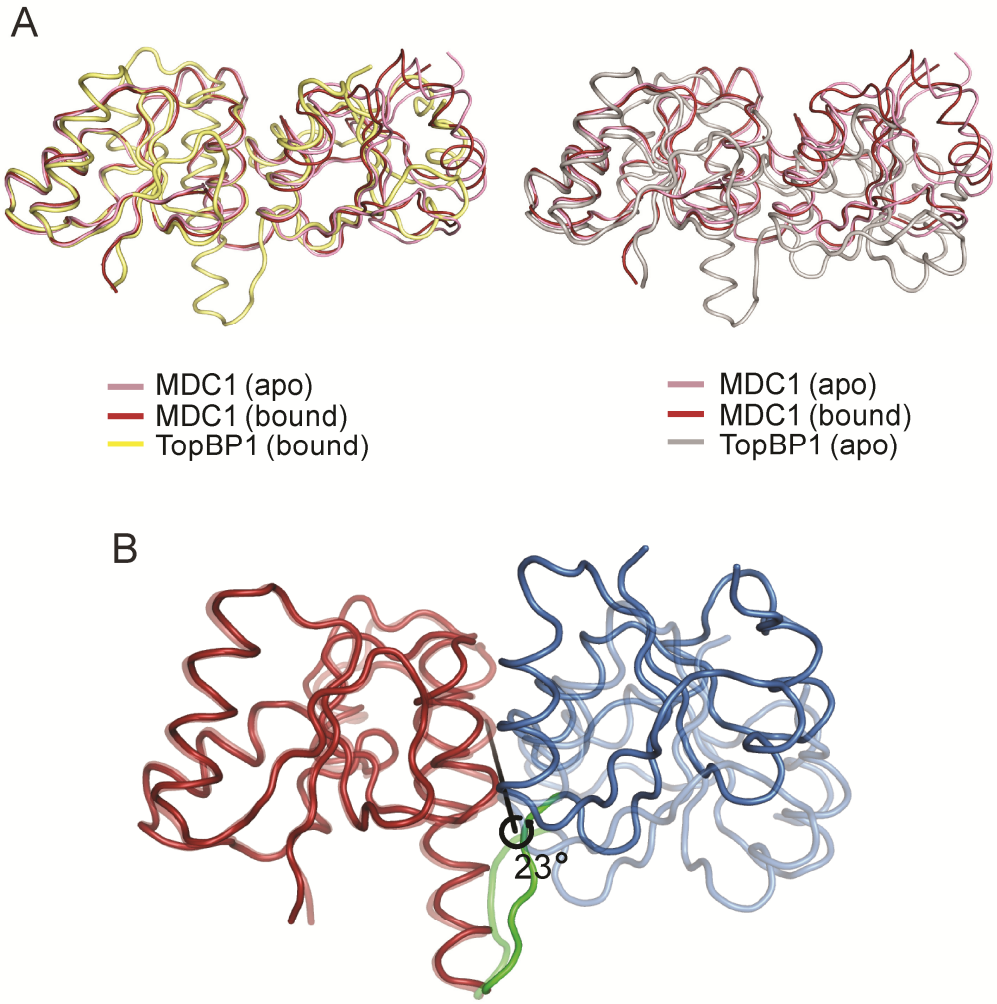

Figure 4-3. BACH1 binding induces domain rotation at the BRCT-BRCT domain interface. (A) Structural alignment of TopBP1 BRCT7/8 and MDC1 BRCT1/2 structures. The apo and peptide-bound structures of MDC1 are superimposed with the TopBP1 peptide-bound structure (left) or apo structure (right). (B) Representation of the structural rearrangement of TopBP1 BRCT7/8 around the central rotation axis. The initial apo state is represented at 50% transparency. The fixed domain (red), moving domain (blue) and inter-domain bending residues (green) are coloured.

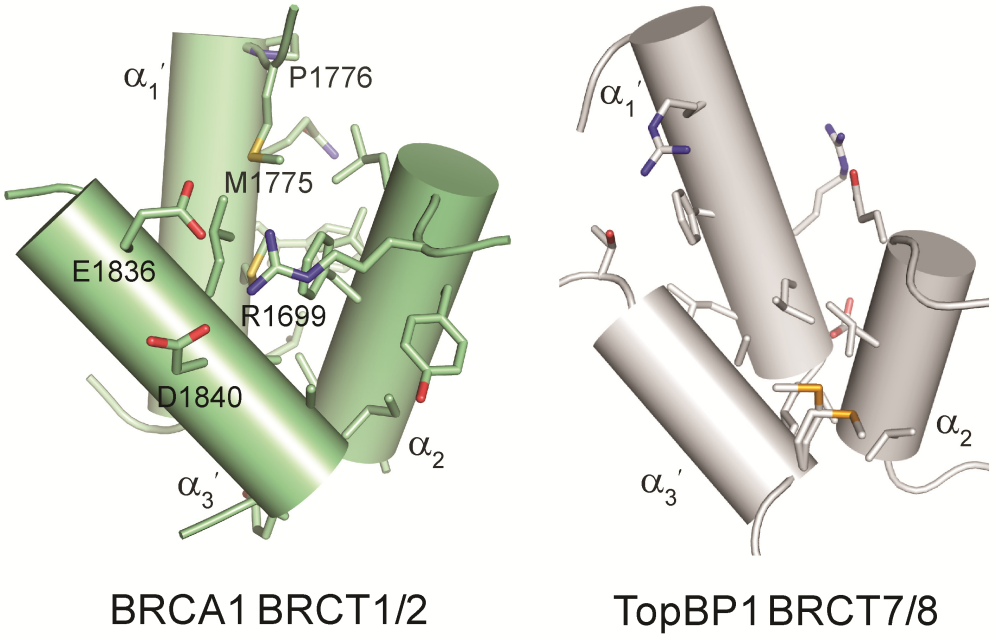

Figure 4-4. Comparison of the hydrophobic packing interface of BRCA1 BRCT1/2 and TopBP1 BRCT7/8. Helices are represented as cylinders and labelled. Residues involved in interface packing are shown as sticks. Residues involved in BRCA1 and not in TopBP1 BRCT packing are labelled.

4.2.2. Conserved pThr binding pocket of TopBP1 BRCT7/8

The pThr binding pocket of TopBP1 BRCT7/8 is made up of phosphate binding residues that are conserved in other phosphate-binding BRCT repeats. The phosphate moiety makes conserved interactions with the side chains of Ser1273 and Lys1317, as well as with the main chain amide of Ser1274 (Fig. 4-5A, Fig. 4-2). In addition, the guanidinium group of Arg1280 makes a novel bidentate interaction with two phosphate oxygen atoms, and is supported by a secondary hydrogen bond with the main chain of the peptide at the -2 position. In comparison to the bound state, the phosphate-binding pocket of TopBP1 BRCT7/8 in the apo form does not appear to be in a favourable conformation for binding. A sulfate ion is bound in the apo crystal structure and mimics the phosphate group in the binding pocket (Fig. 4-5B). Due to the open conformation in the apo state, Lys1317 is pulled away from the phosphate pocket and does not interact with the correct oxygen on the sulfate. Because of the loss of the peptide backbone contact with Arg1280, the guanidinium group of this residue shifts, contacting the sulfate and the main chain of Leu1272 instead. In the phosphate binding pocket of canonical BRCT repeats, the conserved Ser1273 side chain (Ser1655/Thr1898 in BRCA1/MDC1, respectively) is normally held in the optimal rotamer by hydrogen bonding with a conserved threonine residue (Thr1700/Thr1934 in BRCA1/MDC1, respectively) across the pocket. Since the residue at this position in TopBP1, Asn1315, is incapable of making such an interaction in TopBP1, Ser1273 is free to adopt multiple side chain conformations and is not held in the proper hydrogen bonding distance or orientation in the apo structure (Fig. 4-5B).

To examine the phosphate binding specificities of the TopBP1 BRCT7/8 phosphate-binding pocket *in vitro*, we used a fluorescence polarization (FP) assay to first test for the ability of TopBP1 BRCT7/8 to specifically bind to a

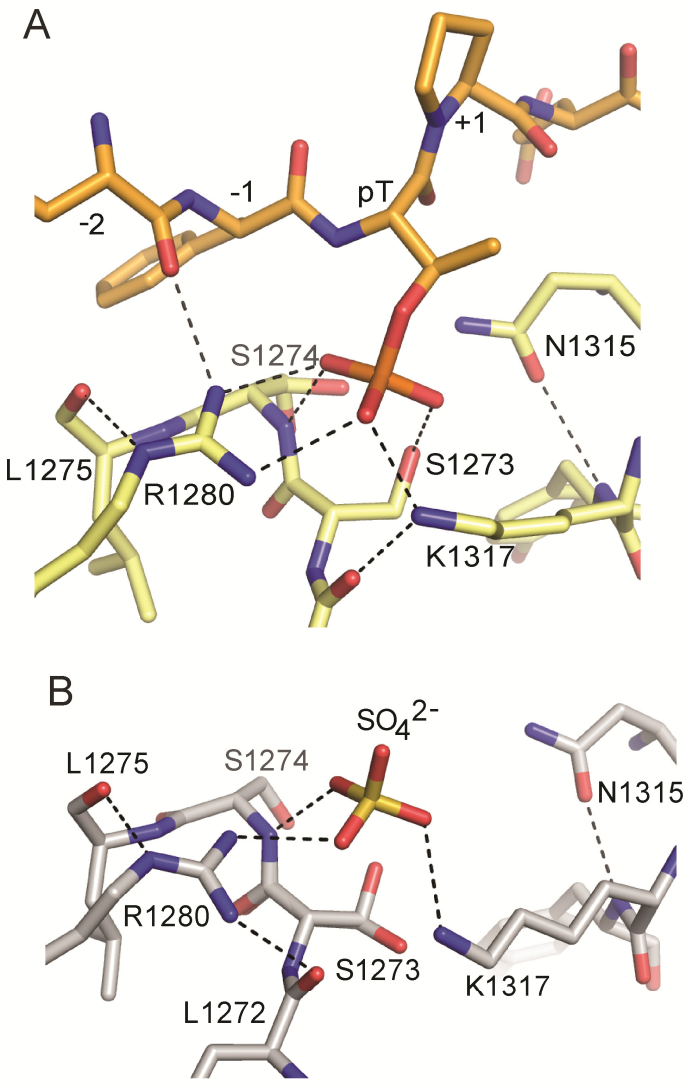

Figure 4-5. Phosphate-binding pocket of TopBP1 BRCT7/8. (A) Stick representation of the TopBP1 BRCT7/8 (yellow) in complex with the BACH1 phospho-peptide (orange). Hydrogen bonding and electrostatic interactions are indicated by dotted lines. (B) Phosphate binding pocket of apo TopBP1 BRCT7/8. The Ser1273 side chain has alternate side chain conformations that are visible in the electron density.

FITC-labelled BACH1 pThr1133 peptide (ESIYFpTPELYDPEDT). The BACH1 phospho-peptide was specifically recognized by TopBP1 BRCT7/8 and not the tandem BRCT domains of BRCA1 (K_d = 2.1 ± 0.6 μM for TopBP1 BRCT7/8, K_d > 400 μM for BRCA1 BRCT1/2) (Fig. 4-6A). To further investigate the requirement for BACH1 phosphorylation at Thr1133, FP was carried out on the FITC-labelled BACH1 phospho-peptide with or without prior λ PPase treatment. The addition of λ PPase significantly diminished binding of the phospho-peptide to TopBP1 BRCT7/8 (K_d > 1 mM), whereas incubation with an inactive λ PPase had no effect (K_d = 1.8 ± 0.5 μM) on the interaction (Fig. 4-6B).

We next mutated a series of residues in the TopBP1 BRCT7/8 phosphate-binding pocket to assess their roles in phosphate binding. Mutation of the conserved Ser1273 or Arg1280 residues in GST-tagged TopBP1 BRCT7/8 markedly reduced binding to the peptide compared to wild-type (K_d = 92 ± 8 μM for S1273A, K_d = 104 ± 11 μM for R1280Q), providing further evidence that Arg1280 is required for phosphate binding (Fig. 4-6C). In contrast, the N1315A mutation (K_d = 4.6 ± 0.3 μM) showed similar levels of binding as wild-type, suggesting that Asn1315 is not required for phosphate binding.

4.2.3. pThr/pSer specificity of tandem BRCT domains

Given BACH1 pThr1133 is the first validated pThr target for a BRCT domain, we were interested in whether TopBP1 BRCT7/8 also has the ability to bind pSer phospho-peptides. We compared the ability of a pSer1133 derivative of the BACH1 binding motif to bind TopBP1 BRCT7/8 in a FP competition assay. Surprisingly, both pThr and pSer BACH1 phospho-peptides competed with the FITC-labelled BACH1 phospho-peptide equally (K_i = 7.7 ± 0.2 μM for pThr and K_i = 8.6 ± 2.4 μM for pSer), demonstrating that TopBP1 BRCT7/8 does not discriminate between pThr and pSer (Fig. 4-7A). In contrast, previous studies of tandem BRCT repeats indicate a preference for pSer phospho-peptide targets

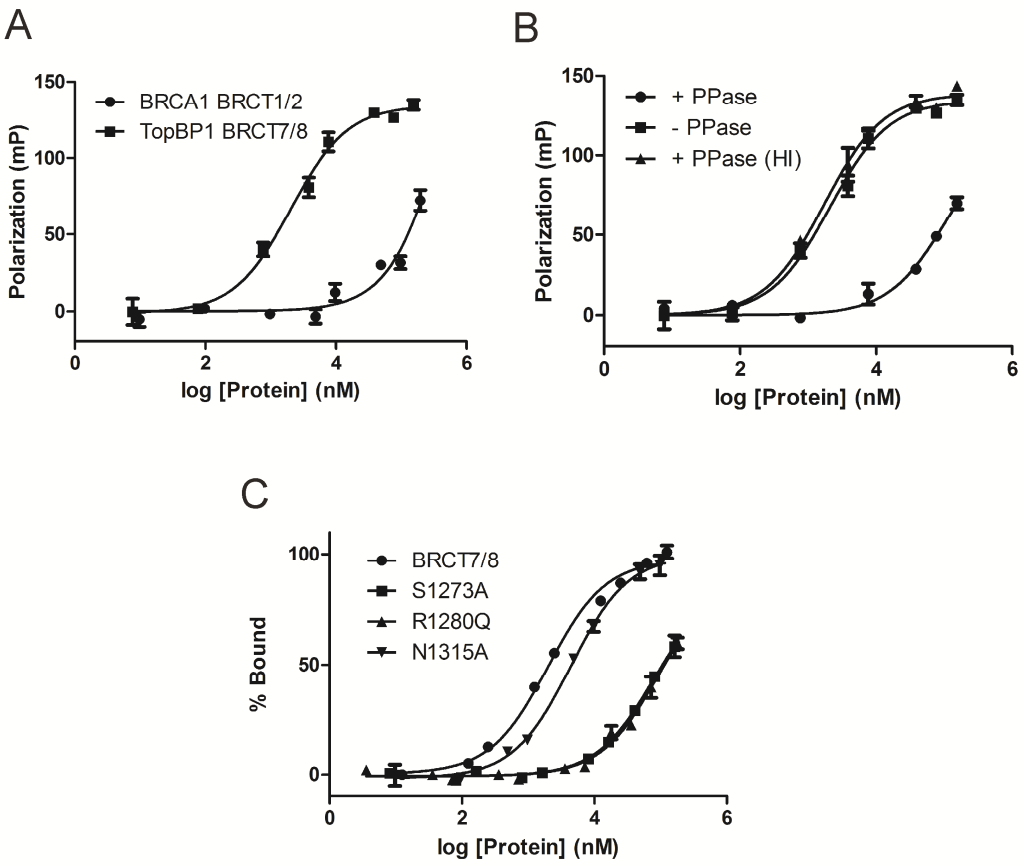

Figure 4-6. FP binding studies of TopBP1 BRCT7/8 and a BACH1 pThr1133-peptide. (A) FP binding results for a FITC-labelled BACH1 phospho-peptide with TopBP1 BRCT7/8 and BRCA1 BRCT1/2. (B) Effects of λ phosphatase treated FITC-BACH1 phospho-peptide on binding TopBP1 BRCT7/8. The peptide was treated with either active PPase (+ PPase), heat inactivated PPase (+ PPase (HI)) or without PPase (- PPase) before performing binding studies. (C) Effects of phosphate-binding pocket mutants on binding the BACH1 phospho-peptide. GST-fusion BRCT7/8 variants were purified and used in the assay.

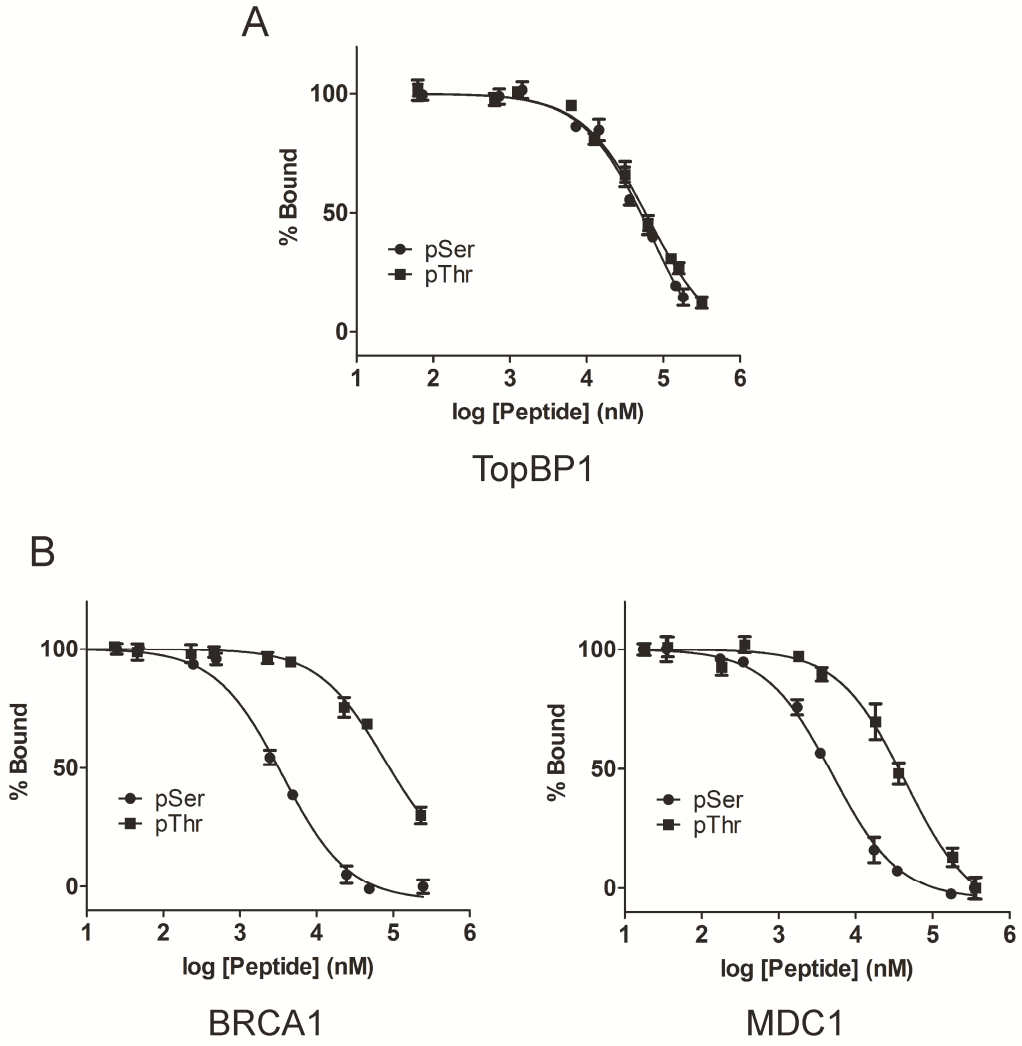

Figure 4-7. TopBP1 BRCT7/8 has specificity for pThr and pSer binding motifs. (A) FP competition assay in which FITC-labelled BACH1 phospho-peptide in complex with TopBP1 BRCT7/8 is challenged with pThr and pSer derivative peptides. (B) FP competition assays with BRCA1 BRCT1/2 (left) and MDC1 BRCT1/2 (right) cognate pSer and pThr derivative phospho-peptides.

over pThr (Manke et al, 2003; Rodriguez et al, 2003). Using the FP competition assay, we confirm that both the BRCA1 and MDC1 BRCT repeats prefer pSer in their respective minimal tetra-peptide targets (K_i = 1.5 ± 0.1 μM for pSer and K_i = 39.7 ± 8.0 μM for pThr in BRCA1, K_i = 0.9 ± 0.1 μM for pSer and K_i = 9.4 ± 3.2 μM for pThr in MDC1) (Fig. 4-7B). The degree of preference for pSer, however, is more dramatic for BRCA1.

A comparison of the structure of the TopBP1 BRCT7/8-BACH1 phospho-peptide complex with those of the BRCA1 and MDC1 BRCT repeats bound to their respective targets suggest why these proteins exhibit different pThr vs. pSer binding specificities. Superposition of the phosphate-binding residues in BRCA1, MDC1 and TopBP1 reveals that although the conserved phosphate contacts (S1273/S1655/T1898, K1317/K1702/K1936 and S1274/G1656/G1899 in TopBP1/BRCA1/MDC1, respectively) are maintained, the position of the phosphate group and orientation of the peptide backbone differ between the TopBP1 complex and either the BRCA1 or MDC1 complexes (Fig. 4-8A). The specific backbone and pThr1133 position in the BACH1 phospho-peptide bound to TopBP1 is supported by the additional contacts TopBP1 Arg1280 makes with the -2 main chain and the phosphate group. The difference in phosphate position of pSer compared to pThr is a result of the large discrepancy in χ_2 angles. The pThr residue in the TopBP1 complex is *gauche+*, but the pSer residues in the BRCA1 and MDC1 complexes are *trans* (Table 4-1), which may account for the selectivity of BRCA1/MDC1 for pSer phospho-peptides. Modeling of the pThr derivative in the BRCA1 and MDC1 structures clearly illustrates how addition of the γ-methyl group in a χ_2 *trans* orientation causes a steric clash with the phosphate oxygen atom (Fig. 4-8B). Introduction of this methyl group also clashes with two conserved waters that mediate interactions between the phospho-peptide and phosphate binding pocket, which may also impact phospho-peptide binding. The more dramatic preference for pSer

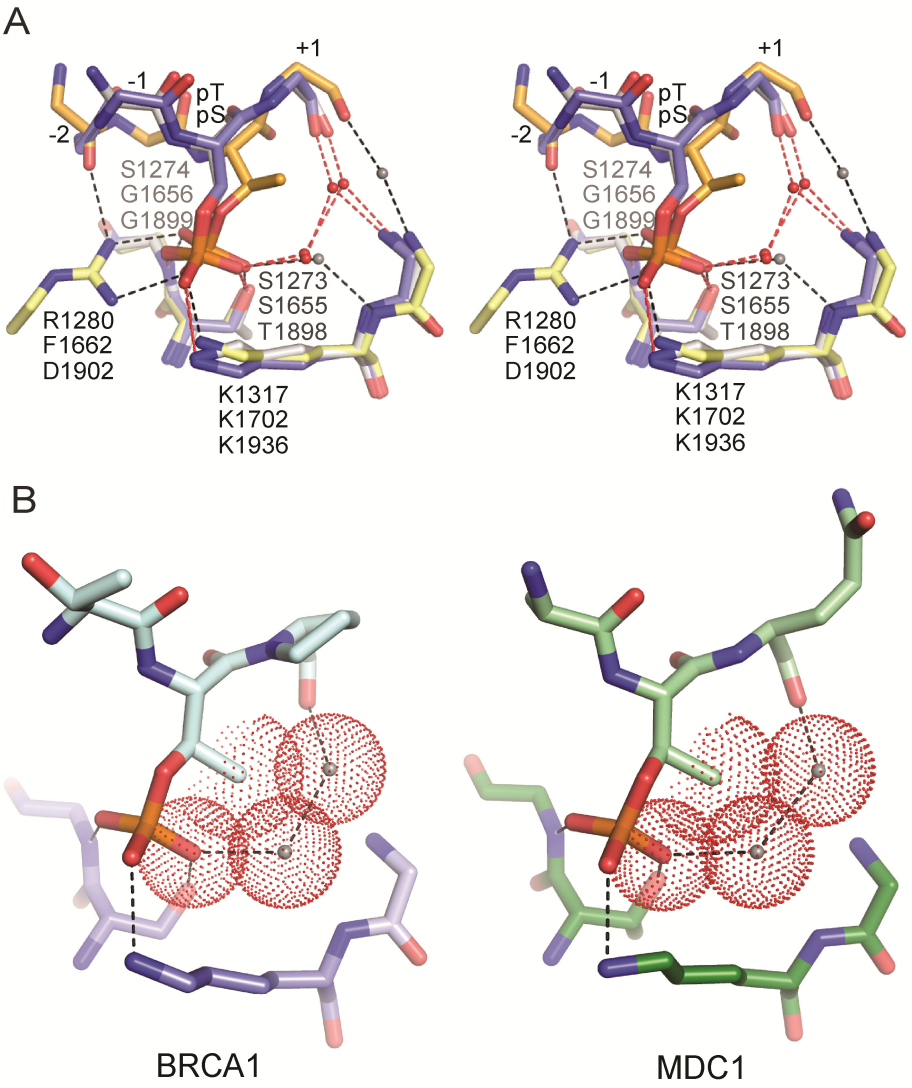

Figure 4-8. Comparison of the pThr/pSer coordination. (A) Stereoview of the superimposed pSer peptide-specific coordination of BRCA1 (blue, PDB ID: 1T15) and MDC1 (gray, PDB ID: 2AZM) with pThr peptide-specific coordination of TopBP1 (orange-yellow). Residues are labelled for TopBP1 (top), BRCA1 (middle) and MDC1 (bottom). Hydrogen bonding and electrostatic interactions in the complex are represented as dotted lines for TopBP1 (black) and BRCA1/MDC1 (red). Conserved waters mediating peptide-BRCT domain interactions are shown as spheres for TopBP1 (gray) and BRCA1/MDC1 (red). (B) Modelling of a pThr-derivative peptide in BRCA1 (left) and MDC1 (right) phosphate binding pockets. Clashing of the methyl group with neighbouring atoms and water molecules are illustrated by the overlap in van der Waals surface (dots).

Table 4-1. Comparison of torsion angles of pSer/pThr in peptide-bound BRCT and FHA domain complexes.

		Torsion Angle (°)			
pS/pT	**Recognition Domain**	ϕ	ψ	χ_1	χ_2
BACH1 pS990	BRCA1 BRCT1/2	-70	125	-58	168
γ-H2AX pS140	MDC1 BRCT1/2	-62	131	-72	156
BACH1 pT1133	TopBP1 BRCT7/8	-59	126	-50	109
XRCC1 pT519	PNKP FHA	-66	142	-52	113

observed by BRCA1 over MDC1 may arise from the differences in the +1 residue of their cognate peptides (Pro/Gln for BRCA1/MDC1, respectively). The presence of a +1 Pro in the BRCA1 target peptide restricts the backbone geometry, perhaps limiting conformational changes that might otherwise facilitate binding of the pThr peptide. In contrast to the pSer-specific rotamer in the BRCA1 and MDC1 complexes, the *gauche+* χ_2 orientation of pThr1133 in the TopBP1 complex permits the coexistence of the γ-methyl group and phosphate oxygen without steric hindrance. This specific orientation of pThr also resembles that seen in structures of pThr in complex with FHA domains, which are known to be selective for pThr binding motifs (Table 4-1).

3.2.4. +3/+4 binding pocket of TopBP1 BRCT7/8

To gain a better understanding of the specificity of the BACH1 binding motif for TopBP1 BRCT7/8, we performed alanine scanning mutagenesis to identify the residues in BACH1 important for the TopBP1 interaction *in vitro*. Using a FP competition assay, we show that alanine mutations of BACH1 +5 (D1138A) and +1 (P1134A) result in little or no change in competition compared to wild-type (Fig. 4-9A). In contrast, mutations at +3 (L1136A) and +4 (Y1137A) almost completely abolish competition with the FITC-labelled cognate peptide, providing evidence that the +3 and +4 residues of BACH1 are the most critical specificity determinants. The fact that the +3 residue is absolutely required for specific binding is characteristic of the common mode of BRCT repeat recognition, although the additional importance of the +4 residue is surprisingly different. Mutation at +2 (E1135A) also yields a smaller but significant reduction in competition.

The observed peptide binding specificity can be explained by the TopBP1 BRCT7/8-BACH1 phospho-peptide complex crystal structure. Both +3 and +4 BACH1 residues are nestled in a deep hydrophobic cavity in TopBP1 BRCT7/8 that is sculpted upon peptide binding (Fig. 4-9B). In the apo structure, the +3/+4

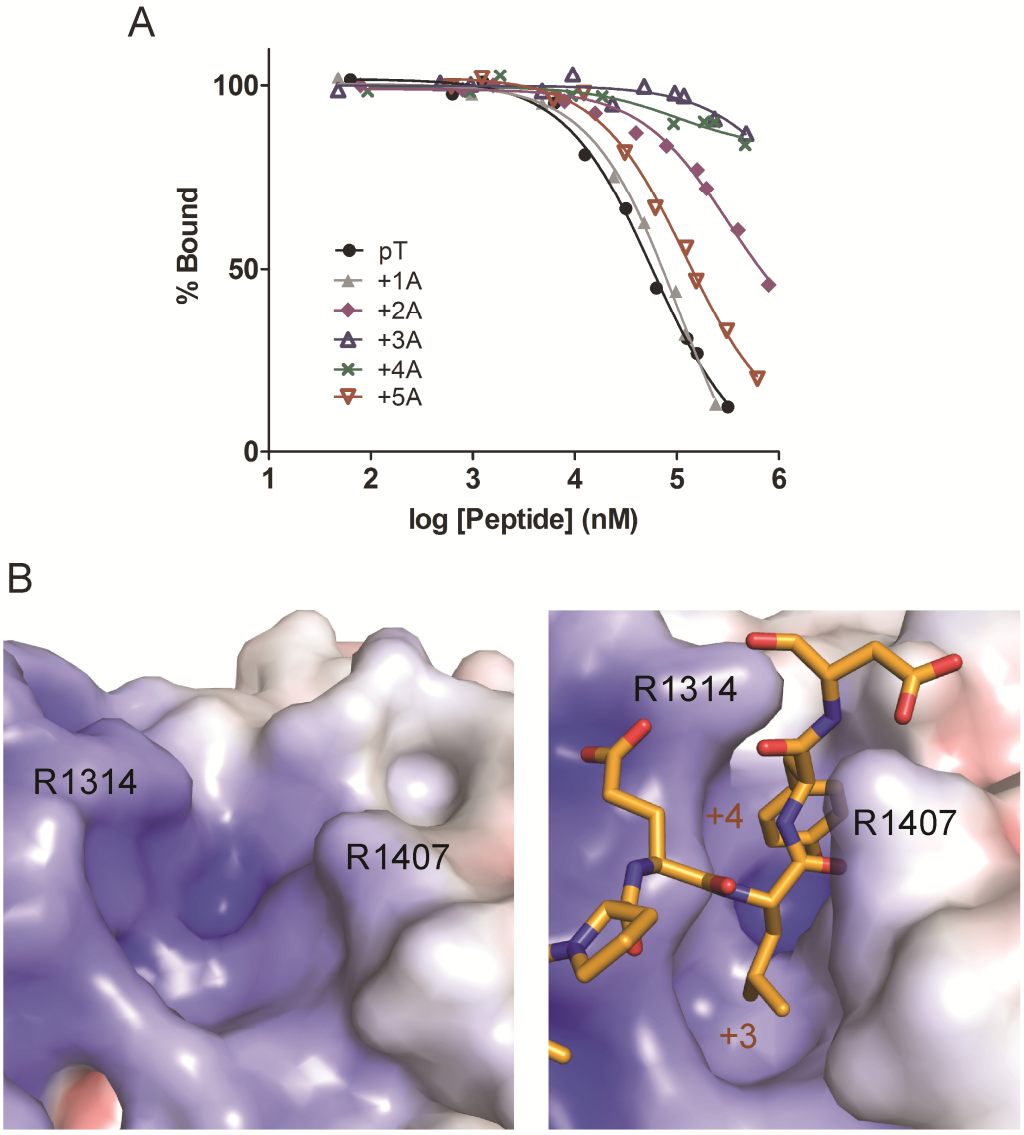

Figure 4-9. TopBP1-BACH1 interaction at the +3/+4 binding pocket. (A) FP competition analysis of the BACH1 binding motif using alanine scanning mutagenesis. BACH1 phospho-peptides mutated to alanine at +1 to +5 positions were used to compete with the FITC-labelled phospho-peptide bound to TopBP1 BRCT7/8. (B) Electrostatic potential surface of the TopBP1 BRCT7/8 +3/+4 binding pocket in the apo (left) and peptide-bound (right) structures. TopBP1 R1314 and R1407 residues are mapped on the surface.

pocket is held open by the open conformation of TopBP1 BRCT7/8. Binding of the peptide initiates closure of the walls of the +3/+4 pocket, creating a tight, narrow cleft that accommodates the hydrophobic side chains of the peptide. The pocket in TopBP1 BRCT7/8 is both larger and deeper than the +3 binding pockets of other established phospho-peptide binding BRCT repeats. For example, although the same Leu +3 peptide residue exists in the *S. Pombe* Brc1-γH2A complex (Williams et al, 2010), the Leu side chain packs horizontally across the shallow +3 pocket created by Brc1 BRCT repeats. The base of the TopBP1 BRCT7/8 +3/+4 binding pocket is made up of a number of residues at the hydrophobic BRCT interface: Leu1319, Phe1411, Leu1414, Ile1469 and Arg1470. Additional residues (Arg1314, Glu1316, Arg1407, Gly1410, Thr1466 and Glu1467) constitute the sides of the +3/+4 pocket (Fig. 4-2). The pocket complements the charge and shape of the +3 Leu and +4 Tyr residues perfectly. Besides the hydrophobic interactions made between the hydrophobic residues, the +4 Tyr side chain also hydrogen bonds with the main chain of Thr1466 and stacks against the guanidinium group of Arg1314 of TopBP1.

Two essential arginine residues (Arg1314 and Arg1407), neatly placed on opposite sides of the +3/+4 binding pocket, effectively shape the sides of the pocket by making a number of interactions with the phospho-peptide. Mutations of Arg1314 (R1314Q) and Arg1407 (R1407A) markedly reduce binding to the FITC-BACH1 phospho-peptide in the FP assay (K_d = 56.4 ± 3.8 μM for R1314Q, K_d = 63.4 ± 4.5 μM for R1407A), highlighting their importance in phospho-peptide binding (Fig. 4-10A). As a function of the rotational movement of BRCT8, Arg1407 makes a dramatic switch by breaking an existing salt bridge with Asp1440 in order to form a new salt bridge with the +5 side chain and make a water-mediated interaction with the +2 main chain (Fig. 4-10B). Arg1314 is conserved in other tandem BRCT domains and has a major role in recognition of the +3 main chain or carboxy tail of the cognate peptide (Campbell et al, 2010). In canonical tandem BRCT repeats, the conserved arginine (Arg1699 in BRCA1,

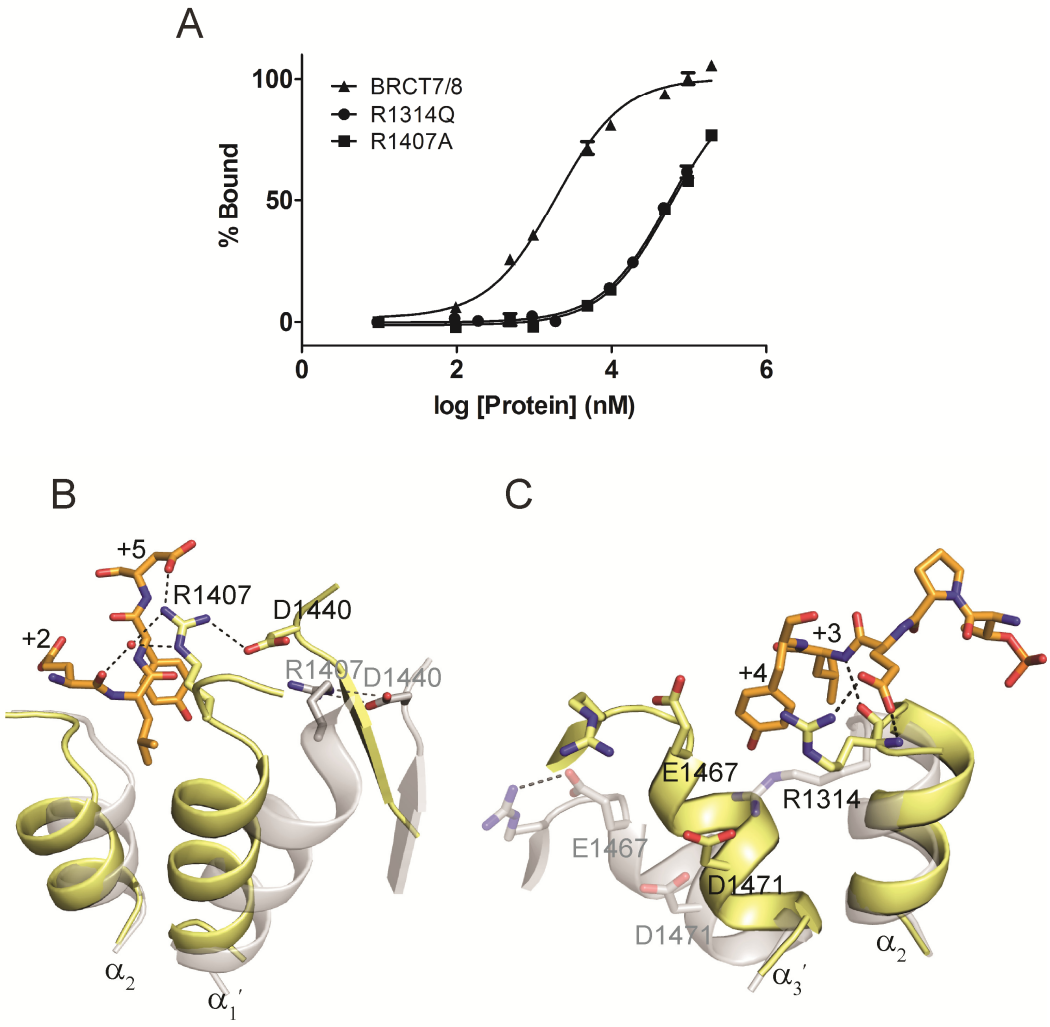

Figure 4-10. Role of Arg1407 and Arg1314 for phospho-peptide binding. (A) FP binding curves of TopBP1 BRCT7/8 +3/+4 pocket mutants with FITC-labelled BACH1 phospho-peptide. GST-fusion BRCT7/8 variants were purified and used in the assay. (B) Role of Arg1407 in the TopBP1-BACH1 complex. TopBP1 BRCT7/8 in the apo (gray) and complex (yellow) structures are superimposed. Residues involved in interacting with R1407 are labelled. (C) Role of Arg1314 in +2/+3 binding of the BACH1 peptide. TopBP1 BRCT7/8 in the apo (gray) and complex (yellow) structures are superimposed.

Arg1933 in MDC1) contributes to the BRCT interface and is held in place by salt bridge interaction(s) with conserved acidic residues (Glu1836 and Asp1840 in BRCA1, Glu2063 in MDC1) across the interface. Although the role of the Arg1314 main chain in binding the +3 main chain is preserved, the Arg1314 side chain has a number of additional roles that appears to be unique to TopBP1 BRCT7/8. In the apo state, Arg1314 is too far from the conserved Glu1467 and Asp1471 residues across the BRCT interface to make contact (Fig. 4-10C). The inherent mobility of Arg1314 is further supported by the relatively poor electron density and higher b-factors associated with the Arg1314 side chain. Consequently in the peptide-bound state, Arg1314 is free to adopt a different rotamer in order to interact with the +2 side chain and form a cation-π interaction with +4 Tyr side chain. Taken together, the structural plasticity of the +3/+4 pocket, which is imparted by the rearrangement of TopBP1 BRCT7/8, is required for the specific TopBP1-BACH1 interaction.

4.2.5. In vivo binding specificities of the TopBP1 BRCT7/8-BACH1 interaction

To further characterize the TopBP1 BRCT7/8-BACH1 binding specificities, we assessed the effects of mutations on the TopBP1 BRCT7/8-BACH1 interaction *in vivo*. Immunoprecipitation localization experiments were performed by Dr. Zihua Gong (Chen lab). From our *in vitro* FP binding results, we showed that mutations in the conserved phosphate-binding pocket residues (S1273A and R1280Q) and in the +3/+4 binding pocket (R1314Q) significantly reduce binding to the FITC-labelled BACH1 phospho-peptide. To determine the effects of these mutations in human cells, Myc-tagged full-length TopBP1 harbouring these mutations were cotransfected with SFB-tagged BACH1. None of the mutants formed a complex with BACH1, as indicated by the absence of Myc-TopBP1 in BACH1 immunoprecipitates (Fig. 4-11A). Using alanine scanning mutagenesis, we also concluded that BACH1 +2 to +4 residues are critical for TopBP1 binding specificity. In support of this, mutants of SFB-tagged BACH1 +2 (E1135A),

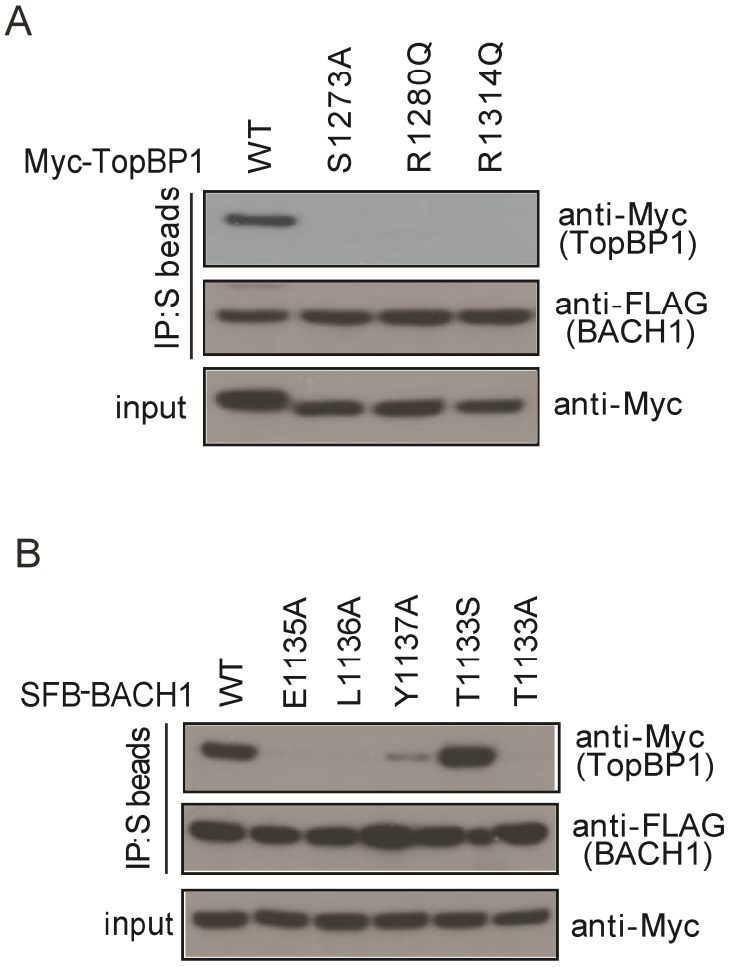

Figure 4-11. *In vivo* binding specificities of the TopBP1-BACH1 interaction. Experiments were performed by Dr. Zihua Gong of the Chen lab. (A) Effects of TopBP1 BRCT7/8 mutations in binding BACH1. Constructs encoding Myc-tagged wild type and mutants of TopBP1 were co-transfected with plasmids encoding SFB-BACH1. Immunoprecipitation reactions were performed using S-protein beads and then subjected to Western blot analyses using antibodies as indicated. (B) Effects of BACH1 mutations in binding TopBP1. Lysates for immunoprecipitation were prepared from cells expressing Myc-tagged TopBP1 along with SFB-tagged wild type or mutants of BACH1.

+3 (L1136A) and +4 (Y1137A) failed to bind myc-TopBP1 in BACH1 immunoprecipitates (Fig. 4-11B). However, mutation at +2 seemed to have a more detrimental effect on binding than at +4 in our *in vivo* co-immunoprecipitation. Although the TopBP1 BRCT7/8 mutants failed to bind BACH1 *in vivo*, we note that this is not a consequence of a defect in overall TopBP1 function since these mutants still colocalize with γ-H2AX to IR-induced foci like wild-type TopBP1 (Fig. 4-12). This is consistent with our previous reports suggesting that TopBP1 BRCT7/8 does not have a role in TopBP1 localization following DNA damage (Gong et al, 2010; Yamane et al, 2002).

To address the pThr/pSer specificity of TopBP1 BRCT7/8 *in vivo*, we tested the ability of BACH1 T1133A and BACH1 T1133S mutants to bind TopBP1. As expected, TopBP1 failed to co-immunoprecipitate with SFB-tagged BACH1 T1133A (Fig. 4-11B), however BACH1 T1133S restored binding to TopBP1, suggesting that BACH1 T1133S is similarly phosphorylated in cells and interacts with TopBP1 BRCT7/8 in the same manner as wild-type BACH1. Consistent with our *in vitro* results, this indicates that the TopBP1 BRCT7/8, unlike the BRCA1 and MDC1 BRCT repeats, is competent to bind both pThr and pSer peptide motifs with similar affinities.

4.3 Discussion

The role of TopBP1 as a facilitator of diverse signals that control the replication stress response critically depends on its nine BRCT domains that dictate diverse molecular interactions. Here we present the first structural information providing insight into how TopBP1 binds one of its critical partners in the DNA damage response, BACH1. The BRCT7/8 tandem pair of TopBP1 functionally interacts with another phosphorylated region of BACH1 that is distinct from that recognized by the BRCA1 BRCT repeats (Gong et al, 2010). This interaction is required for the proper loading of RPA onto ssDNA regions near stalled replication forks in a manner that is also dependent upon the helicase

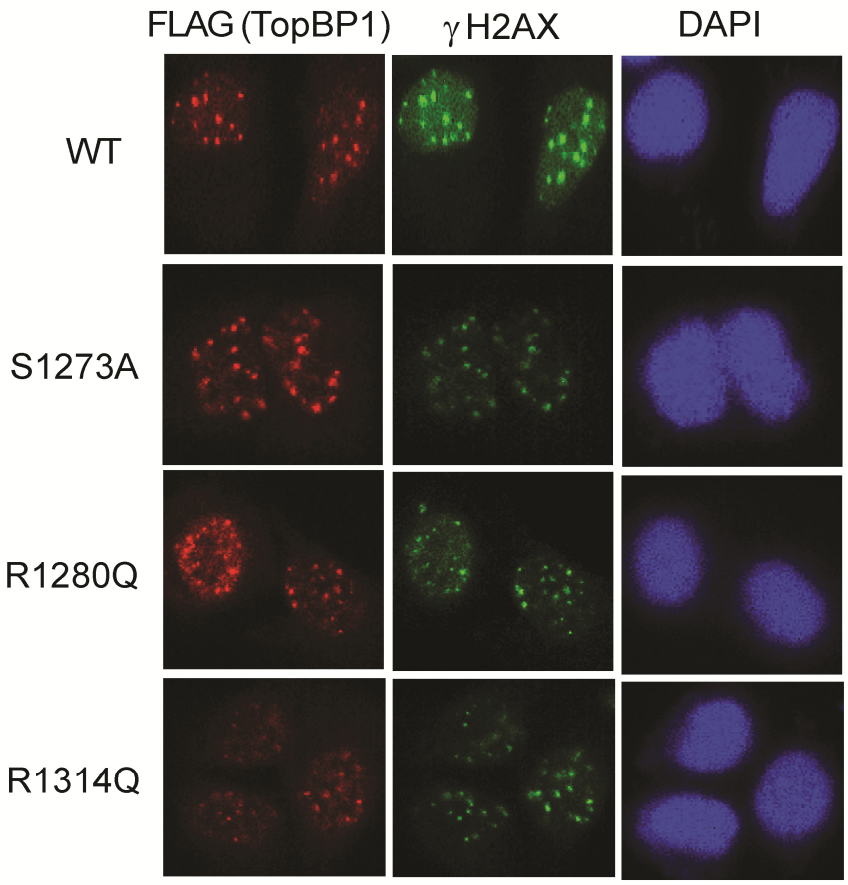

Figure 4-12. TopBP1 mutants deficient in binding BACH1 maintain localization to IR-induced foci. Experiments were performed by Dr. Zihua Gong of the Chen lab. U2OS cells transfected with plasmids encoding SFB-tagged wild-type or mutants of TopBP1 were exposed to 10 Gy of ionizing radiation. Cells were fixed and immunostained with anti-FLAG and anti-γH2AX antibodies.

activity of BACH1 and ultimately leads to ATR-dependent phosphorylation signalling. Our structural and functional analysis reveals intriguing differences in the way that TopBP1 recognizes its BACH1 target compared to the canonical BRCA1 recognition of BACH1 that govern how these two tandem BRCT repeats bind their respective phospho-targets with a high degree of specificity.

A major difference is the fact that phospho-peptide binding induces a large scale rearrangement in the packing of the TopBP1 BRCT7/8 repeats, whereas the conventional BRCT repeats are much more rigid and fixed in a conformation very similar to the bound form. The conformational change in TopBP1 BRCT7/8 upon peptide binding corresponds to a 23 ^{o} rotation of one BRCT with respect to the other about the extended linker helix (α_L). The bound form of TopBP1 BRCT7/8 closely resembles the standard packing of BRCT domains found in the other tandem BRCT structures, while the unbound form represents a more relaxed structure, with opened binding pockets for both the phosphate and peptide +3/+4 residues. The plasticity of TopBP1 BRCT7/8 compared to the other BRCT repeats is likely due to reduced packing of the BRCT repeats. This increased flexibility could allow TopBP1 BRCT7/8 to recognize a more divergent array of peptide targets. In addition to the interaction with BACH1, BRCT7/8 has also been shown to interact with an Akt-phosphorylated region of TopBP1 between the 6th and 7th BRCT to regulate the oligomerization of TopBP1 (Liu et al, 2006) and an ATR autophosphorylation motif (Liu et al, 2011). The +3/+4 positions of these targets (TopBP1: pS^{1159}NLQWPS, ATR: pT^{1989}PPEGK) are not conserved with the BACH1 target sequence, and it may be that recognition of these peptides involve a further rearrangement of the TopBP1 BRCT7/8 specificity pocket. While TopBP1 is more flexible than the other tandem BRCT proteins, a certain degree of flexibility in packing of the tandem repeats of BRCA1 likely also exists in solution, as suggested by both NMR (Botuyan et al, 2004) and thermodynamic stability studies (Ekblad et al, 2002; Nomine et al, 2008). A BRCT interface rotation is also observed in the NBS1

BRCT domains, although it appears to be initiated by a mechanism dependent on the neighbouring FHA domain. Binding of the peptide with the FHA domain initiates a helical rearrangement of the FHA-BRCT1 interface and an approximately 20 ° rotation at the BRCT1-BRCT2 interface (Williams et al, 2009). In contrast to the rearrangement in TopBP1 BRCT7/8 however, this rotation is in an orthogonal direction and its significance is still unknown.

The other intriguing difference between TopBP1 BRCT7/8 and other tandem BRCT proteins is its recognition of a pThr target peptide. We demonstrate that both BRCA1 and MDC1 BRCTs are specific for pSer- and not pThr-containing targets, while TopBP1 has a relaxed specificity, binding both pSer and pThr peptides. The sequence conservation of the different BACH1 binding motifs also complements this notion, as BACH1 Thr1133 exists as a Ser residue in some mammalian species, whereas BACH1 Ser990 is absolutely conserved throughout. Furthermore, other phospho-peptide targets of TopBP1 BRCT7/8 reported in TopBP1 (Liu et al, 2006) and ATR (Liu et al, unpublished) include phosphorylation on both Ser (pS1159) and Thr (pT1989), respectively. The difference in specificity between BRCA1/MDC1 and TopBP1 relies on subtle differences in the geometry of the coordinated phosphorylated amino acid, likely driven by the presence of the additional Arg1280 residue in the phosphate binding pocket of TopBP1 BRCT7/8 (Fig. 4-8A). Arg1280 is also conserved in a number of BRCT domains, suggesting a possible conserved mechanism of phosphate recognition (Fig. 4-13). For example, the equivalent arginine side chain in *S. Pombe* Crb2 (Arg558) makes a single water-bridged interaction with the phosphate of γ-H2A in the Crb2 BRCT1/2-γH2A crystal structure (Kilkenny et al, 2008). The bidentate mode of recognition by Arg1280 may also be conserved, as suggested by the interaction of TopBP1 Arg121 with a sulfate ion in the TopBP1 BRCT0/1/2 crystal structure (Rappas et al, 2011).

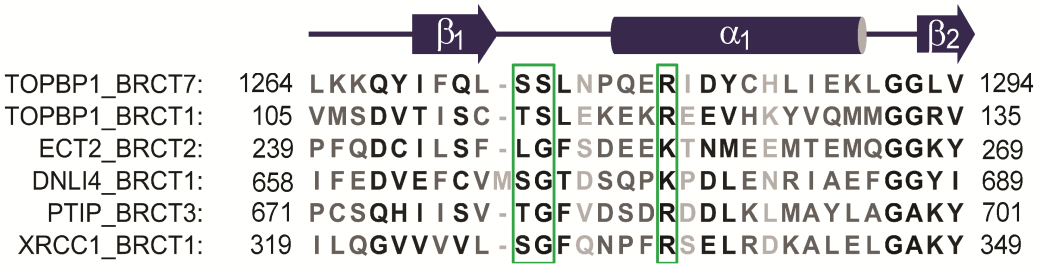

Figure 4-13. Sequence alignment of the phosphate-binding residues in other BRCT domains. Residues are shaded based on conservation. Secondary structure elements are mapped above the sequence. Conserved phosphate binding residues in the β_1-α_1 loop and α_1 are boxed. ECT2: Epithelial cell-transforming sequence 2; DNLI4: DNA ligase 4. PTIP: PAX-interacting protein 1; XRCC1: X-ray repair cross-complementing protein 1.

Interestingly, this recognition of the pThr side chain is similar to that employed by FHA domains, which specifically bind pThr-peptides through conserved arginine residues (Liang & Van Doren, 2008; Yaffe & Smerdon, 2001). For example, Arg61 of the RNF8 FHA domain makes a bidentate interaction with the phosphate of its target pThr, while Arg42 mediates an interaction between the phosphate group and -2 of the peptide backbone. These interactions anchor the pThr side chain and the backbone configuration of the peptide in a similar conformation to that observed in the TopBP1 BRCT7/8 complex (Fig. 4-14). TopBP1 Arg1280 fulfills the roles of the conserved RNF8 Arg61 and Arg42 residues by concurrently contacting both the phosphate and the -2 of the peptide backbone. It has been suggested that FHA domains prefer pThr because binding of the pThr binding motif places the pThr in an orientation that allows the γ-methyl group to pack in a small hydrophobic cavity in the FHA domain. Substitution to a pSer would result in loss of these particular van der Waals interactions (Pennell et al, 2010). In the case of TopBP1 BRCT7/8, the pSer binding ability can be explained by the absence of the FHA γ-methyl cavity, which is substituted by the water mediated network of interactions (Fig. 4-8A).

The interaction between TopBP1 and BACH1 is crucial for the response to DNA replication stress. Recognition of phosphorylated BACH1 by the tandem BRCT7/8 domains of TopBP1 drives RPA chromatin loading, which is a prerequisite for ATR activation and DNA replication checkpoint control. This study provides the structural basis of this critical interaction, as well as new insights into the surprising versatility of tandem BRCT domain function in the DNA damage response.

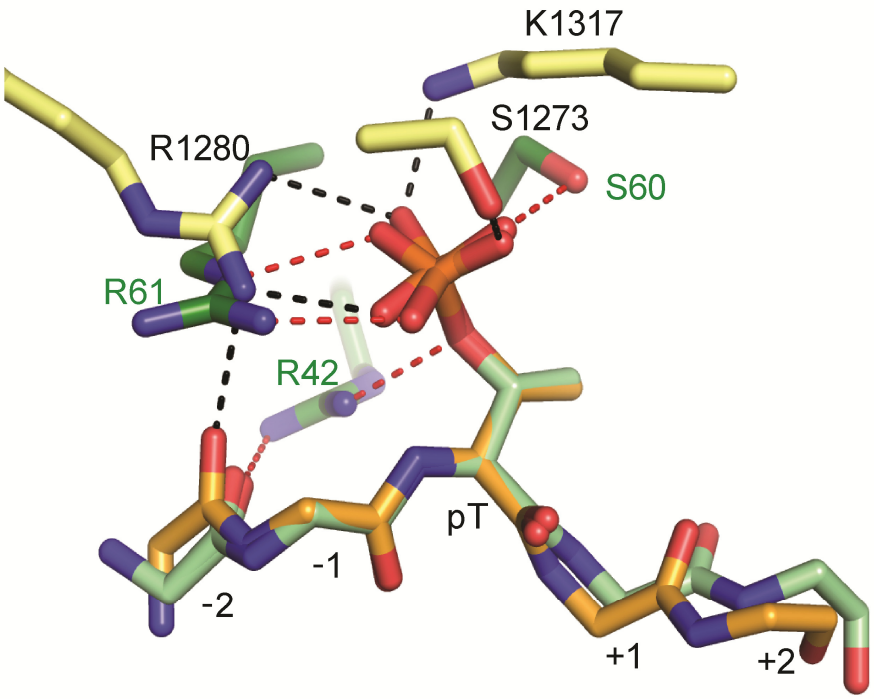

Figure 4-14. The bound pThr-peptide orientation is similar in TopBP1 BRCT7/8 and FHA domains. Structural alignment of the TopBP1 BRCT7/8-pThr peptide complex (yellow/orange) with the RNF8 FHA-pThr peptide complex (green, PDB ID: 2PIE). Conserved residues are labelled for TopBP1 (black) and RNF8 (green).

4.4 References

Botuyan MV, Nomine Y, Yu X, Juranic N, Macura S, Chen J, Mer G (2004) Structural basis of BACH1 phosphopeptide recognition by BRCA1 tandem BRCT domains. *Structure* **12:** 1137-1146

Bridge WL, Vandenberg CJ, Franklin RJ, Hiom K (2005) The BRIP1 helicase functions independently of BRCA1 in the Fanconi anemia pathway for DNA crosslink repair. *Nat Genet* **37:** 953-957

Campbell SJ, Edwards RA, Glover JN (2010) Comparison of the structures and peptide binding specificities of the BRCT domains of MDC1 and BRCA1. *Structure* **18:** 167-176

Cantor SB, Bell DW, Ganesan S, Kass EM, Drapkin R, Grossman S, Wahrer DC, Sgroi DC, Lane WS, Haber DA, Livingston DM (2001) BACH1, a novel helicase-like protein, interacts directly with BRCA1 and contributes to its DNA repair function. *Cell* **105:** 149-160

Cimprich Ka, Cortez D (2008) ATR: an essential regulator of genome integrity. *Nat Rev Mol Cell Biol* **9:** 616-627

Clapperton Ja, Manke Ia, Lowery DM, Ho T, Haire LF, Yaffe MB, Smerdon SJ (2004) Structure and mechanism of BRCA1 BRCT domain recognition of phosphorylated BACH1 with implications for cancer. *Nat Struct Mol Biol* **11:** 512-518

Ekblad CM, Wilkinson HR, Schymkowitz JW, Rousseau F, Freund SM, Itzhaki LS (2002) Characterisation of the BRCT domains of the breast cancer susceptibility gene product BRCA1. *J Mol Biol* **320:** 431-442

Glover JN, Williams RS, Lee MS (2004) Interactions between BRCT repeats and phosphoproteins: tangled up in two. *Trends Biochem Sci* **29:** 579-585

Gong Z, Kim JE, Leung CC, Glover JN, Chen J (2010) BACH1/FANCJ acts with TopBP1 and participates early in DNA replication checkpoint control. *Mol Cell* **37:** 438-446

Hayward S, Berendsen HJ (1998) Systematic analysis of domain motions in proteins from conformational change: new results on citrate synthase and T4 lysozyme. *Proteins* **30:** 144-154

Kilkenny ML, Doré AS, Roe SM, Nestoras K, Ho JCY, Watts FZ, Pearl LH (2008) Structural and functional analysis of the Crb2-BRCT2 domain reveals distinct roles in checkpoint signaling and DNA damage repair. *Genes Dev* **22:** 2034-2047

Levran O, Attwooll C, Henry RT, Milton KL, Neveling K, Rio P, Batish SD, Kalb R, Velleuer E, Barral S, Ott J, Petrini J, Schindler D, Hanenberg H, Auerbach AD (2005) The BRCA1-interacting helicase BRIP1 is deficient in Fanconi anemia. *Nat Genet* **37:** 931-933

Liang X, Van Doren SR (2008) Mechanistic insights into phosphoprotein-binding FHA domains. *Acc Chem Res* **41:** 991-999

Litman R, Peng M, Jin Z, Zhang F, Zhang J, Powell S, Andreassen PR, Cantor SB (2005) BACH1 is critical for homologous recombination and appears to be the Fanconi anemia gene product FANCJ. *Cancer Cell* **8:** 255-265

Liu K, Paik JC, Wang B, Lin FT, Lin WC (2006) Regulation of TopBP1 oligomerization by Akt/PKB for cell survival. *EMBO J* **25:** 4795-4807

Liu S, Shiotani B, Lahiri M, Marechal A, Tse A, Leung CC, Glover JN, Yang XH, Zou L (2011) ATR Autophosphorylation as a Molecular Switch for Checkpoint Activation. *Mol Cell* **43:** 192-202

Manke Ia, Lowery DM, Nguyen A, Yaffe MB (2003) BRCT repeats as phosphopeptide-binding modules involved in protein targeting. *Science* **302:** 636-639

Mohammad D, Yaffe MB (2009) 14-3-3 proteins, FHA domains and BRCT domains in the DNA damage response. *DNA Repair* **8:** 1009-1017

Nomine Y, Botuyan MV, Bajzer Z, Owen WG, Caride AJ, Wasielewski E, Mer G (2008) Kinetic analysis of interaction of BRCA1 tandem breast cancer c-terminal domains with phosphorylated peptides reveals two binding conformations. *Biochemistry* **47:** 9866-9879

Pennell S, Westcott S, Ortiz-Lombardia M, Patel D, Li J, Nott TJ, Mohammed D, Buxton RS, Yaffe MB, Verma C, Smerdon SJ (2010) Structural and functional analysis of phosphothreonine-dependent FHA domain interactions. *Structure* **18:** 1587-1595

Rappas M, Oliver AW, Pearl LH (2011) Structure and function of the Rad9-binding region of the DNA-damage checkpoint adaptor TopBP1. *Nucleic Acids Res* **39:** 313-324

Rodriguez M, Yu X, Chen J, Songyang Z (2003) Phosphopeptide binding specificities of BRCA1 COOH-terminal (BRCT) domains. *J Biol Chem* **278:** 52914-52918

Shen Y, Tong L (2008) Structural evidence for direct interactions between the BRCT domains of human BRCA1 and a phospho-peptide from human ACC1. *Biochemistry* **47:** 5767-5773

Shiozaki EN, Gu L, Yan N, Shi Y (2004) Structure of the BRCT repeats of BRCA1 bound to a BACH1 phosphopeptide: implications for signaling. *Mol Cell* **14:** 405-412

Stucki M, Clapperton Ja, Mohammad D, Yaffe MB, Smerdon SJ, Jackson SP (2005) MDC1 directly binds phosphorylated histone H2AX to regulate cellular responses to DNA double-strand breaks. *Cell* **123:** 1213-1226

Varma AK, Brown RS, Birrane G, Ladias Jaa (2005) Structural basis for cell cycle checkpoint control by the BRCA1-CtIP complex. *Biochemistry* **44:** 10941-10946

Williams JS, Williams RS, Dovey CL, Guenther G, Tainer JA, Russell P (2010) gammaH2A binds Brc1 to maintain genome integrity during S-phase. *EMBO J* **29:** 1136-1148

Williams RS, Dodson GE, Limbo O, Yamada Y, Williams JS, Guenther G, Classen S, Glover JN, Iwasaki H, Russell P, Tainer JA (2009) Nbs1 flexibly tethers Ctp1 and Mre11-Rad50 to coordinate DNA double-strand break processing and repair. *Cell* **139:** 87-99

Williams RS, Green R, Glover JN (2001) Crystal structure of the BRCT repeat region from the breast cancer-associated protein BRCA1. *Nat Struct Biol* **8:** 838-842

Williams RS, Lee MS, Hau DD, Glover JN (2004) Structural basis of phosphopeptide recognition by the BRCT domain of BRCA1. *Nat Struct Mol Biol* **11:** 519-525

Yaffe MB, Elia aE (2001) Phosphoserine/threonine-binding domains. *Curr Opin Cell Biol* **13:** 131-138

Yaffe MB, Smerdon SJ (2001) PhosphoSerine/threonine binding domains: you can't pSERious? *Structure* **9:** R33-38

Yamane K, Wu X, Chen J (2002) A DNA damage-regulated BRCT-containing protein, TopBP1, is required for cell survival. *Mol Cell Biol* **22:** 555-566

Yu X, Chini CC, He M, Mer G, Chen J (2003) The BRCT domain is a phospho-protein binding domain. *Science* **302:** 639-642

Chapter 5

Molecular basis of MDC1 recognition by TopBP1 BRCT4/5 in DNA replication checkpoint control

5.1 Introduction

The emergence of TopBP1 as a key regulator of the DNA replication checkpoint is highlighted by interactions mediated by various BRCT domains in TopBP1. The TopBP1 N-terminal BRCT0/1/2 domains interact with the Rad9 tail of the 9-1-1 complex to activate ATR via the ATR activation domain (AAD) of TopBP1. In an earlier step in checkpoint activation, TopBP1 BRCT7/8 domains bind BACH1/FANCJ to regulate the helicase activity of BACH1 and increase ssDNA and subsequent RPA loading. The structural basis for this interaction is described in Chapter 4. Despite these findings, it remained elusive how TopBP1 accumulated at stalled replication forks, since TopBP1 localization is independent of BACH1 and Rad9 interactions (Gong et al, 2010; Yan & Michael, 2009).

Previous reports by our collaborator, Dr. Junjie Chen (University of Texas MD Anderson Cancer Center), indicated that the fifth BRCT domain of TopBP1 is responsible for TopBP1 localization to stalled replication forks (Yamane et al, 2002). Excitingly, recent work by their group revealed that a critical interaction between TopBP1 BRCT5 and MDC1, an adaptor protein best characterized for its involvement in DNA DSB repair, was indeed the basis for TopBP1 localization (Wang et al, 2011). In response to DNA DSBs, the histone H2AX is phosphorylated at Ser139 (γ-H2AX) by the Ser/Thr kinase ATM. γ-H2AX is recognized by the tandem BRCT domains of MDC1, and functions as a platform to recruit various DDR proteins such as RNF8 and NBS1 to sites of DNA damage (Bennett & Harper, 2008; Huen & Chen, 2010). A region in MDC1 spanning amino acids 210-460 contains six highly conserved Ser-Asp-Thr (SDT) motifs that are constitutively phosphorylated by Casein kinase 2 (CK2). These di-phosphorylated motifs are recognized by the conserved phospho-peptide binding FHA and BRCT domains of the supramodular FHA-BRCT-BRCT domain repeat in NBS1, a component of the MRE11-RAD50-NBS1 (MRN) complex, to

recruit the MRN complex to sites of DNA DSBs (Chapman & Jackson, 2008; Melander et al, 2008; Spycher et al, 2008; Wu et al, 2008).

Like the phospho-peptide binding domains in NBS1, TopBP1 BRCT5 directly interacts with the phosphorylated MDC1 SDT repeats, and this binding is required for sustaining and amplifying ATR activity for checkpoint activation (Wang et al, 2011). Interestingly, unlike conventional tandem BRCT domains that require both BRCT domains to form a viable phospho-peptide binding surface, only the C-terminal BRCT5 of the tandem BRCT4/5 pair is needed for MDC1 interaction. In light of this knowledge, we sought to delineate the molecular basis of TopBP1-MDC1 interaction by characterizing, both structurally and functionally, the interaction between the tandem TopBP1 BRCT4/5 domains and a MDC1 di-phospho-peptide containing a consensus sequence of the SDT repeats. We show that TopBP1 BRCT4/5 adopts an unusual tandem BRCT repeat structure with a phosphate-binding pocket in the C-terminal BRCT5 domain. In collaboration with the Chen lab, we reveal that BRCT5 contains an extended positively charged surface that is critical for TopBP1 localization and mediates MDC1 di-phospho-peptide binding. Unexpectedly, interactions with a single MDC1 di-phospho-peptide require two BRCT5 domains, suggesting a novel mechanism for BRCT domain recognition by phospho-peptides.

5.2 Results

5.2.1. Crystal structure of TopBP1 BRCT4/5

The crystal structure of TopBP1 BRCT4/5 was solved to 1.9 Å resolution. The tandem BRCT pair adopts a unique domain packing, where the juxtaposition of the two BRCT domains is head-to-head (where head is defined as the α_1-α_3 face and tail as the α_2 face) rather than the head-to-tail arrangement characteristic of canonical BRCT repeats (Fig. 5-1). This is likely driven by a combination of the variant BRCT fold in the N-terminal BRCT4 and a

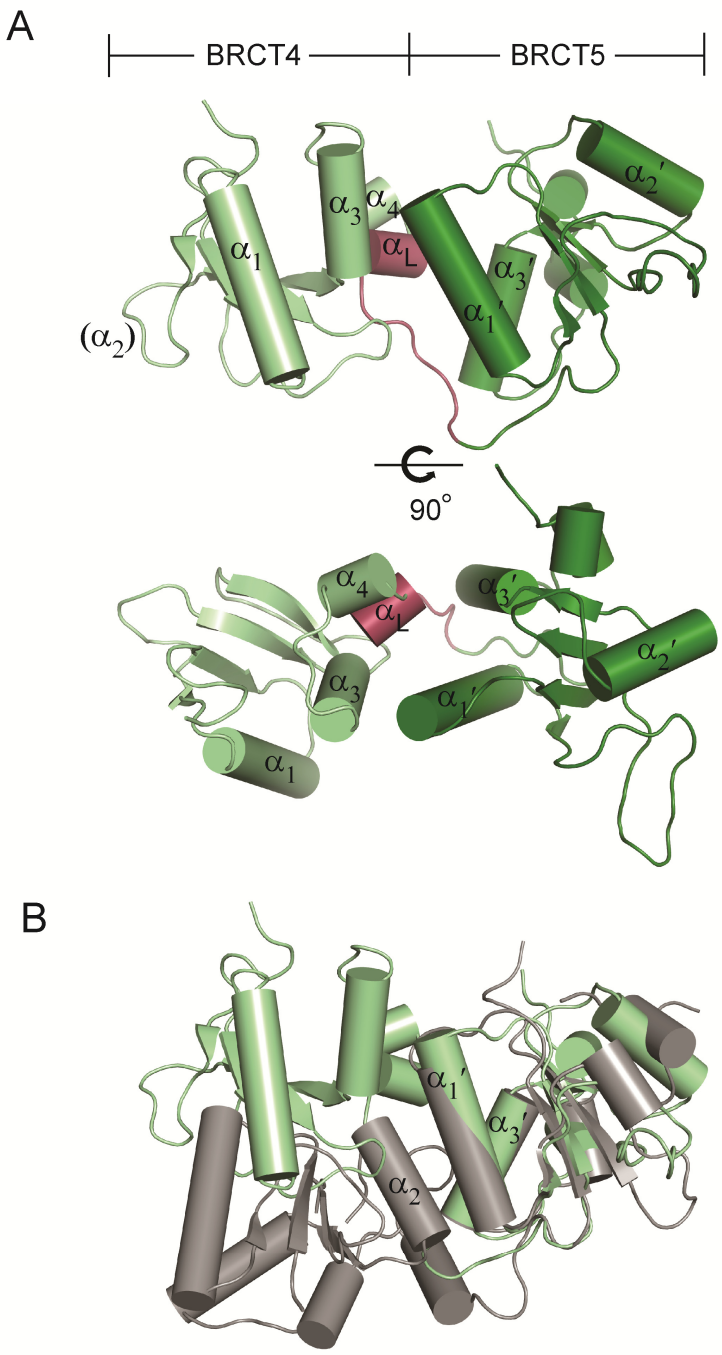

Figure 5-1. Crystal structure of TopBP1 BRCT4/5. (A) Cartoon representation of BRCT4/5, with BRCT4 (light green), inter-BRCT linker (red) and BRCT5 (dark green) coloured accordingly. α-helices are represented as cylinders and labelled. (B) Structural alignment of TopBP1 BRCT4/5 (green) with BRCA1 BRCT1/2 (grey, PDB ID: 1JNX). The α_1, α_1' and α_3'-helices for BRCA1 are labelled.

significantly shorter linker region between BRCT4 and BRCT5. TopBP1 BRCT4 lacks a α_2-helix, which in canonical BRCT repeats houses conserved residues that participate in phosphate-binding and the hydrophobic BRCT-BRCT interface (Fig. 5-1, 5-2). Instead, the BRCT4 α_2 is replaced by a short loop that is solvent exposed rather than being involved at the BRCT-BRCT interface. A short linker helix (α_L) composed of three residues (Pro632, Leu633 and Phe634) is also part of a significantly shorter inter-BRCT linker in TopBP1 BRCT4/5 (Fig. 5-1, 5-2). The inter-BRCT linker packs tightly in between the adjacent BRCT domains to stabilize the BRCT-BRCT interface. In particular, Phe634, Thr635 and Pro636 packs against BRCT4 while Pro632, Leu633, Val637, Pro638, Val639, M640 makes extensive hydrophobic contacts with BRCT5 (Fig. 5-3A).

As a consequence of the unusual head-to-head domain arrangement, the composition of the N-terminal domain face that contacts the C-terminal domain is significantly different from the one employed in conventional BRCT repeats (Fig. 5-1B). The N-terminal domain face consists of residues from α_3 (Val617 and Thr618) , the β_3-β_4 loop (Leu598 and Leu599) and linker region (Pro632, Leu633, Val637, Pro638 and Val639). Contributions from these different regions substitute for the α_2-helix, which is typically found but is absent in BRCT4 (Fig. 5-3B, left panel). Conversely, the C-terminal domain face that contacts the N-terminal domain involves the α_1' and α_3' helices, which are the same secondary structure elements utilized in canonical BRCT repeats. Residues that form this hydrophobic face include Ala659, Ser663, Leu664, Phe666, Leu667 and Leu670 of α_1' and Ile718, Leu722, Ala725 and Arg726 of α_3' (Fig. 5-3B, right panel). Together, the α_3, β_3-β_4 loop, linker region, α_1' and α_3'-helices form an extensive hydrophobic interface that enables a head-to-head domain packing in TopBP1 BRCT4/5.

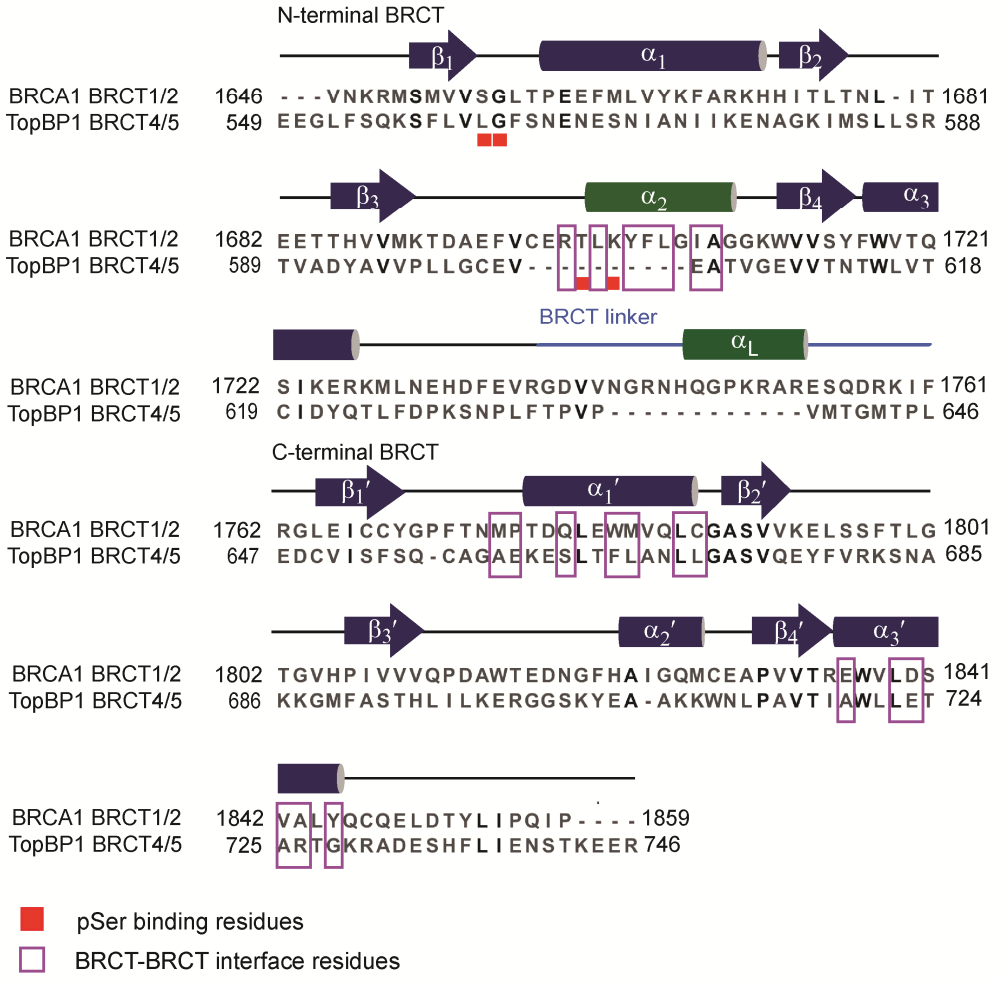

Figure 5-2. Alignment of TopBP1 BRCT4/5 with BRCA1 BRCT1/2. The alignment is based on a combination of sequence alignment, secondary structure prediction and fold recognition (Kelley & Sternberg, 2009). The secondary structure elements of BRCA1 are indicated above the sequence. BRCA1 residues involved in phosphate binding are indicated as red squares and BRCT-BRCT interface residues are boxed in purple.

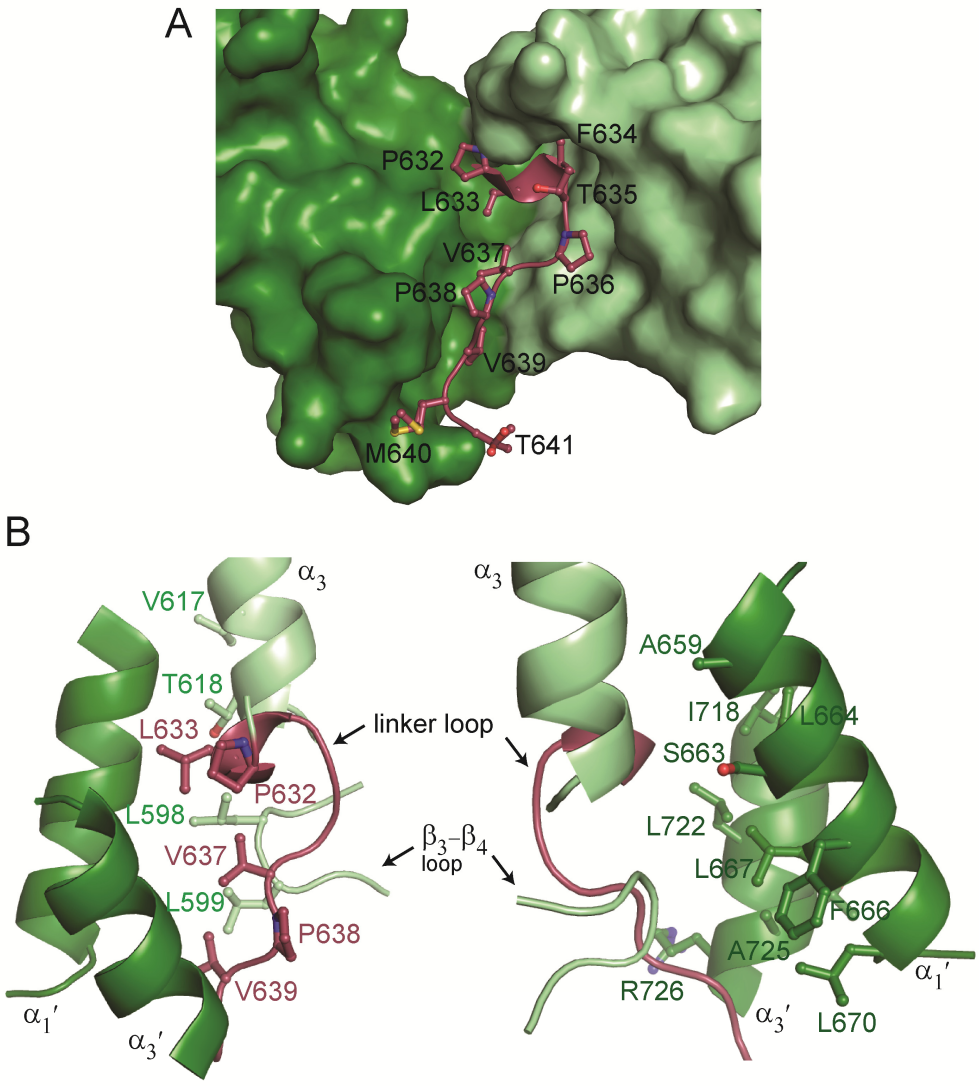

Figure 5-3. TopBP1 BRCT4/5 BRCT-BRCT domain interface. (A) The inter-BRCT linker stabilizes packing with the N- and C-terminal BRCT domains. Residues are shown as sticks and labelled. (B) Residues at the N-terminal domain face (left) and C-terminal domain face (right) involved in the BRCT-BRCT interface are indicated in sticks and labelled. Secondary structure elements are also indicated.

5.2.2. The C-terminal BRCT5 contains the putative phosphate-binding pocket

To date, the phosphate-binding pockets identified in BRCT repeats are found in the N-terminal BRCT. This allows BRCT repeats to select for the +3 residue in a targeted phospho-peptide through a secondary pocket formed at the BRCT-BRCT interface. The putative phosphate-binding pocket in BRCT4 is highly acidic, and conserved phosphate-binding residues are instead substituted with Leu561, Glu568 and Glu604 (Fig. 5-4A, left panel). Strikingly, an intact phosphate-binding pocket is found in the C-terminal BRCT5 (Fig. 5-4A, right panel). Structural alignment of the BRCT5 pocket with known phosphate-binding pockets in BRCA1 and MDC1 also indicate that the conserved phosphate-binding residues (S654, Q655 and K704 in TopBP1; S1655, G1656 and K1702 in BRCA1; T1898, G1899 and K1702 in MDC1) are in optimal orientations for phosphate coordination (Fig. 5-4B). Although the presence of a C-terminal phosphate-binding pocket is perplexing in comparison to other BRCT repeats, the ability for BRCT5 to recognize a phosphate supports previous findings that BRCT5 interacts with MDC1 to control the DNA replication checkpoint (Wang et al, 2011).

5.2.3. A positively charged surface on BRCT5 is required for TopBP1 localization and function

To probe for potential protein binding surfaces on TopBP1 BRCT4/5, we first examined the electrostatic potential surface of TopBP1 BRCT4/5. Although the BRCT repeat structure carries an overall negative charge, a highly positively charged surface is located on BRCT5 (Fig. 5-5A). This region is rich in basic residues that extend from the putative phosphate-binding pocket (K661 and K704) to the extended β_2'-β_3' loop (R681, K682, K686 and K687) and C-terminus of α_2' (K710) (Fig. 5-5B).

Alignments of various tandem BRCT domains indicate that the β_2'-β_3' loop is the most variable region in the BRCT family (Glover et al, 2004). In

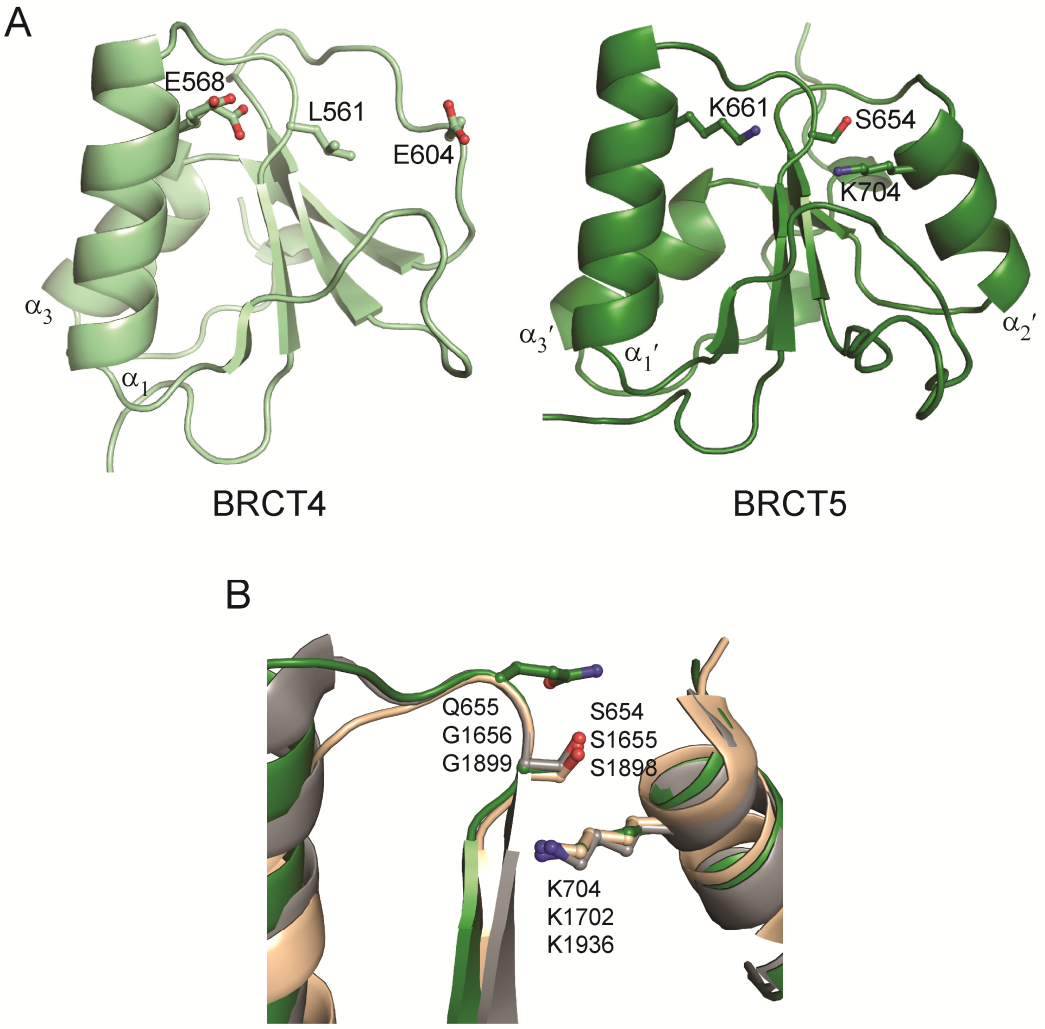

Figure 5-4. TopBP1 BRCT5 contains an intact phosphate-binding pocket. (A) Comparison of conserved phosphate-binding residues in BRCT4 (left) and BRCT5 (right). (B) Structural alignment of the conserved phosphate-binding pocket in BRCT5 (green) with BRCA1 (grey) and MDC1 (beige). Equivalent phosphate-binding residues are shown as sticks and labelled for TopBP1 (top), BRCA1 (middle) and MDC1 (bottom).

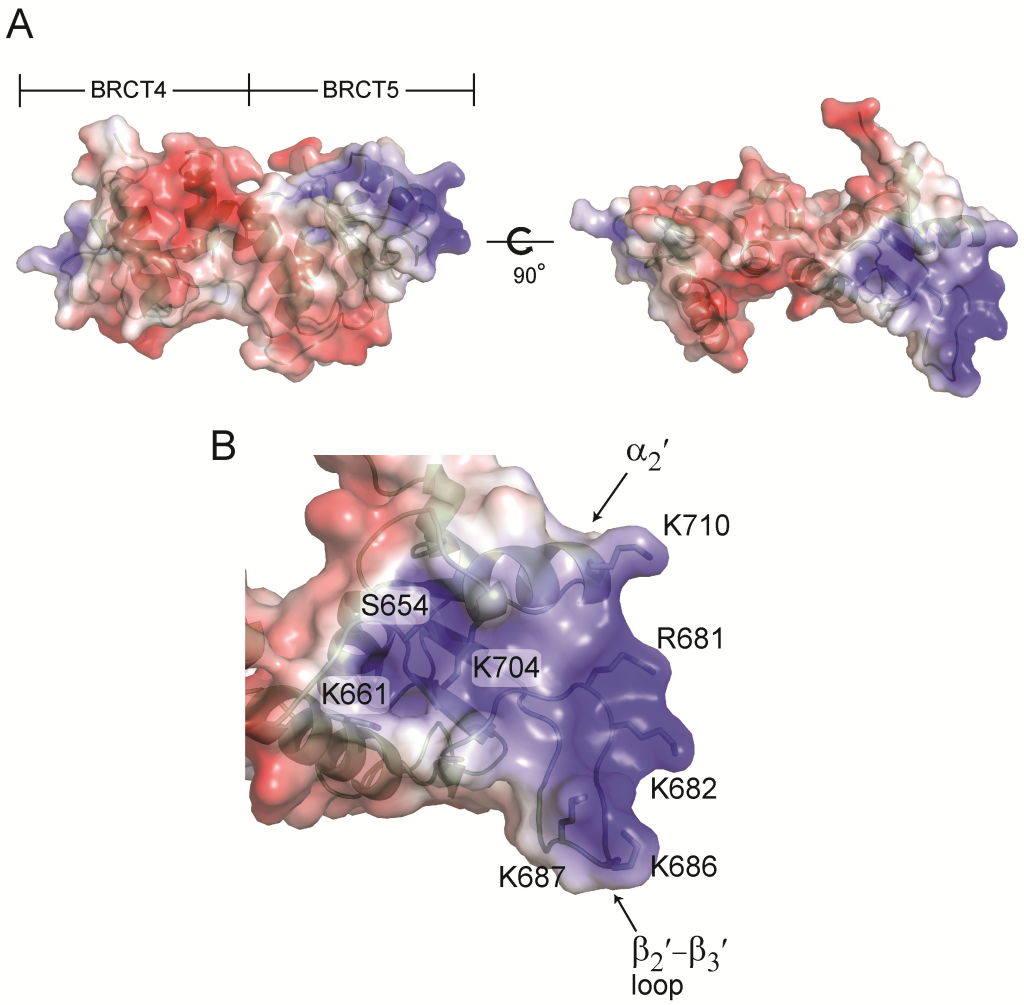

Figure 5-5. TopBP1 BRCT5 contains a conserved positively charged surface. (A) Electrostatic surface representation of TopBP1 BRCT4/5. (B) Residues that make up the basic surface on BRCT5 are marked as sticks and labelled. The conserved Ser654 in the phosphate-binding pocket is also shown.

TopBP1 BRCT5, the β_2'-β_3' loop adopts an unusually extended, structured protrusion. A series of main chain hydrogen bonds mediated by Asn684, Ala685, Lys687, Gly688, Met689 and Ala691 ensure rigidity of the loop (Fig. 5-6A). The side chains of Asn684 and Ser683 also participate in hydrogen bonds with the loop main chain. This provides a structural platform for the four basic loop residues (Arg681, Lys682, Lys686 and Lys687) to create a positively charged concave pocket (Fig. 5-5B). Furthermore, the loop residues, especially Asn684 and the group of basic residues, are highly conserved among TopBP1 homologs (Fig. 5-6B).

Since TopBP1 BRCT5 is required for TopBP1 accumulation at stalled replication forks (Yamane et al, 2002), we hypothesized that the conserved basic surface may be responsible for TopBP1 localization and MDC1 binding. Dr. Zihua Gong (Chen lab) performed experiments to assess the effects of BRCT5 mutants on TopBP1 foci formation in response to hydroxyurea (HU)-induced replication stress. As shown in Table 5-1, mutations in the putative phosphate-binding pocket (K704A) or in the β_2'-β_3' loop (RK681/682EE) abolished foci formation, suggesting that the basic surface is in fact functionally important. The other β_2'-β_3' loop mutant (KK686/687EE) showed a slight defect, perhaps a result of being positioned at the distal edge of the putative binding surface. Interestingly the S654A mutation, which is of a conserved phosphate-binding residue (Ser1655/Thr1898 in BRCA1/MDC1), had no effect on TopBP1 foci formation. Previous studies in BRCA1, MDC1 and TopBP1 BRCT7/8 have shown that mutation of this critical serine significantly compromises binding to their respective phospho-peptides (Clapperton et al, 2004; Leung et al, 2011; Stucki et al, 2005; Williams et al, 2004). The localization data of these various mutants also correlated with MDC1 binding *in vivo* (Zihua Gong, personal communication), suggesting that the positively charged surface in BRCT5 is responsible for interactions with MDC1 in DNA replication checkpoint signalling.

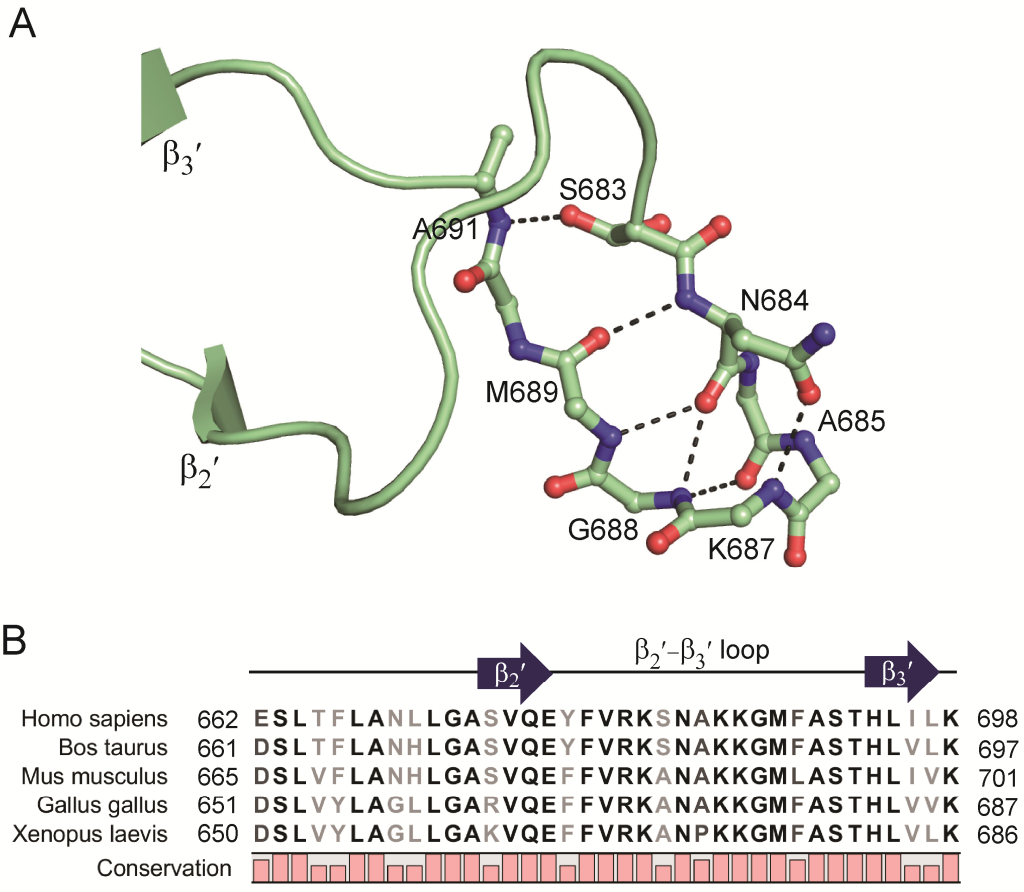

Figure 5-6. The BRCT5 β_2'-β_3' loop is structured and conserved. (A) Hydrogen bonding network of the β_2'-β_3' loop. Residues involved in hydrogen bonding (dotted lines) are labelled. Side chain residues that make loop main chain contacts are shown. (B) Sequence alignment of the β_2'-β_3' loop in various homologs. Conservation is represented as a bar graph under the sequence.

Table 5-1. Effects of TopBP1 BRCT5 mutants on TopBP1 focus formation.

TopBP1 BRCT5 Variant	Focus Formation (full-length TopBP1)
Wild type	+++
KK686/687EE	++/+
RK681/682EE	+/-
K704A	+/-
S654A	+++

5.2.4. Interactions between TopBP1 BRCT4/5 and MDC1 di-phospho-peptide

Previous studies demonstrated that TopBP1 BRCT4/5 can interact with a MDC1 di-phospho-peptide encoding a consensus sequence of the six SDT repeats (Wang et al, 2011). Using a streptavidin-biotin pull-down assay, GST fusion proteins of TopBP1 BRCT4/5 and BRCT5 were pulled down by an immobilized biotin-labelled MDC1 di-phospho-peptide but not the non-phoshorylated counterpart. However, Wang et al. noted that the interaction was very weak and reproducibility of the pull-down assay was difficult (Jiadong Wang, personal communication). Taking a more quantitative approach, we attempted to use fluorescence polarization (FP) and isothermal titration calorimetry (ITC) to further test for this interaction *in vitro*. Unfortunately, we were unable to detect an interaction between a consensus MDC1 di-phospho-peptide (GFIDpSDpTDVEEE) and TopBP1 BRCT4/5 with ITC. However, we were successful in measuring a binding response using FP.

As in our previous studies with the TopBP1-BACH1 interaction (Chapter 4), we tested for the requirement of MDC1 phosphorylation for binding TopBP1 BRCT4/5 using λ phosphatase in conjunction with the FP assay. Dephosphorylation of the FITC-labelled MDC1 di-phospho-peptide showed a significant reduction in binding affinity to TopBP1 BRCT4/5 (K_d = 164 ± 18 μM for PPase (inactive), K_d > 1500 μM for PPase), supporting the preference for binding phosphorylated MDC1 (Fig. 5-7A). The relatively modest difference in peptide affinities compared to other BRCT-phospho-peptide interactions suggests that phosphate binding may play a less important role in the TopBP1-MDC1 interaction. To assess whether binding to phosphorylated MDC1 only requires the C-terminal BRCT5 domain, we performed the FP assay using GST-fusion proteins of TopBP1 BRCT4/5 and BRCT5. Loss of BRCT4 only slightly reduced binding affinities to the FITC-labelled MDC1 di-phospho-peptide (K_d = 159 ± 13 μM for GST-BRCT5, K_d = 82.4 ± 10 μM for GST-BRCT4/5), suggesting that BRCT4

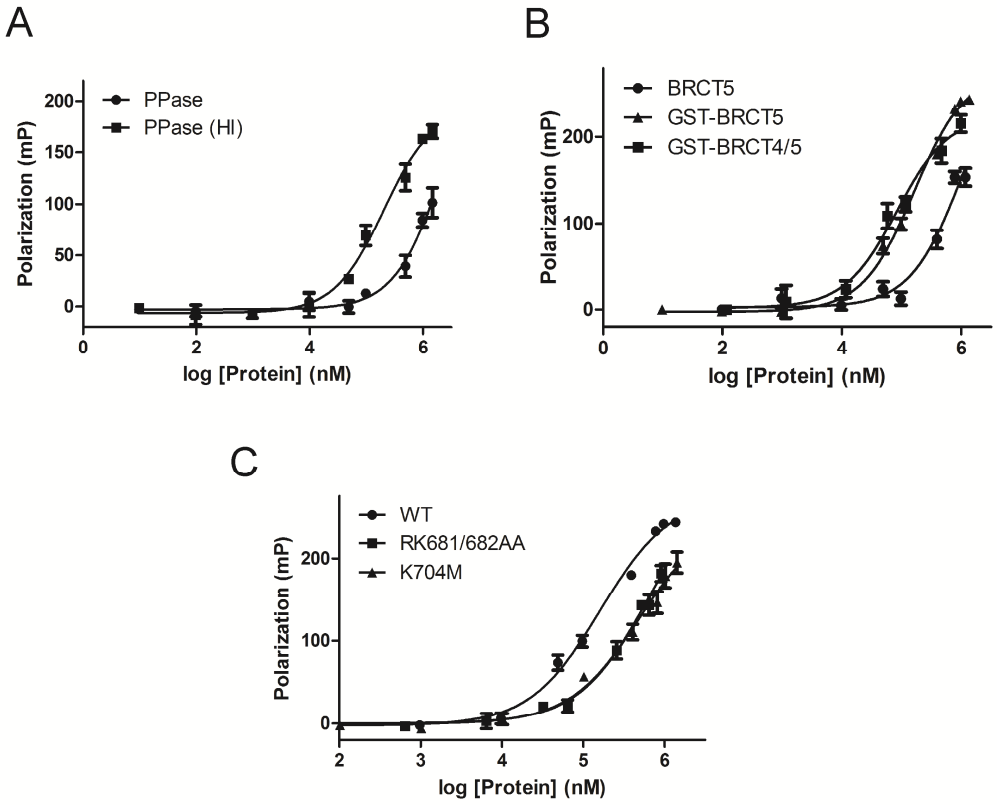

Figure 5-7. Binding specificity studies of TopBP1 BRCT4/5 and BRCT5 with a MDC1 di-phospho-peptide. (A) FP experiments of λ phosphatase treated FITC-MDC1 di-phospho-peptide with TopBP1 BRCT4/5. The peptide was incubated with PPase or heat inactivated (HI) PPase prior to setting up FP assays. (B) FP studies of FITC-MDC1 di-phospho-peptide with various TopBP1 BRCT4/5 and BRCT5 proteins. (C) FP studies of FITC-MDC1 di-phospho-peptide with various GST-BRCT5 mutants.

may not be essential for the MDC1 interaction (Fig. 5-7B). Interestingly, untagged TopBP1 BRCT5 protein displayed a marked reduction in binding to the di-phospho-peptide (K_d > 1000 μM). This implied that GST-induced dimerization of BRCT5 may have an indirect effect on peptide binding. We next performed FP studies on various BRCT5 mutants to test whether the conserved positively charged surface is responsible for interactions with MDC1. Consistent with our *in vivo* localization data, mutations in either the putative phosphate-binding pocket (K704M) or β_2'-β_3' loop (RK681/682AA) reduced binding to the MDC1 di-phospho-peptide compared with wild type ($K_d \geq 600$ μM for K704M, $K_d \geq 500$ μM for RK681/682AA) (Fig. 5-7C).

We were particularly intrigued with the idea that MDC1 is a di-phosphorylated binding motif, since previous studies showed that phosphorylation of the SDT motif at Thr is more important than Ser for interactions with the NBS1 FHA-BRCT-BRCT phospho-peptide binding repeats (Lloyd et al, 2009). Therefore, we asked whether the TopBP1 BRCT4/5 interaction requires phosphorylation of the Ser, Thr or both residues. To test for this *in vivo*, Dr. Zihua Gong performed a series of pull-down assays to test for TopBP1 binding to different MDC1 SDT repeat mutants. Taking a TopBP1-binding defective MDC1 mutant in which the Ser/Thr residues in all six SDT repeats were mutated to alanine (12A), one full SDT site was restored with both Ser/Thr (10ASDTD) or only Thr (11AADTD) or Ser (11ASDAD) to look for its effects in rescuing interactions with TopBP1 in a pull-down assay. As shown in Figure 5-8, adding back one wild type SDT site (10ASDTD) restored partial binding to full-length TopBP1 that was higher than the either single Ser (11ASDAD) or Thr (11AADTD) restored proteins. Interestingly, an intact Thr (11AADTD) in MDC1 bound slightly better than a Ser (11ASDAD), hinting that the pThr may be more important than pSer for interactions with TopBP1. However, since the relative degree of phosphorylation of these proteins is not accounted for, these results can only be taken in a highly qualitative manner. Therefore, we are currently

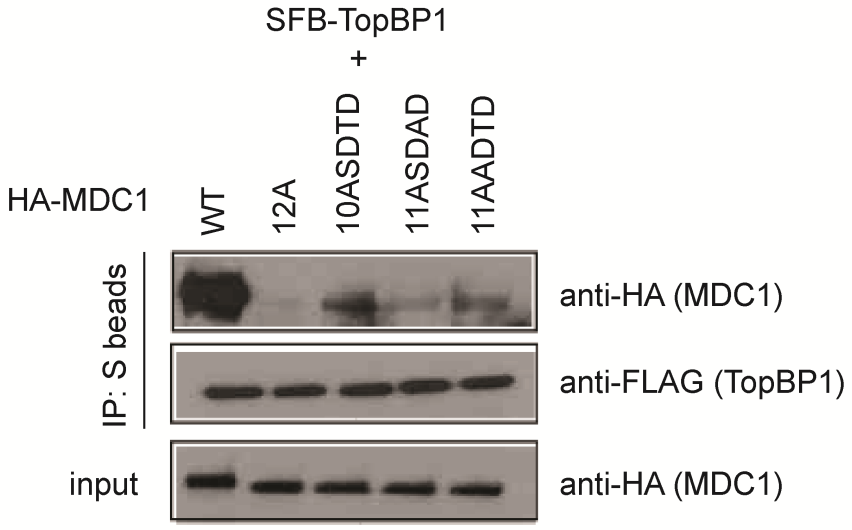

Figure 5-8. Effects of MDC1 SDT mutations on TopBP1 binding *in vivo*. Experiments were performed by Dr. Zihua Gong (Chen lab). Constructs encoding HA-tagged wild type and mutants of MDC1 were co-transfected with plasmids encoding SFB-TopBP1. Immunoprecipitation (IP) reactions were performed using S protein beads and then subjected to Western blot analyses using antibodies as indicated.

using single phosphorylated FITC-labelled MDC1 phospho-peptides (pThr: GFIDSDpTDVEEE, pSer: GFIDpSDTDVEEE) in the FP assay to investigate the phosphorylation requirements for TopBP1 BRCT5 recognition.

5.2.5. Overall crystal structure of TopBP1 BRCT4/5 in complex with MDC1 di-phospho-peptide

To further characterize the TopBP1-MDC1 interaction, we co-crystallized and solved the structure of TopBP1 BRCT4/5 in complex with a MDC1 di-phospho-peptide to 2.6 Å resolution. The crystal asymmetric unit contains four TopBP1 BRCT4/5 molecules that are arranged as two dimers (AB and CD, Fig. 5-9). The two dimers are related by 2-fold non-crystallographic symmetry, which was used as a restraint in the refinement process. Within each dimer, the MDC1 di-phospho-peptide is bound in an extended conformation by two BRCT4/5 protomers on opposite sides (designated A and B, Fig. 5-10). Comparisons of the apo and bound structures indicate that BRCT4/5 is structurally rigid and does not change significantly upon peptide binding (RMSD for Cα = 0.380 and 0.475 with protomer A and B, respectively). The two protomers are oriented in an orthogonal manner in the dimer and interact indirectly through the MDC1 phospho-peptide, except for a single hydrogen bond between the Tyr622 side chain of protomer A and the Gly702 main chain of protomer B. Consistent with previous data for BRCT5-mediated MDC1 binding, the MDC1 di-phospho-peptide exclusively contacts the two BRCT5 domains from each protomer.

Although the MDC1 di-phospho-peptide interacts with two BRCT5 domains, their binding interfaces are not symmetrical and are significantly different in size and composition. The majority of interactions with protomer A are contributed by the peptide pThr residue, and bury a total solvent accessible surface area of 434 Å^2. This relatively small contact interface suggests that peptide interactions with protomer A are unlikely to be stable on its own. In contrast, the interface between the di-phospho-peptide and protomer B is more

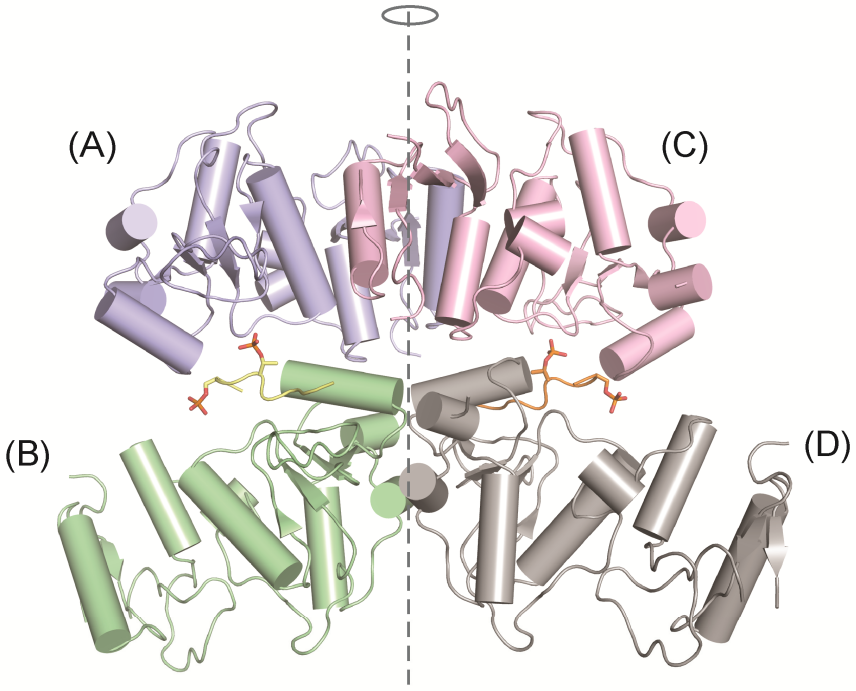

Figure 5-9. Crystal structure of the bound TopBP1 BRCT4/5 dimers related by 2-fold non-crystallographic symmetry. The four BRCT4/5 molecules are denoted A-D and the di-phospho-peptides are coloured yellow and orange.

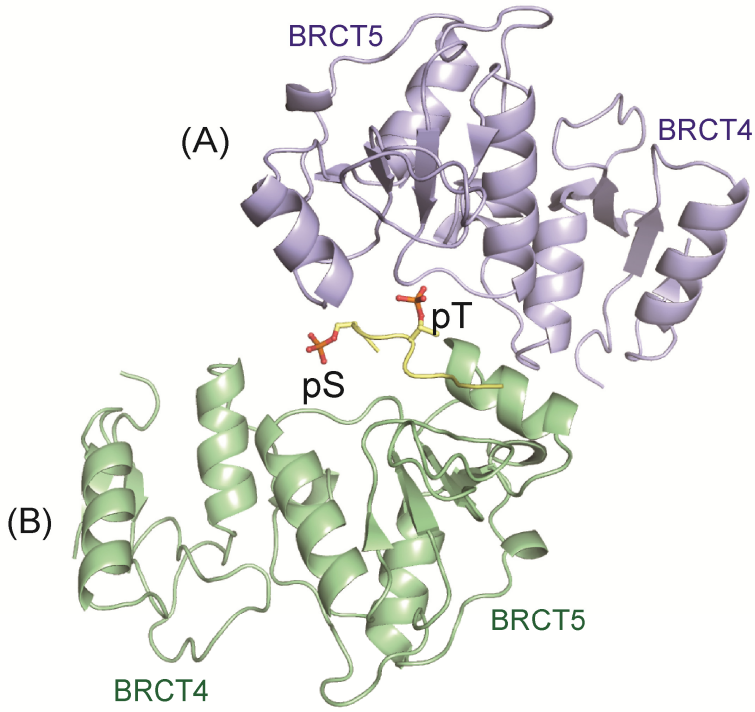

Figure 5-10. Crystal structure of a single BRCT4/5 dimer in complex with a MDC1 di-phospho-peptide. The pS and pT residues in the phospho-peptide (yellow) are shown as sticks and labelled.

extensive, spanning residues -3 to +4 relative to the pThr, and burying 919 $Å^2$ of solvent accessible surface area.

5.2.6. MDC1 di-phospho-peptide binding specificities

Interactions with BRCT5 of protomer A involve the MDC1 pThr and -1 peptide residues. The pThr is coordinated in the phosphate-binding pocket, but only participates in one direct interaction with the conserved Lys704 side chain (Fig. 5-11A). The pThr also makes several water-bridged interactions with the main chains of Cys656 and Lys704, as well as the side chain of Ser703 of protomer B. The -1 Asp side chain also hydrogen bonds to the Ser703 main chain. Unexpectedly, the -3 Asp, rather than the -2 pSer, points into the phosphate-binding pocket of protomer B (Fig. 5-11B). The aspartate side chain makes a number of hydrogen bonds with the Gln655 main chain, Ser654 side chain and a water molecule bridging interactions with the Lys704 side chain and the -1 main chain. Other contacts include a main chain-main chain hydrogen bond between the +1 Asp and Phe679 and water-bridged interactions involving the Tyr678 side chain and the -1 and +1 Asp side chains.

We were intrigued with the observation that the pSer was relatively ordered, given that it was not coordinated in the phosphate-binding pocket and solvent exposed. A phosphate oxygen atom is 5.4 Å away from the ε-amino nitrogen of Lys661 in protomer A and could potentially make weak electrostatic interactions (Fig. 5-11C). On the opposite side of the pSer, a different oxygen atom makes a water-bridged H-bond with the Arg700 main chain of protomer B. These opposing interactions from protomers A and B could help stabilize the pSer side chain and explain why it is ordered in the crystal structure. In addition, the long range electrostatic interactions could also contribute to binding energy and confer minor selectivity for a pSer.

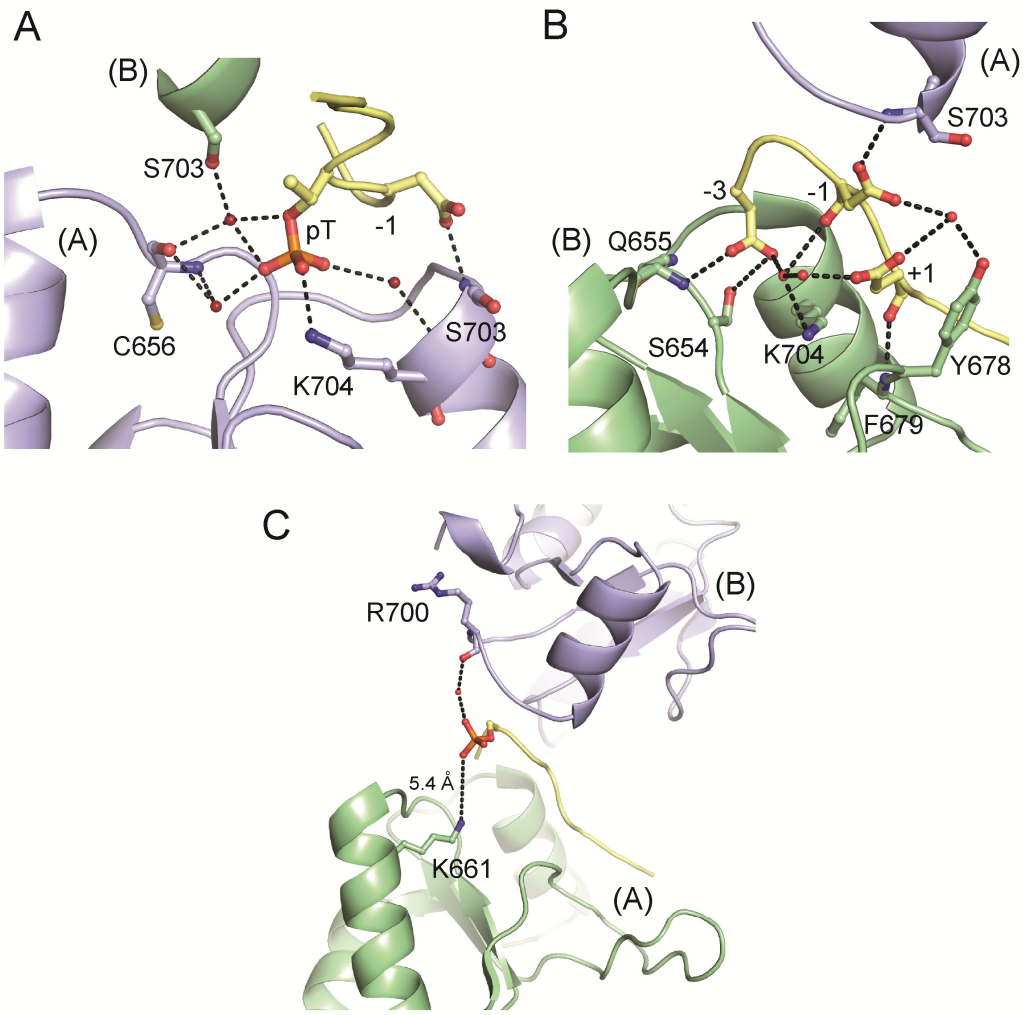

Figure 5-11. TopBP1 BRCT4/5 phosphate-binding pocket interactions. (A) Peptide interactions with BRCT4/5 protomer A. Hydrogen bonds and electrostatic interactions are indicated as dotted lines. Waters are represented as red spheres. (B) Peptide interactions with the phosphate-binding pocket in protomer B. (C) pSer interactions with protomers A and B.

Perhaps the greatest sequence specificity involves the recognition of the C-terminal residues of the conserved MDC1 SDT motif. As part of the larger binding interface established by protomer B, the +2 to +4 residues are recognized by the BRCT5 basic surface that extends from the phosphate-binding pocket to the β_2'-β_3' loop (Fig. 5-12A). The +2 Val sits in a small hydrophobic pocket situated between the basic phosphate-binding pocket and β_2'-β_3' loop. Residues that contribute to this pocket include Ala707 and Trp711 from α_2' and Phe679 from the β_2'-β_3' loop (Fig. 5-12B). The conserved +3 and +4 Glu residues are cradled in the β_2'-β_3' loop and make electrostatic interactions with Lys687 and Lys682, respectively (Fig. 5-12B). Overall, the specificity for the MDC1 SDT motif correlates with our mutational analysis and provides a rationale for the unusually structured and positively charged β_2'-β_3' loop exclusive to TopBP1 BRCT5.

5.2.7. TopBP1 BRCT5 has in vitro DNA binding activity

BRCT domains have also been implicated in DNA binding, although there is still uncertainty as to the specificity of these interactions for different types of DNA structures and their relevance to the biological functions of BRCT proteins. Studies by Yamane et al have previously demonstrated that single and tandem BRCT domains in TopBP1, BRCA1 and XRCC1 can bind various dsDNA substrates *in vitro* (Yamane et al, 2000; Yamane & Tsuruo, 1999). However, the ability for TopBP1 BRCT4/5 to bind DNA was not addressed. Therefore, we were interested to test whether TopBP1 BRCT4/5, specifically the positively charged surface on BRCT5, has DNA binding activity.

To detect for *in vitro* DNA binding activity, we performed EMSA on ^{32}P-labelled DNA substrates. As shown in Figure 5-13A, TopBP1 BRCT4/5 and BRCT5 preferentially binds with similar affinities to an 18 bp dsDNA, suggesting that the observed shift is specific for BRCT5. In contrast, BRCT6 shows weaker affinity to the same dsDNA substrate. BRCT5 also binds tighter to dsDNA compared to an

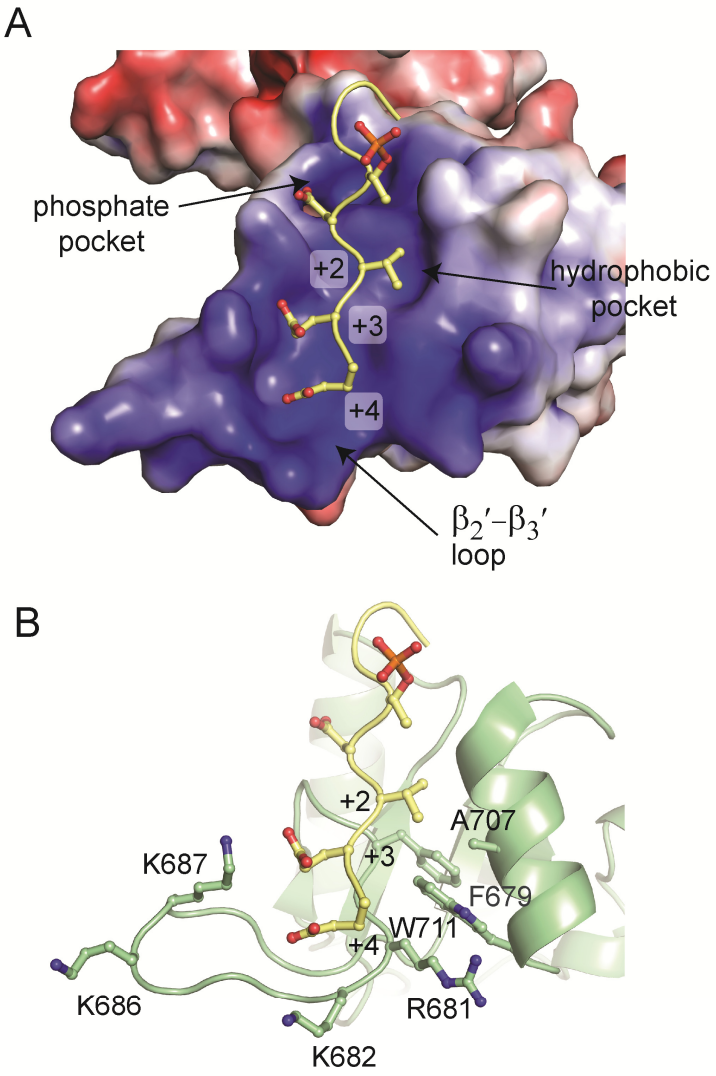

Figure 5-12. BRCT5 basic loop recognizes MDC1 di-phospho-peptide C-terminal residues. (A) Di-phospho-peptide C-terminal residues (sticks) bound to TopBP1 BRCT5 basic surface (represented as electrostatic surface). (B) Details of interactions between di-phospho-peptide C-terminal residues and TopBP1 BRCT5 basic surface.

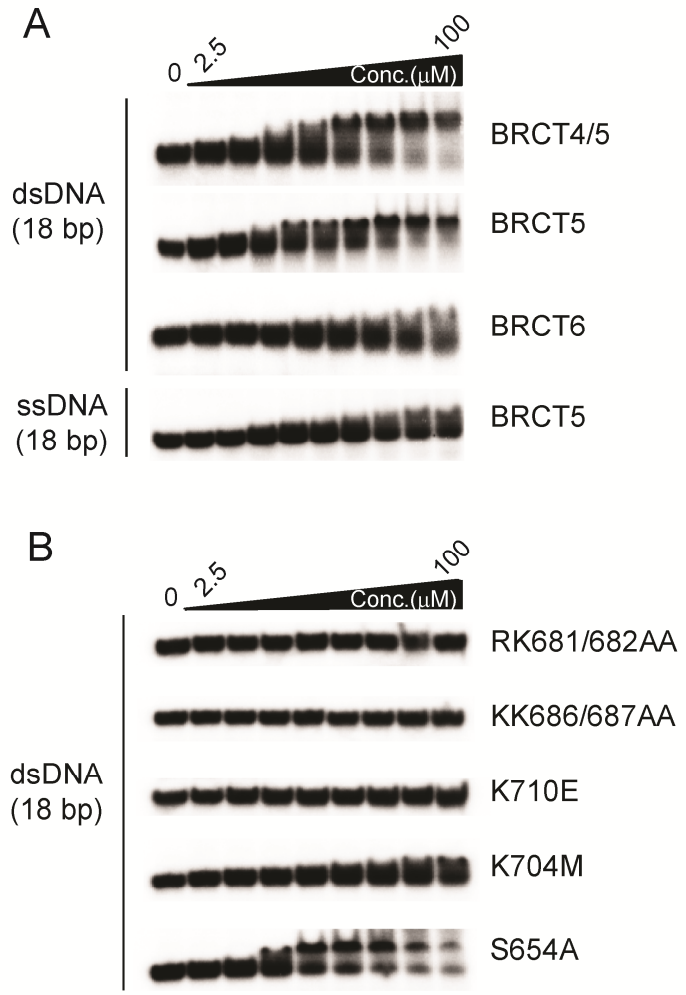

Figure 5-13. TopBP1 BRCT5 binds DNA *in vitro*. (A) Binding of a ssDNA and dsDNA substrate to various TopBP1 BRCT domains. (B) Effects of BRCT5 mutations on binding to a dsDNA substrate.

18 bp ssDNA substrate. To test whether DNA binding is a result of the positively charged surface on BRCT5, we generated a series of mutants to test for their abilities to bind the 18 bp dsDNA. Double mutants of the β_2'-β_3' loop (RK681/682AA and KK686/687AA) completely abolish interactions with DNA (Fig. 5-13B). In addition, Lys mutants in the phosphate-binding pocket (K704M) and α_2' (K710E) also compromise DNA binding activity. Interestingly, mutation of the conserved serine in the phosphate-binding pocket (S654A) binds to the dsDNA substrate similarly to wild-type BRCT5. This also correlates with our localization data (Table 5-1), which shows that the S654A mutant does not affect localization of TopBP1. Although there is more evidence supporting MDC1 binding as the mechanism for TopBP1 localization at sites of stalled replication forks, our DNA binding data may suggest an additional way TopBP1 could gather at replication forks to stimulate ATR activity.

5.3 Discussion

The recognition of MDC1 by TopBP1 is critical for DNA replication checkpoint control in response to replication stress. TopBP1 BRCT5 directly binds to the conserved SDT repeats of MDC1, and this specific interaction is necessary for sustaining and amplifying ATR activation. In the context of phospho-peptide recognition by BRCT domains, the interaction between TopBP1 BRCT5 and the MDC1 SDT motifs was intriguing for several reasons. Firstly as part of a tandem BRCT pair, the functional requirement for only the C-terminal BRCT5 domain suggested that TopBP1 BRCT4/5 does not follow the canonical BRCT repeat mode of recognition. Secondly, the MDC1 SDT repeats are established di-phospho-peptide motifs that are also targets for NBS1 in DNA DSB repair. Since BRCT domain phosphate-binding pockets can bind to both pSer and pThr peptides, TopBP1 BRCT5 could potentially recognize only the pSer, pThr or even both phosphorylated residues via other interactions outside the putative phosphate-binding pocket. Here we present the molecular basis for TopBP1

BRCT5 recognition of a MDC1 di-phospho-peptide containing a consensus SDT repeat sequence. Our structural and functional analysis provide insight into the questions raised above, but also reveal other surprising aspects of BRCT phospho-peptide binding that were previously unknown.

TopBP1 BRCT4/5 contains a number of structural features that diverges from a conventional BRCT repeat. An unexpected BRCT-BRCT packing interface results in a head-to-head arrangement of the BRCT domains. This is a consequence of an absent α_2-helix and constraints imposed by the relatively short inter-BRCT linker region. Rather than the α_2-α_1'-α_3'triple helix bundle associated with typical BRCT repeat interfaces, TopBP1 BRCT4/5 incorporates the same α_1'-α_3' helices from BRCT5 and a novel surface composed of α_3 and the β_3-β_4 loop from BRCT4. Unconventional BRCT-BRCT interfaces have also been observed in the triple BRCT repeat, TopBP1 BRCT0/1/2, which coincidently also contains relatively shorter inter-BRCT linkers. However, the interfaces between BRCT0/1 and BRCT1/2 are distinct from BRCT4/5 and their respective C-terminal domain faces do not involve the α_1' and α_3' helices (Fig. 5-14). Another difference is the presence of a phosphate-binding pocket in BRCT5 rather than the N-terminal BRCT4. Although this is rare in tandem BRCT domains, it is also found in the BRCT1/2 repeats in PAX-interacting protein 1 (PTIP) (Lechner et al, 2000), suggesting that TopBP1 BRCT4/5 could represent a new class of tandem BRCT domains. It is not clear, however, whether PTIP BRCT1/2 can bind phospho-peptides, and further structural and functional work will be needed to provide evidence for this potential group of BRCT repeats that recognize phospho-peptides via a C-terminal BRCT pocket.

Perhaps the most surprising aspect of phospho-peptide recognition by TopBP1 BRCT5 is the apparent dimerization of BRCT5 induced by MDC1 binding.

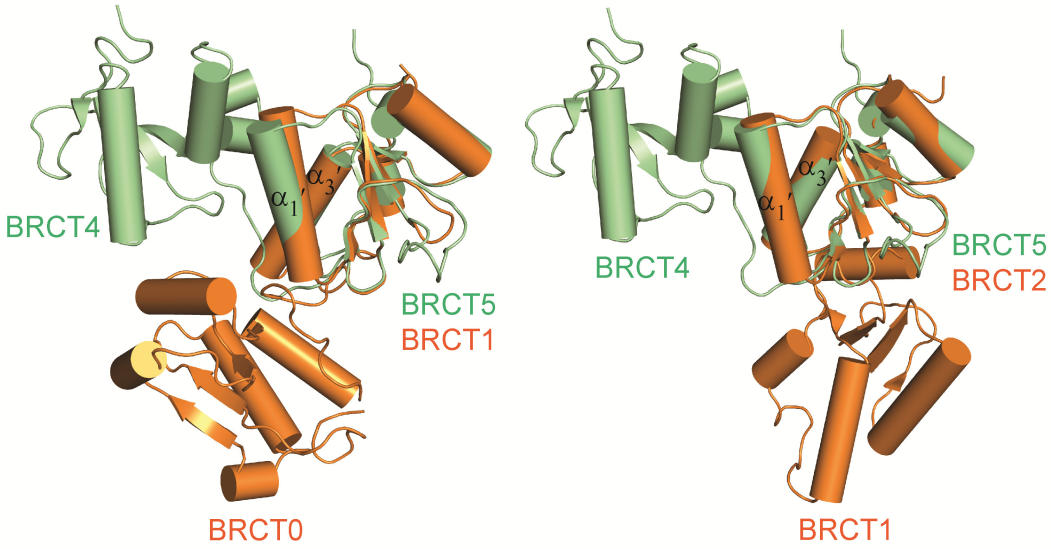

Figure 5-14. Comparison of BRCT domain packing interfaces of TopBP1 BRCT4/5 and TopBP1 BRCT0/1/2. The C-terminal BRCT of BRCT4/5 (green) is superimposed with the C-terminal BRCT in BRCT0/1 (left) and BRCT1/2 (right) (PDB ID: 2XNK). The α_1′ and α_3′-helices are labelled.

We were unable to isolate or trap the peptide-induced dimer in solution using gel-filtration chromatography, chemical cross-linking or EMSA, suggesting that the interactions driving dimer formation with the phospho-peptide may be too transient to form a tight complex. As indicated by our FP binding studies (Fig. 5-7), the interaction between TopBP1 BRCT5 and the MDC1 di-phospho-peptide is relatively weak compared to other established BRCT-phospho-peptide interactions. Interestingly, GST-fusion proteins of BRCT5 or BRCT4/5 bound to the di-phospho-peptide with higher affinity than the untagged protein. GST-induced dimerization may indirectly stabilize two BRCT5 domains in a state that favours the formation of the peptide-induced dimer observed in our crystal structure. Because no significant contacts are made between BRCT4/5 protomers, oligomerization of BRCT5 would require interactions from other regions in TopBP1. Indeed, TopBP1 has been shown to oligomerize through a TopBP1 BRCT7/8-mediated recognition of an Akt-dependent internal TopBP1 pSer motif (pSer1159) (Liu et al, 2006). Liu et al. provided evidence that TopBP1 oligomerization is needed for TopBP1 BRCT6 to bind E2F1, an interaction that we investigated and failed to detect with ITC or FP (see Chapter 3). It is also possible that other unidentified TopBP1 BRCT-mediated interactions may also oligomerize TopBP1.

The crystal structure of TopBP1 BRCT4/5 bound to a MDC1 di-phospho-peptide provides mechanistic insights into the basis for this interaction. The peptide pThr makes one direct bond with Lys704 and a number of water-bridged interactions with other residue main chains in protomer A. On the other side, the -3 Asp substitutes as a phospho-mimetic and hydrogen bonds with the Asn655 main chain, Ser654 side chain, and also the Lys704 side chain via a water molecule. The unusual specificity of the BRCT5 phosphate-binding pockets is supported by our mutational analysis of residues in the pocket. The lack of peptide interactions involving the conserved Ser654 (Ser654 of protomer A has no contacts; Ser654 of protomer B makes a single hydrogen bond with the -3 Asp

that may not be essential for overall Asp recognition) is supported by the unperturbed HU-induced TopBP1 foci formation of a S654A mutation *in vivo* (Table 5-1). In contrast, the conserved Lys704 has a more significant role, most likely providing charge complementation for the negatively charged pThr and -3 Asp residues of the di-phospho-peptide. Mutation of Lys704 compromises TopBP1 foci formation in response to replication stress in cells and reduces binding to a MDC1 di-phospho-peptide compared to wild type *in vitro* (Table 5-1, Fig. 5-7C). The reason both BRCT5 pockets do not tightly coordinate a phosphate in a conventional manner might be reflected in the requirement to recognize different moieties in the di-phospho-peptide via the same binding pocket. This is further complemented by the amount of main chain and water-mediated contacts rather than specific side chain contacts with the di-phospho-peptide, which allow the two protomers to bind without being highly sequence specific. In contrast, there is a high degree of sequence specificity for the C-terminal phospho-peptide residues by the highly structured β_2'-β_3' loop of BRCT5. The +2 Val is complemented by a shallow hydrophobic pocket, while the +3 and +4 Glu residues make electrostatic interactions with the basic β_2'-β_3' loop residues. In support of this, mutations of the positively charged β_2'-β_3' loop residues also show defects in TopBP1 foci formation and MDC1 di-phospho-peptide binding (Table 5-1, Fig. 5-7C). It is plausible that the major binding specificity involves BRCT5 interactions with the peptide +2 to +4 residues, while upstream interactions with the two phosphate-binding pockets and the negatively charged acidic and phosphorylated residues may rely on general charge effects.

Previous studies from the Chen lab clearly demonstrated that only the C-terminal BRCT5 is needed for TopBP1 localization and MDC1 binding (Wang et al, 2011; Yamane et al, 2002). In their experiments, a defect in TopBP1 function is only observed when BRCT5, and not BRCT4, is deleted. This suggests that BRCT5 may in fact function as a single BRCT domain without a requirement for BRCT4. Our structural and functional characterization of the TopBP1-MDC1 interaction

also supports this notion. In the crystal structure of TopBP1 BRCT4/5 in complex with a MDC1 di-phospho-peptide, BRCT5 of protomers A and B exclusively interacts with the di-phospho-peptide. Other than crystal packing contacts, no interactions are observed between the BRCT4 domains with the di-phospho-peptide and only a single hydrogen bond is found between BRCT4 and BRCT5 of different protomers. Our FP binding data also show that GST-fusion proteins of BRCT4/5 or BRCT5 bind to a FITC-labelled MDC1 di-phospho-peptide with relatively similar affinities, supporting the functional requirement of BRCT5 only. We have previously purified and crystallized TopBP1 BRCT5 on its own, although the solubility of BRCT5 is slightly lower than tandem BRCT4/5 in solution. It is likely that BRCT5 can exist as a functional single BRCT unit, and BRCT4 may only have a minor role in maintaining the structural integrity of BRCT4/5. This also resembles the nature of the TopBP1 BRCT0/1/2 triple BRCT repeat, where structural and functional studies have shown that the degenerate BRCT0 is dispensable for Rad9 binding by the tandem BRCT1/2 domains of TopBP1 (Huo et al, 2010; Rappas et al, 2011). Like BRCT4 in BRCT4/5, BRCT0 may only be involved in sustaining structural integrity of the overall BRCT repeat.

Studies with human NBS1 provide evidence that both the FHA and tandem BRCT domains in the FHA-BRCT-BRCT repeat can bind MDC1 SDT motif di-phospho-peptides (Lloyd et al, 2009). Whereas the FHA domain is highly specific for the pThr, the NBS1 tandem BRCTs appear to favour binding to a di-phospho-peptide with both pSer and pThr residues intact. Our data demonstrates that TopBP1 BRCT5 is specific for the pThr, and suggests that TopBP1 may compete with NBS1 FHA and BRCT repeat for binding to the MDC1 SDT motifs. It is also possible that the presence of six SDT motifs could allow both TopBP1 and NBS1 to dock onto different sites in MDC1 at the same time. Interestingly, TopBP1 has also been shown to bind to NBS1 via the N-terminal TopBP1 BRCT domains (Ramirez-Lugo et al, 2011). Because recognition of pThr and the rest of the phospho-peptide by BRCT5 of protomer B involve a relatively

smaller interface, one could imagine a possible scenario where the MDC1 di-phospho-peptide induces a heterodimer with NBS1 FHA domain and TopBP1 BRCT5 (protomer A). However, modeling of this potential complex suggests significant clashing of the BRCT5 α_2'-helix with the NBS1 FHA β_4-β_5 and β_{10}-β_{11} loops, which are critical for NBS1 FHA domain phospho-peptide recognition (Fig. 5-15). Unless there are significant conformational changes to the di-phospho-peptide, it is unlikely that NBS1 and TopBP1 can bind to the same SDT motif. In support of this, we were also unable to detect a MDC1 di-phospho-peptide induced complex of TopBP1 BRCT4/5 and the NBS1 FHA-BRCT-BRCT repeat using FP and EMSA experiments.

Our structural data also suggests that MDC1 SDT repeat phosphorylation of the Thr is more important than Ser for TopBP1 binding. Whereas the pThr is bound by the phosphate-binding pocket of one BRCT5 protomer, the pSer does not make significant interactions with the BRCT5 dimer. Our *in vivo* pull-down results (Fig. 5-8) also provides subtle clues for a larger requirement for pThr. Since the efficiency of CK2 phosphorylation of these various SDT mutants may vary and is not measured, it is difficult to make any conclusions regarding the differential binding effects of these MDC1 mutants with TopBP1. As a result, we have planned experiments for FP to test the binding preference of TopBP1 BRCT5 to pSer and pThr MDC1 phospho-peptides *in vitro*. Nonetheless, if only the pThr is required for interactions with both TopBP1 and NBS1, why is a conserved pSer found in these MDC1 SDT motifs? Although a number of studies have demonstrated that both Thr and Ser residues are phosphorylated *in vivo* (Beausoleil et al, 2004; Olsen et al, 2006; Villen et al, 2007), the relative quantities of pThr and pSer have not been tested. It is possible that pThr may be more prevalent than pSer within the MDC1 SDT repeats in cells; therefore, proteins are designed to target the pThr in these motifs. Another possibility is that other unidentified MDC1 protein partners may select for the pSer.

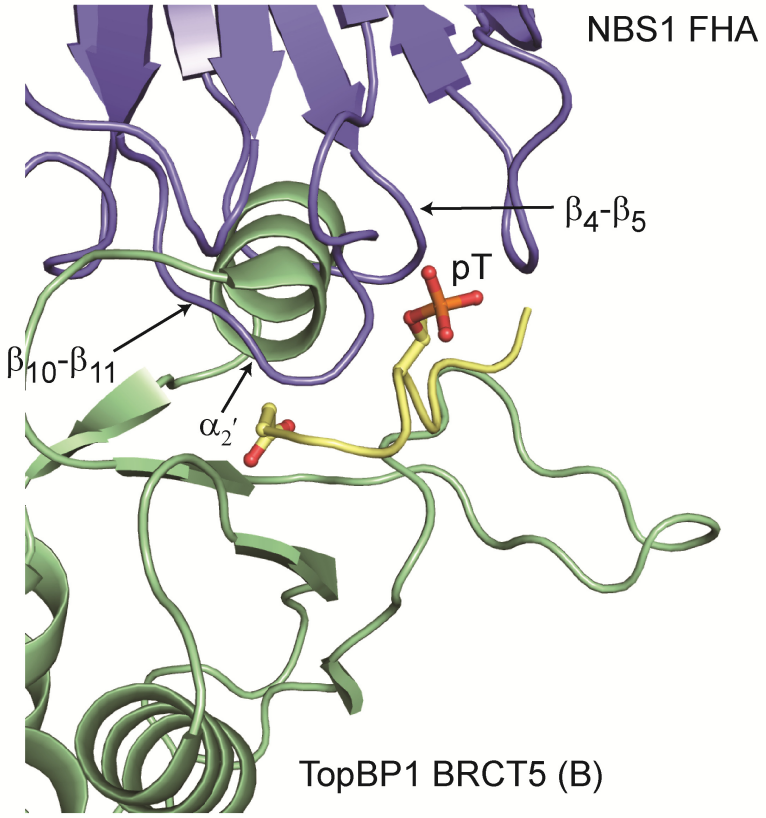

Figure 5-15. Model of a MDC1 phospho-peptide bound to TopBP1 BRCT5 and NBS1 FHA domain. Clashing of the BRCT5 (green) α_2'-helix and FHA (blue, PDB ID: 3HUF) β_4-β_5 and β_{10}-β_{11} loops are shown.

Clearly, further studies are needed to investigate how these unique di-phospho-peptide motifs in MDC1 are recognized by a host of proteins in DDR.

Our DNA binding experiments also indicate that TopBP1 BRCT5 can bind to dsDNA in a sequence independent manner. Interestingly, our mutational analysis of DNA binding activity also correlates with TopBP1 localization (Table 5-1). Although our data is preliminary, it implies an intriguing possibility that TopBP1 accumulation at stalled replication forks could be mediated by direct binding to dsDNA in addition to protein interactions. Tandem and single BRCT domains in various proteins can bind DNA, although conflicting evidence for their binding specificities and biological relevance exists. Further investigation into BRCT domain DNA binding specificities will be needed to substantiate our *in vitro* TopBP1 BRCT5 DNA binding results.

Like the TopBP1-BACH1 interaction, the interaction between TopBP1 and MDC1 is also crucial for DNA replication checkpoint control. This study provides structural insights into the mechanism that underlies another key TopBP1-mediated interaction that contributes to ATR activation and checkpoint signalling. Moreover, the structural basis of MDC1 binding by TopBP1 BRCT5 uncovers novel aspects of BRCT domain phospho-peptide recognition that further illustrates the diversity of BRCT domain function in the DNA damage response.

5.4 References

Beausoleil SA, Jedrychowski M, Schwartz D, Elias JE, Villen J, Li J, Cohn MA, Cantley LC, Gygi SP (2004) Large-scale characterization of HeLa cell nuclear phosphoproteins. *Proc Natl Acad Sci U S A* **101:** 12130-12135

Bennett EJ, Harper JW (2008) DNA damage: ubiquitin marks the spot. *Nat Rev Mol Cell Biol* **15:** 20-22

Chapman JR, Jackson SP (2008) Phospho-dependent interactions between NBS1 and MDC1 mediate chromatin retention of the MRN complex at sites of DNA damage. *EMBO Rep* **9:** 795-801

Clapperton Ja, Manke Ia, Lowery DM, Ho T, Haire LF, Yaffe MB, Smerdon SJ (2004) Structure and mechanism of BRCA1 BRCT domain recognition of phosphorylated BACH1 with implications for cancer. *Nat Struct Mol Biol* **11:** 512-518

Glover JNM, Williams RS, Lee MS (2004) Interactions between BRCT repeats and phosphoproteins: tangled up in two. *Trends Biochem Sci* **29:** 579-585

Gong Z, Kim JE, Leung CC, Glover JN, Chen J (2010) BACH1/FANCJ acts with TopBP1 and participates early in DNA replication checkpoint control. *Mol Cell* **37:** 438-446

Huen MS, Chen J (2010) Assembly of checkpoint and repair machineries at DNA damage sites. *Trends Biochem Sci* **35:** 101-108

Huo Y-G, Bai L, Xu M, Jiang T (2010) Crystal structure of the N-terminal region of human Topoisomerase IIβ binding protein 1. *Biochemical and biophysical research communications* **401:** 401-405

Kelley LA, Sternberg MJ (2009) Protein structure prediction on the Web: a case study using the Phyre server. *Nat Protoc* **4:** 363-371

Lechner MS, Levitan I, Dressler GR (2000) PTIP, a novel BRCT domain-containing protein interacts with Pax2 and is associated with active chromatin. *Nucleic Acids Res* **28:** 2741-2751

Leung CC, Gong Z, Chen J, Glover JN (2011) Molecular basis of BACH1/FANCJ recognition by TopBP1 in DNA replication checkpoint control. *J Biol Chem* **286:** 4292-4301

Liu K, Paik JC, Wang B, Lin F-T, Lin W-C (2006) Regulation of TopBP1 oligomerization by Akt/PKB for cell survival. *EMBO J* **25:** 4795-4807

Lloyd J, Chapman JR, Clapperton JA, Haire LF, Hartsuiker E, Li J, Carr AM, Jackson SP, Smerdon SJ (2009) A supramodular FHA/BRCT-repeat architecture mediates Nbs1 adaptor function in response to DNA damage. *Cell* **139:** 100-111

Melander F, Bekker-Jensen S, Falck J, Bartek J, Mailand N, Lukas J (2008) Phosphorylation of SDT repeats in the MDC1 N terminus triggers retention of NBS1 at the DNA damage-modified chromatin. *J Cell Biol* **181:** 213-226

Olsen JV, Blagoev B, Gnad F, Macek B, Kumar C, Mortensen P, Mann M (2006) Global, in vivo, and site-specific phosphorylation dynamics in signaling networks. *Cell* **127:** 635-648

Ramirez-Lugo JS, Yoo HY, Yoon SJ, Dunphy WG (2011) CtIP interacts with TopBP1 and Nbs1 in the response to double-stranded DNA breaks (DSBs) in Xenopus egg extracts. *Cell Cycle* **10:** 469-480

Rappas M, Oliver AW, Pearl LH (2011) Structure and function of the Rad9-binding region of the DNA-damage checkpoint adaptor TopBP1. *Nucleic Acids Res* **39:** 313-324

Spycher C, Miller ES, Townsend K, Pavic L, Morrice Na, Janscak P, Stewart GS, Stucki M (2008) Constitutive phosphorylation of MDC1 physically links the MRE11-RAD50-NBS1 complex to damaged chromatin. *J Biol Chem* **181:** 227-240

Stucki M, Clapperton Ja, Mohammad D, Yaffe MB, Smerdon SJ, Jackson SP (2005) MDC1 directly binds phosphorylated histone H2AX to regulate cellular responses to DNA double-strand breaks. *Cell* **123:** 1213-1226

Villen J, Beausoleil SA, Gerber SA, Gygi SP (2007) Large-scale phosphorylation analysis of mouse liver. *Proc Natl Acad Sci U S A* **104:** 1488-1493

Wang J, Gong Z, Chen J (2011) MDC1 collaborates with TopBP1 in DNA replication checkpoint control. *J Cell Biol* **193:** 267-273

Williams RS, Lee MS, Hau DD, Glover JN (2004) Structural basis of phosphopeptide recognition by the BRCT domain of BRCA1. *Nat Struct Mol Biol* **11:** 519-525

Wu L, Luo K, Lou Z, Chen J (2008) MDC1 regulates intra-S-phase checkpoint by targeting NBS1 to DNA double-strand breaks. *Proc Natl Acad Sci U S A* **105:** 11200-11205

Yamane K, Katayama E, Tsuruo T (2000) The BRCT regions of tumor suppressor BRCA1 and of XRCC1 show DNA end binding activity with a multimerizing feature. *Biochemical and biophysical research communications* **279:** 678-684

Yamane K, Tsuruo T (1999) Conserved BRCT regions of TopBP1 and of the tumor suppressor BRCA1 bind strand breaks and termini of DNA. *Oncogene* **18:** 5194-5203

Yamane K, Wu X, Chen J (2002) A DNA damage-regulated BRCT-containing protein, TopBP1, is required for cell survival. *Mol Cell Biol* **22:** 555-566

Yan S, Michael WM (2009) TopBP1 and DNA polymerase-alpha directly recruit the 9-1-1 complex to stalled DNA replication forks. *J Cell Biol* **184:** 793-804

Chapter 6

Conclusions

A version of this chapter is accepted in:

Leung CC, Glover J N (2011) BRCT domains: Easy as one, two three. *Cell Cycle*. **10**:2461-70.

6.1. TopBP1 has multiple regulatory roles in DNA replication checkpoint control

The DNA replication checkpoint is critical for the prevention of genomic instability during DNA replication in cells. It is now clear that TopBP1 is key to the success of checkpoint activation by operating at multiple and distinct steps of ATR activation. The unusual abundance of conserved BRCT domains in TopBP1 provides extraordinary specificity to target different replication fork proteins.

To date, there are at least three different TopBP1 BRCT-mediated protein interactions involved in DNA replication checkpoint activation (Fig. 6-1). Firstly, TopBP1 BRCT7/8 interacts with phosphorylated BACH1 in an early step to facilitate BACH1 driven DNA unwinding. This amplifies the amount of ssDNA and ensuing RPA loading that is needed to potentiate ATR activation. Activation of ATM and ATR depends on the types of DNA structures at the damaged sites. Whereas ATM is activated by DSBs with blunt ends or short single-stranded overhangs, ATR is specific for longer stretches of ssDNA (Shiotani & Zou, 2009). The TopBP1-BACH1 interaction is therefore necessary to generate the DNA substrates specific for ATR activation. Following the recruitment of the 9-1-1 complex and ATR-ATRIP by RPA, TopBP1 then participates in a second interaction involving the N-terminal BRCT0/1/2 repeats and phosphorylated Rad9 of 9-1-1. This binding perhaps brings TopBP1 in close proximity to ATR, enabling the direct stimulation of ATR via the ATR activation domain (AAD) of TopBP1. Low levels of ATR activity are not sufficient for checkpoint activation, however, which requires further amplification and stimulation of ATR. This is achieved through a third BRCT-mediated interaction between phosphorylated MDC1 and TopBP1 BRCT5. Recognition of MDC1 retains TopBP1 accumulation at stalled replication forks, thus allowing TopBP1 to continually activate and amplify ATR activity.

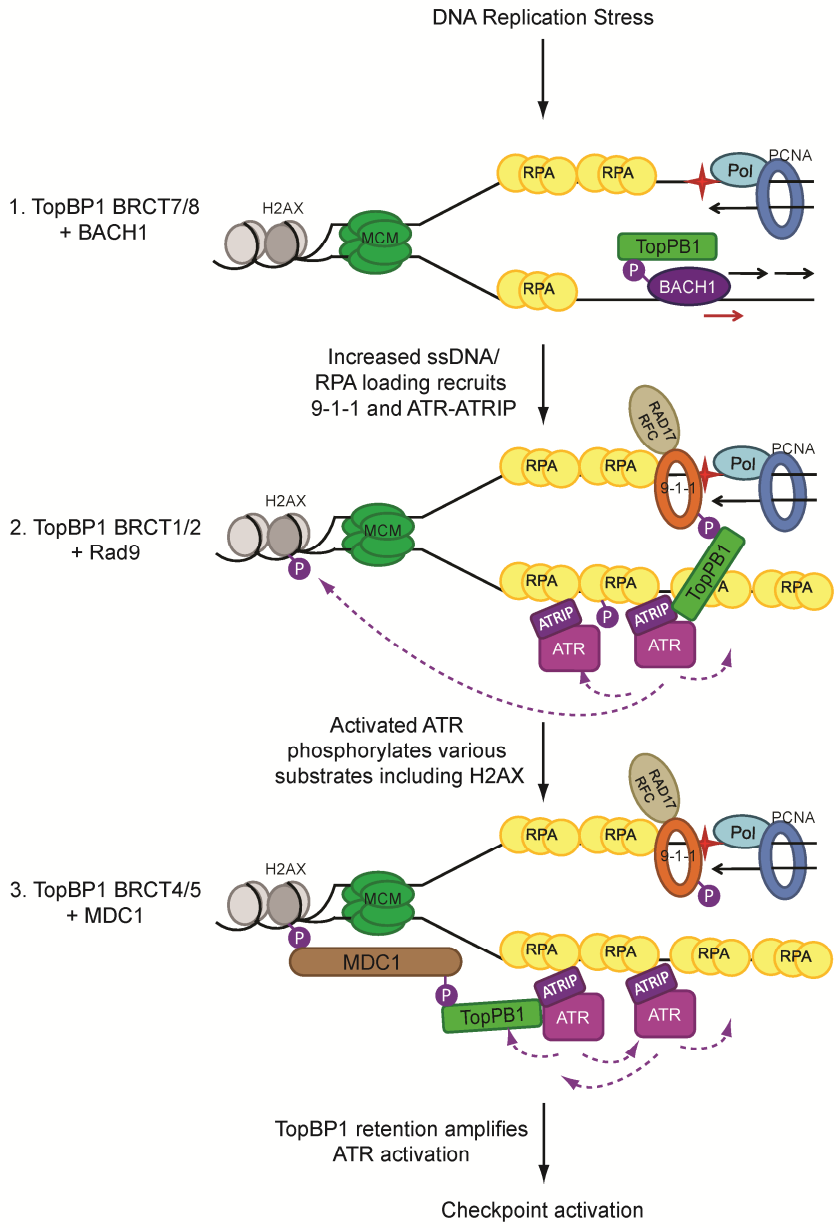

Figure 6-1. TopBP1 BRCT-mediated interactions in DNA replication checkpoint control. Tandem BRCT interactions with BACH1, Rad9 and MDC1 at different stages contribute to the overall ATR and checkpoint activation.

Why are there multiple mechanisms required to activate ATR in response to replication stress? ATR is considered the master regulator of the DNA replication checkpoint and the multistep regulation by TopBP1 and other proteins may enable tighter control of checkpoint activation at various stages in the pathway. One intriguing possibility is that the degree of checkpoint response may be finely tuned against different types of DNA damage. Less disruptive lesions or barriers may not require a fully firing ATR cascade, since repair or removal of the barrier can be more readily achieved. In these cases, replication fork stability may be the main priority so that replication can resume once the lesion and barrier is fixed or removed. In contrast, more cytotoxic lesions such as DNA DSBs may involve a larger investment by cells and therefore need a fully active checkpoint response. For example, DSBs require homologous recombination repair, which entitles an additional battery of proteins at the collapsed replication fork. It is evident that we are only starting to understand the complexity involved in ATR and checkpoint activation in response to DNA replication stress.

6.2. Novel aspects of BRCT domain phospho-peptide recognition

Our studies in TopBP1 have revealed new aspects of phospho-peptide binding by tandem BRCT domains that were previously unknown. From our structural studies of TopBP1 BRCT7/8, both free and in complex with a BACH1 phospho-peptide, we uncovered the molecular basis for pThr specificity by BRCT domains. This implies that at least two different classes of phosphate binding pockets may exist in BRCT domains. The phosphate-binding pockets of BRCA1 and MDC1 serve as prototypes for the first class, which are selective for pSer (Fig. 6-2, left panel). In this class, the phosphate moiety interacts with two side chains (S1655/T1898, K1702/K1936 in BRCA1/MDC1, respectively) and a main chain NH (G1656/G1899 in BRCA1/MDC1). TopBP1 BRCT7/8 represents the second class, which contains additional specificity for pThr peptide targets. In

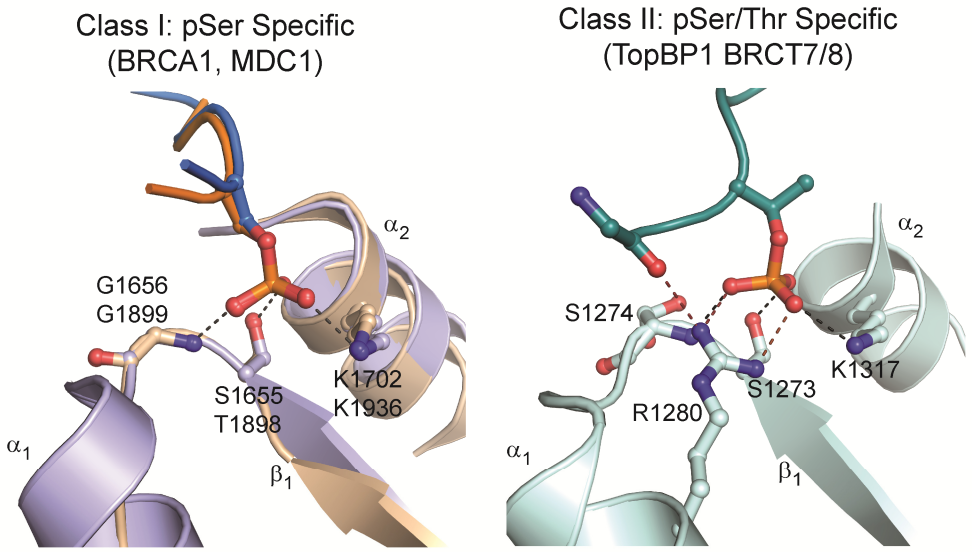

Figure 6-2. Different classes of BRCT domain phosphate-binding pockets. pSer coordination by BRCA1/MDC1 (left panel) and pThr coordination by TopBP1 BRCT7/8 (right panel). Phosphate contact residues for BRCA1/MDC1 (top/bottom) and TopBP1 are labelled. Equivalent hydrogen bonding and electrostatic interactions are indicated by black dotted lines and additional contacts by TopBP1 R1280 are shown as red dotted lines.

addition to interactions that are conserved with the class I pocket that involve Ser1273, Lys1317 and the main chain NH of Ser1274, the phosphate group is also recognized by the side chain guanidinium of Arg1280 (Fig. 6-2, right panel). The combination of differences in the peptide backbone orientation and coordination of the pThr residue, likely facilitated by additional interactions with the conserved TopBP1 R1280, allows incorporation of the γ-methyl group without steric hindrance in the pocket.

Another feature of TopBP1 BRCT7/8 is the dramatic conformation change at the BRCT-BRCT interface initiated upon phospho-peptide binding. Alterations in the hydrophobic packing interface between BRCT repeats may present a means to alter phospho-peptide specificity. Due to the extent of hydrophobic interactions between α_2-α_1′-α_3′ helices, the BRCT domain pair is typically held rigid and only show small deviations in domain movement upon peptide binding. This is perhaps reflected in the absolute conservation of the cognate phospho-peptide motif sequence for BRCA1, where all validated binding partners contain the consensus motif, pSer-Pro-Thr-Phe (Kim et al, 2007; Liu et al, 2007; Manke et al, 2003; Miki et al, 1994; Ray et al, 2006; Wang et al, 2007; Yu & Chen, 2004; Yu et al, 2003). In contrast, the significantly smaller hydrophobic interface in TopBP1 BRCT7/8 allows for a dramatic domain rotation (23 °) at the BRCT-BRCT interface upon phospho-peptide binding in order to shape the larger +3/+4 pocket, as well as the phosphate-binding pocket to a lesser extent. Since TopBP1 BRCT7/8 has also been implicated in binding other TopBP1 phospho-peptide motifs with divergent sequences (pS-N-L-Q-W-P-S in TopBP1 (Liu et al, 2006) and pT-P-P-E-G-K in ATR (Liu et al, 2011)), the plasticity at the BRCT-BRCT interface in TopBP1 BRCT7/8 could potentially cater to a larger variety of peptide targets.

TopBP1 BRCT4/5 represents a novel group of BRCT repeats that contains a phosphate-binding pocket in the C-terminal BRCT rather than the N-terminal

BRCT domain. In accordance with *in vivo* studies by Wang et al (Wang et al, 2011), our biochemical and structural data suggests that the N-terminal BRCT4 contains a degenerate BRCT fold that is dispensable for MDC1 binding and TopBP1 localization at stalled replication forks. The crystal structure of TopBP1 BRCT4/5 in complex with a MDC1 di-phospho-peptide reveals an unexpected mechanism of phospho-peptide binding that is consistent with the unusual BRCT repeat arrangement. In contrast to the 1:1 stoichiometry in previously identified BRCT repeat-phospho-peptide complexes, recognition of the MDC1 di-phospho-peptide involves interactions from two TopBP1 BRCT5 domains. Both BRCT5 phosphate-binding pockets are utilized to bind the pThr and Asp side chains of the phospho-peptide, suggesting that the nearby pSer is not as critical for the interaction. Additionally, an unusual positively charged BRCT5 loop complements the conserved negatively charged C-terminal residues in the MDC1 binding motif. Although the unique characteristics of TopBP1 BRCT4/5 are uncommon in other tandem BRCT domains, the dimerization mode of binding observed by BRCT5 may in fact provide a molecular basis for how single BRCT domains could bind phospho-peptides. In support of this, studies have shown that recognition of an E2F1 phospho-peptide motif by the TopBP1 single BRCT6 domain is dependent on oligomerization of TopBP1 via another BRCT-mediated interaction involving TopBP1 BRCT7/8 and a phosphorylated motif in TopBP1 (Liu et al, 2006). Although there is evidence that other single BRCT domains can bind phospho-peptides (Yu et al, 2003), the structural basis for these interactions are still unknown. Compared to tandem BRCT domains, single BRCT domains are limited to a smaller phospho-peptide binding surface that is likely to facilitate weaker or more transient binding interactions. Oligomerization of single BRCT domains may provide a means to stabilize phospho-peptide interactions that may otherwise be too weak to support.

6.3. Expanding diversity of BRCT domain structure and function

BRCT domains have proven to be remarkably versatile binding modules in DNA damage signalling. Starting from the single BRCT domain building block, the ability to incorporate different functions by altering or adding different structural features grants unprecedented advantages to establish regulation and specificity for various targets such as phospho-peptides, proteins, DNA and PAR (Fig. 6-3). Within a single BRCT domain, implementing phosphate binding residues in a positively charged pocket, such as in the N-terminal BRCT of BRCA1 (Clapperton et al, 2004; Shiozaki et al, 2004; Williams et al, 2004) and TopBP1 BRCT7/8 (Leung et al, 2011), allows specific coordination to a pSer or pThr in phospho-peptide motifs. Residues on the BRCT domain surface can also present binding surfaces for protein-protein interactions, like in the XRCC1-DNA ligase III BRCT-BRCT heterodimer (Cuneo et al, 2011). Other binding surfaces, such as in the N-terminal single BRCT in XRCC1, may also recognize post-translational modifications such as PAR (El-Khamisy et al, 2003; Pleschke et al, 2000). Single BRCT domains can be further modified by the addition of other structural features to yield different functions. An extra N-terminal α-helix flanking the single BRCT of RFC creates a binding module for specific dsDNA substrates (Kobayashi et al, 2006).

The expansion of single BRCT domains to tandem repeats increases variables needed to garner further functional diversity. Canonical tandem BRCT domains incorporate a C-terminal BRCT alongside the N-terminal phosphate-binding BRCT domain. The inherent interface between the adjacent BRCTs establishes a secondary +3 (eg. BRCA1) or +3/+4 (eg. TopBP1 BRCT7/8) pocket that is critical for phospho-peptide binding (Glover et al, 2004; Leung et al, 2011). Inter-BRCT linkers between BRCT repeats can also play a role in forming binding interfaces for protein-protein interactions (Watts & Brissett, 2010). For example, the inter-BRCT linker of DNA LigIV adopts a clamp-like structure that

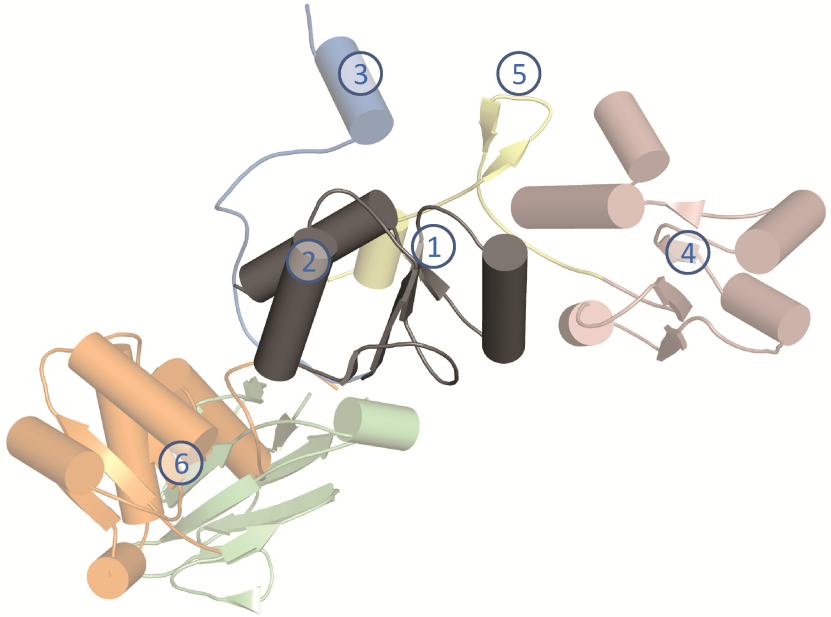

	Feature	Description	Examples
1	Phosphate-binding residues	Binding to phosphate, specificity for pS or pS/pT	pS: BRCA1; pT/pS: TopBP1 BRCT7/8
2	Surface residues	Protein-protein interactions, PAR binding	Protein: XRCC1-Lig3; PAR binding: XRCC1
3	N-terminal insert	N-terminal helix binds DNA	RFC p140
4	C-terminal BRCT	BRCT-BRCT interface determines +3 or +3/+4 specificity in phospho-peptides	+3: BRCA1; +3/+4: TopBP1 BRCT7/8
5	Inter-BRCT linker	Protein-protein interactions	LigIV-XRCC4
6	N-terminal domain	BRCT, FHA and FN3 - may provide further specificity/regulation for BRCT function	BRCT: TopBP1 BRCT4/5; FHA: NBS1; FN3: *S. cerevisiae* Chs5p

Figure 6-3. Summary of BRCT domain variation and function. The fundamental single BRCT domain is represented in black. Each feature is marked and coloured in the schematic.

specifically wraps around the coiled-coil tails of the XRCC4 homodimer (Dore et al, 2006; Sibanda et al, 2001; Wu et al, 2009). Finally, an additional N-terminal domain can buttress single or tandem phosphate-binding BRCT domains. These N-terminal domains may regulate activities of the BRCT domains, as demonstrated by the ability for FHA domain phospho-peptide binding to initiate a structural rearrangement of the BRCT repeats in the NBS1-FHA-FHA repeat of NBS1 (Williams et al, 2009).

Although the phospho-peptide and phosphorylation-independent protein binding functions of tandem BRCT domains have been structurally and functionally characterized, less is clear about the particular role of single BRCT domains, aside from the DNA binding activity of the RFC BRCT domain. Indeed, further work is needed to elucidate the mechanisms behind the multitude of functions associated with BRCT domains.

6.4. TopBP1 as a target for cancer therapies

TopBP1 may prove to be a viable target for cancer therapies since it is essential for the maintenance of genomic integrity. As a key regulator in the DNA replication checkpoint, inhibiting TopBP1 function may render severe replication stress that would lead to cell death. Studies have shown that TopBP1 deficiency is embryonic lethal and ablation of TopBP1 in cultured cancer cells induces DNA DSBs and apoptosis through multiple mechanisms (Jeon et al, 2011; Kim et al, 2005; Liu et al, 2009; Liu et al, 2006; Yamane et al, 2002). In addition, although synthetic lethal interactions have not been found for TopBP1 in mammalian cells, there are synthetic lethal interactions in *S. cerevisiae* between the TopBP1 homolog, Dpb11, and a number of genes such as *Cdc45*, *MCM10* and *Sld2/Drc1* (Araki et al, 2003; Reid et al, 1999; Wang & Elledge, 1999).

An effective chemotherapy drug can be measured by a high therapeutic index, which is described as the ratio of drug dosage that causes tumour cure compared to normal tissue complications. Specificity for targeting cancer cells is

perhaps the biggest challenge for chemotherapies. Most cancer drugs take advantage of the rapid DNA replication and proliferation cancer cells undergo in comparison to normal cells. Therefore, many drugs target various aspects of DNA replication or the cell cycle to stimulate cancer cell killing or sensitize remaining cells to other chemo- or radio-therapies to effectively increase the therapeutic indexes. A current approach to cancer drug discovery is the targeting of checkpoint signalling (Zhou & Bartek, 2004). By inhibiting cell cycle arrest, DNA damage accumulates in cells and drives apoptosis. XL844 (Exelexis) is a small molecule inhibitor of the checkpoint kinases, CHK1 and CHK2, that has gone through Phase I clinical trials (ClinicalTrials.gov Identifier: NCT00475917) as combination therapy with gemcitabine, a deoxycytidine analogue that normally causes cell-cycle arrest and apoptosis. An ATM inhibitor, KU55933 (AstraZeneca), is also in preclinical development.

Our studies provide insight into how multiple BRCT-mediated interactions in TopBP1 help control the DNA replication checkpoint. Failure of any of these BRCT domain interactions leads to a defective DNA replication checkpoint, suggesting that the numerous BRCT domains, namely BRCT0/1/2, BRCT4/5 and BRCT7/8 could all be potential targets for inhibitor design. Targeting BRCT domains may also be a general approach for cancer drug discovery since BRCT domains are predominantly found in proteins involved in numerous aspects of DDR signalling. Stephen Campbell and Dr. Nico Coquelle from our lab and others (Dr. Amar Natarajan, University of Nebraska Medical Center) are currently using various approaches to identify an inhibitor of the BRCA1 BRCT repeats. In the case of BRCA1 targeting, a validated BRCA1 inhibitor may work in concert with PARP inhibitors to mimic the synthetic lethality seen with PARP inhibition in BRCA1-deficient breast cancers (Ashworth, 2008; Farmer et al, 2005). Ultimately, understanding the molecular basis of BRCT-phospho-peptide interactions is crucial to the design of BRCT domain inhibitors that may one day be used in cancer therapies.

6.5 References

Araki Y, Kawasaki Y, Sasanuma H, Tye BK, Sugino A (2003) Budding yeast mcm10/dna43 mutant requires a novel repair pathway for viability. *Genes Cells* **8:** 465-480

Ashworth A (2008) A synthetic lethal therapeutic approach: poly(ADP) ribose polymerase inhibitors for the treatment of cancers deficient in DNA double-strand break repair. *J Clin Oncol* **26:** 3785-3790

Clapperton Ja, Manke Ia, Lowery DM, Ho T, Haire LF, Yaffe MB, Smerdon SJ (2004) Structure and mechanism of BRCA1 BRCT domain recognition of phosphorylated BACH1 with implications for cancer. *Nat Struct Mol Biol* **11:** 512-518

Cuneo MJ, Gabel SA, Krahn JM, Ricker MA, London RE (2011) The structural basis for partitioning of the XRCC1/DNA ligase III-{alpha} BRCT-mediated dimer complexes. *Nucleic Acids Res*

Dore AS, Furnham N, Davies OR, Sibanda BL, Chirgadze DY, Jackson SP, Pellegrini L, Blundell TL (2006) Structure of an Xrcc4-DNA ligase IV yeast ortholog complex reveals a novel BRCT interaction mode. *DNA Repair* **5:** 362-368

El-Khamisy SF, Masutani M, Suzuki H, Caldecott KW (2003) A requirement for PARP-1 for the assembly or stability of XRCC1 nuclear foci at sites of oxidative DNA damage. *Nucleic Acids Res* **31:** 5526-5533

Farmer H, McCabe N, Lord CJ, Tutt AN, Johnson DA, Richardson TB, Santarosa M, Dillon KJ, Hickson I, Knights C, Martin NM, Jackson SP, Smith GC, Ashworth A (2005) Targeting the DNA repair defect in BRCA mutant cells as a therapeutic strategy. *Nature* **434:** 917-921

Glover JNM, Williams RS, Lee MS (2004) Interactions between BRCT repeats and phosphoproteins: tangled up in two. *Trends Biochem Sci* **29:** 579-585

Jeon Y, Ko E, Lee KY, Ko MJ, Park SY, Kang J, Jeon CH, Lee H, Hwang DS (2011) TopBP1 deficiency causes an early embryonic lethality and induces cellular senescence in primary cells. *J Biol Chem* **286:** 5414-5422

Kim H, Huang J, Chen J (2007) CCDC98 is a BRCA1-BRCT domain-binding protein involved in the DNA damage response. *Nat Struct Mol Biol* **14:** 710-715

Kim J-E, McAvoy SA, Smith DI, Chen J (2005) Human TopBP1 ensures genome integrity during normal S phase. *Mol Cell Biol* **25:** 10907-10915

Kobayashi M, Figaroa F, Meeuwenoord N, Jansen LET, Siegal G (2006) Characterization of the DNA binding and structural properties of the BRCT region of human replication factor C p140 subunit. *J Biol Chem* **281:** 4308-4317

Leung CC, Gong Z, Chen J, Glover JN (2011) Molecular basis of BACH1/FANCJ recognition by TopBP1 in DNA replication checkpoint control. *J Biol Chem* **286:** 4292-4301

Liu K, Bellam N, Lin HY, Wang B, Stockard CR, Grizzle WE, Lin WC (2009) Regulation of p53 by TopBP1: a potential mechanism for p53 inactivation in cancer. *Mol Cell Biol* **29:** 2673-2693

Liu K, Paik JC, Wang B, Lin F-T, Lin W-C (2006) Regulation of TopBP1 oligomerization by Akt/PKB for cell survival. *EMBO J* **25:** 4795-4807

Liu S, Shiotani B, Lahiri M, Marechal A, Tse A, Leung CC, Glover JN, Yang XH, Zou L (2011) ATR Autophosphorylation as a Molecular Switch for Checkpoint Activation. *Mol Cell* **43:** 192-202

Liu Z, Wu J, Yu X (2007) CCDC98 targets BRCA1 to DNA damage sites. *Nat Struct Mol Biol* **14:** 716-720

Manke Ia, Lowery DM, Nguyen A, Yaffe MB (2003) BRCT repeats as phosphopeptide-binding modules involved in protein targeting. *Science* **302:** 636-639

Miki Y, Swensen J, Shattuck-Eidens D, Futreal Pa, Harshman K, Tavtigian S, Liu Q, Cochran C, Bennett LM, Ding W (1994) A strong candidate for the breast and ovarian cancer susceptibility gene BRCA1. *Science* **266:** 66-71

Pleschke JM, Kleczkowska HE, Strohm M, Althaus FR (2000) Poly(ADP-ribose) binds to specific domains in DNA damage checkpoint proteins. *J Biol Chem* **275:** 40974-40980

Ray H, Moreau K, Dizin E, Callebaut I, Venezia ND (2006) ACCA phosphopeptide recognition by the BRCT repeats of BRCA1. *J Mol Biol* **359:** 973-982

Reid RJ, Fiorani P, Sugawara M, Bjornsti MA (1999) CDC45 and DPB11 are required for processive DNA replication and resistance to DNA topoisomerase I-mediated DNA damage. *Proc Natl Acad Sci U S A* **96:** 11440-11445

Shiotani B, Zou L (2009) Single-stranded DNA orchestrates an ATM-to-ATR switch at DNA breaks. *Mol Cell* **33:** 547-558

Shiozaki EN, Gu L, Yan N, Shi Y (2004) Structure of the BRCT repeats of BRCA1 bound to a BACH1 phosphopeptide: implications for signaling. *Mol Cell* **14:** 405-412

Sibanda BL, Critchlow SE, Begun J, Pei XY, Jackson SP, Blundell TL, Pellegrini L (2001) Crystal structure of an Xrcc4-DNA ligase IV complex. *Nat Struct Biol* **8:** 1015-1019

Wang B, Matsuoka S, Ballif Ba, Zhang D, Smogorzewska A, Gygi SP, Elledge SJ (2007) Abraxas and RAP80 form a BRCA1 protein complex required for the DNA damage response. *Science* **316:** 1194-1198

Wang H, Elledge SJ (1999) DRC1, DNA replication and checkpoint protein 1, functions with DPB11 to control DNA replication and the S-phase checkpoint in Saccharomyces cerevisiae. *Proc Natl Acad Sci U S A* **96:** 3824-3829

Wang J, Gong Z, Chen J (2011) MDC1 collaborates with TopBP1 in DNA replication checkpoint control. *J Cell Biol* **193:** 267-273

Watts FZ, Brissett NC (2010) Linking up and interacting with BRCT domains. *DNA Repair* **9:** 103-108

Williams RS, Dodson GE, Limbo O, Yamada Y, Williams JS, Guenther G, Classen S, Glover JNM, Iwasaki H, Russell P, Tainer JA (2009) Nbs1 flexibly tethers Ctp1 and Mre11-Rad50 to coordinate DNA double-strand break processing and repair. *Cell* **139:** 87-99

Williams RS, Lee MS, Hau DD, Glover JN (2004) Structural basis of phosphopeptide recognition by the BRCT domain of BRCA1. *Nat Struct Mol Biol* **11:** 519-525

Wu P-Y, Frit P, Meesala S, Dauvillier S, Modesti M, Andres SN, Huang Y, Sekiguchi J, Calsou P, Salles B, Junop MS (2009) Structural and functional interaction between the human DNA repair proteins DNA ligase IV and XRCC4. *Mol Cell Biol* **29:** 3163-3172

Yamane K, Wu X, Chen J (2002) A DNA damage-regulated BRCT-containing protein, TopBP1, is required for cell survival. *Mol Cell Biol* **22:** 555-566

Yu X, Chen J (2004) DNA damage-induced cell cycle checkpoint control requires CtIP, a phosphorylation-dependent binding partner of BRCA1 C-terminal domains. *Mol Cell Biol* **24:** 9478-9486

Yu X, Chini CCS, He M, Mer G, Chen J (2003) The BRCT domain is a phospho-protein binding domain. *Science* **302:** 639-642

Zhou BB, Bartek J (2004) Targeting the checkpoint kinases: chemosensitization versus chemoprotection. *Nat Rev Cancer* **4:** 216-225

Appendix A

Ubiquitin binding specificities of the RAP80 tandem UIM domains

A version of this chapter is published in:

Huang J, Huen MS, Kim H, Leung CC, Glover JN, Yu X, Chen J (2009) RAD18 transmits DNA damage signalling to elicit homologous recombination repair. *Nat Cell Biol.* **11**:592-603.

A.1 Introduction

Like phosphorylation, ubiquitylation is a common modification that regulates signalling processes in the DNA damage response Ubiquitylation involves a multistep process that requires at least three enzymes: the ubiquitin (Ub) activating enzyme (E1), Ub conjugating enzyme (E2) and the Ub protein ligase (E3) (Weissman, 2001). In the first step, a free Ub is activated by the E1 in an ATP-dependent manner by forming a thiol-ester bond with the carboxy-terminal glycine of Ub. The activated Ub is then transferred to the E2 by a trans-thiolation reaction at the Ub carboxy terminus. Finally the E3 interacts with the E2 to transfer the Ub onto the ε-amino group of a lysine residue of the substrate. The Ub molecule can also be a substrate itself, resulting in multiple Ub molecules conjugated onto proteins. Because an Ub moiety contains seven lysine residues, different chain linkages exist and result in distinct chain-defined topologies. For example, K48-linked polyUb form compact structures while K63-linked polyUb are extended in solution (Varadan et al, 2004; Varadan et al, 2002). Linear Ub chains can also form through linkages between the C- and N-termini of adjacent Ub molecules (Kirisako et al, 2006). Furthermore, the chain linkage also dictates the functional outcome of ubiquitylated substrates. In general, K48 and K11 polyUb chains destine proteins for proteasomal degradation, whereas K63 polyUb chains are used for cell signalling (Al-Hakim et al, 2010; Pickart & Fushman, 2004).

BRCA1 has well established roles in the repair of DNA DSBs. In response to ionizing radiation (IR), BRCA1 localizes to IR-induced foci to regulate homologous recombination (HR) repair. However, the exact mechanism of recruitment of BRCA1 to IR-induced foci was unclear, until the discovery of Receptor-associated protein 80 (RAP80) as a recruitment factor for BRCA1 (Kim et al, 2007; Sobhian et al, 2007; Wang et al, 2007). RAP80 is part of the multi-protein BRCA1-A complex that also includes Abraxas/CCDC98, BRCC36,

BRCC45/BRE and NBA1/MERIT40 (Huen et al, 2010). This complex is brought to sites of DSBs by the RAP80-specific recognition of K63-linked Ub chains, which are catalyzed by the RNF8/RNF168 E3 Ub ligases in coordination with the UBC13/MMS2 E2 heterodimer (Huen et al, 2007; Kolas et al, 2007; Mailand et al, 2007; Wang & Elledge, 2007). The mechanism of polyUb recognition is mediated by tandem UIM domains in the N-terminus of RAP80 (Kim et al, 2007; Sobhian et al, 2007). To understand the basis for K63-linked chain recognition, we used GST pull-down assays and surface plasmon resonance to characterize the binding specificities of the RAP80 tandem UIM domains. In accordance with other studies, we show that the tandem UIM domains are specific for K63-linked chains and that the binding affinities increase with increasing chain lengths.

A.2 Materials and Methods

A.2.1. Cloning, protein expression and purification

Constructs containing the N-terminal region of RAP80 (RAP80N, aa 1-337) and only the RAP80 tandem UIM domains (RAP80 UIM, aa 74-124) were cloned into pDEST15 (Invitrogen) and pGEX-6P-1, respectively. The RAP80 UIM construct was provided by Dr. Leo Spyracopoulos (University of Alberta). The plasmids were expressed *E. coli* BL21 Gold strain and grown in LB media at 25 °C to an A_{600} of 0.6-0.8 prior to induction with 0.5 mM IPTG overnight at 22 °C.

Harvested cells were resuspended in lysis buffer (50 mM Tris-HCl pH 8.0, 150 mM NaCl and 0.1 % 2-mercaptoethanol) supplemented with Complete EDTA-free protease inhibitor cocktail tablets (Roche Applied Science). To lyse the cells, the suspension was incubated with 1 mg/mL lysozyme (Sigma-Aldrich) for 30 min. on ice and sonicated with 5-10 5 sec. pulses separated by 30 sec. pauses on ice. The lysate was then centrifuged at 17,000 rpm for 45 min. using the JA-17 rotor (Beckman Coulter Inc.) to separate the soluble fraction from insoluble fraction. The GST-fusion proteins were purified using glutathione

affinity chromatography with glutathione sepharose 4B beads (GE Healthcare) and eluted in elution buffer (20 mM Tris-HCl pH 7.5, 150 mM NaCl and 20 mM reduced glutathione).

A.2.2. GST pull-down assay and immunoblotting

Purified proteins were buffer exchanged with an Amicon Ultra-15 centrifugal filter (Millipore) into NETN buffer (20 mM Tris pH 7.5, 150 mM NaCl, 1 mM EDTA and 0.1% BME). GST pull-down experiments were carried out with NETN buffer supplemented with NP-40 (20 mM Tris pH 7.5, 150 mM NaCl, 1 mM EDTA, 0.5 % NP-40 and 0.1 % BME). GST-fusion proteins were incubated with excess bait protein in ice for 30 min. before adding glutathione sepharose 4B beads, which was then further incubated at 4 °C with gentle agitation for 1.5 hours. Samples were washed 4 times in NETN buffer, eluted by adding Laemmli loading buffer dye and resolved using SDS-PAGE.

SDS-PAGE gels were transferred onto Immobilon-PSQ (Millipore) membrane in transfer buffer (18% methanol and 1X Tris/glycine buffer (25 mM Tris pH 8.3, 192 mM glycine)) for 3 hrs at 150 mA in a Mini Trans-Blot cell (Bio-Rad). After transfer, the membrane was blocked in 1 % BSA in TBST buffer (10 mM Tris pH 7.4, 0.9 % NaCl, 0.05 % Tween-20) for 2 hrs at room temperature, followed by incubation with a mouse monoclonal anti-Ub primary antibody (sc-8017, Santa Cruz) overnight at 4 °C. This was followed by incubation with a anti-mouse HRP conjugate (A4416, Simga-Aldrich) for 1 hr at room temperature and detection using the Amersham ECL detection system (GE Healthcare). Gels were exposed on BioMax MR X-ray film (Kodak).

A.2.3. Surface plasmon resonance

Purified proteins were buffer exchanged with an Amicon Ultra-15 centrifugal filter (Millipore) into running buffer (10 mM HEPES pH 7.4, 150 mM NaCl, 0.05% NP-40 and 1 mM DTT). Binding experiments were carried out on the

BIAcore 3000 system (GE-Healthcare). Penta-Ub linked K48 and K63 chains (Boston Biochem) were immobilized using the Amine Coupling Kit (BIAcore-GE). Specifically, two lanes on a CM5 chip were activated using 1:1 N-hydroxysuccinimide (NHS)/1-ethyl-3-(3-dimethylaminopropyl)carbodiimide (EDC) at a flow rate of 5 µl/min for 7 min. Penta-Ub linked K48 chains (1 µM) or K63 chains (1µM) in 10mM sodium acetate buffer (pH 4) were then immobilized at a flow rate of 5 µl/min, followed by blocking with 1M ethanolamine, pH 8.5 for 7 min at a flow rate of 5 µl/min. A total of 70 response units of penta-Ub linked K63 and 400 response units of penta-Ub linked K48 chains were immobilized. A control lane was made by activation and blocking, but without any immobilization of protein. Binding of GST and GST-RAP80 UIM to either penta-Ub linked K48 or K63 chains were carried out at 4 °C with a flow rate of 30 µL/min in running buffer. The amount of specific analyte protein bound was monitored by subtracting the response units from the control lane from the penta-Ub immobilized lane. All sensorgram data points were averaged from duplicate runs and plotted with Excel.

A.3 Results and Discussion

To test for the specificity of RAP80 tandem UIM domains, we used GST pull-down assays and immunoblotting to detect for binding to different Ub chains. Consistent with previous studies (Kim et al, 2007; Sobhian et al, 2007), GST-fusion proteins of the N-terminal region of RAP80 containing the UIM domains (RAP80N) or tandem UIM domains only (RAP80 UIM) were sufficient for recognizing K63 polyUb chains (Fig A-1). In stark contrast, no binding was observed for K48 polyUb. Interestingly, the pattern of K63 polyUb binding suggested that the minimum requirement for RAP80 binding was di-Ub, with a stronger preference for tetra-Ub or longer chains. This apparent preference for tetra-Ub was also shown by Sobhian et al. in their pull-down assays (Sobhian et al, 2007). To confirm the selectivity for K63-linked chains, we used surface

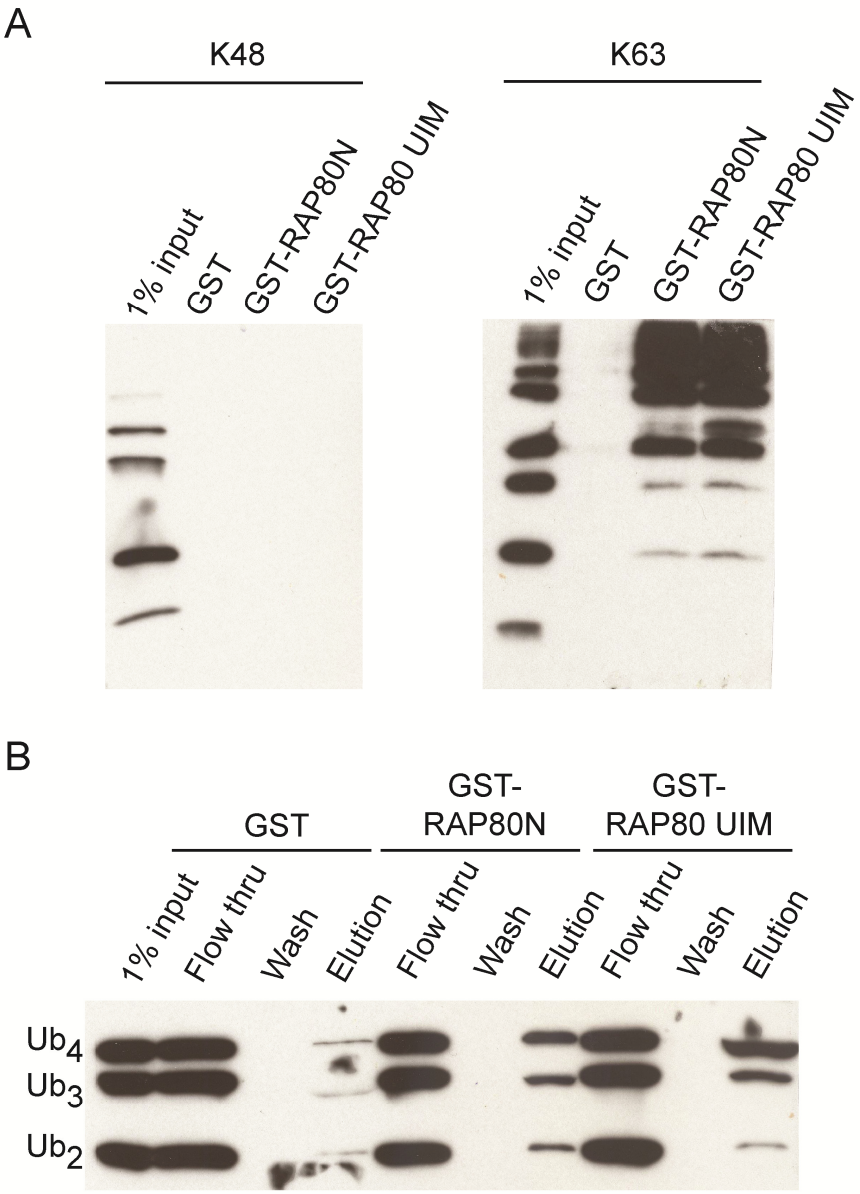

Figure A-1. RAP80 UIM domains binds to polyUb chains in a K63-linkage and length dependent manner. (A) GST pull-down assays using various GST fusion proteins with K48 and K63 Ub conjugates (1-7). Reactions were immunoblotted with anti-Ub antibody. (B) GST pull-down assays with linear-linked di-, tri- and tetra-Ub.

plasmon resonance to assess interactions between RAP80 UIM and K48 or K63 penta-Ub chains. As shown in Figure A-2, RAP80 UIM domains display an absolute specificity for K63 penta-Ub chains, with no detectable binding observed with K48 penta-Ub chains even at high concentrations.

The structure of K63-linked Ub resembles linear Ub chains due to the close proximity of K63 to the N-terminus of Ub. Structural studies of K63 di-Ub and linear di-Ub suggest that both are virtually equivalent in overall conformation, where individual Ub moieties are highly flexible and rotationally unrestrained (Komander et al, 2009). We hypothesized that RAP80 UIM domains may also garner the same specificity for linear Ub chains. Indeed, we noticed the same pattern of binding to linear Ub chains in our GST pull-down assay. As shown in Figure A-1B, linear tetra-Ub binds stronger than tri- or di-Ub chains. However the binding affinities are significantly weaker than K63-linked Ub, since a large excess of linear Ub was required as input in the pull-down experiments (175 μg total linear Ub compared to 5 μg total K63-linked Ub) to detect binding in the elution lanes. Therefore, the apparent higher affinity of the RAP80 UIM domains for K63-polyUb over linear polyUb suggests that the extended conformation of the linear polyUb molecules is not sufficient to mimic specificity for tandem UIM domains.

Due to the problem of attaining high amounts of pure K63-linked di-Ub or tetra-Ub, we attempted to instead crystallize the individual RAP80 UIM domains with mono-Ub. Unfortunately, we were unable to successfully co-crystallize these complexes. At the same time, several studies that included the crystal structure of RAP80 UIM domains in complex to K63-linked di-Ub were published, revealing the structural basis for RAP80 UIM domain specificity for K63-linked Ub (Sato et al, 2009; Sims & Cohen, 2009). Interestingly, no interactions are observed with the K63 iso-peptide linkage. Instead, binding of K63 di-Ub initiates an helical switch of the inter-UIM region, forming a continuous α-helix

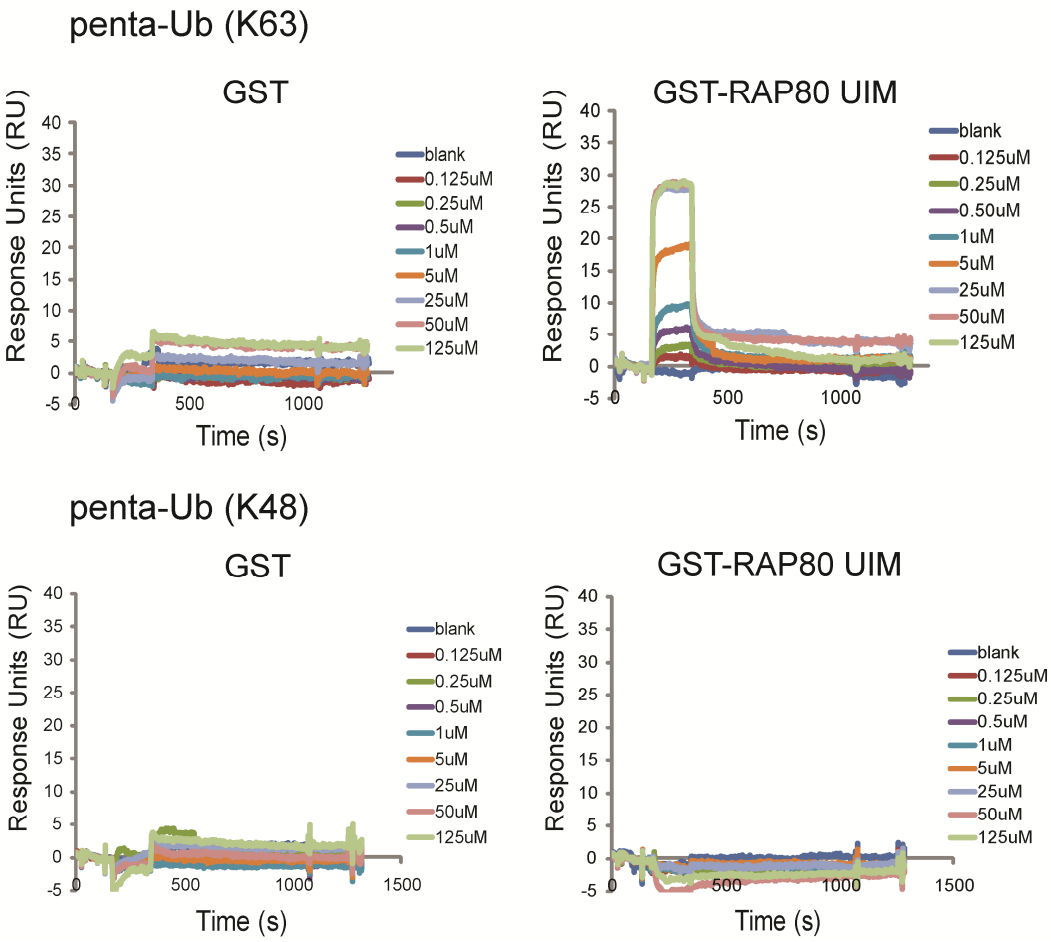

Figure A-2. Surface plasmon resonance sensorgrams of RAP80 UIM domains with K48 and K63-linked Ub chains. Immobilized penta-Ub linked K48 and K63 chains were titrated with increasing concentrations of GST and GST-RAP80 UIM.

spanning both UIM domains for efficient binding across a single K63 linkage (Fig. A-3). This allows both UIM domains to be in the correct cis orientation and distance to recognize the conserved Ile44-centered hydrophobic patch on each Ub molecule. This unique multivalent specificity depends on the length and helical turns of the inter-UIM linker (Cho et al, 2009; Sato et al, 2009; Sims & Cohen, 2009). Whereas addition or subtraction of residues that position the UIM binding sites out of helical phase are the most disruptive for binding, mutants that restore their positions on the same side of the continuous α-helix are less disruptive.

The "molecular ruler" of the RAP80 tandem UIM domains is also sufficient to distinguish K63-polyUb from linear polyUb linkages in extended polyUb chains. Interestingly, different ubiqutin-binding domains (UBDs) are able to distinguish between K63 or linear-linked Ub chains. For example, the NEMO UBAN domain is highly specific for linear polyUb, whereas the Tab2 NZF domain, like the RAP80 tandem UIMs, is highly specific for K63-polyUb (Komander et al, 2009; Lo et al, 2009). The crystal structure of NEMO UBAN domain in complex with linear di-Ub illustrates that an extended interface involving different binding sites on the distal and proximal Ub moieties and residues in the linkage region (Arg72, Leu73, Arg74 in distal Ub; Gln2 in proximal Ub), likely only made possible by the linear linkage, is recognized by the UBAN dimer structure (Rahighi et al, 2009).

The increasing binding affinity for longer K63-linked Ub chains, as shown from our pull-down experiments, was also demonstrated using a combination of solution-state NMR methods and molecular dynamics by Markin et al., suggesting that RAP80 tandem UIM domains interact to an increasing number of mono- and multivalent binding sites as chain length increases (Markin et al, 2010). Our observation for the marked preference for tetra-Ub in our pull-down

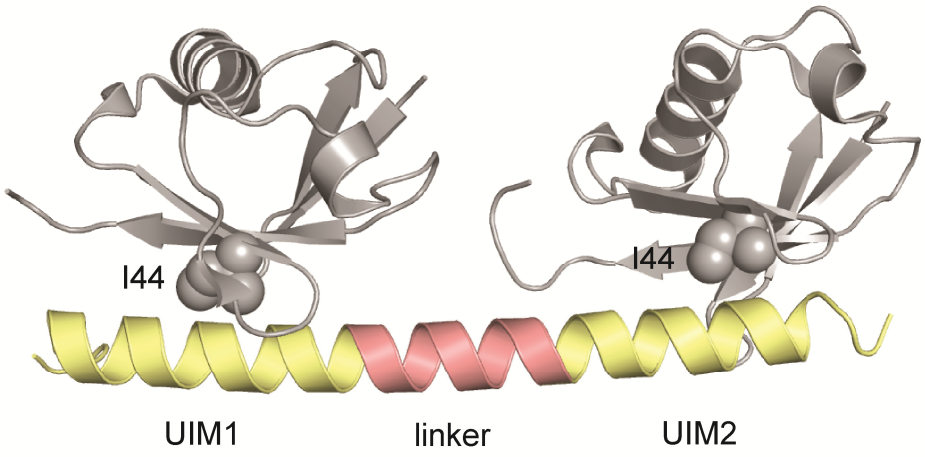

Figure A-3. Structural basis for K63-linked di-Ub binding by RAP80 UIM domains. RAP80 UIM domains (yellow) form a continuous helix with the inter-UIM linker (red) to recognize the K63-linked di-Ub (PDB ID: 3A1Q). Both UIM1 and UIM2 bind to the Ile44 (shown as spheres) centered hydrophobic patch on the two Ub molecules.

assays (Fig. A-1) may be due to the GST-tag induced dimerization by the GST-RAP80 fusion protein used in the pull-down assays.

It is clear that ubiquitylation signalling has evolved to be extraordinarily complex. The fate of ubiquitylated proteins not only depend on whether it is mono- or poly-ubiquitylated, but how the Ub molecules are linked. Unlike phospho-peptide binding modules, which usually recognize residues flanking the phosphorylated residue to garner specificity, UBDs usually only bind the same Ile44-centered face of Ub. Therefore, Ub binding domains have designed clever ways to recognize chain-specific polyUb. The RAP80 tandem UIM domains represent a specific class of UBDs that are specific for K63-linked polyUb. Indeed, future work is needed to elucidate the mechanism of Ub and poly-Ub selectivity by UBDs.

A.4 References

Al-Hakim A, Escribano-Diaz C, Landry MC, O'Donnell L, Panier S, Szilard RK, Durocher D (2010) The ubiquitous role of ubiquitin in the DNA damage response. *DNA Repair* **9:** 1229-1240

Cho HJ, Lee S, Kim H (2009) The linker connecting the tandem ubiquitin binding domains of RAP80 is critical for lysine 63-linked polyubiquitin-dependent binding activity. *BMB Rep* **42:** 764-768

Huen MS, Sy SM, Chen J (2010) BRCA1 and its toolbox for the maintenance of genome integrity. *Nat Rev Mol Cell Biol* **11:** 138-148

Huen MSY, Grant R, Manke I, Minn K, Yu X, Yaffe MB, Chen J (2007) RNF8 transduces the DNA-damage signal via histone ubiquitylation and checkpoint protein assembly. *Cell* **131:** 901-914

Kim H, Chen J, Yu X (2007) Ubiquitin-binding protein RAP80 mediates BRCA1-dependent DNA damage response. *Science* **316:** 1202-1205

Kirisako T, Kamei K, Murata S, Kato M, Fukumoto H, Kanie M, Sano S, Tokunaga F, Tanaka K, Iwai K (2006) A ubiquitin ligase complex assembles linear polyubiquitin chains. *EMBO J* **25:** 4877-4887

Kolas NK, Chapman JR, Nakada S, Ylanko J, Chahwan R, Sweeney FD, Panier S, Mendez M, Wildenhain J, Thomson TM, Pelletier L, Jackson SP, Durocher D (2007) Orchestration of the DNA-damage response by the RNF8 ubiquitin ligase. *Science* **318:** 1637-1640

Komander D, Reyes-Turcu F, Licchesi JD, Odenwaelder P, Wilkinson KD, Barford D (2009) Molecular discrimination of structurally equivalent Lys 63-linked and linear polyubiquitin chains. *EMBO Rep* **10:** 466-473

Lo YC, Lin SC, Rospigliosi CC, Conze DB, Wu CJ, Ashwell JD, Eliezer D, Wu H (2009) Structural basis for recognition of diubiquitins by NEMO. *Mol Cell* **33:** 602-615

Mailand N, Bekker-Jensen S, Faustrup H, Melander F, Bartek J, Lukas C, Lukas J (2007) RNF8 ubiquitylates histones at DNA double-strand breaks and promotes assembly of repair proteins. *Cell* **131:** 887-900

Markin CJ, Saltibus LF, Kean MJ, McKay RT, Xiao W, Spyracopoulos L (2010) Catalytic proficiency of ubiquitin conjugation enzymes: balancing pK(a) suppression, entropy, and electrostatics. *J Am Chem Soc* **132:** 17775-17786

Pickart CM, Fushman D (2004) Polyubiquitin chains: polymeric protein signals. *Curr Opin Chem Biol* **8:** 610-616

Rahighi S, Ikeda F, Kawasaki M, Akutsu M, Suzuki N, Kato R, Kensche T, Uejima T, Bloor S, Komander D, Randow F, Wakatsuki S, Dikic I (2009) Specific recognition of linear ubiquitin chains by NEMO is important for NF-kappaB activation. *Cell* **136:** 1098-1109

Sato Y, Yoshikawa A, Mimura H, Yamashita M, Yamagata A, Fukai S (2009) Structural basis for specific recognition of Lys 63-linked polyubiquitin chains by tandem UIMs of RAP80. *EMBO J* **28:** 2461-2468

Sims JJ, Cohen RE (2009) Linkage-specific avidity defines the lysine 63-linked polyubiquitin-binding preference of rap80. *Mol Cell* **33:** 775-783

Sobhian B, Shao G, Lilli DR, Culhane AC, Moreau La, Xia B, Livingston DM, Greenberg Ra (2007) RAP80 targets BRCA1 to specific ubiquitin structures at DNA damage sites. *Science* **316:** 1198-1202

Varadan R, Assfalg M, Haririnia A, Raasi S, Pickart C, Fushman D (2004) Solution conformation of Lys63-linked di-ubiquitin chain provides clues to functional diversity of polyubiquitin signaling. *J Biol Chem* **279:** 7055-7063

Varadan R, Walker O, Pickart C, Fushman D (2002) Structural properties of polyubiquitin chains in solution. *J Mol Biol* **324:** 637-647

Wang B, Elledge SJ (2007) Ubc13/Rnf8 ubiquitin ligases control foci formation of the Rap80/Abraxas/Brca1/Brcc36 complex in response to DNA damage. *Proc Natl Acad Sci U S A* **104:** 20759-20763

Wang B, Matsuoka S, Ballif Ba, Zhang D, Smogorzewska A, Gygi SP, Elledge SJ (2007) Abraxas and RAP80 form a BRCA1 protein complex required for the DNA damage response. *Science* **316:** 1194-1198

Weissman AM (2001) Themes and variations on ubiquitylation. *Nat Rev Mol Cell Biol* **2:** 169-178

Appendix B

Ubiquitin binding specificities of the RAD18 ZNF domain

A version of this chapter is published in:

Huang J, Huen MS, Kim H, Leung CC, Glover JN, Yu X, Chen J (2009) RAD18 transmits DNA damage signalling to elicit homologous recombination repair. *Nat Cell Biol.* **11**:592-603.

B.1 Introduction

RAD18 is an E3 ubiquitin (Ub) ligase that has roles in DNA damage bypass and post-replication repair (Tateishi et al, 2003; Tateishi et al, 2000). At stalled replication forks, RAD18, in combination with the E2 Ub conjugase RAD6, promotes the mono-ubiquination of proliferating cell nuclear antigen (PCNA) (Hoege et al, 2002; Watanabe et al, 2004), a homotrimeric protein that encircles DNA to maintain the processivity of polymerases and also acts as a scaffold to recruit proteins involved in cell-cycle control and DNA repair (Moldovan et al, 2007). The role of RAD18 in homologous recombination (HR) repair remained elusive, until studies from our collaborator, Dr. Junjie Chen (University of Texas MD Anderson Cancer Center), uncovered a basis for RAD18 function (Huang et al, 2009). In response to DNA DSBs, RAD18 is recruited to sites of DNA strand breaks and facilitates HRR by interacting with the recombinase RAD51C, which functions in the strand exchange of DNA strands during HR. The domain structure of RAD18 includes an N-terminal Really Interesting New Gene (RING) finger domain, a SAF-A/B, Acinus and Pias (SAP) domain and UBZ-type Zinc Finger (ZNF) domain (Notenboom et al, 2007). Interestingly, the recruitment of RAD18 depends on the ZNF domain binding to K63-linked Ub conjugates catalyzed by the RNF8/RNF168 E3 Ub ligases (Huang et al, 2009). This poly-ubiquination signalling is also responsible for the localization of BRCA1-associated complexes to DSBs through the K63-linked Ub binding of RAP80 UIM domains (Bennett & Harper, 2008; Panier & Durocher, 2009). To characterize the binding specificities of RAD18 ZNF Ub binding *in vitro*, we used surface plasmon resonance (SPR) to measure the binding properties of RAD18 ZNF to K48 and K63-linked Ub chains.

B.2 Materials and Methods

B.2.1. Cloning, protein expression and purification

An N-terminal GST-fusion of RAD18 (186-240) was cloned into pDEST15 vector (Invitrogen) and provided by the Dr. Junjie Chen. The plasmid was expressed *E. coli* BL21 Gold strain and grown in LB media at 25 °C to an A_{600} of 0.6-0.8 prior to induction with 0.5 mM IPTG overnight at 22 °C.

Harvested cells were resuspended in lysis buffer (50 mM Tris-HCl pH 8.0, 150 mM NaCl and 0.1 % 2-mercaptoethanol) supplemented with Complete EDTA-free protease inhibitor cocktail tablets (Roche Applied Science). To lyse the cells, the suspension was incubated with 1 mg/mL lysozyme (Sigma-Aldrich) for 30 min. on ice and sonicated with 5-10 5 sec. pulses separated by 30 sec. pauses on ice. The lysate was then centrifuged at 17,000 rpm for 45 min. using the JA-17 rotor (Beckman Coulter Inc.) to separate the soluble fraction from insoluble fraction. The GST-RAD18 ZNF was purified using glutathione affinity chromatography with glutathione sepharose 4B beads (GE Healthcare) and eluted in elution buffer (20 mM Tris-HCl pH 7.5, 150 mM NaCl and 20 mM reduced glutathione). The purified GST-RAD18 ZNF was buffer exchanged with an Amicon Ultra-15 centrifugal filter (Millipore) into running buffer (10 mM HEPES pH 7.4, 150 mM NaCl, 0.05% NP-40 and 1 mM DTT).

B.2.2. Surface plasmon resonance

SPR experiments were carried out as described in Appendix A. Assuming a 1:1 stoichiometry for GST-RAD18 ZNF interactions with either K48 and K63-linked chains, equilibrium dissociation constants (K_d) were fit from the titration data using the equation,

$$R_{eq} = \frac{R_{\max}[RAD18]}{K_D + [RAD18]}$$

where [RAD18] is the concentration of GST-RAD18 ZNF analyte, R_{eq} is the peak response level observed at [RAD18], and R_{max} is the maximum SPR response

level. Fitting of K_d and R_{max} against the experimental data was performed with SigmaPlot software.

B.3 Results and Discussion

Using SPR, we demonstrate that RAD18 ZNF domain is a bona fide Ub binding domain. Interestingly, the ZNF domain does not seem to be specific for the type of Ub linkage, since it displays similar affinities to both penta-K48 and K63-linked Ub chains (K_d = 36 ± 10 nM and 17 ± 4 nM, respectively) (Figure B-1).

The RAD18 ZNF domain belongs to the family of UBZ4 C2HC Zinc finger domains that are also found in the Y-family DNA polymerase κ and the Werner-helicase interacting protein WRNIP1 (Bienko et al, 2005; Hofmann, 2009). Although the molecular basis of UBZ4-Ub recognition remains unresolved, solution structure studies of the UBZ3 domain in Y-family DNA polymerase η (Bomar et al, 2007), which is predicted to adopt the same fold as UBZ4, provide insight into the potential basis for Ub binding by the RAD18 ZNF domain (Fig. B-2A). The UBZ domain utilizes a single α-helix to recognize the conserved hydrophobic surface (centered at the conserved Ile44 residue) of Ub in a manner similar to that of inverted helical Ub-binding (MIU) domains (Fig. B-2B). If the RAD18 ZNF domain recognition of Ub is structurally similar, this may explain the lack of specificity observed for the Ub linkage type, since no interactions are found with the linkage region and the conserved Ile44-centred surface on Ub is accessible in both mono-Ub and different types of poly-Ub chains.

In contrast, the RAP80 UIM domains are specific for binding K63-linked Ub chains, which also matches the chain type catalyzed by the RNF8/RNF168 E3 ligases in HR repair. The apparent lack of Ub linkage specificity of the RAD18 ZNF domain may suggest a more promiscuous role for RAD18 to target differentially ubiquitylated substrates in order to switch from HR repair to post-replication repair at stalled replication forks.

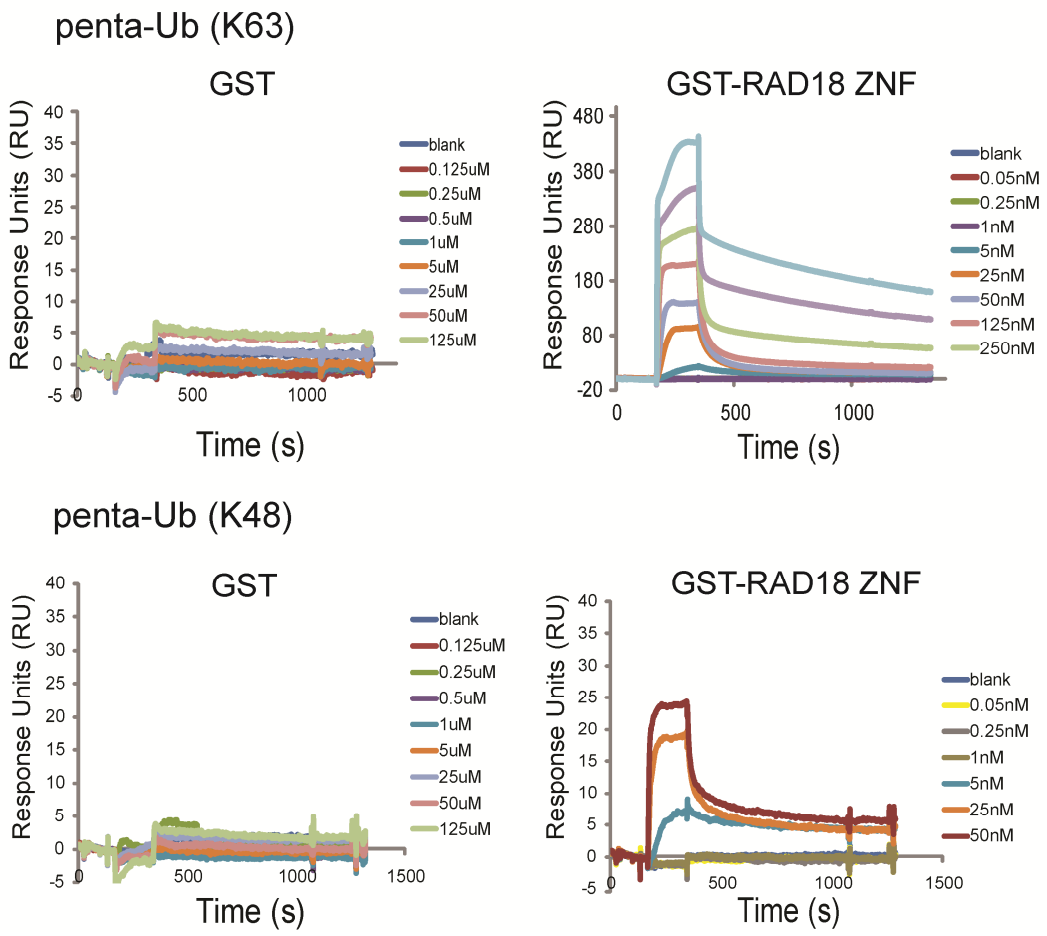

Figure B-1. RAD18 ZNF domain binds to K48 and K63-linked Ub chains. SPR sensorgrams for GST and GST-RAD18 ZNF with immobilized K63 (top) and K48 (bottom) linked penta-Ub chains.

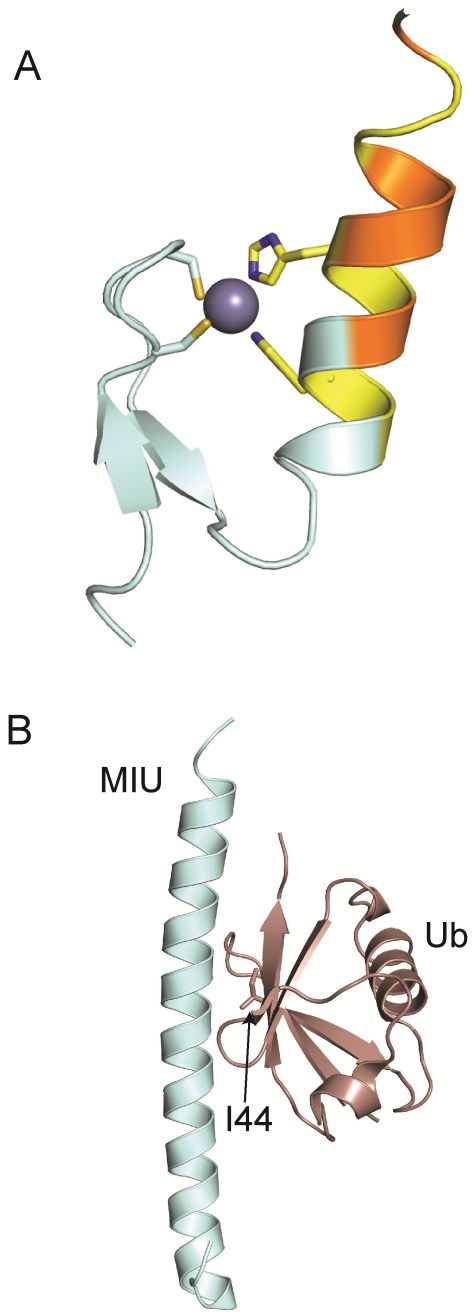

Figure B-2. Proposed Ub binding mode for RAD18 ZNF domain. (A) Solution structure of UBZ3 domain in DNA polymerase η (PDB ID: 2I5O). Residues coordinating the Zn (grey) are shown as sticks. Residues with chemical shift perturbations upon binding Ub are coloured orange (greater than 2σ) and yellow (greater than 1σ). (B) Crystal structure of Rabex-5 MIU domain in complex with Ub (PDB ID: 2FIF).

B.4 References

Bennett EJ, Harper JW (2008) DNA damage: ubiquitin marks the spot. *Nat Rev Mol Cell Biol* **15:** 20-22

Bienko M, Green CM, Crosetto N, Rudolf F, Zapart G, Coull B, Kannouche P, Wider G, Peter M, Lehmann AR, Hofmann K, Dikic I (2005) Ubiquitin-binding domains in Y-family polymerases regulate translesion synthesis. *Science* **310:** 1821-1824

Bomar MG, Pai MT, Tzeng SR, Li SS, Zhou P (2007) Structure of the ubiquitin-binding zinc finger domain of human DNA Y-polymerase eta. *EMBO Rep* **8:** 247-251

Hoege C, Pfander B, Moldovan GL, Pyrowolakis G, Jentsch S (2002) RAD6-dependent DNA repair is linked to modification of PCNA by ubiquitin and SUMO. *Nature* **419:** 135-141

Hofmann K (2009) Ubiquitin-binding domains and their role in the DNA damage response. *DNA Repair* **8:** 544-556

Huang J, Huen MSY, Kim H, Leung CCY, Glover JNM, Yu X, Chen J (2009) RAD18 transmits DNA damage signalling to elicit homologous recombination repair. *Nature cell biology* **11:** 592-603

Moldovan GL, Pfander B, Jentsch S (2007) PCNA, the maestro of the replication fork. *Cell* **129:** 665-679

Notenboom V, Hibbert RG, van Rossum-Fikkert SE, Olsen JV, Mann M, Sixma TK (2007) Functional characterization of Rad18 domains for Rad6, ubiquitin, DNA binding and PCNA modification. *Nucleic Acids Res* **35:** 5819-5830

Panier S, Durocher D (2009) Regulatory ubiquitylation in response to DNA double-strand breaks. *DNA Repair* **8:** 436-443

Tateishi S, Niwa H, Miyazaki J, Fujimoto S, Inoue H, Yamaizumi M (2003) Enhanced genomic instability and defective postreplication repair in RAD18 knockout mouse embryonic stem cells. *Mol Cell Biol* **23:** 474-481

Tateishi S, Sakuraba Y, Masuyama S, Inoue H, Yamaizumi M (2000) Dysfunction of human Rad18 results in defective postreplication repair and hypersensitivity to multiple mutagens. *Proc Natl Acad Sci U S A* **97:** 7927-7932

Watanabe K, Tateishi S, Kawasuji M, Tsurimoto T, Inoue H, Yamaizumi M (2004) Rad18 guides poleta to replication stalling sites through physical interaction and PCNA monoubiquitination. *EMBO J* **23:** 3886-3896